Effect of Microstructure on Thermal Conductivity of Cement-Based Foam

by

Farnaz Batool

A thesis submitted in partial fulfillment of the requirements for the degree of

Doctor of Philosophy

In

Structural Engineering

Department of Civil and Environmental Engineering
University of Alberta

Abstract

The use of thermal insulation has assumed greater importance amidst rising energy costs, with applications in the resource-rich but climatically harsh regions like Canada's North. The thermal performance of structural and non-structural components is singularly determined by the thermal properties of the materials used in its construction. The thermal conductivity which is a material's property is used in designing the insulation. In recent years, the use of cement-based foam has noticeably increased due to its good insulating properties and with potential for utilization of industrial by-products as pozzolanic admixtures.

The microstructure of cement-based foam comprises of two phases i.e. the solid phase and the void phase. The dimension and distribution of the air-void phase are influenced by a change in the overall density or porosity, whereas the properties of the solid phase are affected by the type of mix composition i.e. addition of the pozzolanic admixture, hydration age and moisture content.

This study investigates in detail the influence of air-void parameters and hydrated cement paste on the thermal conductivity of cement-based foam by varying the density and binder types. In the experimental phase, three series of cement-based foams were prepared with cast densities of 800 kg/m^3, 600 kg/m^3 and 400 kg/m^3 respectively. In addition to the reference mix, two mixes were prepared at each cast density containing fly ash, silica fume and metakaolin, where in the cement was replaced 10% and 20% by weight. The result shows that the thermal

conductivity was significantly influenced by the change in density and the substitution of admixtures leads to further reduction. This is mainly due to formation of crystalline and amorphous hydrated products, changes to air-void network and water absorptive property. Adding fly ash, silica fume and metakaolin does not significantly influence the of air-void size distribution. However, pore-size of 0.03 mm diameter had the maximum frequency of occurrence for all the mixes. The shape of the majority of the air-voids in all mixes was circular (i.e. spherical).

An empirical thermal conductivity model was developed based on the measurement of the void phase (porosity), substitution ratio of the pozzolanic admixture and the age of the paste. These observations were recorded in the current study for mixes with and without the pozzolanic admixture. For validation, thermal conductivity predictions were examined against other independent databases, reliable and accurate predictions were found.

Preface

This thesis is an original work by Farnaz Batool. No part of this thesis has been previously published

Acknowledgements

The author want to express her appreciation to Mr. Rizadly Mariano at the Civil Engineering Laboratory and to Mr. Greg Miller at the I.F. Morison Structural laboratory for their technical assistance in setting up different testing equipment and machines for this research. The author also extends her thanks to Dr. Michael Doschak and Muhammad Imran from Department of Pharmacy, University of Alberta for their skilled assistance with X-ray tomography scans. Author is also grateful to the administrative staff of the Department of Civil and Environmental Engineering at University of Alberta for their assistance throughout the years and to the undergraduate summer students namely Mr. John Rodway, Mr. Dennis Rosillo and Mr. Alexander Melnik for their support and help. Importantly, the author thanks all her fellow students for sharing their experience and giving intellectual input due to which this study became possible.

This author would like to thank her supervisor, Dr. Vivek Bindiganavile, for his unconditional trust, faith, moral and financial support and for also believing in the author's potential and abilities. Without him, this research would not have been possible. Finally, the author wants to convey special appreciation and gratitude to her family, especially her parents for their unconditional love, precious prayers and moral support without which this work was not possible. Many thanks also to my friends, students, colleagues at NED University, Karachi, Pakistan for being with me in times of need.

Finally, the financial support and in-kind contribution from Cematrix Canada Inc, Calgary, City of Edmonton's Drainage Services and Natural Sciences and Engineering Research Council (NSERC-Canada) is gratefully acknowledged.

Table of Contents

List of Figures

List of Tables

List of Symbols

$F(\tau)$	Dimensionless time dependent function of τ
$R(t)$	Total resistance at time t
R_0	Initial resistance
α	Temperature coefficient resistivity
$\Delta T(t)$	Average rise in temperature as a function of time (t)
P_o	Total output power
a	Radius of the spiral
K	Thermal conductivity
τ	Dimensionless parameter called the characteristic time ratio
κ	Thermal diffusivity
λ	Wavelength
Θ	Bragg angle
d	Interplanar spacing of parallel lattice planes
n	Number of wavelength
S_{cp}	Spread of cement-based foam
Υ_{cd}	Cast density
F_c	Foam content of cement-based foam
D	Demoulding density of cement-based foam
CH	Calcium hydroxide
CSH	Calcium silicate hydrate
AFt	Trisulfatehydrate
AFm	Momosulfatehydrate

P	Portlandite
E	Ettringite
C	Calcite
G	Gypsum
Q	Quartz
K	Kuzelite
S	Strätlingite
G	Gehlenite
Y	Yeelemite
M	Mullite
J	Jennite
T	Tobermorite /Plombierite-14A
Sl	Sillimanite
GIS	Gismondine
GW	Peak shape
LY	Phase fractions
$\mathbf{A_p}$	Cross-sectional area of void
$\mathbf{P_p}$	Parameter of the void cross section
C	Circularity
$\mathbf{P_p}$	Porosity
$\mathbf{þ_{solid}}$	Density of solid part
$\mathbf{þ_{porous\ material}}$	Density of porous material
Tc	Conductivity of the cement-based foam
$\mathbf{Tc_p}$	Thermal conductivity of cement paste

$\mathbf{T_d}$	Thermal conductivity of cement-based foam at 300^{th} day
t	Age of the paste since the day of casting
$\mathbf{Tc_{pa}}$	Conductivity of cement paste containing admixture
$\mathbf{Tc_v}$	Thermal conductivity of air in pores
$\mathbf{Tc_w}$	Thermal conductivity of water
$\mathbf{\Upsilon_d}$	Dry density
$\mathbf{\lambda_o}$	Constant
$\mathbf{\lambda_1, \lambda_2}$	Regression coefficient
$\mathbf{M_c}$	Moisture content
$\mathbf{\alpha_o}$	Constant
$\mathbf{\alpha_1, \alpha_2}$	Regression coefficient
$\mathbf{\beta_o}$	Constant
$\mathbf{\beta_1, \beta_2, \beta_3}$	Regression coefficient
$\mathbf{\Psi}$	Ratio (Tc / Tc_p)
þ	Porosity
N	Number of observations

1. Introduction

1.1 Background

Addressing the question of finding economically viable thermal insulation materials for both structural and non-structural purposes in the construction industry has assumed greater importance nowadays, in view of the rising cost of energy inputs to operate and maintain the insulation systems. There is greater demand now in the harsh climates of northern Canada where the exploitation of rich minerals is increasing day by day. Beside this, cement industry is also finding alternative building material to achieve the desired level of CO_2 reduction in coming years.

Cement-based foams are increasingly finding application in the construction industry because they are lightweight and can be produced quickly as compared to concrete (Kearsley et al. 2002 and Aldridge 2005). Lightweight foam concrete has in fact been used increasingly in countries including Libya, Russia, Brazil, Malaysia, Mexico, Saudi Arabia, Indonesia, Egypt and Singapore (Mydin 2010).

In Canada, cement-based foams are typically used for tunnel annulus grouting, flowable fills and geotechnical applications (Aldridge 2005, Bindiganavile et al. 2008). For instance, in British Columbia, cement-based foam is used as a lightweight engineered fill, while in the colder regions of the Canadian prairies, it is used for thermal insulation.

Cement-based foam comprises Portland cement, water and foam. The foam may be introduced either by adding surfactants to the mix constituents or by adding a “preformed foam” to the cement slurry. The cast density of this

composite may range from 300-1600 kg/m^3, in which lighter densities, < 800 kg/m^3, are used for non-structural application such as engineered void fill and thermal insulation. The heavier mixes are used for crash cushions, retaining walls and as structural fillers (Aldridge 2005). The low density composites are typically produced without using any fine aggregates although, occasionally, certain lightweight fine aggregates may also be introduced. In some cases, pozzolanic admixtures are also added to the mix.

The thermophysical parameters such as thermal conductivity, thermal diffusivity and specific heat capacity are the main parameters which govern the heat transport in multiphase systems. However thermal conductivity which is the ability of the material to conduct heat is mainly used in designing the insulation. Although mechanical and physical properties of cement-based foam has been subject of intensive study for last past years thus, far, very limited number of studies has been conducted on the functional properties like thermal conductivity.

Published literature (Goual et al. 1999, Khan 2002, Kim et al. 2003, Ochsner et al. 2008) reports that the thermal conductivity of the porous material is significantly influenced by its solid and void phases, size distribution of the air-void, shape of the void and porosity.

Achieving the target density in cement-based foam is only possible through indirect means where the consistency and stability of the base mix are satisfactory. If insufficient water is added, the mixture becomes too stiff and, as a result, foam bubbles break down. On the other hand, if too much water is added to the mixture then segregation takes place (Kearsley 1999, Kearsley et al. 2001, Nambiar et al. 2008, Ramamurthy et al. 2009).

Many important properties of cement-based foams depend upon the foam's microstructure. The microstructure may reasonably be assumed as a two-phase system consisting of a solid phase made of cement-paste and a voids phase made up entirely of an air-void. Protein- or synthetic-based foams are basically used to create a stable air-void network. The greater the foam content, the more the voids and the lower the density of the mix. While adding different types of pozzolanic admixtures changes the properties of the mix composition, depending on the content of each particular admixture.

While a few studies have characterized air-void parameters and their influence on the mechanical properties of cement-based foam, hardly any studies have investigated the effect of the air-void network on thermal conductivity. Also, only a limited investigation has been carried out explaining the role of hydrated products in the thermal conductivity of cement paste, especially when the pozzolanic admixture is part of the mix. Past research suggests that adding a pozzolanic admixture generally reduces the thermal conductivity of the mix. The present study was designed to investigate in detail the influence of air-void parameters and hydrated cement paste on the conductivity of cement-based foams.

It is expected that the data base that results from this study will lead to a better understanding of the microstructure parameters of cement-based foams in general, and the factors influencing the thermal conductivity in particular. This study should also make it possible to develop a more reliable analytical model to predict conductivity of cement-based foam.

1.2 Problem Statement

The effect of thermal conductivity for different types of building materials has been the subject of intensive study for decades. Limited information has been generated so far on characterizing the microstructure of cement-based foam and its influence on the thermal conductivity, especially by varying the density and mix composition. As a result, many fundamental questions, such as the following, remained unanswered:

- How much influence do the pozzolanic admixtures and different cast densities have on the thermal conductivity of cement-based foam?

- Which are the microstructural parameters influencing the thermal conductivity of cement-based foams ?

- Which are the governing hydrated products and how they are affected in the presence of a pozzolanic admixture? How much influence these hydrated products have on conductivity.

- What influence air-void parameters have on thermal conductivity for different mix compositions?

- What standards need to be drawn to measure the various parameters affecting the thermal properties? What would a better measurement technique entail?

- Are the existing models capable of fairly accurately predicting the effective conductivity for cement-based foam with different mixes in view of the irregular shapes and distribution of the voids prevalent in

the foams? If not, which parameters need modification and how they can be linked with these models?

This study addresses the above questions in detail to lead to a better and more reliable understanding of the factors affecting the microstructure of foams and their thermal conductivity.

1.3 Research Objectives

In order to fill the knowledge gaps identified in Chapter 2, the objectives of this study are:

- To investigate properties of mixes of cement-based foam in their fresh state.

- To identify and quantify the hydrated products of cement-based foam and establish a mathematical relationship between these hydrated products and thermal properties.

- To characterize and quantify the air-void parameters of cement-based foam samples.

- To experimentally evaluate the thermal conductivity of cement-based foam for different cast densities and with pozzolanic admixtures in two different substitutions (10% and 20% by weight).

- To develop and validate the proposed analytical model for the thermal conductivity of cement-based foam.

1.4 Scope of the Study

This study is intended to address the following:

- Experimentally measure the thermal properties by using transient plane source technique at room temperature and on air-dried cement-based foam specimens.

- Employ the X-ray tomography technique (XRT) to investigate the air-void network of cement-based foam specimens. The measurement of pores is limited to air-void (macro pores) of the specimen only.

- Quantify the crystalline products of hydrated cement paste by using the Rietveld Quantitative X-ray diffraction (RQXRD) method.

1.5 Significance of the Study

Cement-based foam has been the subject of many studies but not much data is available on the role of various parameters on the mechanical, physical, chemical and especially thermal properties. This research project was designed primarily to bridge gaps in the knowledge as ascertained during the literature review. Especially the understanding of the various factors influencing not only the thermal properties but also the mechanical properties. Further, the investigation into different pozzolans at various dosages will also shed more light on what role these admixture play in the consistency of cement-based foam in its fresh state. In particular, the development of a reliable model should be incorporating into the code of practice, so as to provide the end users with a handy tool for both manufacturing and designing future cement-based foams.

1.6 Thesis Organization

This thesis is organized into nine chapters and two appendices.

Chapter 1 provides the general introduction to this study, the problem statement, objective, scope and the research significance.

Chapter 2 reviews and discusses in detail the published literature on various aspects of lightweight cementitious systems, cement-based foam, cement slurries with and without foam, and the presence of pozzolanic admixture. The literature on the properties of fresh cement mix, thermal characteristics, measurement techniques and the microstructure have been dealt with in detail. The chapter examines the theoretical models used for predicting the thermal conductivity of porous materials, and also identifies their limitations. In addition, this chapter identifies the gaps in current knowledge and highlights the difficulties in measurement techniques.

Chapter 3 presents the experimental program and setup for this study. Details of the mix design, constituent materials and the preparation techniques of various specimens are presented. The setup for thermal property evaluation and techniques for the characterization of the microstructure and identification and quantification of various hydrated products are also described in detail. The technique employed to analyse the images taken during the course of the above are also included.

Chapter 4 displays the results of an experimental program to determine the fresh-state properties of cement-based foam. The fresh-state properties include stability, consistency, foam content and density of cement-based foam. The predicted model for spreadability and foam content are also formulated and included in the discussion.

Chapter 5 presents the results of a detailed experimental investigation to quantify the hydrated cement paste. The results include the identification of mineral phases and their quantification with and without mineral admixtures. A law for the thermal conductivity of cement-based foam is also presented. Moreover, the contribution of hydrated products in thermal conductivity, especially when a pozzolanic admixture is present in the mix is also included.

Chapter 6 characterizes the air-void parameters and the affect these parameters have on thermal conductivity.

Chapter 7 discusses the experimental results of thermal conductivity of cement paste and cement-based foams. Factors such as pozzolanic admixture type and content, moisture content, density, porosity and air-void parameters, all of which influence thermal conductivity, are investigated and included.

Chapter 8 presents analytical models for predicting the thermal of conductivity of cement-based foam containing pozzolanic admixture and the reference mix. The formulation of the cement hydrated paste model and its correlation to porosity and moisture content are also discussed. A comparison between the proposed model arising out of this study and the existing thermal conductivity models is also included. The validations of the models from this study are also investigated with the available database.

Chapter 9 summarizes the major findings of this study and lists the conclusions. Appendix A reports the detailed test results for XRD and X-ray tomography discussed in chapters 5 and 6. Appendix B presents the detailed output results of regression models.

2. Literature Review

2.1 Introduction

In this chapter, the relevant literature for cement-based foam, its constituent material, fresh state properties, thermal conductivity and design procedure is reviewed. Previous research on microstructure of cement-based foam is also discussed along with its influence on the thermal conductivity. The measurement techniques are also added in this discussion. In addition to this, the existing thermal conductivity models for the porous material from previous research are also reviewed. Moreover, summary of the literature review is also presented at the end.

2.2 Cement-Based Foam

Historically, it is noted that cellular concrete although in use now for decades, is not a century old yet. The first patent was taken in 1923 (Valore 1954) and its use was primarily for non- structural applications like ground fills. Brady et al. (2001) report that it is only after 1987 that its use was extended to other semi structural works like trench reinstatement, backfills behind retaining walls, in roof tiles as sandwich material, in precast works, as sound and thermal insulators, in foundation insulation or in pipe line works as fillers. In Canada especially, cellular concrete composites are being used quite extensively for thermal insulation in geo-structural applications. Therefore, the emphasis is on achieving low thermal conductivity at a given density and strength. The foamed concrete and cement-based foam belongs to same class i.e. cellular concrete; the difference is of aggregate which is part of foam concrete while cement-based foam is without it.

According to ACI 523.1R (2006), ACI 523.2R (1996) this material is defined as "A light weight product consisting of Portland cement and/or lime with siliceous fine material, such as sand, slag, or fly ash, mixed with water to form a paste that has a homogeneous void or cell structure is referred to as cellular or aerated concrete. The cellular structure is attained essentially by the inclusion of macroscopic voids resulting from a gas-releasing chemical reaction or the mechanical incorporation of air or other gases (autoclave curing is usually employed)".

In addition to this the BCA (1994) has defined the cellular concrete as "a light-weight material produced by incorporating preformed foam, into a base mix of cement paste or mortar, using a standard or proprietary mixing plant". The entrapped air bubbles reduce the density of the base mix and have a strong plasticizing effect on it.

However, the cement-based foam comprises of Portland cement, water and foam and the foam may be introduced either by adding surfactants to the mix constituents or by the addition of a preformed foam to the starting mix slurry. The density of this composite typically ranges between 300-1600 kg/m^3(Aldridge 2005, Jones et al. 2005b, Puttappa et al. 2008, Ramamurthy et al. 2009). Cast density less than 800 kg/m^3 is used in non-structural application such as engineered void fill and thermal insulation etc. These low density composites are typically produced without using any fine aggregates. While certain lightweight fine aggregates may be introduced, it is commonplace to use pozzolanic admixtures also (Kearsley 1999, Aldridge 2005, Jones et al. 2005a, Jones et al. 2005b).

2.3 Constituents Materials

As mentioned earlier, cement-based foam is made up of cement, water, mineral admixtures and foam. It is seen that the literature mentions about using cements other than type GU such as high alumina and calcium sulphoaluminate and rapid hardening Portland cements respectively (Kearsley et al. 2001, Jones et al. 2004, Jones et al. 2005b, Ramamurthy et al. 2009, Mydin 2010).

2.3.1 Surfactants (Foaming Agent)

The air bubbles in cement-based foam are incorporated by using a foaming surfactant. Two types of foaming agent; synthetic and protein-based has been reported by past researchers. Aldridge 2005, Jones et al. 2005a, Bindiganavile et al. 2008, Ramamurthy et al. 2009, Mydin 2010 have reported that protein based surfactants are made from refined animal products such as hoof, horn and skin whereas synthetic based foaming agents are made using man-made chemicals used in shampoos and soap. In another report Bindiganavile et al. (2008) have summarized that synthetic agents are made of amine, amine oxides and naphthalene sulphonate formaldehyde condensates.

According to McGovern (2000), Tikalsky et al. (2004), Bindiganavile et al. (2008), Mydin (2010) and Mamun (2010) protein based surfactant have more stable and strong bubble structure as compared to the foam produced using synthetic surfactants. These authors also state that synthetic foams give a lower density mix because of better expansion of the foam. Also, the shelf life of synthetic foams is less about 6 months only as compared to the protein derivatives which can be stored for up to 12 months.

The literature reveals that the foaming agents can further be classified into two types, where the respective type is capable of producing predominantly an open cell or a closed cell internal air-void network. The factors which influences the stability of the foam and which may lead to the breakdown of foam bubbles are identified by the above literature as vibration, evaporation, wind, temperature and other environmental factors. Therefore, the generated foam must be firm and stable so that it resists the pressure of the mortar until the cement takes its initial set and a strong skeleton of concrete is built up around the void filled with air.

Feng-qing et al. (2011) have reported three parameters which evaluate the performance of the foaming agent namely 1) foaming capacity which is the ratio of the final volume of foam to the volume of the solution before air-voids is form. 2) The bleeding rate is the amount of water seeped through the generated foam in an hour and 3) the collapse rate measured as the collapse length of the foam in test-tube within one hour.

2.3.2 Pozzolanic Admixtures

Bapat (2013) reported in his book that the "pulverized fuel ash" (PFA) also known as fly ash (FA) is commonly used as a pozzolanic admixture in cement and concrete. It is a product of the pulverized coal firing system, mostly used in the thermal power plants. It was further added that the presence of fly ash improves the performance of cement and concrete in terms of strength and the durability.

The PFA is divided into two classes; Class F and Class C these two classes are distinguished on the basic of their chemical compositions (Siddique et al. 2011, ACI 232.2 2003).

The Class F has pozzolanic properties and has low calcium oxide (CaO) content whereas, Class C has high calcium oxide content resulting in both pozzolanic and cementitious properties. Past research (Lee et al. 2003, Mehta et al. 2006) have shown that fly ash can be used in the range of 10–75% as cement replacement to reduce the cost, enhance consistence of mix, reduce the water demand and to reduce the heat of hydration whereas, the early-strength development can be affected by high fly ash content. Furthermore, the partial replacement of cement with fly ash also helps to prevent autogenous shrinkage (Lee et al. 2003).

Similarly, Siddique et al. (2011) and Bapat (2013) reported that silica fume (SF) is a pozzolanic admixture mainly consist of submicron particles of amorphous silicon dioxide. Silica fume commonly used in cement and concrete is the by-product of silicon metal and ferrosilicon alloys. It was further added that the American concrete institute (ACI) defines silica fume as ‘‘very fine non crystalline silica produced in electric arc furnaces as a by-product of production of elemental silicon or alloys containing silicon’. In addition, to this it was also added by the authors that addition of silica fume increases the strength and the durability because it increases the content of CSH, which is a principal strength giving compound.

Among, these pozzolanic admixture metakaolin is generally produced by the calcination of raw kaolin clay (Bapat 2013) and it conforms to ASTM C618 (2012) specifications. Furthermore, ACI 116R (2000) defines the MK as “either a raw or calcined natural material that has pozzolanic properties (for example, volcanic ash or pumicite, opaline chert and shales, tuffs and some diatomaceous earths)”. In addition to this presence of metakaolin increases the strength and durability of concrete. Moreover, the addition of metakaolin significantly influences the rheological properties of concrete mix.

Metakaolin has been used at 10% and 25% cement replacement (Siddique et al. 2009) and was seen to improve workability, increases durability, better compression and flexural strength and reduces water permeability. Kearsley et al. (2001) observed that the large volumes of fly ash can be used in foamed concrete. Although the high ash content results in a decrease in the early strength but the long-term strength was improved by replacing up to 75% of cement with fly ash. In another study, Jones et al. (2004) reported that the use of fly ash with high carbon content may require more foam to maintain desired plastic density. Recently, Nambiar et al. (2007) reported uniform distribution of air-voids in the foam concrete in the presence of fly ash.

In addition, Kearsley (1996), Jones et al. (2005a) and Ramamurthy et al. (2009) have reported that the compressive strength of the foamed concrete improves significantly with the replacement of silica fume up to 10% by mass of cement. Whereas, when the substitution percentage of silica fume was increased to 30%, then the influence on the strength noticed was not substantial. Furthermore, Ramamurthy et al. (2009) reported that ground granulated blast furnace slag has also been used as partial replacement of cement at levels between 30 to 50% respectively in foamed concrete.

2.4 Design Procedure

Presently, there is no standard method available for mix design of cement-based foam or foam concrete (Kearsley et al. 2005, Bindiganavile et al. 2008, Ramamurthy et al. 2009, Mamun 2010, Mydin 2010).The mix proportioning of the cement-based foam or foamed concrete is different from the regular concrete as the former not only depends on a specified strength, but also on the required cast density.

McCormick (1967) proposed a rational proportioning method based on solid volume for a given mix proportion. The design aid of ACI Committee 523 was used to select the cement content and water-cement ratio for a given strength and density. In addition to this ASTM C 796 (2012) provides a method of calculation of foam volume required to make cement slurry of known water–cement ratio and target density. Furthermore, Kearsley et al. (2005) have proposed a set of equations, which are written in terms of the mixture composition, for calculating the foam volume and cement content. These equations take the target cast density, the water-cement ratio, the water–fly ash ratio, the water–sand ratio, the fly ash–cement ratio and the sand–cement ratio as input parameters. The two equations are as follows:

$$\rho_m = x + x\left(\frac{w}{c}\right) + x\left(\frac{a}{c}\right) + x\left(\frac{s}{c}\right) + x\left(\frac{a}{c}\right)\left(\frac{w}{a}\right) + x\left(\frac{s}{c}\right)\left(\frac{w}{s}\right) + RDfVf \qquad \text{Eq 2.1}$$

$$1000 = \frac{x}{RDc} + x\left(\frac{w}{c}\right) + \frac{x\left(\frac{a}{c}\right)}{RDa} + \frac{x\left(\frac{s}{c}\right)}{RDs} + x\left(\frac{a}{c}\right)\left(\frac{w}{a}\right) + x\left(\frac{s}{c}\right)\left(\frac{w}{s}\right) + Vf \qquad \text{Eq 2.2}$$

Where,

ρm = target cast density (kg/m^3)

x = cement content (kg)

w/c = water/cement ratio

a/c = fly ash/cement ratio

RDc = relative density of cement (specific gravity)

RDf = relative density of foam

s/c = sand/cement ratio

w/a = water/ash ratio

w/s = water/sand ratio

Vf = volume of foam (l)

RDa = relative density of fly ash

RDs = relative density of sand

ACI 523.3R (2014) explains a design procedure for the cellular concrete. In this method a target cast density of foamed concrete and water-binder ratio is to be selected. A slurry mixture is then proportioned using the absolute volume method. This method estimates the volume of air required for a unit volume of cellular concrete by calculating the sum of the absolute volume of the cement, water and aggregates. The foam volume can easily be estimated by taking the foam-air ratio as 1.05 to 1.07 which gives the value of air volume required.

2.5 Properties of Cement-Based Foam

The cement-based properties can be divided into two parts; fresh and hardened properties. The flow characteristics are the part of fresh property whereas, the hardened properties are classified into physical, mechanical, durability properties and functional characteristics (thermal conductivity, acoustical properties and fire resistance).

2.5.1 Fresh State Properties

Researchers (Nambiar et al. 2008, Ramamurthy et al. 2009) have reported that the two important fresh properties to be considered in any cement-based foam are its flowability and self-compatibility. Normally these two properties are evaluated in terms of consistency and stability of foam concrete, which are in turn influenced by the water/binder ratio, foam content and other constituents like pozzolanic admixture.

Nambiar et al. 2008 conducted marsh cone and flow cone tests for the measurement of “spreadability” and “flowability” of foam concrete. They have reported the influence of water/binder ratio, the foam content itself and the addition of admixture on these parameters. The mixes considered

by them were prepared by replacing sand with 20 to 100% fly ash and using foam volume content from 10 to 50%. The author concluded that the stability and the consistency of the foam concrete was influenced by the water content and amount of the foam added along with other mix constituents. Based on the study Nambiar et al. (2008) has proposed an equation to predict the spreadability of foam concretes as follows:

$$S_F = -266.1 - 0.615(F_A) + 1010(w/s) + 2.775(F_V) - 1.546(F_A)(w/s) + 0.014(F_A)(F_V) - 11.56(w/s)(F_V) \quad \text{Eq 2.3}$$

where,

S_F = spread flow (%)

F_V = foam volume (%)

F_A = fly ash replacement (%)

w/s = water/solids ratio

The water-binder ratio is an important factor which significantly influences the consistency and stability of the foam concrete, a typical range of water-binder ratio given by past researcher (Bindiganavile et al. 2008, Ramamurthy et al. 2009) is between 0.4–1.25. Kearsley (1999) and Jones et al. (2005a) observed that at lower water content the mix become too stiff and the cement paste extracts water from the foam bubbles causing the bubbles to break. Whereas, higher water content makes the mix too thin to hold the bubbles leading to separation of bubbles from the mix and thus segregates.

Ramamurthy et al. (2009) reviewed the past studies and have reported that in the presence of coarse fly ash in foam concrete makes the spread 2.5 times higher as compared with cement-sand mix without fly ash. This difference is attributed to the difference in particle shape and size of the fine aggregate. It was also found that large foam content was required in the

presence of fly ash to achieve the design plastic density, which was attributed to the high fluid consistency in the base mix and high residual carbon in the ash. Agulló et al. (1999) tested the fluidity of the cement paste mix with 5%, 10% and 15% silica fume by using the Marsh cone method. It was reported that the superplasticizer dosage required increases with low water/cement ratio and with a higher silica fume content. It was also reported, that the addition of other mineral admixtures, such as micronized diatomites which has higher water demand requires more dosages of superplasticizer as compared with silica fume.

Studies have reported that the ratio between the measured cast density/ target density should be nearly one to achieve a consistency at which the base mix of foam concrete is stable (Kearsley et al. 2005, Jones et al. 2005a Ramamurthy et al. 2009). When this value shifts higher or lower than unity, then it implies that either the mix was too stiff or segregation is ensured. Ramamurthy et al. (2009) have further added that the stability of the mix can also be assessed by comparing the calculated and measured quantity of foam, required to achieve a plastic density within 50 kg/m^3 of the target density. In addition to this another approach is to check the calculated and measured water/cement ratio.

2.5.2 Thermal Conductivity of Cement-Based Foam

Recently, Awang et al. (2012) investigated the thermal conductivity of light weight foamed concrete for the density range of 600-1400 kg/m^3. The measured conductivity values were in the range of 0.19-0.59 w/m/k respectively. The samples were oven dried before the testing and Transient Plane Source (TPS) method was used for evaluating the thermal conductivity. The water/cement ratio used was 0.45 and the cement/sand ratio was 1:1.5 respectively. Furthermore, the author also observed the thermal conductivity in the range of 0.17-0.58 w/m/k for the mixes with

15% fly ash and 0.16-0.61 w/m/k for 30% fly mixes respectively for the same cast density range. In case of foam concrete, Jones et al. (2005a) have carried out studies on specimens and reported the thermal conductivity between 0.1 and 0.7 w/m/k for 600–1600 kg/m^3 dry densities. However, for dry densities of 1000 and 1200 kg/m^3 the thermal conductivity reported was between 0.23 and 0.42 w/m/k respectively. Cheung et al. (2012) measured the thermal conductivity of foamed concrete for the density range of 1800-1200 kg/m^3 and reported the values between 0.68-0.32 w/m/k. When the same mixes were replaced by 7% silica fume then the reduction in the conductivity recorded was from 0.55 to 0.29 w/m/k.

Fang et al. (2011) proposed an equation for calculating the thermal conductivity of foamed concrete with water/binder ratio of 0.35 and with the substitution of 20% fly ash and 20% steel slag. The relationship between thermal conductivity and bulk density is expressed in equation 2.4.

$$\lambda = 0.07985 + 0.1457d \quad \text{(w/m/k)} \qquad \text{Eq 2.4}$$

where, λ is the thermal conductivity and d is the bulk density. This equation can predict the thermal conductivity when the bulk density is known and cannot be used when fly ash and steel slag have different substitution ratios. The reliability of this equation is a question mark as the author did not address it.

2.5.3 Factors Influencing the Thermal Conductivity

Besides the foregoing studies, Kim et al. (2003) lists that the conductivity is influenced to different degree by moisture content, (water/binder) ratio, types of admixtures, aggregate volume fraction and temperature. The age of concrete however, did not have much affect after the early age i.e. 28th day.

Khan (2002) investigated the influence of moisture content on the thermal conductivity of mortar and concrete. The specimens were prepared with cement, fine aggregates and coarse aggregates in the ratio of 1:2.33:4.66 with 0.60 water/cement ratio. It was observed that the presence of moisture content increases the thermal conductivity of mortar and concrete. The difference of 38% and 50% was reported between the dry and saturated state of mortar and concrete samples.

Recently, Liu et al. (2011) reported the effect of moisture content on the thermal conductivity of mortar containing expanded perlite aggregates. The author reported that the mortar samples with 75 and 100% replacement of expanded perlite aggregate exhibit 60 and 80% reduction in thermal conductivity when oven dried. Jones et al. (2005a), Jones et al. (2005b), Aldridge (2005) and Awang et al. (2012) have found a linear relationship between conductivity and cast density for specimens of densities varying from 450-1500 kg/m^3.

2.6 Measurement Techniques for Thermal Properties

The measurement of thermal conductivity is based on two regimes namely, the steady state and the non-steady method or transient methods. The guarded hot plate (ASTM C1043 2010) and radial heat flow methods (ASTM D6574 2013) are well established steady state evaluation methods and are best suited for homogenous systems. However, the processing time of these methods is too long (He 2005) and in most cases they require large sample sizes. Moreover, the laser flash method, hot wire, transient hot strip method and the transient plane source method are all examples of the non-steady state (He 2005). However, laser flash method only calculates the thermal diffusivity and in order to obtain the thermal conductivity, it is

necessary to evaluate the heat capacity of the sample from separate measurements. Although this method is quite fast in recording the measurement but the sample preparation requires significant time and efforts (precise dimension, soldering). In addition, hot wire methods measures the thermal conductivity only whereas, transient methods evaluates both the thermal conductivity and the thermal diffusivity. Scott et al. (1986) have reported that transient heat source tests are best for heterogeneous systems especially those containing moisture.

The hot disk technique ISO/DIS 22007-2.2(2008), which is a transient plane source technique was described by Gustafsson (1991) and later discussed and analysed in detail by He (2005). Recently, this technique has gained popularity as a tool for measuring the thermal conductivity of a wide range of materials, including materials with low electrical conductivity (such as fused quartz), building materials (e.g. cement and brick powder), stainless steel, copper powder, anisotropic solids (crystalline quartz) and thin metallic materials (He 2005). The TPS device can rapidly measure the thermal conductivity at a range of 0.01 to 400 w/m/k with accuracy better than 5%, and reproducibility better than 1%, the measuring time can be adjusted from 20 s to 520 s. This device not only measures the thermal conductivity but also evaluates the thermal diffusivity and specific heat at the same time.

Bentz et al. (2011) investigated the thermal properties of high volume fly ash mortars and concrete by using a transient plane source method. The author replaced cement with 50% of fly ash or more. Their findings show a dependence of conductivity on the density-at-test and more importantly on the source of aggregates whether it is siliceous or calcareous. The TPS method is reported to be reliable for cases of cement mixes containing high percent of fly ash at room temperature.

Similarly, Awang et al. (2012) observed the thermal conductivity values for lightweight foamed concrete (LFC) by using transient plane source method. The lightweight foamed concrete specimens were casted at the density of 600 to 1800 kg/m^3 respectively and cement was replaced by fly ash in the ratio of 15% and 30%. Their findings also report accuracy in TPS measurements.

2.7 Microstructure of Cement-Based Foam

2.7.1 Air-Void Characterization

Past researchers have reported that the pore system in cement-based material can be classified as micropores, mesopores and macropores. In foam concrete/ cement-based foam macropores are deliberately produced by adding foam in to the mix whereas other pores i.e. gel pores, capillary pores is the result of hydration process.

Nambiar et al. (2007) characterised the air-void structure of foam concrete by identifying air-void parameters like void size distribution, shape factor, spacing factor and then studying their influence on density and strength. The foam concrete mixes used for the study include cement/sand and cement/fly ash mixes with a filler/cement ratio of 2 and foam volume in the range of 10% - 50% which results in cast density of 550-1200 kg/m^3. The dimensions of the specimens for image analysis were 50 × 50 × 25 mm. The images were captured with the help of optical microscope connected with the computer. Later image analysis software was used to identify and quantify the air-void parameters i.e. air-void size distribution, shape factor and spacing factor for each mix. The effect of air-void distribution on density and strength of this study for two mixes is summarized in Figure 2.1 and 2.2 below. Nambiar et al. (2007) concludes that mixes with a narrower

range of air-void size distribution showed higher strength. Whereas, at lower density which mean higher foam content, larger size of voids and wider distribution of voids were formed resulting in reduced strength. In comparison, cement-fly ash mixes showed higher strength at lower density which is likely due to more uniform distribution of air-voids than with only fine sand. Further, the author summarized that the shape factor of the voids itself have no influence on the properties of foam concrete.

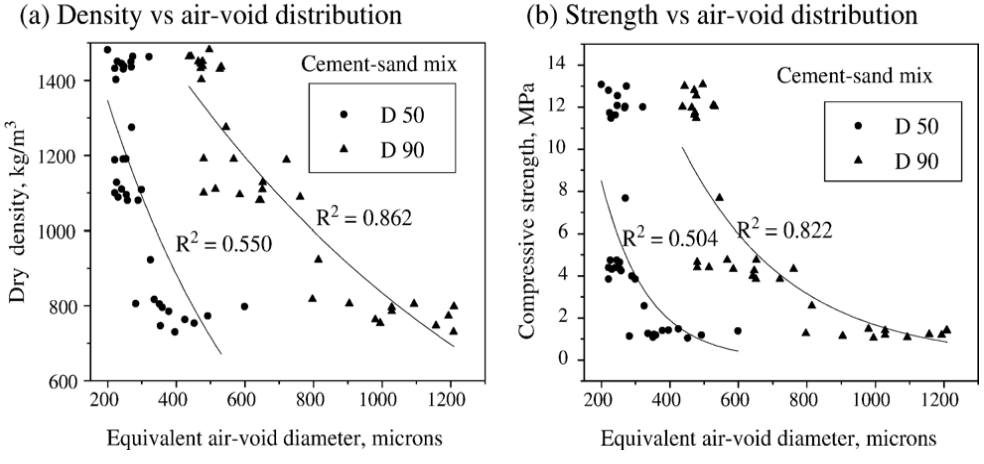

Figure 2.1: Relationship of Density and Strength with air-void size distribution parameters for cement/sand mix (Nambiar et al. 2007).

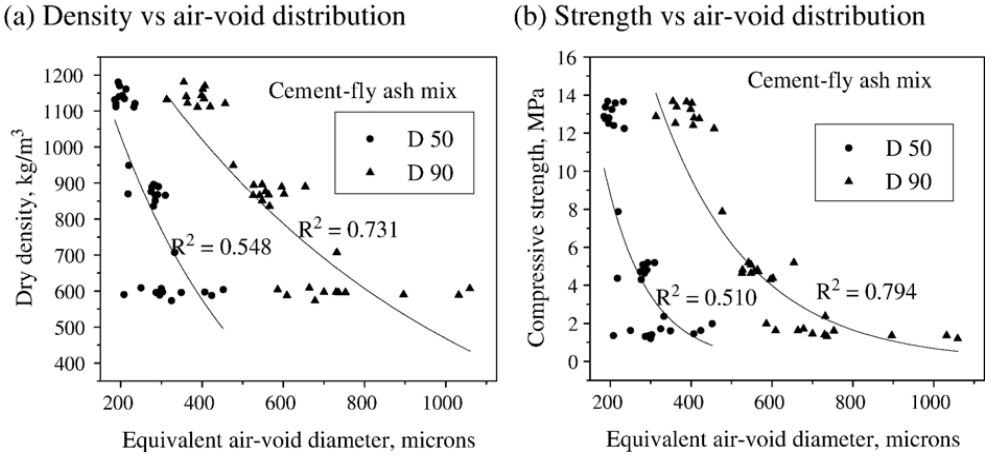

Figure 2.2: Relationship of Density and Strength with air-void size distribution parameters for cement/Fly ash mix (Nambiar et al. 2007).

Wee et al. (2006) investigated the air-void parameters and their effect on mechanical properties of cement-based foam. The mix was prepared with 50% of normal Portland cement and 50% of Ground Granulated Blast Furnace Slag (GGBFS) by weight, with 0.3 water/cement ratio. For the cast density of 600 to 1900 kg/m^3 the compressive strength obtained was in the range of 2 to 58 MPa. The Linear Traverse Method (ASTM C457) was used to determine air-void parameters like air-void size and spacing factor. The author found that the spacing factor influences the compressive strength of the cement-based foam and also have inverse relationship with the density as illustrated in Figure 2.3. In addition to this, it was also reported that optimal values for spacing factor, air-void size, and air content was 0.04 mm, 0.12 mm and 42%, respectively at which high strength-to-weight ratio can be achieved. It was also noticed that same mix with different air content significantly influences the mechanical properties of cement-based foam.

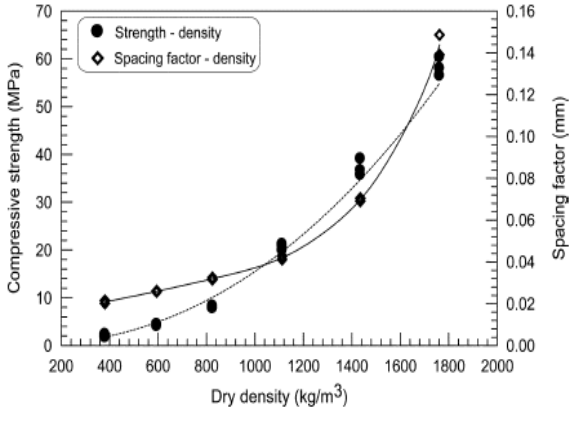

Figure 2.3: Relationship between dry density, compressive strength and spacing factor (Wee et al. 2006).

Kearsley (1999) and Kearsley et al. (1999) investigated the air-void parameters namely, void size distribution and void spacing of the foamed concrete. The mixes were prepared at cast densities of 1000, 1250 and 1500 kg/m^3 with 50%, 66.7% and 75% fly ash replacement of cement. Optical microscope was used for recording the images and the magnification was

such that voids with diameters in excess of 20 μm could be easily identified. Each photograph that was taken represented an area 1954 μm wide and 1872 μm high. Kearsley (1999) summarizes that with drop in the density there was a concomitant increase in the air-void diameter. This in turn led to a drop in the spacing between the voids. Further it is also mentioned that the ash type or content does not appear to have a significant effect on the entrained air-void size and distribution. It was also reported that the porosity is largely dependent on the density not on ash type or content.

2.7.2 Methods for Characterizing Air-Void Network

Aligizaki (2005) and Nambiar et al. (2007) reviewed the measurement techniques for the pore structure of cement-based material and have reported that the pore structures can be ascertained by indirect methods such as mercury porosimetry, gas adorption, thermoporometry, displacement methods and small-angle scattering. In these methods an external stimulus is applied to the material and the response is recorded. The pore parameters are evaluated indirectly from other properties like adsorptive, density etc. Researchers have also investigated the direct methods using image analysis techniques which capture the physical images of the pore structures and the software evaluates the parameters. Optical microscopy, scanning electron and latest one is X-ray computed tomography all are listed in this category. Among the foregoing techniques, the X-ray tomography and SEM seem to be popular among many researchers (Bentz et al. 2000, Shen et al. 2004, Lu et al. 2006, Cnudde et al. 2009, Hoseini 2013) for the characterization of microstructure of cement-based material and for other engineering materials. XRT is a completely non-destructive method in as much as the sample remains intact even after the test. However, in other techniques such as Scanning Electron Microscopy (SEM) and optical microscopy most of the sample information

is lost or altered in the process of sample preparation. Moreover, in XRT one can capture 3D images from the whole specimen while other methods can only provide two-dimensional information of the surface of a very small part or just one section at a time. However, this technique has certain specimen size limits due to the need for high-flux X-ray sources of narrow energy distribution which increases with larger specimen. Nevertheless, it was concluded by the past researchers Martz et al. (1993), Bentz et al. (2000), Masad (2002), Maire (2003), Chotard et al. (2003), Helfen et al. (2004), Rattanasak et al. (2005), Gallucci et al. (2007), Zhang et al. (2010) and Hoseini (2013) that XRT method is able to identify different phases in the cementitious material. In addition to this the image analysis also quantifies the various required microstructural parameters like air-void size, spacing of void, shape factor etc.

2.7.3 Hydrated Cement Paste

Many studies (Kosmatka et al. 2003, Korpa et al. 2009, Scrivener et al. 2011, Bapat 2013, Thomas 2013) on the hydration process with and without pozzolanic admixture have been carried out. The researches have concluded that during the hydration process multiple phases of cements and their corresponding hydration products are formed. These phases are mostly influenced by the hydration age and the type of pozzolanic admixture. Importantly, the accurate knowledge about the phase composition at a given time of hydration and in the presence of admixture is needed for the elucidation of complex hydration processes and their associated mechanisms and products. Demirboğa (2003) investigated the affect of silica fume (SF), class C fly ash (FA) and blast furnace slag (BFS) on the thermal conductivity of cement paste with natural sand content. SF, FA and BFS were added as replacement for cement by decreasing the cement in the ratios of 10, 20 and 30% by weight. The author observed the thermal conductivity of cement paste value equal to 1.186 w/m/k and also noticed

decrease in the conductivity with the addition of admixture. The reductions noticed due to addition of silica fume were 17, 31 and 40% for 10, 20 and 30% SF (replacement for cement), respectively. However, when fly ash was the part of the mix the drop of 14, 26 and 33% for 10, 20 and 30% fly ash was recorded. Moreover, BFS effect on the thermal conductivity was approximately the same at all percent and the reduction reported was between 12 and 14% respectively.

With regards to plain concrete including lightweight concrete, Demirboğa et al. (2003) and Demirboğa (2007) have studied in detail the conductivity characteristics with silica fume, slag and fly ash present in the mixes. Similarly Raheem et al. (2011) and Bentz et al. (2011) investigated the conductivity of plain concrete and light weight with the addition of fly ash, silica fume and blast furnace slag in different ratio. Figure 2.4 and 2.5 shows the effect of these pozzolanic admixtures with the thermal conductivity as reported by the aforementioned authors. It is seen that the conductivity drops with an increases in the percentage of admixture substituted.

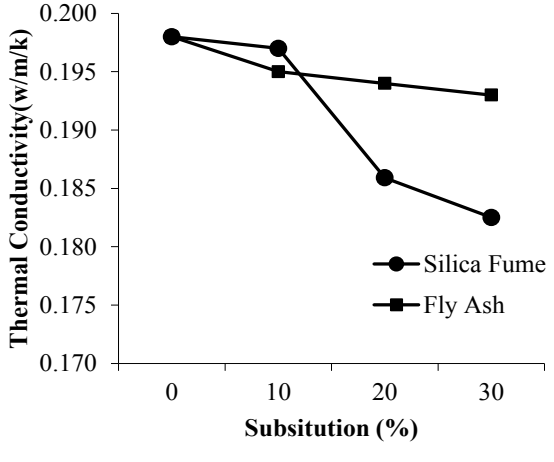

Figure 2.4: Relationship of admixture with thermal conductivity (Demirboğa et al. 2003).

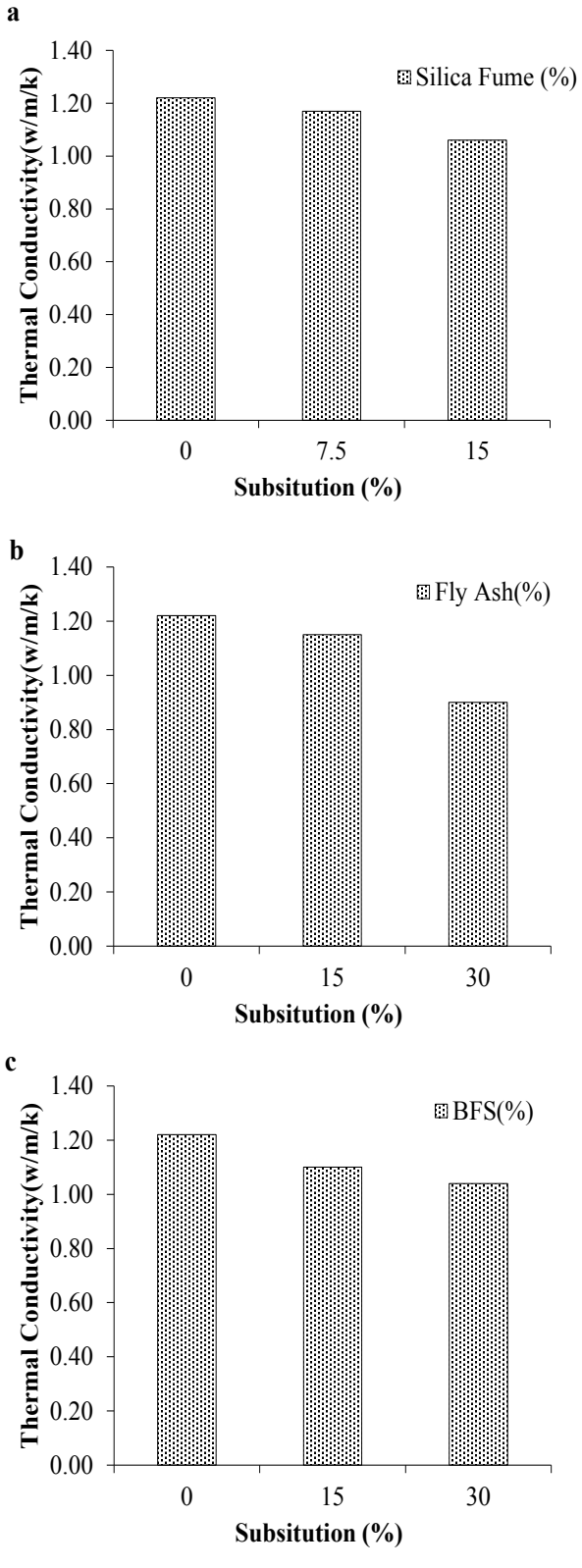

Figure 2.5: Relationship of admixture with thermal conductivity; a) Silica Fume; b) Fly Ash; c) Blast Furnace Slag (Demirboğa 2007).

2.7.4 Methods for Quantifying the Hydrated Cement Paste

Several authors (Odler et al. 1983, Ramachandran et al. 2002, Roszczynialski et al. 2002, Vedalakshmi et al. 2003, Korpa et al. 2009, Chancey et al. 2010, Ou et al. 2011, Esteves 2011, Deschner et al. 2012 and Dittrich et al. 2014) have used Fourier Transform Infrared Spectroscopy (FT-IR), thermal analysis, thermogravimetric analysis (TGA), scanning electron microscopy (SEM), energy dispersive X-ray spectroscopy (EDX) and X-ray diffraction (XRD) techniques for the investigation of hydration products in cement paste.

The TGA method works efficiently in the case when small phases are present in the system and is used to estimate the quantity of CH (Esteves 2011). On the other hand, SEM technique has less potential for differentiating hydrated phases whereas, EDX techniques is helpful when the identification of the element is required (Esteves 2011).

Hence, X-ray diffraction provides the ideal means to understand structures of minerals and other crystalline matter on an atomic scale. The first X-ray diffraction experiment using single crystals of copper sulfate and zinc was performed by Friedrich et al. (1912). This experiment helped Max von Laue to develop his theory of X-ray diffraction in crystals as in a three-dimensional diffraction grating. At the same time W. L. Bragg and W. H. Bragg performed their diffraction experiments to confirm Barlow's hypothetic model of rock salt, thus performing the first X-ray diffraction analysis of single crystals (Borisov et al. 2012). The detail of Barlow's hypothetic model can be found in literature Bragg (1975).Since then Laue conditions and the Bragg equation are the basis of X-ray diffraction of crystalline material.

Subsequently, in the last few years the quantitative analysis of cements, clinkers, supplementary cementitious materials and hydrated cementitious systems has been done by Jimeneza et al. (2006), Korpa et al. (2009), Chancey et al. (2010), Rietveld (2010), Aranda et al. (2012), Ibáñez et al. (2013) and Soin et al. (2013) by using Rietveld quantitative X-ray diffraction (RQXRD) methods. Majority of these authors recommended that XRD is a powerful tool and can be easily used for the qualitative analysis of cementitious materials.

The Rietveld remarkable concept: "*To use measured powder pattern intensities instead of reflection (peak) intensities*" gives the breakthrough in the field of powder diffraction analysis (Aranda et al. 2012). The method was first described in 1966 by Hugo M. Rietveld (Rietveld 1967 and Rietveld 1969) to refine crystal structures from powder data measured on neutron diffractometers.

Moreover, Meier (2012) and Aranda et al. (2012) explains that the Rietveld method is based on the fact that the overall scale of a phase is proportional to its content in a phase mixture. Whereas, the intensity relationship between peaks in a diffraction pattern is governed by the crystal structure like atomic positions, occupation factors and atomic displacement parameters for each of the phases present in the mixture. Actually, this method is based on least square approach in which first a model is calculated and then it is optimized until it is best fitted with the measured powder diffraction profile (XRD patterns) (Aranda et al. 2012). The Equation 2.5 given below is used by Rietveld analysis software to perform this optimization.

$$Sy = \sum_i wi|yi(obs) - yi(cal)|^2 \qquad \text{Eq 2.5}$$

Where, *Sy* is the function to be minimized, *wi* is the statistical weight, and *yi* (obs) and *yi*(cal) are the observed and calculated powder diffraction intensities for the i-point of the powder pattern, respectively.

During the review it was found that these studies Rietveld (1969), David et al. (1993), Madsen et al. (2000), Madsen et al. (2001), Madsen et al. (2008), Korpa et al. (2009), Esteves (2011), Meier (2012), Aranda et al. (2012) applied the Rietveld method for the quantitative XRD analysis from powder diffraction data on different material and found satisfactory results.

2.8 Theoretical Models for Porous Material

Thermal conductivity is the material property and is defined as the amount of heat crossing a unit area of the material per unit time per unit temperature gradient. The thermal conductivity of a material is expressed by Fourier's equation as follow

$$q = K\, dt/dz \qquad \text{Eq 2.6}$$

where, K is the thermal conductivity of the system, dt/dz is the temperature gradient and q is the amount of heat passing through unit area per unit time (heat flux). Heat propagates by three modes in the porous material: conduction, radiation and convection. Convection is neglected when the size of pores are small and radiation play important role at high temperature (Arthur 1954).

Heat conduction in porous materials is a complex and complicated phenomenon and is usually described macroscopically by averaging the microscopic heat transfer process over a representative elementary volume (Kaviany 1995). Ochsner et al. (2008) reported that the existing theoretical

models can be classified on the basis of three approaches namely, the Field approach, the Resistor approach and Phase Averaging approach. This classification is illustrated in Figure 2.6. Verma et al. (1991) defined the field approach, in which the path of heat flow is affected by the presence of a dispersed phase and so, the flux lines form concentrated field regions in the vicinity of grains. Whereas, when the heat flux follows a straight path and different phases on the way are considered as thermal resistors obeying Ohm's Law, it is known as the resistor approach. However, if the effective thermal conductivity is obtained as an averaged property of the mixture, the model is based on the phase averaging approach.

Francl et al. (1935), Russell (1935), Bave (1980), Goual et al. (1999), Narayanan et al. (2000) and Ochsner et al. (2008) carried out investigation to evaluate the thermal conductivity of porous materials made up of different material such as sintered metal powders, clayey aerated concrete, bricks, calcium silicate boards etc. These studies reported that the thermal conductivity of a porous material depends on various parameters including thermal properties of constituent phases and the microstructural parameters. Especially, the volume fraction of constituent phases, the geometrical distribution of the phases and the geometry of the pore structure, porosity, moisture content, density and the type of binder used (cement/admixture ratio).

Several researchers, in particular, Maxwell (1904), Wiener (1904), Burgers (1919), Fricke (1924), Frey (1932), Russell (1935), Bruggeman (1935), De varies (1952) and Pande (1984) have developed equation for predicting the thermal conductivity of porous materials considering a uniformly dispersed void network with regular geometry in a continuous medium that may be solid or fluid. These model are limited in applicability and do not cater to a random distribution of void sizes. Another, major draw-back which limit

the applicability is the requirement of porosity and thermal conductivity of solid and air values as an input. These values have to be determined through separate experimental set ups which is time consuming and requires lot of efforts.

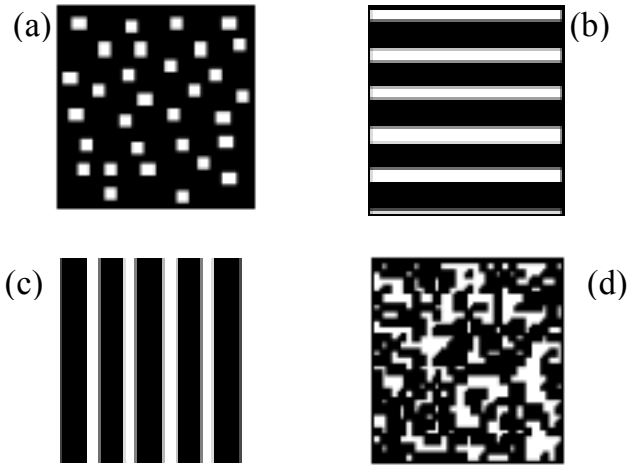

Figure 2.6: Schematic diagram a) Field approach b) Resistor approach: series c) Resistor approach: parallel d) Phase averaging. Note: black part is solid phase and white part dispersed phases (Wang et al. 2008).

Maxwell (1904) used Laplace equation and derived by rigorous analysis a formula for the electrical conductivity of a two-phase medium assuming random size spheres dispersed into a continuous medium, the model is formulated as shown in Equation 2.7

$$K_{maxwell}=k_{solid}\frac{(2ksolid+kpore-2p(ksolid-kpore))}{(2ksolid+kpore+p(ksolid-kpore))} \quad \text{Eq 2.7}$$

This model is based on field approach and can be applied for fully dry and wet conditions. In addition to this, Maxwell's work has been modified for particles having ellipsoidal and cylindrical shape by Burgers (1919), Fricke (1924) and Bruggeman (1935) respectively. Russell (1935) in connection with the thermal conductivity of refractory brick, derived the effective thermal conductivity of a dry porous material from the properties of its component gas and solid for a distribution of uniform pores of cubical

shape arranged in a simple cubic lattice. He assumed parallel heat flow and neglected convection across the pores. When the dispersed phase is a fluid and the solid phase is a continuous one, then Russell expresses the model as Equation 2.8.

$$K_{russell} = k_{solid} \frac{p^{2/3} + v(1-p^{2/3})}{p^{2/3} - p + v(1-p-p^{2/3})} \quad \text{Eq 2.8}$$

The theory of Frey (1932) involves the same variables as that of Russell except that the former assumes a series heat flow and neglects the convection and radiation of heat across the pores. The Frey model is as shown in Equation 2.9. The expressions given by Russell and Frey are based on the resistor approach and both expressions require the value of thermal conductivity of solid and porosity as input parameters, similar to the Maxwell equation.

$$K_{frey} = k_{solid} \frac{(v(1-p^{1/3}+p)+p^{1/3}-p)}{v(1-p^{1/3})+p^{1/3}} \quad \text{Eq 2.9}$$

Wiener (1904) used parallel and series configuration of constituent phases to develop a model based on the resistor approach. In parallel configuration, the plane of phases was set parallel to the direction of heat flow and the effective thermal conductivity was evaluated as the weighted arithmetic mean of the conductivities of the solid phase and void phase. The parallel configuration results in a maximum value for the effective thermal conductivity while offering minimum insulation (Ochsner et al. 2008). In addition to this, the parallel approach also serves as the upper bound (Carson et al. 2005) as expressed in Equation 2.10. However, in the case of series configuration, the constituent phases are in series with the direction of heat flow. The effective thermal conductivity is given by the weighted harmonic mean of the conductivity of the constituent phases as shown in Equation 2.11.This configuration offers the maximum insulation resulting

in a minimum thermal conductivity and thus serves as the lower bound (Carson et al. 2005 and Ochsner et al. 2008).

$$K_{parallel} = (1-p)ksolid + p * kpore \quad \text{Eq 2.10}$$

$$K_{series} = \frac{1}{\frac{1-p}{ksolid} + \frac{p}{kpore}} \quad \text{Eq 2.11}$$

$$K_{brugg} = K_{solid}\left[v + (1-p)(1-v)\left(\frac{kBruggeman}{ksolid}\right)^{\frac{1}{3}}\right] \quad \text{Eq 2.12}$$

$$K_{horai} = \frac{Kseries + kparallel}{2} \quad \text{Eq 2.13}$$

$$K_{EMT} = \frac{1}{4}[(3p-1)kpore + (3(1-p)-1)ksolid + \sqrt{[(3p-1)kpores + (3*(1-p)-1)kpore]^2 + 8kporeksolid}] \quad \text{Eq 2.14}$$

where,

$K_{maxwell}$	Effective thermal conductivity (w/m/k)
$K_{russell}$	Effective thermal conductivity (w/m/k)
K_{frey}	Effective thermal conductivity (w/m/k)
$K_{parallel}$	Effective thermal conductivity (w/m/k)
K_{series}	Effective thermal conductivity (w/m/k)
$K_{bruggeman}$	Effective thermal conductivity (w/m/k)
K_{Horai}	Effective thermal conductivity (w/m/k)
K_{EMT}	Effective thermal conductivity (w/m/k)
k_{solid}	Thermal conductivity of solid material (w/m/k)
k_{pores}	Thermal conductivity of pores in the porous material (w/m/k)
v	k_{pores}/k_{solid} (w/m/k)/ (w/m/k)
p	porosity

The two-phase porous medium consists of solid and void phase whereas if moisture is considered into the void then it becomes three phase system. Chaudhary et al. (1968) has extended the two-phase empirical relation for evaluating the effective thermal conductivity into three-phases as expressed in Equation 2.15. If moisture is considered into the void then it becomes three-phase system otherwise it is called two-phase system.

$$K=K_w^{\Phi} K_a^{(p-\Phi)} K_s^{(1-p)} \quad \text{Eq 2.15}$$

where, K_w is the conductivity of water , K_a is the conductivity of air containing water, K_s is the conductivity of solid whereas, Φ is the fractional moisture content and p is the porosity. Number of investigation (Khan 2002, Matiasovsky et al. 2005, Matiasovsky 2008, Rahmanian et al. 2009) has been done using these thermal conductivity structural models for calculating the effective thermal conductivity of porous building material like clay brick, plaster, gypsum board, clayey aerated concrete, plain concrete etc. and the researcher find agreement between the experimentally evaluated and those predicted values.

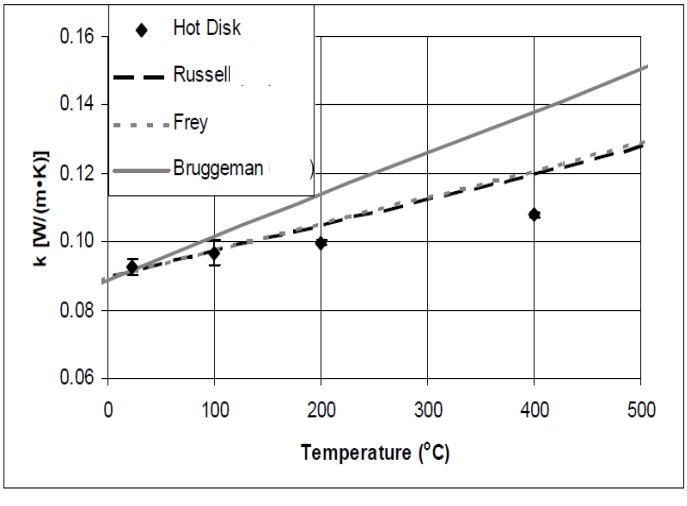

Figure 2.7: Measured and predicted thermal conductivities for fire resistive material (Do et al. 2007).

Recently, Do et al. (2007) investigated thermal conductivity of hydrated calcium silicate boards. During the study, the thermal conductivity values of calcium silicate boards with different densities were evaluated experimentally by TPS. Later was compared with the effective thermal conductivity structural models by Russell, Frey and Bruggeman (Eq 2.12). It can be notice in Figure 2.7 that the theories of Russell and Frey provide

quite similar predications for the thermal conductivity values and that these two theories generally capture the trend observed in the experimental data better than the theory of Bruggeman.

Wyrwal et al. (2008) in his investigation used different theoretical models to predict the thermal conductivity value for different types of concrete (basalt concrete, limestone concrete, sandstone concrete, composite fibre reinforced concrete) samples under wet and dry condition. It was noticed during the comparison that Maxwell and EMT (Eq 2.14) models give close results but in general the analyzed models of effective heat conductivity give different, and sometimes very divergent, results. It has been found that these models can better predict heat conductivity for wet materials than dry one. The only exception is porous brick which is characterized by relatively low heat conductivity of skeleton, which has the influence for lower heat conductivity of dry material. Figure 2.8 summarizes the results for Wyrwal et al. (2008) finding for cement mortar and porous brick samples by using Eq 2.7,Eq 2.10,Eq 2.13 and Eq 2.14 respectively.

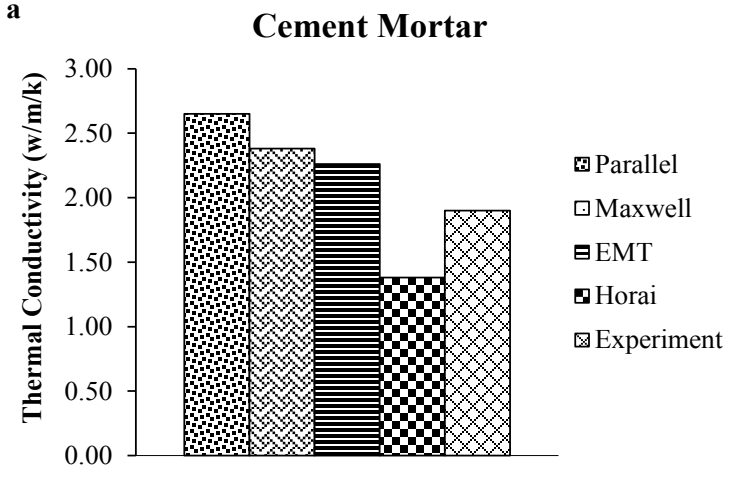

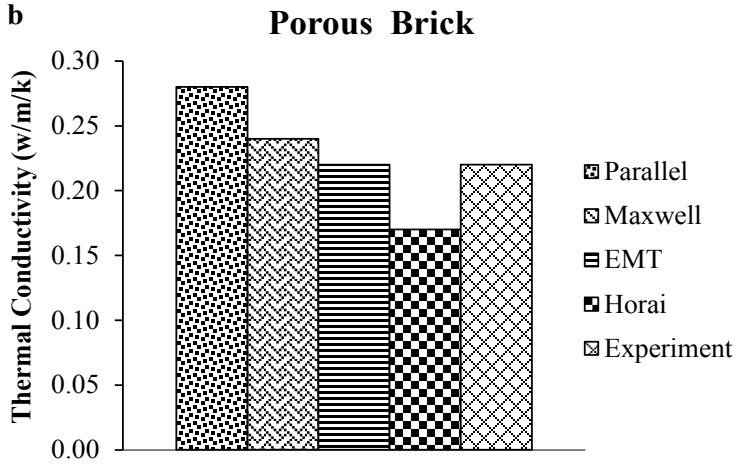

Figure 2.8: Measured and Predicted thermal conductivity of different building materials (Wyrwal 2008).

2.9 Conclusion

The literature review reveals that cement-based foam have the density range of 300-1600 kg/m^3. The lighter densities (≤800 kg/m^3) are especially attractive in insulation while the heavier mixes are used for crash cushions, retaining walls and fillers. But most of the studies deal with the densities ≥800 kg/m^3 whereas, few investigations were carried out for cast densities ≤ 800 kg/m^3. In addition to this most of the authors have used protein type foaming agent and very limited studies are available with synthetic type foaming agent.

Consequently, number of researchers has used fly ash, silica fume and blast furnace slag as a cement replacement material to improve the properties of cement-based foam. However, to author knowledge no investigation has been done so far replacing metakaolin in cement-based foam.

The water binder ratio is the most important factor of cement-based foam which significantly influences the consistency and stability of the base mix. Researchers have observed that at lower water content the mix becomes too stiff causing the bubbles to break. On the other side, high water content makes the mix too thin to hold the bubbles leading to separation of bubbles from the mix. As a result, the target and hardened density is affected. No comprehensive study has been reported so far on fresh state characteristics of the cement-based foam with and without pozzolanic admixture.

Also revealed by this literature review is the fact that while a good number of researchers have dealt with the mechanical and physical properties of but limited work has been done on thermal conductivity of cement-based foam. Similarly no work appears to have been done on studying the effect of microstructure of the phases in cement-based foam on its thermal properties.

Subsequently, researchers have concluded that air-void network significantly influences the mechanical and other properties of cement-based foam. Few studies have characterized the air-void parameters and their influences on the strength and density of cement-based foam but hardly any study investigates the effect of air-void network on the thermal conductivity of cement-based foam. Furthermore, the techniques adopted for the measurement of the air-void network by the past researches were capable of visualizing only two dimensional images of a specimen or of thin slices.

The object structure itself used to get altered by the preparation technique and the distance between the slices used for observation by the past study was usually too coarse to avoid loss of 3-D information whereas in the case of cement-based foam the 3-D information of microstructure is quite important as air-voids are in the form of bubbles.

Furthermore, literature review reveals that addition of admixture reduces the thermal conductivity of the hydrated paste but hardly any study is available which explains the contribution of different hydrated products in increases or decreasing the thermal conductivity.

As far as the available theoretical models for thermal conductivity evaluation are concerned, they are only applicable for well-defined void shapes and for a uniform distribution of voids. These models take the parameters of porosity and thermal conductivity of solid and air as an input, and these quantities vary widely in the context of cement-based foams. So far author knowledge is concern these model has never been used before for predicting the thermal conductivity for cement-based foam.

No, equations are available which can predict the thermal conductivity of cement-based foam for different age of paste and for different substitution of pozzolanic admixture.

3. Experimental Program

3.1 Introduction

This chapter presents the experimental program adopted for this study. Here, therefore, the mix designs, the specimen preparation, the thermal testing set up, the X-ray diffraction set up, the X-ray tomography technique (including image acquisition and analysis methods used in the present study) and other properties are described in detail.

3.2 Materials

A typical cement-based foam mix contained cement, water, foam and pozzolanic admixture. No aggregates were used in the mixes in this study as the focus was on obtaining lightweight mixes without adding more parameters. The detail of the materials is as follow.

3.2.1 Cement

High early age Type HE Portland cement, conforming to CAN/CSA-A3000 (2013) standards or ASTM C150/C150 M (2012) specification, supplied by local manufacture was used in this investigation. Type HE was selected because of its quick strength gaining ability under cold climates. This is the reason it is commonly used in Canada in the production of cement-based foam. The chemical and the physical properties of type HE cement provided by the suppliers are listed in Table 3.1 and 3.2 respectively.

Table 3.1: Physical Properties of HE Type Cement

Property	Value
Retained on #325 sieve (%)	5.27
Blaine fineness (m^2/kg)	406
Specific gravity	3.15
Density kg/m^3	3100
Particle size (μm)	10-15
Colour	grey
Autoclave Expansion (%)	0.055
Sulphate Expansion (%)	0.028
Vicat Initial Set	95
False Set (%)	62
Air Content (%)	8.13

Table 3.2: Typical Chemical Composition of Pozzolanic Admixture and HE Type Cement

Component	**FlyAsh** (Type CI)	**Silica Fume**	**Metakaolin**	**High Early** (Cement)
	Local Manufacturer	Local Manufacturer	Siddique et al. (2011)	Local Manufacturer
	(%)	**(%)**	**(%)**	**(%)**
SiO_2	55.80	98.90	51.52	21.00
Fe_2O_3	3.80	0.07	1.23	4.40
Al_2O_3	23.40	0.13	40.18	4.00
CaO	9.20	0.10	2.00	62.00
MgO	1.20	0.01	0.12	3.34
SO_3	0.20	0.00	0.99	2.08

3.2.2 Foaming Agent

Presently, there is no selection criterion for the foaming agents of foamed concrete. Except that the generated foam must be firm and stable enough to resist the pressure from the mortar until the cement hardens around the air-voids.

In this study the air-void network in the slurry was created with the help of a stable foam, generated using a 3% (by volume) solution of a synthetic foaming agent mixed with water and then aerated to a density of 40 kg/m^3. This foaming agent was supplied by local manufacturer which produces a predominantly closed-cell internal structure confirming to ASTM C869 (2011). Moreover, this synthetic foaming agent was selected because very few studies are done using this type and it is a common practice in Canada to use this agent for the production of foams.

A general description of ingredients in the foaming agent as provided by the supplier is shown in Table 3.3 and 3.4. The measured performance parameters of the synthetic foaming agent are tabulated in Table 3.5. The foaming capacity was calculated by measuring the final volume of foam generated and the volume of the solution before air entrainment through the generator. In addition to this the bleeding rate was evaluated by measuring the quantity of seeping water from foam after an hour filled in a container of known weight.

3.2.3 Pozzolanic Admixture

The pozzolanic admixtures are often used in concrete mixes to improve the mechanical properties and to reduce the cement contents. In this study, these pozzolanic admixtures were used to investigate their effect on the thermal properties. Therefore, three pozzolanic admixtures fly ash, silica fume and metakaolin were selected to be used as a cement replacement material in this research.

The fly ash was supplied from a local coal-fed thermal power plant whereas silica fume and metakaolin were sourced commercially. The representative chemical compositions of these admixtures and cement are tabulated in Table 3.2. Moreover, Figure 3.1 illustrates these admixture and cement in powder form. For metakaolin, this information was taken from a paper by Siddique et al. (2011) who had used a very similar source.

The type CI fly ash, conforming to ASTM C618 (2012a) have a particle size which are generally spherical in nature and typically in size range of 10 to 100 μm. These particles are finer than the ordinary Portland cement particles. ASTM C618 (2012a) limits the maximum amount of fly ash retained on the 45 μm (#325) mesh sieve on wet sieving as 34% and the loss on ignition equals to 6%. It may be noted that Canadian fly ashes were found to have specific gravity in the range of 1.94 and 2.94, whereas American ashes have slightly higher specific gravity ranging between 2.14 and 2.69 (Siddique et al. 2011). The typical physical properties are given in Table 3.6.

Similarly, silica fume conforming to ASTM C1240 (2012) have extremely small particle sizes, being less than 1μm which is two orders of magnitude

smaller compared with cement particle (Siddique et al. 2011). Its typical physical properties are given in Table 3.7. As per ASTM C1240 (2012) the loss on ignition is less than 4% and the maximum amount of silica fume retained on the 45 μm (#325) mesh sieve was as 10%.

Table 3.3: Composition of the Foaming Agent Provided by Local Manufacturer

Ingredient	**Weight (%)**
Fatty Alcohol	1-10
Alcohol	6.5-35
Fatty Acid	10-65

Table 3.4: Physical and Chemical Properties of the Foaming Agent Provided by Local Manufacturer

Appearance	Transparent to opaque amber liquid
Odour	Alcohol odour
Flash Point (C)	92
Boiling Point (C)	117
Specific Gravity	0.94-0.99
pH Value	9-11
Solubility in water	Infinite

Table 3.5: Performance Parameters of Synthetic Foaming Agent

Foaming Performance Values	
Foaming capacity ratio	0.97
Bleeding Rate (kg/h)	5

The metakaolin conforms to ASTM C618 (2012a) Class N pozzolans specification. The average particle size is in the range of 1–10μm again being about one order of magnitude smaller than that of ordinary cement and but larger than silica fume particles (Bapat 2013). Moreover, ASTM C618 (2012a) defines the maximum moisture content in metakaolin (MK) as 3% and loss of ignition as 10% whereas, the maximum amount retained on the 45 μm (#325) mesh sieve on wet sieving was limited to 34%. The typical physical properties of metakaolin are given in Table 3.8.

3.3 Mixture Composition

Since in Canada and USA, lightweight CBF is extensively used for thermal insulation, the mixes in this study were aimed at densities less than 800 kg/m^3. Hence, a series of samples were prepared with three different cast densities, namely 800 kg/m^3, 600 kg/m^3 and 400 kg/m^3, with each of the three different pozzolanic admixtures. In addition to this, a reference mix was made with Portland cement as the sole component of the binder (i.e without any pozzolanic admixture).

Previous investigation by Bapat (2013) reported that the cement-based mixes containing silica fume and metakaolin within 10%-25% replacement range, exhibit improved performance in terms of strength and durability. However, it is noted that without sacrificing much the strength or durability a wider range of replacement of cement by fly ash can be used. In addition to this no data of thermal conductivity is available for 10%-25% cement replacement with any of the above pozzolans in cement-based foam. Therefore, based on these finding from existing literature it was decided to replace the cement (by weight) with fly ash (FA), silica fume (SF) and metakaolin (MK) in the proportion of 10% and 20% respectively.

Table 3.6: Physical Properties of Fly Ash (as given by supplier)

Property	Value
Retained on #325 sieve (%)	20.5%
Blaine fineness (cm^2/g)	1579-5550
Specific gravity(Canadian)	1.94 - 2.94
Moisture content (%)	0.05%
Particle size (μm)	10-100
Colour	Tan to dark grey

Table 3.7: Physical Properties of Silica Fume (as given by supplier)

Property	Value
Density (kg/m^3)	480-720
Surface Area (m^2/g)	18-20
Specific gravity	2.22
Particle size (μm)	≤1
Colour	Dark grey

Table 3.8: Physical Properties of Metakaolin (Bapat 2013)

Property	Value
Bulk Density (ton/m^3)	0.3-0.4
Surface Area (m^2/g)	9.5–18
Specific gravity	2.5-2.6
Particle size (μm)	1-9.5
Colour	Off white

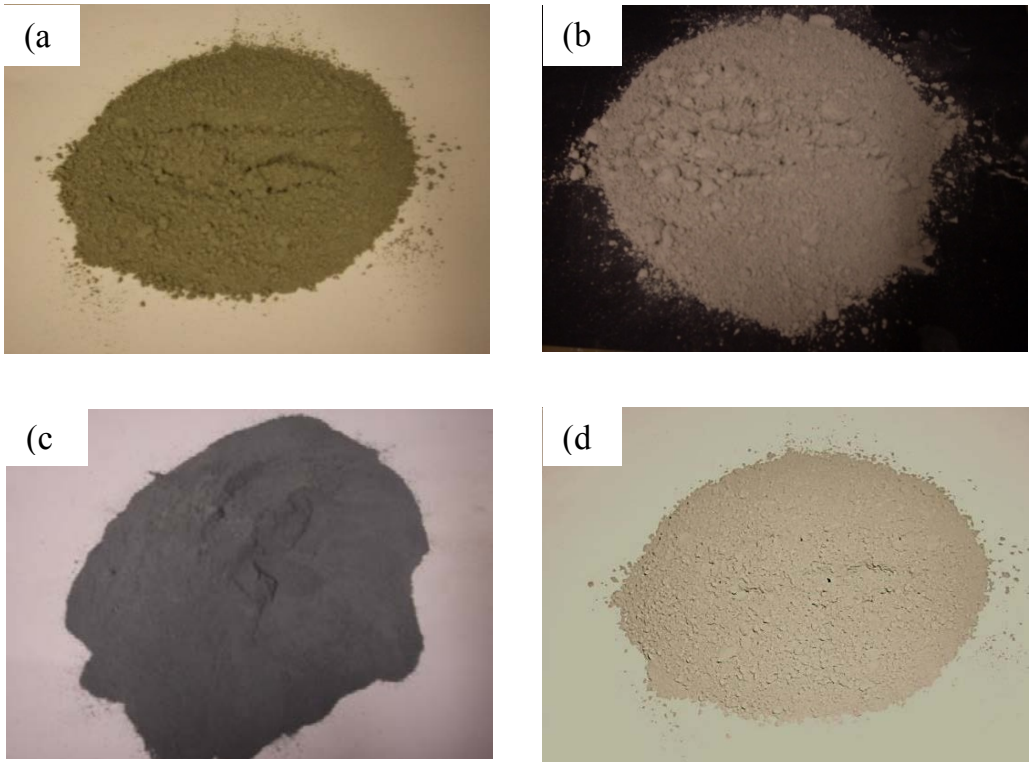

Figure 3.1:Portland cement and pozzolanic admixture powder; a) HE cement; b) Fly Ash; c) Silica Fume; d) Metakaolin.

In the production of every cement-based foams mix, an optimal water/cement ratio is desired. If the w/c is too low, it leads to the instability of the foam and if too high, then it leads to poor strength and durability. Thus, realizing the importance of consistency and the water demand due to the high early strength cement, a number of trials were carried out to select the most appropriate water/cement ratio. This was found to be in the range of 0.70-0.78 to accommodate all the compositional variations in this study. The detailed mix proportion of the seven mixes for each cast density is presented in Table 3.9. The foam volume was evaluated as the percentage of total volume of the mix and the design method is in conformity with ACI 523.3R (2014) standards.

Table 3.9: Mix Proportions of Cement-Based Foam

Mixes	Cast Density kg/m^3	Cement kg/m^3	Water kg/m^3	Pozzolanic Admixture kg/m^3	Foam Volume (%)	Water /Binder Ratio
Reference Mix	800	474	327	0	52	0.69
	600	355	245	0	66	
	400	237	164	0	83	
Fly Ash (FA 10%) (90%Cement+10%FA)	800	430	327	43	51	0.69
	600	323	245	32	66	
	400	215	163	22	83	
Fly Ash (FA 20%) (80%Cement+20%FA)	800	395	327	79	50	0.69
	600	296	245	59	65	
	400	198	164	40	82	
Silica Fume (SF 10%) (90%Cement+10%SF)	800	430	327	43	48	0.69
	600	323	245	33	63	
	400	215	164	22	81	
Silica Fume (SF 20%) (80%Cement+20%SF)	800	395	327	79	44	0.69
	600	296	245	59	61	
	400	198	164	40	79	
Metakaolin (MK 10%) (90%Cement+10%MK)	800	430	327	43	48	0.69
	600	323	245	33	64	
	400	216	164	22	81	
Metakaolin (MK 20%) (80%Cement+20%MK)	800	395	327	79	45	0.69
	600	296	245	60	61	
	400	198	164	40	79	

3.4 Preparation of the Mixes

The preparation of the cement-based foam mixes was in three steps. Firstly, slurry is prepared by adding water, cement and the pozzolanic admixture. In the second step stable foam is generated by using a synthetic foaming agent mixed with water in a separate, in a mini ½ inch open air foam generating system activated by compressed air source at 0.70 MPa pressure. The experimental set-up of foam generator is shown in Figure 3.2. Finally a rotating, inclined drum mixer was used for mixing the cementitious slurry together with the pre-formed foam that was added gradually to the slurry. The mixing was carefully monitored so that foam is perfectly blended into the slurry and also to avoid the loss of internal air-void structure.

Moreover, the density of the composite was checked intermittently and the addition of foam was continued until reaching the desired cast density. Once the desired density was reached, a set of cylinders specimens were cast in plastic molds of size 150 mm in height and 75 mm in diameter. In order to allow easy removal from the molds, 'freezer paper' liners was placed in each mold before casting specimens, with the plastic film side towards the cement-based foam surface. Soon after filling, these cylinders were carefully covered with plastic covers to avoid loss of moisture. After 48 hours these specimens were demoulded and then placed in the curing room for 28 days.

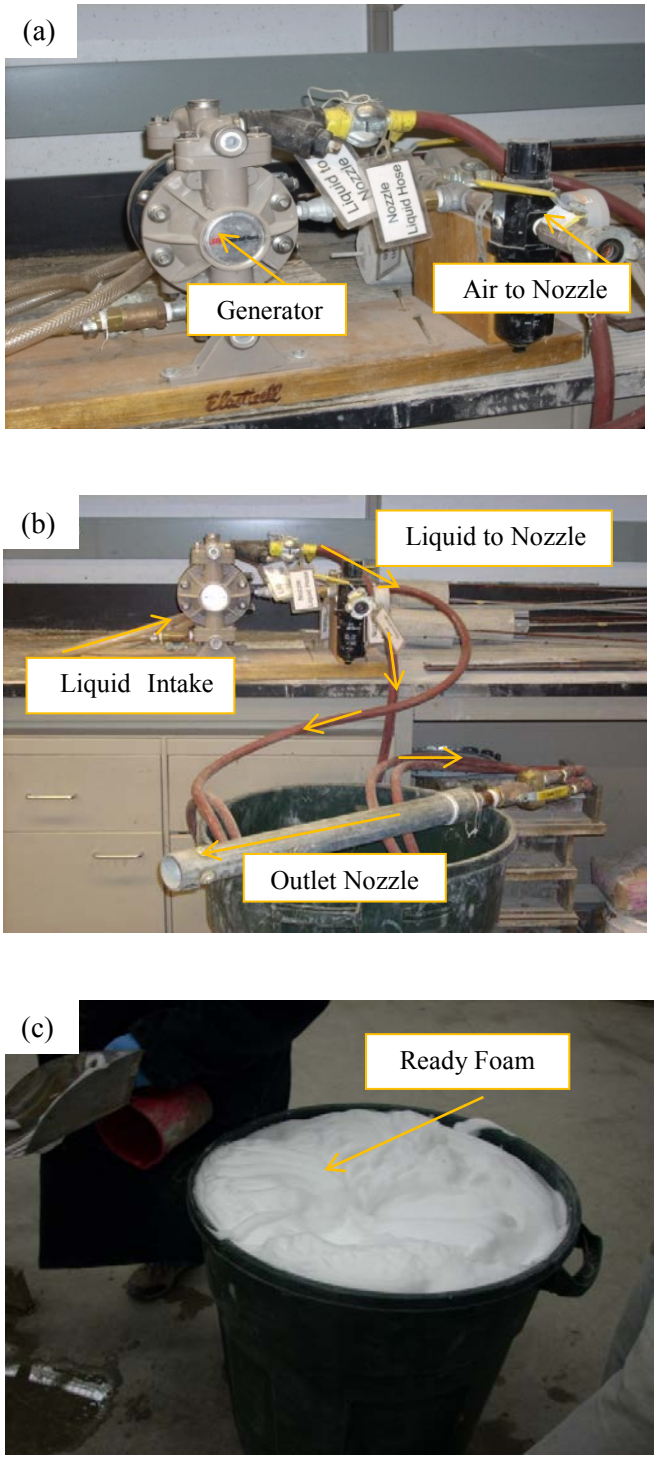

Figure 3.2: Equipment for foam making; a) Foam generating machine; b) Foam generating machine with nozzles; c) Prepared foam ready to use.

3.5 Specimen Preparation

3.5.1 Specimen for Thermal Test

The method adopted for thermal testing was Thermal Plane Source (TPS) method. This method requires a hot disk thermal analyser in which two identical pieces of the sample's disks are used with the thermal sensor to be sandwiched between these disks. Therefore, from the cylinders cast and cured discs of 75 mm diameter and 22 mm thickness were sawn as shown in Figure 3.3. This is the largest size which can easily fit in the dimensional limitations of the hot disk thermal analyser used in this study.

For results comparison purposes, it was decided to prepare specimen before adding the foam in to the slurry. Thus, three pairs of specimens of slurry mix (without any foam added) and six pairs of cement-based foam specimens for each density from the seven mixes including the reference mix were prepared. This resulted respectively in three and six replicates for the thermal tests. Thus, 21 specimens-pairs of slurry mix and 126 pairs of cement-based foam were used in all for studying the thermal parameters as shown in Table 3.10.

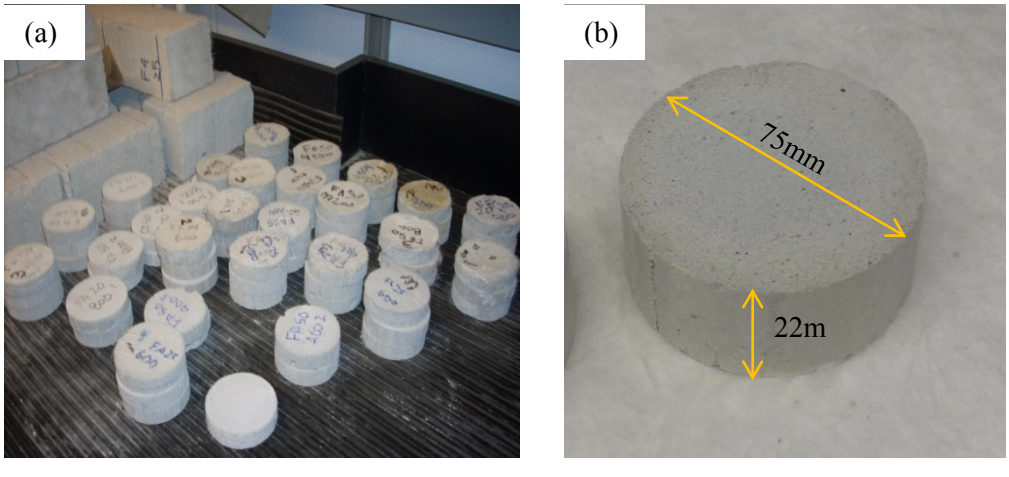

Figure 3.3: Thermal test specimens; a) Discs for seven mixes and for three cast densities; b) Dimension of the specimen.

Table 3.10: Details of Specimens Prepared for Experimental Testing

No. of Specimens							
Mixes	**Cast Density kg/m^3**	**Slurry Mix (without foam)**	**Cement-Based Foam**			**Slurry Mix (without foam)**	**Cement-Based Foam**
		TPS (pairs)		**XRD**	**XRT**	**Moisture Content**	
Reference Mix	800	3	6	1	1	3	3
	600		6		1	3	3
	400		6		1	3	3
Fly Ash (FA) 10%	800	3	6	1	1	3	3
	600		6		1	3	3
	400		6		1	3	3
Fly Ash (FA) 20%	800	3	6	1	1	3	3
	600		6		1	3	3
	400		6		1	3	3
Silica Fume (SF) 10%	800	3	6	1	1	3	3
	600		6		1	3	3
	400		6		1	3	3
Silica Fume (SF) 20%	800	3	6	1	1	3	3
	600		6		1	3	3
	400		6		1	3	3
Metakaolin (MK) 10%	800	3	6	1	1	3	3
	600		6		1	3	3
	400		6		1	3	3
Metakaolin (MK) 20%	800	3	6	1	1	3	3
	600		6		1	3	3
	400		6		1	3	3
Total		21	126	7	21	63	63

3.5.2 Specimen for XRD

X-ray Diffraction (XRD) test requires small amounts of dust type powder. So pieces from the specimens of the seven mixes were finely ground separately to get particle sizes between 25-35μm. This particle size is recommended by the past researchers. On the whole, seven samples, one from the reference mix and one each with the pozzolanic materials were prepared for identifying and characterizing the crystalline phases in the cement-based foams.

Figure 3.4: X-ray powder diffraction specimen.

3.5.3 Specimen for Moisture Content

The samples for moisture evaluation were disks of 75 mm diameter with a thickness of 22 mm as used for thermal evaluation. Samples from the slurry and cement-based foam samples for each density from seven mixes as shown in Table 3.10 were prepared resulting in three replicates for the moisture content test. Thus, a total of 63 samples were examined to determine the moisture content.

3.5.4 Specimen for XRT Scanning

X-ray tomography scanning machine have some limitation on the size of the sample. Therefore, square pieces of size 35 mm x 35 mm with height of 20 mm as shown in Figure 3.5 were cut from the cylindrical specimens of each density for each of the seven series. Thus, total 21 samples were prepared for X-ray tomography scanning and CT images were recorded within the width of 14 mm as shown in the Figure 3.5.

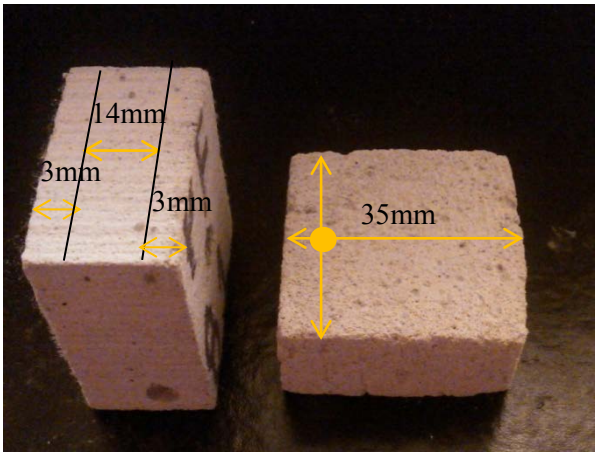

Figure 3.5: X-ray tomography scanning specimens with 14 mm region for CT scanning.

3.6 Testing Conditions

3.6.1 Curing Regimen

All the moulds containing the cast specimens were stored at the temperature 21 ± 2°C for the first 48 hours after casting. Thereafter, the samples were then demoulded and stored in a curing room for water curing and were allowed to remain there under a controlled temperature of 22 ± 2°C and at 95 ± 5% control humidity for 28 days. After 28 days of curing all the samples were removed from the curing room and was left for air drying for about 25 days at the temperature of 21 ± 2°C with average relative humidity of 65 ± 5%.

3.6.2 Temperature

Testing was carried out at 21 ± 2°C temperature and with an average relative humidity of 65 ± 5%.

3.6.3 Samples Ages at Different Tests

The thermal and XRD testing were carried out at four different ages of the specimen namely 60^{th}, 120^{th}, 210^{th} and 300^{th} days. However, the XRT tests were done at age of 300^{th} day. This age was chosen to eliminate any inherent moisture that could influence the tomographic readings.

3.7 Test Set Up

3.7.1 Thermal Conductivity Test

The Transient Plane Source (TPS) which is a non-steady state method, conforming to ISO/DIS 22007-2.2(2008) was used here to measure the thermal conductivity of specimen. All the measurements were carried out at room temperature and on air dried samples. This method is based on the use of a transiently heated plane sensor in its most common adaptation referred to as the Hot Disk Thermal Constants Analyser. This Hot Disk sensor acts both as a heat source for increasing the temperature of the sample and as a "resistance thermometer" for recording the time dependent temperature increase. The transient plane heat source technique was described by Gustafsson (1991) and later discussed and analysed in detail by He (2005). Figure 3.6a shows the experimental set up for the transient plane source (thermal conductivity).The Hot Disk thermal constant analyser is connected with a sensor cable and on other side is attached with the computer which has the operating software in it. The Hot Disk thermal constant analyser consists of designed Wheatstone bridge and Keithley 2400 source meter,

which ensures a constant supply of voltage across the bridge. As shown in Figure 3.6b and 3.6c the Hot Disk sensor which is made of double spiral nickel encased in insulating layers of Kapton has to be placed between the two smooth surfaces of adjacent disc specimens. Moreover, the specimens can be locked into place with the help of a hand-tightened screw and the disks were covered with the help of insulating container as shown in Figure 3.6d.

The transient plane source testing is operated by Hot Disk analysis software. This software requires input of two experimental parameters for the transient recording, for instance "output of power" which is total output power from the sensor during the reading and "measuring time" which is time for the transient recording. After doing number of trails, the parameters tabulated in Table 3.11 were selected for the testing in this study. Upon clicking the "Run experiment" button the Hot Disk starts heating the samples and at the same time record 200 data points of the temperature increases of the sensor.

Table 3.11: Measurement Parameters for TPS Testing

Measuring Time	160 sec
Output Power	0.09 watts
Calculation Range	40-180 points
Radius of Sensor	6.403 mm
Analysis	Fine-Tuned Analysis
TCR* (Room temp)	0.00470(1/K)

***** Temperature Coefficient of Resistivity

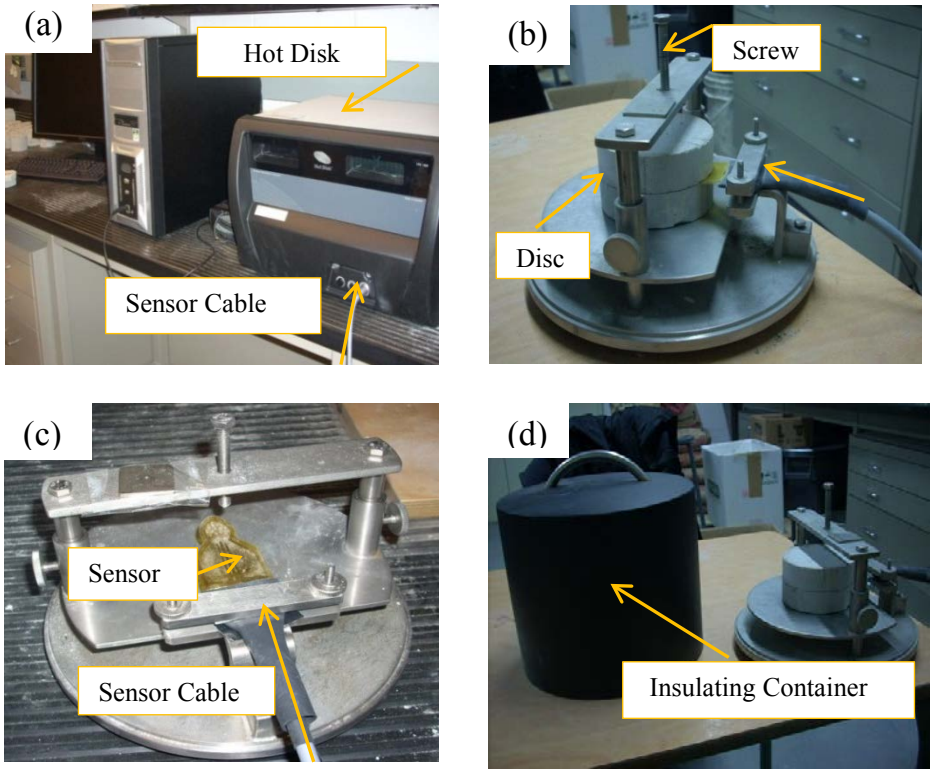

Figure 3.6: a) Thermal Plane Source Analyser; b) Disc placed in the strand; c) Sensor; d) Insulating container.

These 200 data points are the maximum points recorded and are irrespective of the selected total time of the transient recording. A constant voltage is supplied by a Keithley 2000 source meter across the Wheatstone Bridge. The Bridge automatically balanced itself before the final reading and as the resistance of the sensor increased, the bridge became increasingly unbalanced. Afterwards, unbalanced voltage is recorded by the Keithley 2000 digital voltmeter, which is equipped with a multiplexing card (Manual TPS 2010).

The accompanying software analyses these voltage readings to yield the thermal properties. The temperature against time graph shown in Figure 3.7 is displayed by the software when the transient recording is completed. This graph indicates the temperature increase of the sensor during the measuring

time. Usually the processing of data is terminated if the graph does not increase smoothly over the period of time for the selected analysis.

After this step, the calculation of thermal properties was carried out by selecting the suitable data point in the range of 0 to 200. As mentioned earlier, in each experiment, 200 data point are collected during the prescribed measuring time.

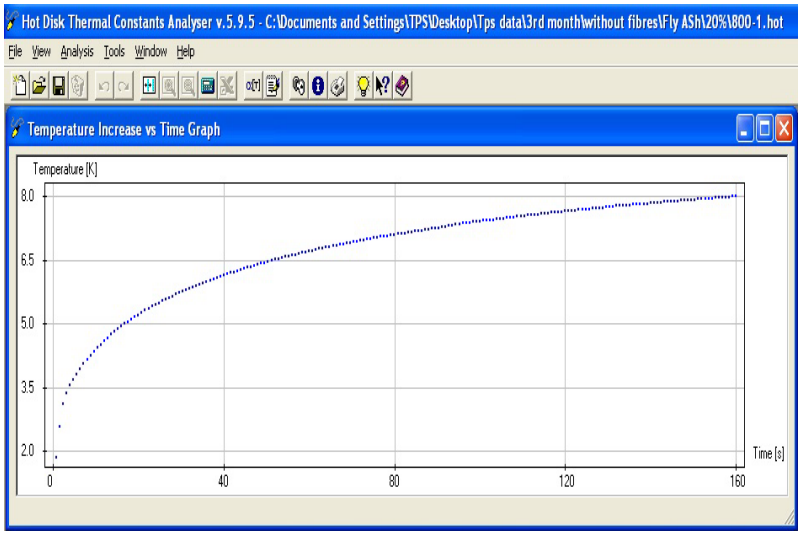

Figure 3.7: Relationship between the temperature increases and time.

These points are usually selected on the basis of graph displayed in Figure 3.7 or trials are done for most appropriate selection. For this study the range of 40-180 points was selected after number of trails. The initial reading points were eliminated to minimize the effect of heat capacity of the sensor whereas the end points might get affected by the limited size of the samples.

When the calculation for the thermal properties is completed with the fine-tuned analysis, the temperature increase verses $F(\tau)$ (dimensionless time function) window (Figure 3.8a) and the difference temperature versus sqrt (time) window appear automatically on the computer as illustrated in Figure

3.8b. The temperature against $F(\tau)$ graph gives an inclined straight line and from the slope of this line the thermal conductivity is calculated. The random scatter of the data points around this straight line is displayed in the difference temperature against sqrt (time) graph as shown in Figure 3.8a. As per requirement if the scatter is not random a new set of data points should be selected and the calculation process should be repeated.

The experimental results window as shown in Figure 3.8c gives the measured values of thermal conductivity, thermal diffusivity and specific heat per unit volume respectively. Moreover, it also reflects the measured indicators for the data analysis such as probing depth which is a distance from any part of the sensor to the nearest outside boundary of the sample and another important one is total to characteristic time which is a ratio that gives the total time of the analysis divided by the characteristic time ratio. And characteristic time ratio can be defined as the square of the radius of the Hot Disk sensor divided by the thermal diffusivity.

Theoretically, the Hot Disk analyzer measures thermal properties by optimizing the relationship between the rise in average temperature and a dimensionless parameter associated with thermal diffusivity. Details of the derivation of this relationship can be found in literature He (2005). The rise in average temperature surrounding the sensor surface is measured by monitoring the electrical resistance of the senor and that can be calculated by employing the Equation 3.1 (He 2005). The average temperature rise can be evaluated as a function of time.

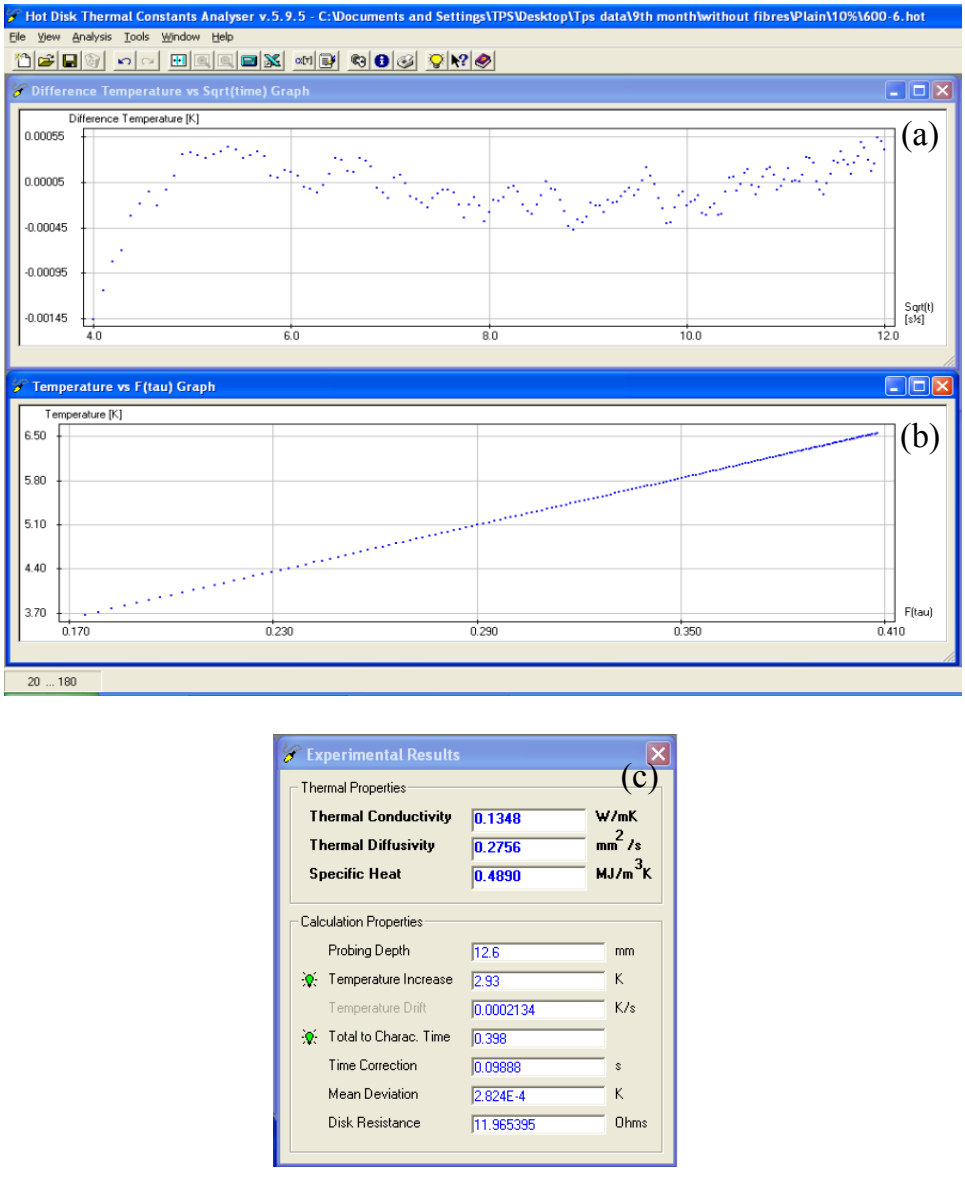

Figure 3.8: a) Relationship between difference temperature and Sqrt (time); b) Relationship between the temperature increases and $F(\tau)$;c) Experimental results window.

$$R(t) = R_0[1 + \alpha \Delta T(t)] \quad \text{Eq 3.1}$$

Here, R(t) is the total resistance (Ohm) at time t, R_0 is the initial resistance (Ohm), α is the temperature coefficient resistivity (TCR) this value is related to the material of the sensor and ΔT (t) is the average rise in temperature as a function of time (t). Furthermore, this equation can easily estimate the value of ΔT as the function of time. The average temperature increase in the sensor surface as the function of τ can be expressed as shown in Equation 3.2 (He 2005). The term $\frac{P_o}{\pi^{3/2} aK}$ (He 2005) is the slope of the line from which the thermal conductivity can be evaluated. Where, P_o is the total output power (watt), a is the radius of the spiral, K is the thermal conductivity, and $F(\tau)$ is a dimensionless time dependent function of τ.

$$\Delta T(\tau) = \frac{P_o}{\pi^{3/2} aK} F(\tau) \quad \text{Eq 3.2}$$

$$\tau = \sqrt{\kappa t}/a \quad \text{Eq 3.3}$$

Hence τ is a dimensionless parameter called the characteristic time ratio and can be calculated by using Equation 3.3 (He 2005) if κ (thermal diffusivity) is known. If it is unknown then by taking a range of κ values, a series of ΔT (t) versus $F(\tau)$ plots can be obtained. Upon optimization, the plot associated with the correct value of κ will yield a straight line and as the slope is known the thermal conductivity can be calculated.

3.7.2 X-Ray Diffraction Test

The X-ray diffraction principle is based on the interaction between electromagnetic radiation and electron of the material. Briefly, the principle is as follows: When the electromagnetic X-rays wave strikes the objects with a certain frequency they are scattered by the electrons of the object in the direction of the polarization of the incident light. The electrons in turn create secondary waves of the same frequency and the wavelength like primary waves (Dinnebier et al.1999). These waves superimpose and form constructive interactions in particular directions giving rise to the different diffraction phenomena. X-ray diffractions are stable and strong if the interacted material shows a periodicity in the distribution of electrons comparable to the X-ray wavelength (λ). The wavelength of X-rays, ranging from 0.1 to 100 Å (equivalent to energies of about 120 to 0.1 keV) is in the range of interatomic distances or unit cell sizes (Lavina et al. 2014). A mathematical method for computing diffraction direction is explained by Bragg's equation as follows

$$n.\lambda=2.d.\sin\Theta \qquad \text{Eq 3.4}$$

Here, λ is the wavelength of the X-rays, n is the number of wavelength, 2Θ as the diffraction angle and d (Å) as the interplanar spacing of parallel lattice planes generating a diffraction peak. This may be easily calculated from observed diffraction angles provided the wavelength is known. Nowadays X-ray diffractometer are used to perform the X-ray powder diffraction analysis. These XRD instruments are equipped with filters and/or monochromators which records the intensity of the diffracted beam electronically at precise angles as the specimen is scanned over Θ angles as shown in Figure 3.9a, where Θ is the Bragg angle measured in degrees (Jumate et al. 2011).

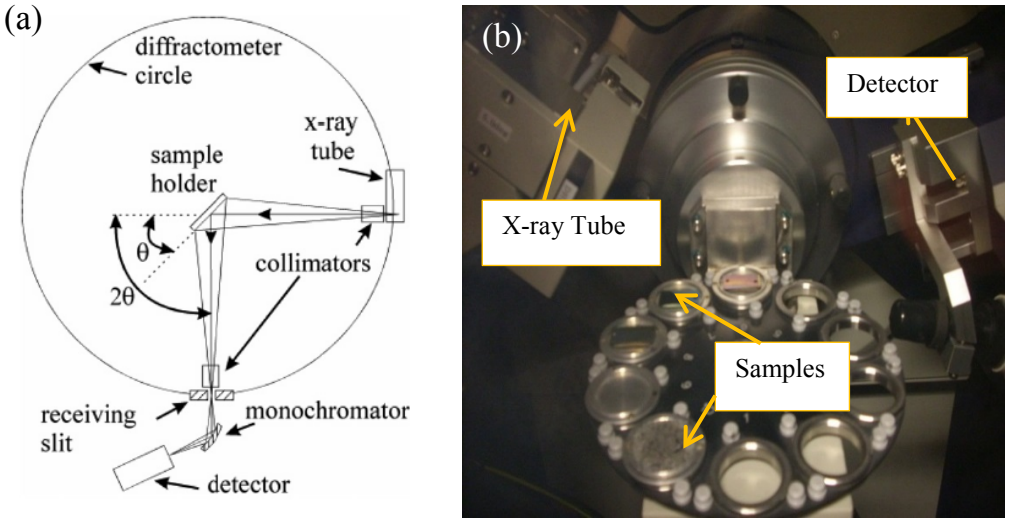

Figure 3.9: a) Schematic illustration of X-ray diffractometer components (Harris et al. 2007); b) Components of diffraction machine used for this study.

In this study the X-ray powder diffraction (XRD) tests were performed using a Rigaku Ultima IV (X-ray diffractometer) with Cross Beam Optical (PB/BB diffracted beam monochromator) with the automatic alignment capability as shown in Figure 3.9b. In addition the intensity of cobalt tube was set to 38 kV and 38 mA with a wavelength K equal to 1.790Å. Furthermore, spin and scan speed was set as 30.0 rpm and 0.600 deg/min with scan mode as continuous. These settings were recommended by the manufacturer. To avoid maximum overlapping of the peaks two hour run time was selected for each specimen. Data collected by the diffractometer is in the form of XRD spectrum/powder histogram with 2Θ on one axis and intensity counts on other axis as shown in Figure 3.10.

The crystalline peaks of spectrum were identified by matching them with PDF (powder diffraction file). In this study the identification and analysis of crystalline peaks were done with the help Jade version 9.1 which is X-ray powder diffraction analytical software.

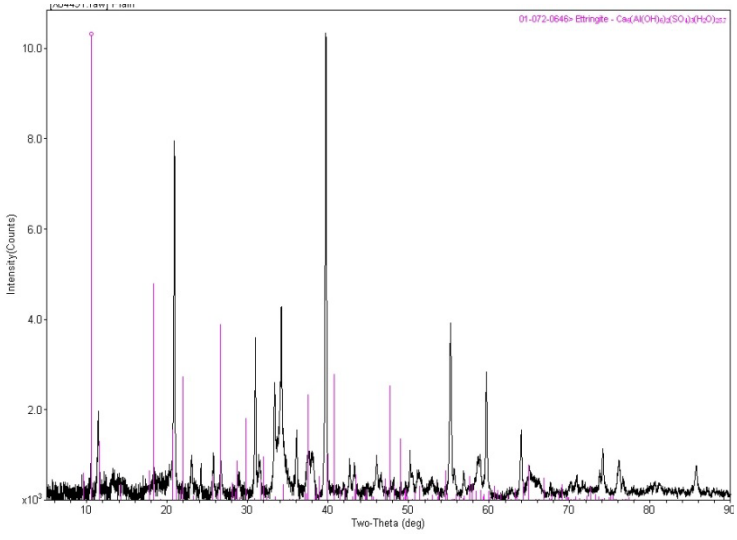

Figure 3.10: XRD pattern with phases identified.

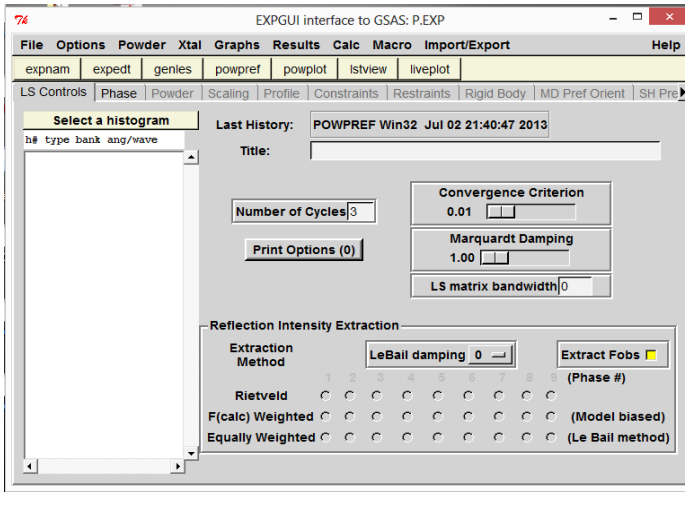

Figure 3.11: GSAS interface with EXPGUI.

After the identification of crystalline phases, Rietveld quantitative X-ray diffraction (RQXRD) analysis was carried out with the help of generalized structure analysis system (GSAS) software with EXPUGI interface as shown in Figure 3.11. This software takes X-ray diffraction spectrum/powder histogram and CIF (crystallographic information file) as an input.

The X-ray diffraction spectrum/powder histogram was measured with the help of X-ray diffraction whereas the crystallographic information files (CIF) were taken from the American mineralogist crystal structure database (AMCSD). After the analysis the weight fraction for the crystalline phases were quantified and analyzed. More details on the software parameter and results are discussed in chapter 5.

3.7.3 X-Ray Tomography

X-ray tomography is a three-dimensional imaging technique that measures the internal structure of the material through its X-ray absorption (Flannery et al. 1987). This technique was first introduced to medical science in 1971 and since then it has been used extensively for the diagnosis purposes. This technique is identical in practice to medical computed axial tomography (CAT) or Computed Axial Tomography (CATSCAN).

Recent advancements in X-ray tomography present a non-destructive technique due to which accurate and in depth microstructure characterization of engineering materials has become possible. The XRT procedure is carried out by directing the X-rays through the specimen, collecting large number of CT images from discrete view angles. The specimen is rotated around a single axis with an angular increment between 0^o to 180^o by using a rotation stage and keeping the rotation axis perpendicular to the X-ray beam (Hoseini 2013, Meier et al. 2012). Schematic illustration of XRT set-up is shown in Figure 3.12. A specialized algorithm is used to reconstruct the distribution of X-ray in the slice plane and stack of contiguous series of 2D CT images is obtained. Afterwards, these images can be easily converted into 3D object.

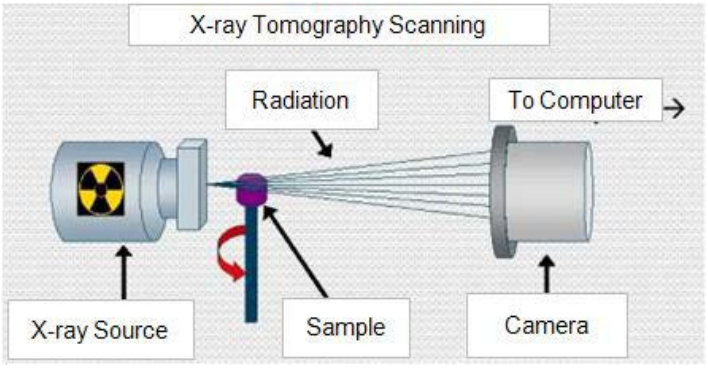

Figure 3.12: A schematic illustration of XRT set-up (taken from Hoseini 2013).

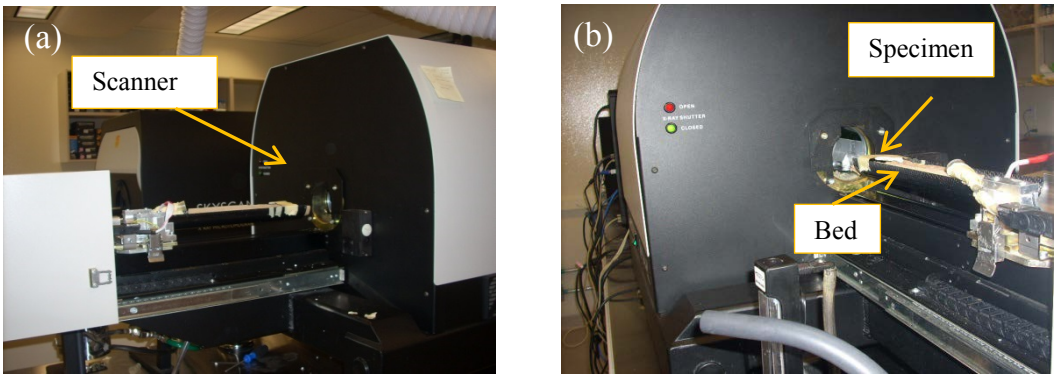

Figure 3.13:a);b); Skyscan 1076 X-ray Computed Tomography Machine used for this study.

The scanning of the specimens (CT Scan) in this study was done with the help of Skyscan 1076 X-ray computed tomography machine. The experimental set up of this scanner is shown in Figure 3.13. This machine is in the micro-tomography laboratory in the Department of Pharmacy, University of Alberta. The SkyScan 1076 was equipped with a high performance micro-CT scanner with X-ray source supply of 20-100kV with X-ray detector of 4000 x 2672 pixels size.

The cement-based foam specimens were placed in the bed of the X-ray machine and any possible movements of these specimens were restrained using masking tape. An X-ray voltage and electric current source was set 100 kV and 100 µA respectively to take 2D projections through a 1.0 mm

aluminum filter. After, doing number of trails it was found that the low voltage and electric current are most suitable for porous material. Moreover, the images were taken at the intervals of 0.009 mm corresponding to a spatial resolution of 9 μm and the reconstruction of the CT images (raw images) done with the help of SkyScan NRecon software available with Department of Pharmacy, University of Alberta.

The Feldkamp Back-Projection Algorithm was used during the image reconstruction. A total of 1500 reconstructed images from the width of 14 mm as shown in Figure 3.5 of the specimens were taken and are referred to as the "image-dataset". After the reconstruction of the raw images the 2D quantitative analysis of all the cement-based foam specimens were done by using the Skyscan CT-analyzer software provided by Department of Pharmacy, University of Alberta.

The Image-dataset of reconstructed raw images was loaded in the software as shown in Figure 3.14a. After that raw images were processed by first selecting a fixed region of interest on the database images. In this study circular region was selected to have similarity with the actual samples as shown in Figure 3.14b.

Next, those selected region of the images were then converted into a binary format using a thresholding technique. Thresholding is the method of image segmentation that converts grey scale images in to binary scale (Jähne 2005). This scale is basically image pixel and has the range of 0 to 255. The accuracy of the results depends a lot on the threshold value making it the most important factor of analysis process. Therefore, this value was selected manually by comparing binary images produced from several threshold values against the original grayscale image.

For example the threshold value for the image shown in Figure 3.14c was set as 33 to 255. The white color which is solid in these images represents areas within the range of the binary threshold selection and the areas outside this selection are pores which is black in color. After binary operation, the software performs the 2D analysis and the pore structure parameters like porosity, air-void size distribution, air-void spacing and shape factors were analyzed and quantified as shown in Figure 3.14d.

3.7.4 Scanning Electron Microscopy

Scanning Electron Microscope (SEM) examination was done to illustrate the microstructures of the test specimens. This test was conducted to build the understanding about the geometry of microstructure of specimens. As due to low resolution used in XRT test this microstructure is not very visible. However, it is essential to exclude any moisture in the specimens therefore this test was done after air drying the samples for 6 months. Scanning electron microscopy needs to be performed in high vacuum, as molecules in the air can interfere with the electron beam. Also, specimens need to be coated with a thin layer of gold which acts as a reflective surface for the electron beam. Therefore, before scanning a, “Sputter Machine” was used to apply the gold coating, which deposited a thin layer of 10 to 20 nm. Finally, specimens were placed under the microscope and high-resolution images were taken at a desired location with 100X, 150X and 500X magnifications respectively.

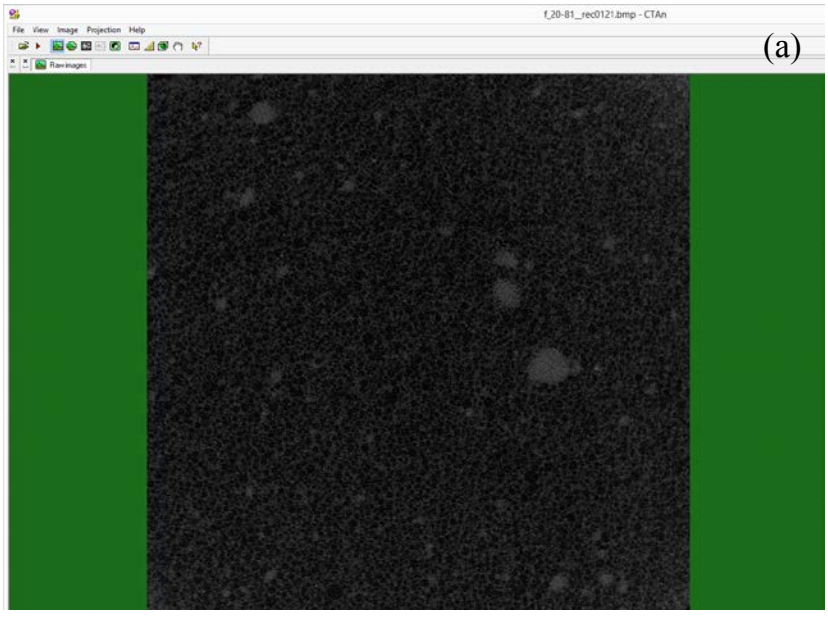
f_20-81_rec0121.bmp - CTAn
File View Image Projection Help
Raw images

(a)

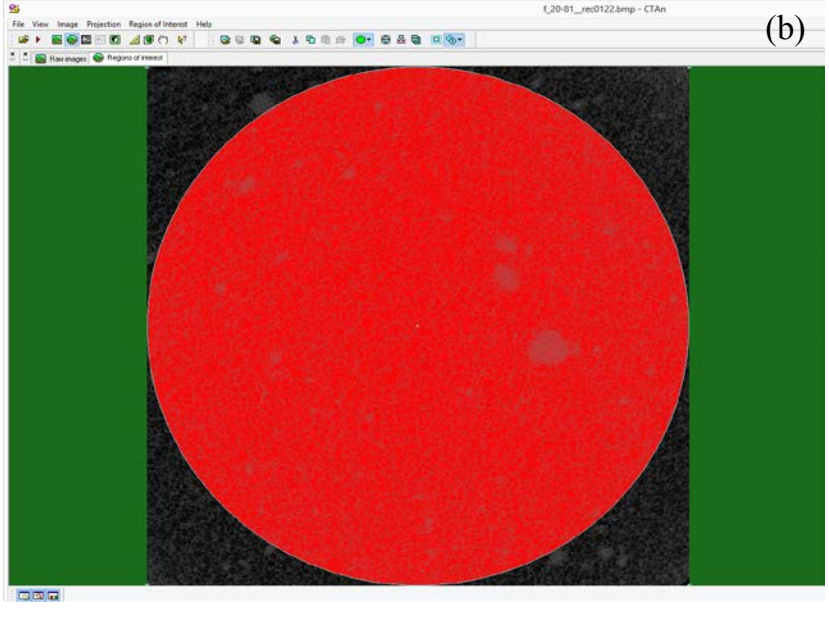
f_20-81_rec0122.bmp - CTAn
File View Image Projection Region of Interest Help
Raw images
Regions of interest

(b)

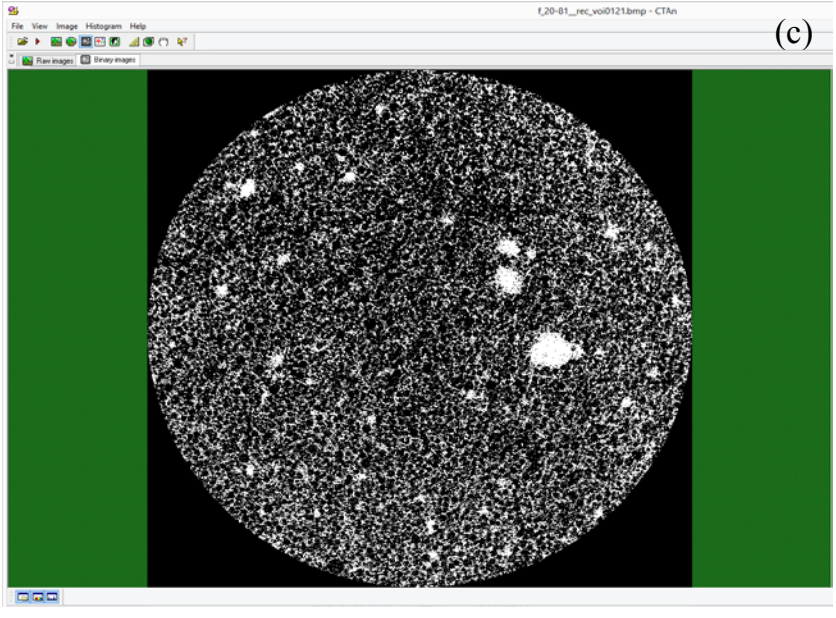

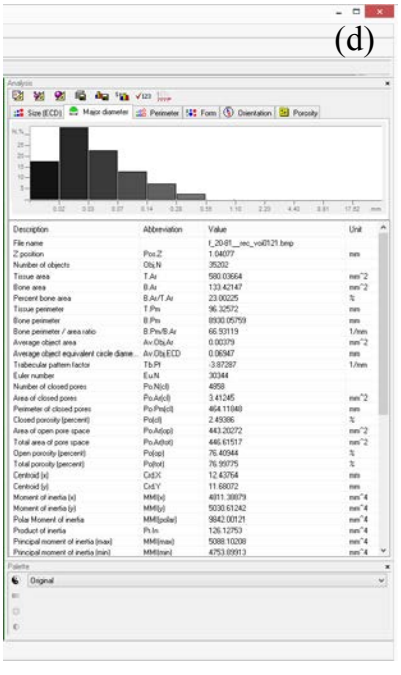

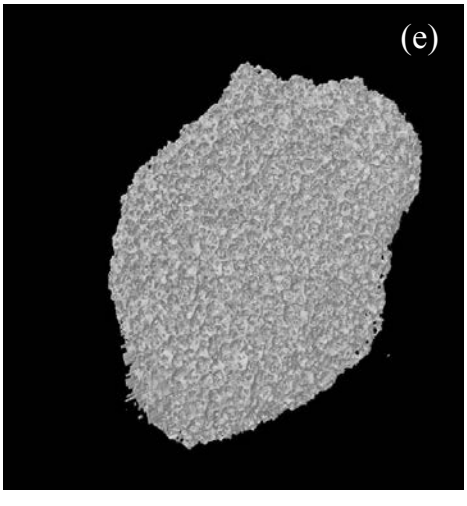

Figure 3.14: Different Stages of Image Analysis; a) Raw Image; b) Region of Interest; c) Thresholding; d) Processed Image with results; e) 3D rendered image of sample.

3.7.5 Moisture Content Evaluation

The oven drying test procedure which confirms to ASTM C566 (2013) standards was used here to measure the moisture content of the specimen. This test was carried out at four different ages of the specimen namely 60^{th}, 120^{th}, 210^{th} and 300^{th} days respectively. In addition to this all the measurements were carried out at room temperature and on air dried samples. As per specification all the samples were placed in an oven at 110°C for 24 hours after weighting them. After 24 hours the samples were removed from the oven and the weight of the samples were measured again. The moisture content in the specimen was determined by using Equation 3.5 as shown below.

$$M_c = \left(\frac{W-D}{D}\right) * 100 \qquad \text{Eq 3.5}$$

where,
M_c = total evaporable moisture content of sample (%)
W = mass of sample (g)
D = mass of oven-dried sample (g)

3.7.6 Consistency Test: Marsh Cone Test

Marsh Cone test belongs to group of orifice tests known as the V funnel or the ORIMET (Roussel 2005). Similar approach is given by ASTM C 939 (2010) flow cone test for grouts. This test measures the fluidity of the paste as the inverse of the flow time, by measuring the time taken for a 350 ml of base mix to flow through a cone opening as shown in Figure 3.15a. Longer the flow time, lower the fluidity is. In addition, Marsh cone helps in determining the consistency (flowability) of the base mix and the water requirement for making stable cement-based foam. Therefore, for all the

base mixes, Marsh cone test was performed by pouring 350 ml of the paste in to the cone and recording the time as shown in Figure 3.15. This time was then compared with other researcher findings as no standards and specifications are available on the flow time of specific base mixes.

3.7.7 Consistency Test: Flow Cone Test

Another test of consistency was done by using the Flow Cone Test which conforms to ASTM C 230 (2008) standard as shown in Figure 3.16. This test was used here to measure the spreadability of cement-based foam in the fresh state.

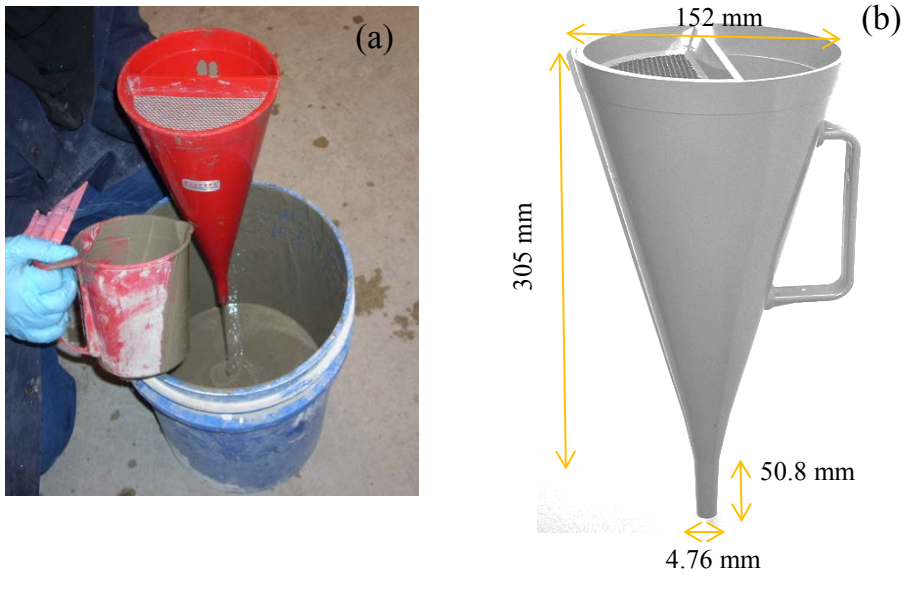

Figure 3.15: a) Slurry flowing through the Marsh cone; b) Schematic illustration of Marsh cone.

After filling the cone with the cement-based foam fresh mixture, the cone was lifted up slowly and gradually allowing the mix to flow without any vibration. In the end the average flow of the mix was measured as the maximum dimension of the spread mix with the help of ruler and this test was carried out for all the mixes.

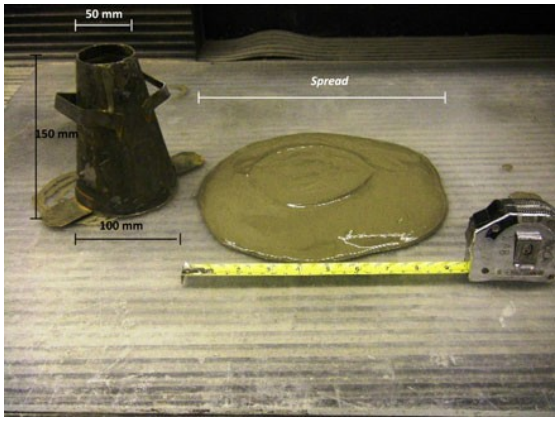

Figure 3.16: Flow cone apparatus with spread (Kramar et al. 2011).

3.7.8 Density

As mentioned earlier, during the preparation of cement-based foam the density of the mixture was measured intermittently and the addition of foam was continued until the required density is achieved. This density is known as “cast density” and is determined by filling a small container of known weight and volume with cement-based foam from the mixer. Another density which is the desire density is also termed as “Target density”. Test specimens were demoulded after 48 hours of casting and the density was measured. This density is known as demoulding density or the wet density of that specific specimen. The density measured on the date of test is designated as “density-at-test”.

4. Fresh State Properties of Cement-Based Foam

4.1 Introduction

Limited numbers of studies are reported so far on the characteristics of fresh cement-based foam and those reported (Kearsley 1999, Kearsley et al. 2001, Jones et al. 2005a, Nambiar et al. 2006, Ramamurthy et al. 2009) have showed that even a small variation in density significantly influences the material property. In cement-based foam, the target density or the density ratio (defined as the ratio of the density achieved to the desire density) closer to unity can only be achieved at a particular consistency of the fresh mix. The consistency depends on the water/cement ratio, foam content and pozzolanic admixture, if any. The spreadability and flowability are the two measurement indicators of consistency for the fresh base mix. These two indicators can be measured by using Flow cone and Marsh cone respectively (Agulló et al. 1999, Jones et al. 2003, Jones et al. 2005a, Nambiar et al. 2008).

In this chapter experimental results of (i) spreadability, (ii) flowability, (iii) foam content and (iv) demoulding density for the mixes with and without pozzolanic admixture are analysed and discussed. Subsequently, the "regression equation" for predicting the spread, flow and demoulding density of cement-based foam is also derived and presented here.

4.2 Stability of Cement-Based Foam Mixes

Past researchers have defined the cement-based foam mixes with density ratio (cast/target) closer or equal to unity as a stable mix. This stability in cement-based foam mixes is achieved by selecting workable water/cement ratio. When insufficient water is added, the mixture becomes too stiff and as a result foam bubbles breaks down, if too much water is added to the mixture then segregation takes place (Kearsley 1999, Kearsley et al. 2001, Nambiar et al. 2008, Ramamurthy et al. 2009). Along with this there is a narrow range of water/cement ratio reported by the researchers that makes cement-based foam stable i.e. 0.4 to 1.25.

Understanding the importance of an optimum w/c ratio, numbers of trials were done to select the workable water/cement ratio for this program. The ratios used are indicated in Table 3.9, it is important to note that these ratios do not include the water brought by the foam to the mixture. It was noticed during the trials that the water demand of Type HE is higher as compared to Type GU Portland cement. For Type GU cement the water/binder ratio required was in the range of 0.54 to 0.58 but for Type HE, the suitable ratio was found to lie in the range of 0.65 to 0.69. Thus, to facilitate comparison across mixes in the present study, a uniform w/binder ratio of 0.69 was chosen.

4.3 Consistency of Cement-Based Foam Mixes

As mentioned earlier the consistency for the fresh cement-based foam mix is measured in term of spreadability and flowability. Past researcher have used brewer spread test, slump flow test, flow table, flow cone test for measuring spreadability of cement-based foam. However, the marsh cone test is used here to measure the flowability (also indicates the plastic

viscosity) of the cement paste. This test is done by measuring the time taken for a certain volume of paste to flow through a cone with a small opening (Agulló et al. 1999, Jones et al. 2003, Jones et al. 2005a, Nambiar et al. 2008). Here, in this study marsh cone test was done of cement paste without any foam whereas, the flow cone test was done of a mixture with foam. These tests allow the selection of water/cement ratio and also indicate about the suitability of the process used to design the mixes.

4.3.1 Effect of Pozzolanic Admixture and Content

4.3.1.1 Flowability of Cement Paste (Marsh Cone Test)

Figure 4.1 plots the time recorded by marsh cone for the cement paste with and without pozzolanic admixture. Here, the "marsh cone time" is the indicator of flowability or the plastic viscosity of the cement paste (Nambiar et al. 2008). It can be noticed that the flow time for the mixes with pozzolanic admixtures was higher than that for the reference mix which means addition of admixtures makes the mixes more viscous also supported by (Jones et al. 2003, Nambiar et al. 2008, and Roussel et al. 2005). This is corroborated through studies that show these admixture increases the plastic viscosity. In comparison, mixes containing metakaolin takes longer time to flow or in other words, this mix have less fluidity (or more viscous) as compare to other mixes. A possible reason is high water demand when incorporating metakaolin same was as stated by Siddique et al. (2009). A similar increase in the water demand was recorded for silica fume also. It is likely that the fineness of these two admixtures could lead to a cohesive mix with an increase in the flow time (Agulló et al.1999 and Nambiar et al. 2008). Thus, it can be said that the present study Marsh's cone test results are in accordance with other researcher's findings.

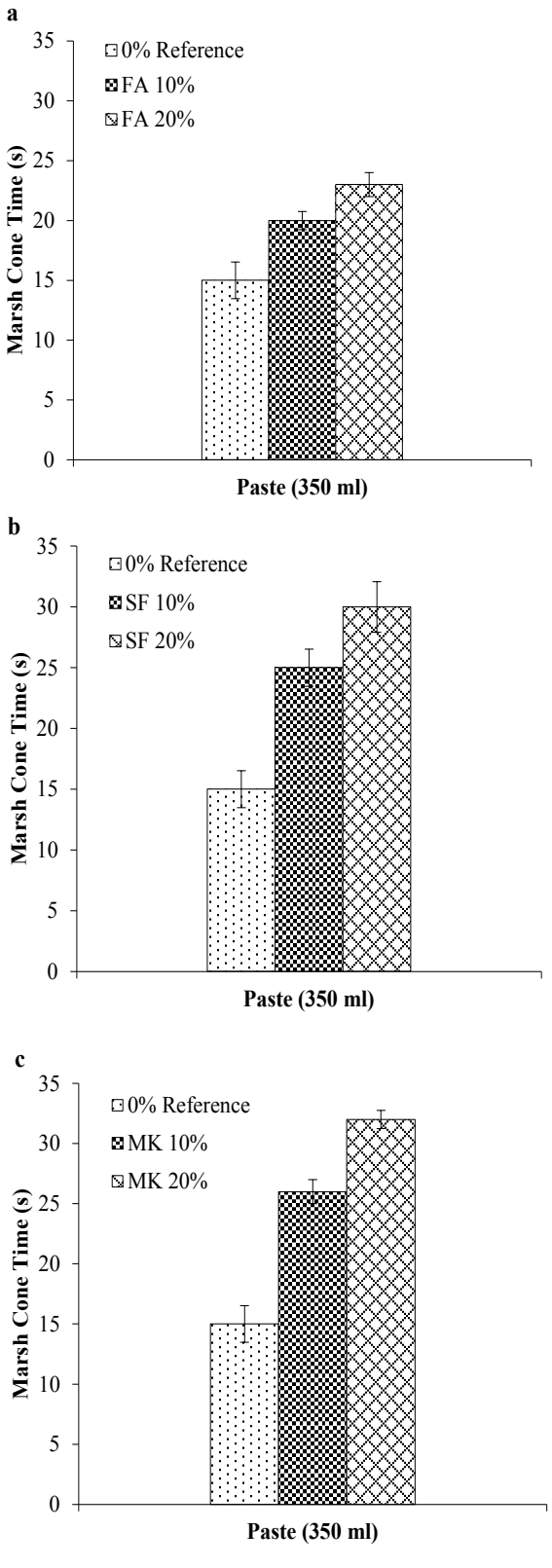

Figure 4.1: Effect of pozzolanic admixture on the flow time; a) Fly Ash; b) Silica Fume; c) Metakaolin. Error bars indicate standard deviation in Marsh Cone Time values based on three measurements.

4.3.1.2 Spreadability (Flow Cone Test)

The relationship between the average spread values and the cast density for the cement-based foam mixes is plotted in Figure 4.2. It was seen that the spread is the function of density so that as the density increases there was a corresponding increases in the spread. Nambiar et al. (2006) and Nambiar et al. (2008) explain this, due to loss of weight which increases the cohesion in presence of air bubbles.

When fly ash was incorporated at 10% and 20% substitution of Portland cement, it was found that the spread was higher compared with the 0% reference mix. The percentage difference noticed for 10% cement substituted mix was 9% and for 20% mix was 5% for the density range of 800 to 400 kg/m^3 respectively. Whereas, the drop between the mixes (FA10% and FA20%) was 5% for the 800 to 400 kg/m^3 density range respectively. Interestingly, increase in the substitution of fly ash ratio, decreases the spread value. This implies that the addition of fly ash reduces the viscosity and no doubt at a certain substitution, the viscosity will increase and the spread of the fly ash mix will likely be equal to the reference mix. Nambiar et al. (2008) have reported the value of spread for 0% reference mix without foam for 0.55 water/binder ratio equal to 19 cm. Similarly, Kearsley et al. (2005) reported the spread value equal to 22.5 cm for cement paste for 0.35 water/binder ratio and 25 cm when fly ash was added. The present study, spread values are close to these studies.

Subsequently, similar observations as of fly ash were recorded for mixes with silica fume. In fact, that the spread for the mix containing 20% SF as cement substitution was nearly equal to that of reference mix.

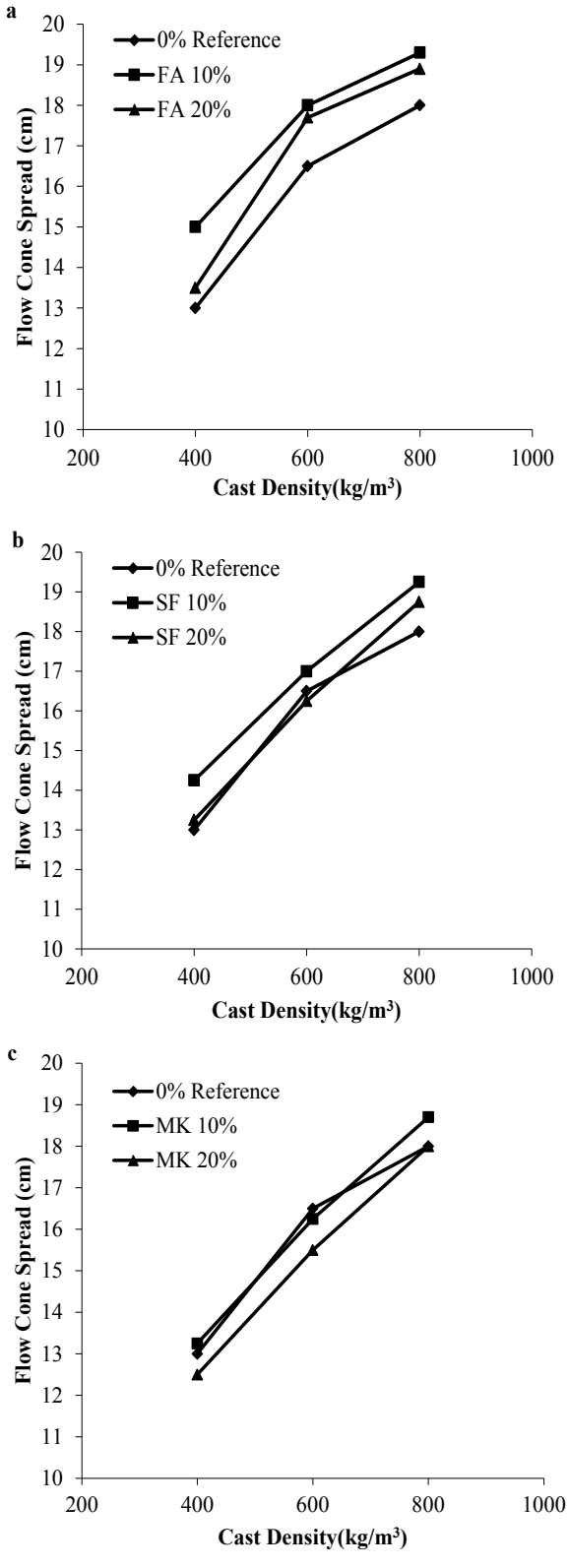

Figure 4.2: Relationship between the Spread and Cast Density for the mixes; a) Fly Ash; b) Silica Fume; c) Metakaolin.

Here, because of its fine particle size and being less prone to segregation, silica fume likely imparts cohesion to the mix (ACI 234R 2006). Therefore, percentage difference noticed between having 10% SF and 20% SF mixes was 6% and 1% respectively for the density range of 800 to 400 kg/m^3 compared with reference mix. In comparison between mixes, as expected silica fume led to more cohesive mixes than was observed in the case of fly ash. Furthermore, when cement was substituted with metakaolin in the ratio of 10% and 20%, the trend in spread values was opposite of that seen with silica fume and fly ash. At higher substitutions, there was a reduction in the spread, which implies that the addition of metakaolin increases the viscosity.

4.3.2 Predicted Equation for Spreadability

From the experimental output, a multiple linear regression model is used to describe the relationship between the spread of cement-based foam and two independent variables, namely cast density and admixture/cement ratio. This regression model can be applied to fly ash, silica fume and metakaolin when substituting cement from 0% to 20%. The spread of cement-based foam containing pozzolanic admixture is expressed in Equation 4.1 as follow:

$$S_{cp} = \beta_o + \beta_1 \Upsilon_{cd} + \beta_2 (ratio) \qquad \text{Eq 4.1}$$

where,

S_{cp} = spread of cement-based foam (cm)

β_o = constant (table 4.1)

β_1, β_2 = regression coefficient (table 4.1)

ratio = admixture/cement ratio (by weight)(fraction)

Υ_{cd} = cast density (kg/m^3)

The model summary indicates the R-square value for fly ash, silica fume and metakaolin is 86.7% (N=9), 94.4% (N=9), 97% (N=9) respectively whereas, the adjusted R-square for the corresponding pozzolanic admixture is 82.3%,92.6%,96%. The ANOVA table from the SPSS output indicates that the p-value for the regression model F-test is 0.000 which shows that model is highly significant. The p-value and F-test is explained in detail in chapter 8. The predicted spreadability of cement-based foam is plotted against the measured one in Figure A.1 (Appendix). Which illustrate that the Equation 4.1 was reasonable in predicting the spreadability.

Table 4.1: Constants for Equation 4.1

Constant	Fly Ash	Silica Fume	Metakaolin
β_o	8.872	8.375	8.019
β_1	0.012	0.013	0.013
β_2	4.333	1.250	-2.500

4.4 Foam Content

4.4.1 Effect of Pozzolanic Admixture and Content

The required density of cement-based foam is achieved by adding certain amount of foam into the slurry. This amount depends on the cast density, type of the pozzolanic admixture, ratio and type of foaming agent used i.e. protein or synthetic based (Kearsley et al. 2005, Kearsley et al. 2001, Mydin et al. 2012).

Figure 4.3 illustrates the relationship between the measured foam content and the cast density for all the mixes. It is seen that as the required density increases, the foam content decreases and interestingly, this trend does not even change in the presence of pozzolanic admixture. Kearsley et al. (2001) and Mydin et al. (2012) investigated the foam content of foam concrete and reported the same relationship between the density and the foam content. In addition to this (Figure 4.3), for fly ash mixes with higher substitution ratio the demand of foam content increases. The rise difference noticed for 10% and 20% fly ash was 11% and 18% for the cast density range of 800-400 kg/m^3 respectively, compared to the reference mix. Further 10% difference in the foam for the two mixes of fly ash was noticed. Similarly, when silica fume was added, higher foam content was noticed for higher substitution ratio. In comparison with 0% reference mix the percentage difference noticed in rise was 5% for 10% and 11% for 20% mixes respectively.

However, as opposed to the above two cases, in mixes with metakaolin, higher substitution reduces the foam content demand. The reduction value in foam demand noticed when compared with reference mix was 7% for mixes with 10% cement substitution and 24% for those with 20% substitution of cement by metakaolin respectively. Whereas, the difference in the actual drop of foam demand for these two series was measured to be 13% for the set density range.

Thus, summarizing these observations, it can be said that in the presence of fly ash the demand of foam content increases due to high fluid consistency in the base mix and high residual carbon in the ash. For silica fume fine particle could be the reason for higher foam content value. However, for metakaolin the drop noticed could be due to its particle size and high water absorptive property, same was reported by Siddique et al. (2011) and Bapat (2013).

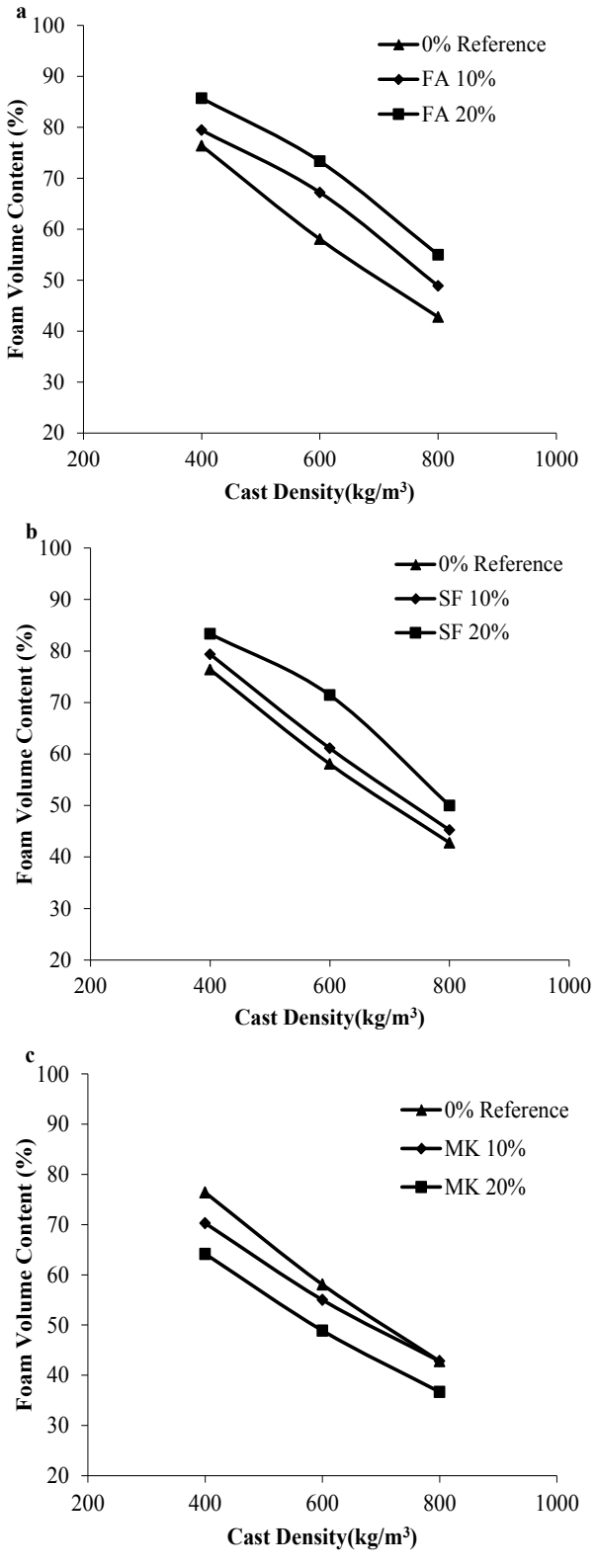

Figure 4.3: Relationship between the Foam Content and Cast Density for the mixes; a) Fly Ash; b) Silica Fume; c) Metakaolin.

4.4.2 Predicted Equation for Foam Content

A model which can predict the foam content of cement-based foam was formulated by using multiple linear regression analysis using the experimental data shown in Figure 4.3. The two independent variables were, cast density and admixture ratio. The model was based on substitution of cement from 0% to 20% with one of the three pozzolanic admixture examined here and the density range within 400-800 kg/m^3.The predictive model foam content is expressed in Equation 4.2 as follow:

$$F_c = \beta_o + \beta_1 \Upsilon_d + \beta_2 (\text{ratio}) \qquad \text{Eq 4.2}$$

where,

F_c = Foam volume content of cement-based foam (%)

β_o = constant (table 4.2)

β_1, β_2 = regression coefficient (table 4.2)

ratio = admixture/cement ratio (by weight)(fraction)

Υ_d = cast density (kg/m^3)

The R-square value recorded was 99% (N=9), 97% (N=9), 98.5% (N=9) respectively in case of mixes with fly ash, silica fume and metakaolin regression models. The corresponding adjusted R-square was equal to 98.7%, 96.0% and 98.0% respectively. The ANOVA table from the SPSS output indicates that the p-value for the regression model F-test is 0.000 which shows that model is highly significant. However, the detail of these outputs is explained in chapter 8. The predicted foam content of cement-based foam is plotted against the measured as shown in Figure A.2 (Appendix A). It can be noticed that Equation 4.2 is reasonable good in predicting the foam content. Except the predicted content seem to be slightly overestimating for silica fume mixes.

Table 4.2: Constants for Equation 4.2

Constant	Fly Ash	Silica Fume	Metakaolin
β_o	108.61	110.44	103.00
β_1	-0.08	-0.08	-0.07
β_2	71.66	56.66	-45.00

4.5 Density

4.5.1 Slurry Density

The average fresh slurry density as measured for all the mixes is shown in Figure 4.4. Note that the density was measured before adding any foam to it. It can be noticed that for higher dosages of substitution, the density of the fresh slurry density decreases and this was true for all three types of pozzolanic admixture examined here.

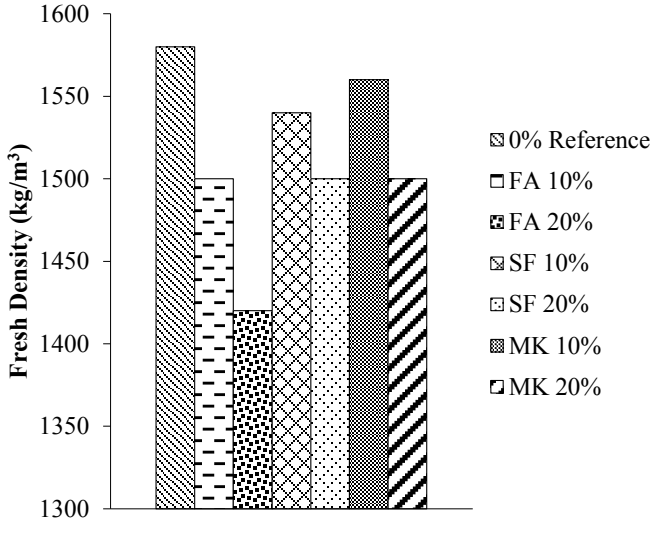

Figure 4.4: Fresh slurry density for all mixes.

4.5.2 Cement-Based Foam Density

The density of cement-based foam is directly related to the percentage of foam added to the slurry. The fact that a small variation in density can cause large difference in thermal properties makes it essential to place strict control on the target density. Therefore, careful measurements were taken to control the foam content so that the cast density and the target density do not vary significantly. Ideally, the ratio of cast and target density should be equal or close to unity but the 5% difference is acceptable and considered as indication of suitability of the method used to design the mixes (Kearsley et al. 2005a). Therefore in this study, it was strictly checked that for all the mixes, the casting densities were within 5% of the target densities.

Hence, as a second check, the ratio between the demoulding (hardened state) and the cast density was also checked to verify the stability, consistency of the base mix and the foam content used.

Figure 4.5 and 4.6 illustrate the comparison between the cast density and the demoulding density for the mixes with and without pozzolanic admixture. The demoulding density was measured after 48 hours of casting at the same time of demoulding of the specimens. It can be noticed that both densities are in good agreement with each other for all mixes the difference recorded was less than 10% which is mainly due to the decreases in moisture content. This implies that the water/binder ratio used here and the mix design method was satisfactory.

Table 4.3: Constants for Equation 4.3

Constant	0% Reference	Fly Ash	Silica Fume	Metakaolin
β_o	-84.114	64.863	-44.716	-147.447
β_1	1.087	1.072	1.121	1.235
β_2	0	-759.276	-316.519	-11.06

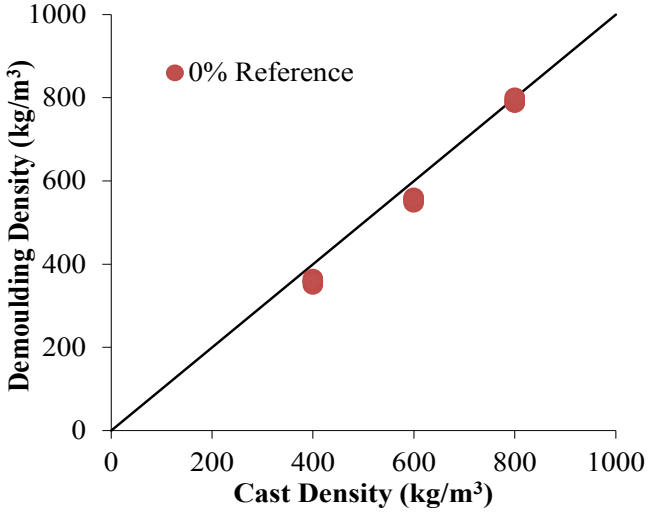

Figure 4.5: Comparison between the demoulding and cast density for 0% reference mix.

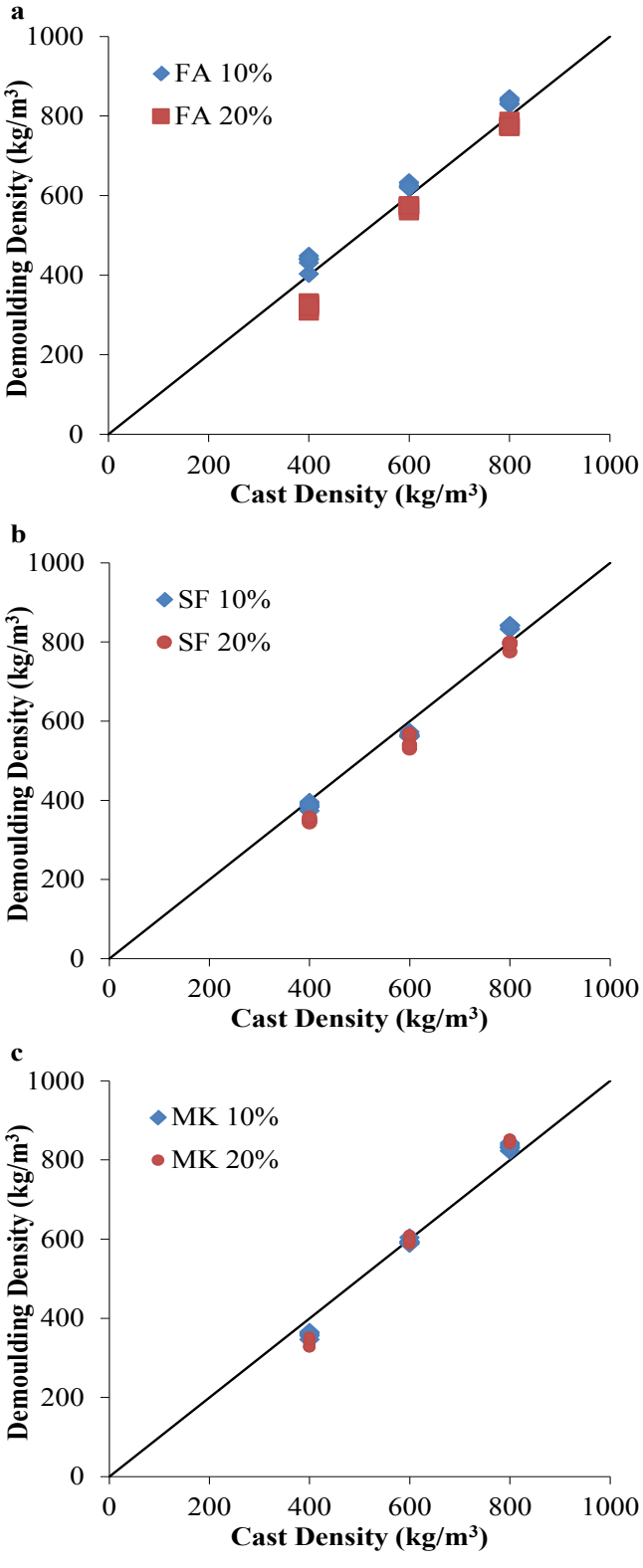

Figure 4.6: Comparison between the demoulding and cast density for mixes; a) Fly Ash; b) Silica Fume; c) Metakaolin.

4.5.3 Predicted Equation for Demoulding Density

Based on the experimental results, a multiple linear regression analysis was done to develop a model which can predict the demoulding density of cement-based foam for three types of pozzolanic admixtures i.e. fly ash, silica fume and metakaolin. The cast density and admixture ratio were treated as two independent variables and the following Equation 4.3 was derived.

$$D = \beta_o + \beta_1 \Upsilon_d + \beta_2 (ratio) \qquad \text{Eq 4.3}$$

where,

D = demoulding density of cement-based foam (kg/m^3)

β_o = constant (table 4.3)

β_1, β_2 = regression coefficient (table 4.3)

Υ_d = cast density (kg/m^3)

ratio = admixture/cement ratio (by weight)(fraction)

The adjusted R-square was equal to 99% (N=18) for the reference series, fly ash, silica fume and metakaolin regression models. The ANOVA table from the SPSS output indicates that the p-value for the regression model F-test is 0.000 which shows that model is highly significant. See chapter 8 for the detail on the outputs coefficients.

4.6 Conclusion

- The spread is a function of density. As the density increases, the spread also increases.

- The density of cement-based foam decreases as the foam content increases. With a higher substitution ratio of fly ash and silica fume, the demand of the foam content increases, whereas adding metakaolin in the mixes decreases this demand.

- The cast density and demoulding density for the mixes with and without the pozzolanic admixture were in agreement, as the difference recorded between the two was less than 10%.

- Mathematical models developed to predict the spreadability and foam content needs validation by the future researchers.

5. Quantitative Analysis of Hydrated Products in Cement Paste

5.1 Introduction

The microstructure of cement-based foam comprises of two phases solid phase and void phase. The solid phase, which is basically hydrated cement paste, significantly influences the thermal conductivity of cement-based materials (Marshall 1972, Kim et al. 2003, Bentz 2007,Choktaweekarn et al. 2009). In order to understand and interpret this influence, it is necessary to identify and quantify the hydration products that form during the hydration process with and without pozzolanic admixtures.

In this chapter experimental results of X-ray diffraction for the mixes with and without pozzolanic admixtures are analysed to identify the phases present in the cement paste. The quantification of X-ray diffraction (QXRD) for the identified phases was done by using the Rietveld Method which is most widely used technique at present. Subsequently, the mathematical relationship between the fraction (weight) and the thermal conductivity of the hydrated phases is also derived and presented here.

5.2 Phases Identification

The hydration of cement is the combination of all chemical and physical processes taking place after contact of the cement powder with water. Cement consists of minerals, mostly calcium silicates and aluminates (C_3S, C_2S, C_3A, C_4AF) and the calcium sulfate (gypsum) as tabulated in Table 5.1. During the hydration process these minerals are transformed into calcium silicate hydrate (CSH), calcium hydroxide (CH), trisulfatehydrate

(AFt) and monosulfatehydrate (AFm) phases respectively (Kosmatka et al. 2003, Bapat 2013). The hydration time, amount and type of pozzolanic admixture if any, are the major factors which greatly influences the formation of different products. Therefore, a technique is required which can identify these hydrated and other additional phases.

Past researchers (Sharma et al. 1999, Agarwal 2006, Veluchamy et al. 2009, Korpa et al. 2009, Jumate et al. 2011, Jumate et al. 2012, Soin et al. 2013) have suggested that X-ray diffraction (XRD) can be used for the characterisation of hydration phases in cementitious materials. The working details of XRD are explained in chapter 3. The presence of major crystalline peaks can be detected by XRD but not so amorphous phases, since amorphous phases do not by nature give reflection peaks in the diffraction pattern. This means that the direct identification of amorphous hydrated products like CSH will be difficult through the direct output of this technique. However amorphous phases can still be quantified only indirectly by the Quantitative XRD method. In this procedure, a defined quantity of crystalline inert material (the internal standard) is added to the sample and the ratio between the usual peak of each crystalline phase and that of the internal standard is determined. The details of this method can be found in literature Torre et al. (2001), Chancey et al. (2010) and Ibáñez et al. (2013) respectively.

However, from the work of Demirboğa et al. (2003), it is common to take the conductivity of the amorphous phases as around $1/15^{th}$ that of crystalline silica. In the present case, the study is made to highlight and quantify only the crystalline phases through peaks from the XRD test.

5.2.1 Hydrated Cement Paste

Figure 5.1 displays the results of X-ray diffraction pattern conducted on the reference mix with no pozzolanic admixture. It can be seen that CH (portlandite) is the dominant peak at all hydration periods as identified by the XRD test. Also in Table 5.2 all the various phases are given along with the symbols for their identification. The formation of CH is basically due to the reaction between C_3S, C_2S and water. Their reactive equations can be found in any textbook on cement and concrete technology (Mindness et al. 2002, Neville 2011). It can be seen for 60^{th} day that the rate of formation of CH peaks was of high intensity. Many peaks of smaller intensity of CH can be seen up till the 120^{th} day. Thereafter, the other hydrated products than CH have peaks with intensity exceeding that of CH. Another product formed due to the reaction of calcium silicates with water was CSH which is amorphous or semi crystalline or both in nature (Bapat 2013) and due to being of this type was not traceable by XRD. However, other hydrated products like jennite (J) and tobermorite (T) which have similar chemical composition as that of CSH were detected by XRD (Gard et al. 1976, Bapat 2013).

In the initial period of 60 and 120^{th} day of hydration, some small and large peaks of jennite (J) and traces of tobermorite (T) were found, but in later stages of 210 and 300^{th} day, tobermorite was more prominent. Quartz was found at the 60^{th} day but later it disappeared. This means it was consumed to form other products. Another set of peaks noticed was of ettringite which belongs to trisulphate *Aft* phase and was formed due to reaction between C_3A and gypsum. It was observed that the peaks of ettringite were of low intensity and even this diminished as the hydration time advanced. Traces of kuzelite (K) which belong to *AFm* phase were also found. Along with

this, some peaks of strätlingite (S) were also noticed during the entire period of hydration.

Interestingly, prominent peaks of calcite were noticed at 120th day whereas before and after this period only traces were recorded. This means by the 120th days the CH reacts with atmospheric carbon dioxide to form calcite and the dissolution of carbon dioxide in water result in the formation of H_2CO_3 which further react with CH to form more calcite. The details of the chemical reaction can be found in literature (Bapat 2013). For the remaining two periods (210 and 300th days) it was expected that calcite amount will not increase significantly as the sample get dry and CH is also consumed by other products (See Figure A.3-A.6, Appendix A).

Table 5.1: Chemical and Compound Composition of HE Type Portland Cement

Notation	Mineral Name	Chemical Composition	Compound Composition (% by mass)
C_3S	Tricalciumsilicate (alite)	$3CaO \cdot SiO_2$	54
C_2S	Dicalciumsilicate (belite)	$2CaO \cdot SiO_2$	19
C_3A	Tricalciumaluminate (aluminate/celite)	$3CaO \cdot Al_2O_3$	3
C_4AF	Tetracalciumaluminoferrite (ferrite)	$4CaO \cdot Al_2O_3 \cdot Fe_2O_3$	13.5

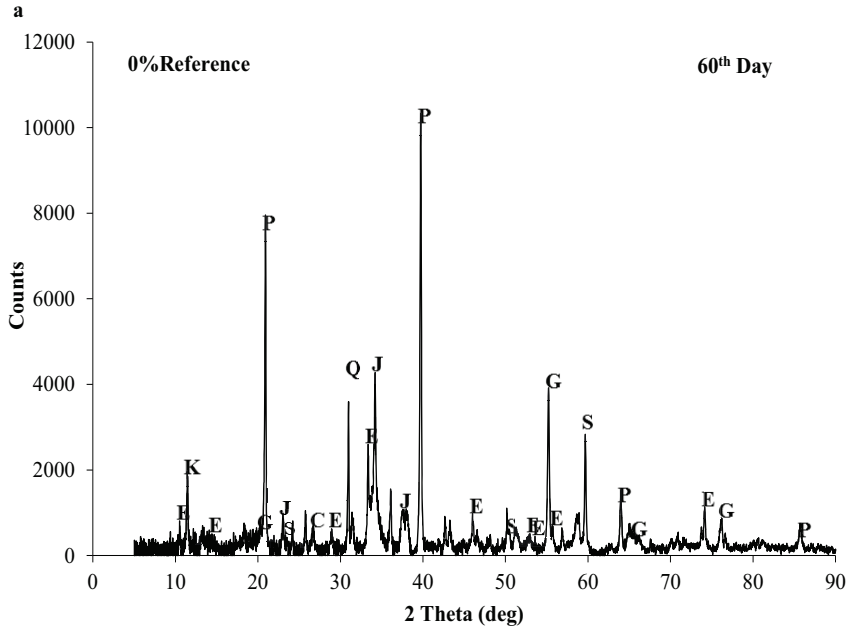
a
0%Reference
60th Day
Counts
2 Theta (deg)

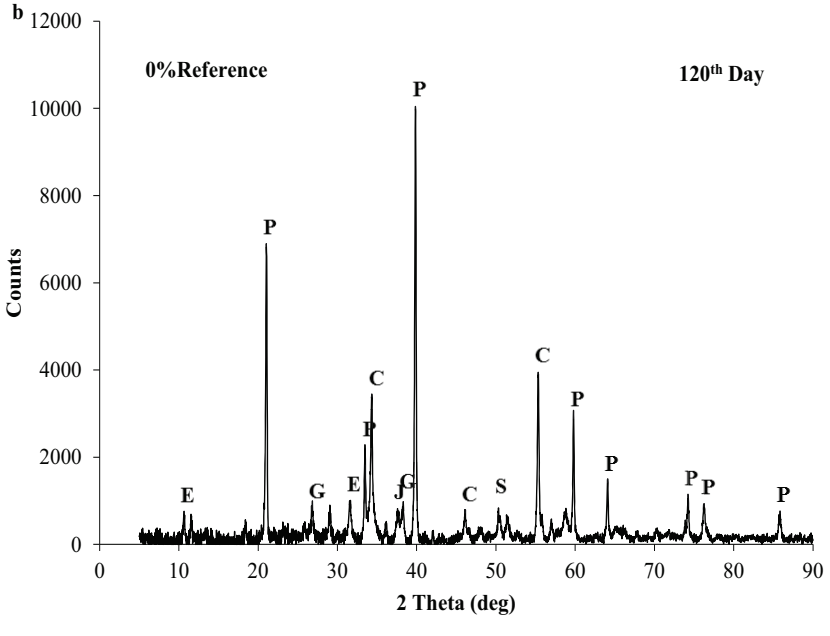
b
0%Reference
120th Day
Counts
2 Theta (deg)

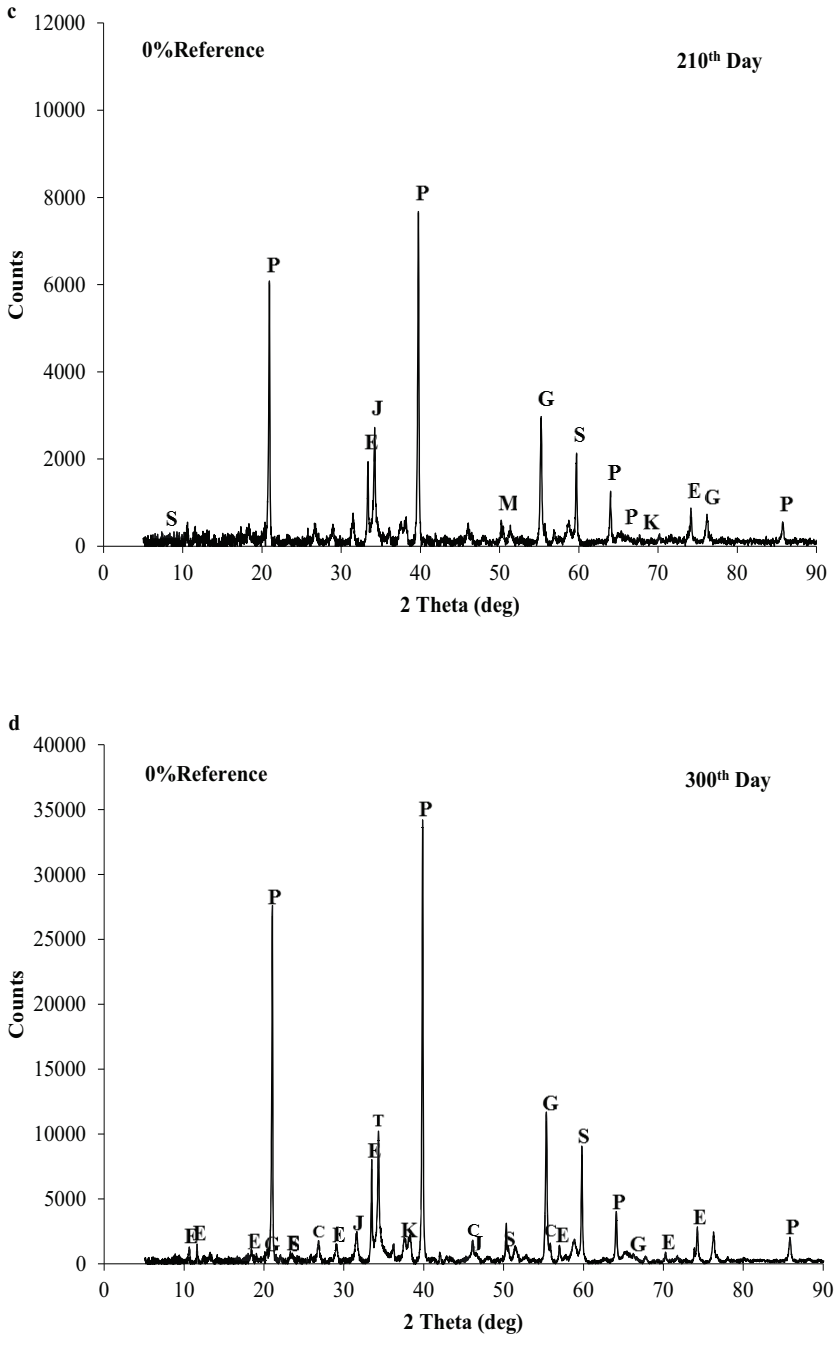

Figure 5.1: X-ray Diffraction Pattern for 0% Reference mix; a) 60th day; b) 120th day; c) 210th day; d) 300th day.

Table 5.2: Details of Crystalline Phases Identified in X-ray Diffraction

Notation	Mineral Name	Chemical Composition	Pdf Codes
P	Portlandite (CH)	$Ca(OH)_2$	00-044-1481
E	Ettringite	$Ca(Al(OH)_6)_2(SO_4)_3(H_2O)_{26}$	01-072-0646
C	Calcite	$CaCO_3$	00-005-0586
Gy	Gypsum	$CaSO_4 \cdot 2H_2O$	00-033-0311
Q	Quartz	SiO_2	00-046-1045
K	Kuzelite	$Ca_4Al_2(OH)_{12}[SO_4] \cdot 6H_2O$	00-050-1607
S	Strätlingite	$Ca_4Al_2(OH)_{12}[AlSi(OH)_8]_2 \cdot 2H_2O$	01-080-1579
G	Gehlenite	$Ca_2Al_2SiO_7$	01-089-5917
Y	Yeelemite	$Ca_4Al_6SO_{16}$	00-042-1478
M	Mullite	Al_4SiO_8	01-073-1389
J	Jennite	$Ca_9Si_6O_{18}(OH)_6 \cdot 8H_2O$	00-018-1206
T	Tobermorite /Plombierite-14A	$Ca_5Si_6O_{16}(OH)_2 \cdot 7H_2O$	00-029-0331
Sl	Sillimanite	Al_2SiO_5	00-038-0471
GIS	Gismondine	$CaAl_2Si_2O_8 \cdot 4H_2O$	00-020-0452
CSH	Calcium Silicate Hydrate	$Ca_{1.5}SiO_{3.5}\ xH_2O$	00-033-0306

5.2.2 Hydrated Cement Paste with Pozzolanic Admixture

5.2.2.1 Hydration of Cement with Fly Ash (FA)

Figure 5.2 and 5.3 illustrates the X-ray diffraction pattern of the 10% and 20% fly ash mixes respectively for 60^{th},120^{th}, 210^{th} and 300^{th} hydration periods. It can be observed from Figure 5.2 that peaks of CH was prominent in the initial hydration period but in later stages these peaks minimizes due to pozzolanic reaction i.e.CH consumption. This consumption is explained (Kosmatka et al. 2003, Siddique et al. 2011, Bapat 2013) as the reaction between amorphous silica present in fly ash with CH of Portland cement which results in the formation of more CSH. The crystalline phases of fly ash type CI described by researchers are tabulated in Table 5.3. Similarly alumina of fly ash reacts with CH in cement to produce strätlingite (S), hydrogarnet (C_3AH_6) and ettringite ($C_3A{\cdot}3CS{\cdot}H_{32}$).

However, strong peak of jennite (J) and tobermorite (T) can be noticed throughout the period of hydration as compared to the peaks in reference mix. This confirms that pozzolanic reaction has taken place. Along with this, ettringite peaks were also quite prominent up till 210^{th} day and after that only trace were found. The peaks of calcite (C) diminish with hydration time and the peaks of gehlenite (G) remained prominent in the entire hydration period. This could be due to the addition of silica and alumina. In addition to this, the traces of mullite (M), sillimanite (S) and kuzelite (K) were also found during the four hydration periods.

Similar XRD pattern and hydration products have been observed by Sharma et al. (1999) after 90^{th} days of hydration with 10% fly ash substitution of cement.

As regards the cement-based foam with 20% cement substitution by fly ash, the XRD trace points out that similar to the case with 10% fly ash in binder, the formation of CH was predominant in the initial stages i.e. 60th day and 120th day. Later periods of hydration show other products like jennite (J), tobermorite (T), strätlingite (S), gehlenite (G) and gismondine (GIS) also. Comparatively, significant difference was not noticed in the hydration products or in their peaks patterns between 10 and 20% fly ash to binder ratio.

Overall, it can be summarized that addition of fly ash increases the consumption of CH leading to the formation of other products because of its pozzolanic actions. However, the two figures also clearly show that increased substitution does not significantly change the XRD pattern nor the hydrated products (Figure A.3-A.6 Appendix A).

Table 5.3: Crystalline Phases of Fly Ash Powder (Siddique et al. 2011)

Notation	**Mineral Name**	**Chemical Composition**
Hm	Hematite	Fe_2O_3
M	Mullite	$Al_6Si_2O_{13}$
Sp	Ferrite Spinel	$(Mg.Fe)(Fe,Al)_2O_4$
Q	Quartz	SiO_2

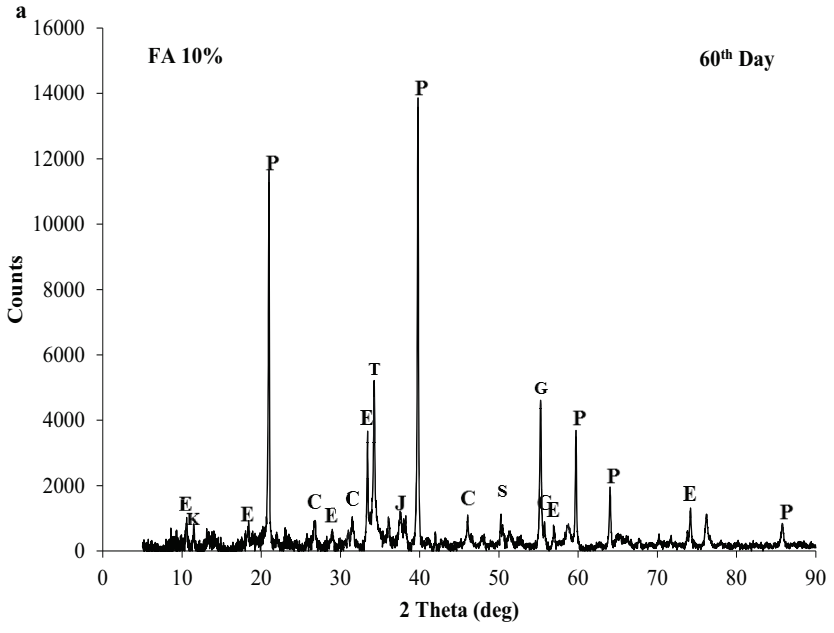
a
FA 10%
60th Day
Counts
2 Theta (deg)
P
E
K
C
T
J
S
G

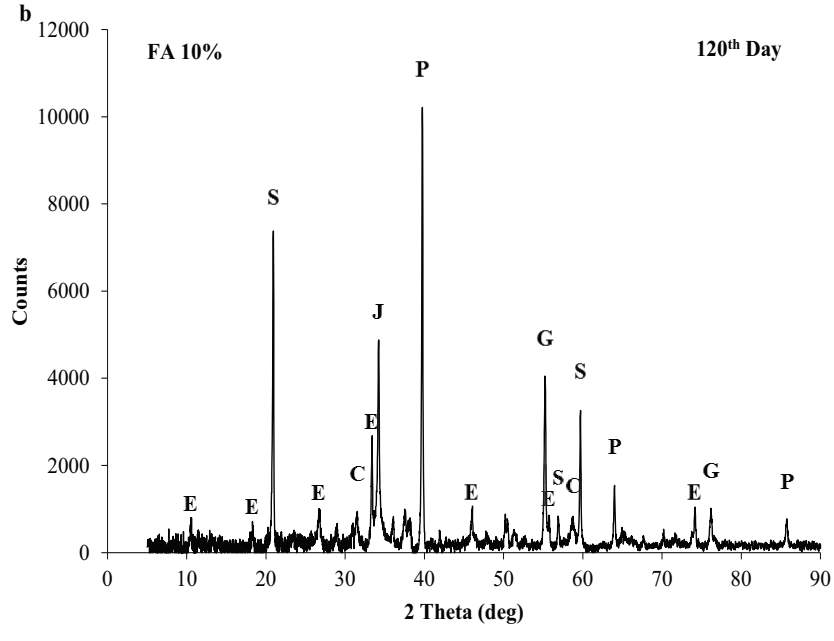
b
FA 10%
120th Day
Counts
2 Theta (deg)
P
S
J
G
E
C

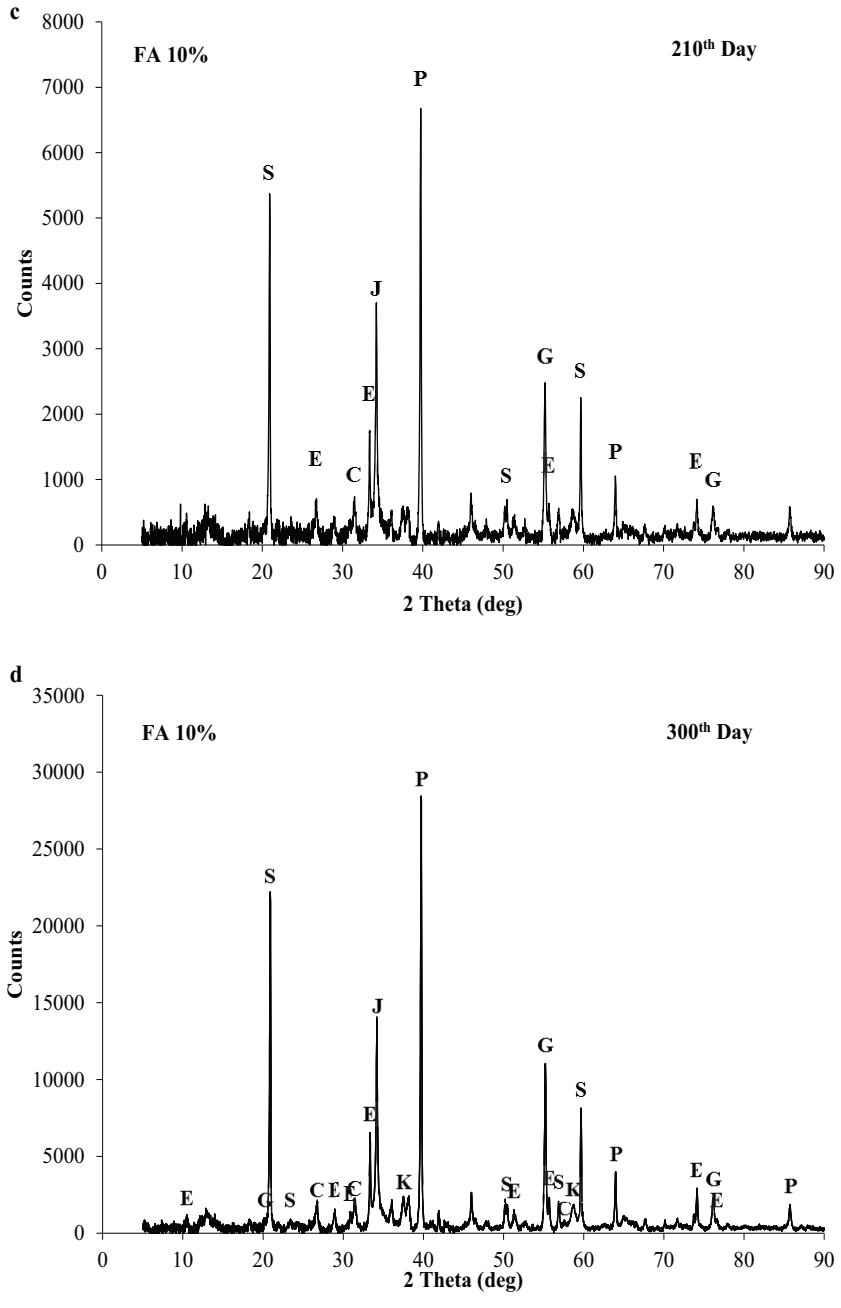

Figure 5.2: X-ray Diffraction Pattern for 10% Fly Ash mix; a) 60th day; b) 120th day; c) 210th day; d) 300th day.

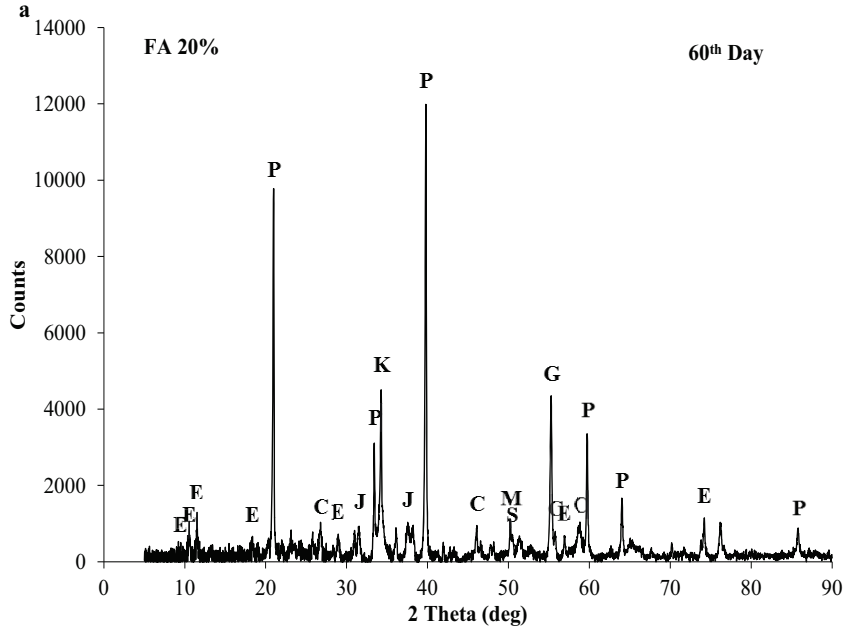
a
FA 20%
60th Day
Counts
2 Theta (deg)
P
K
G
E
C
J
M
S

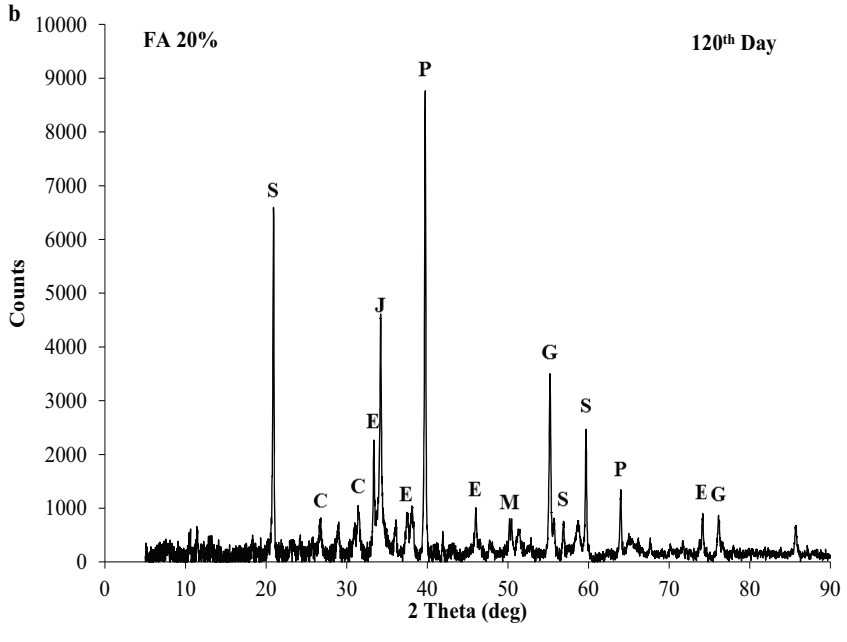
b
FA 20%
120th Day
Counts
2 Theta (deg)
S
P
J
G
E
C
M

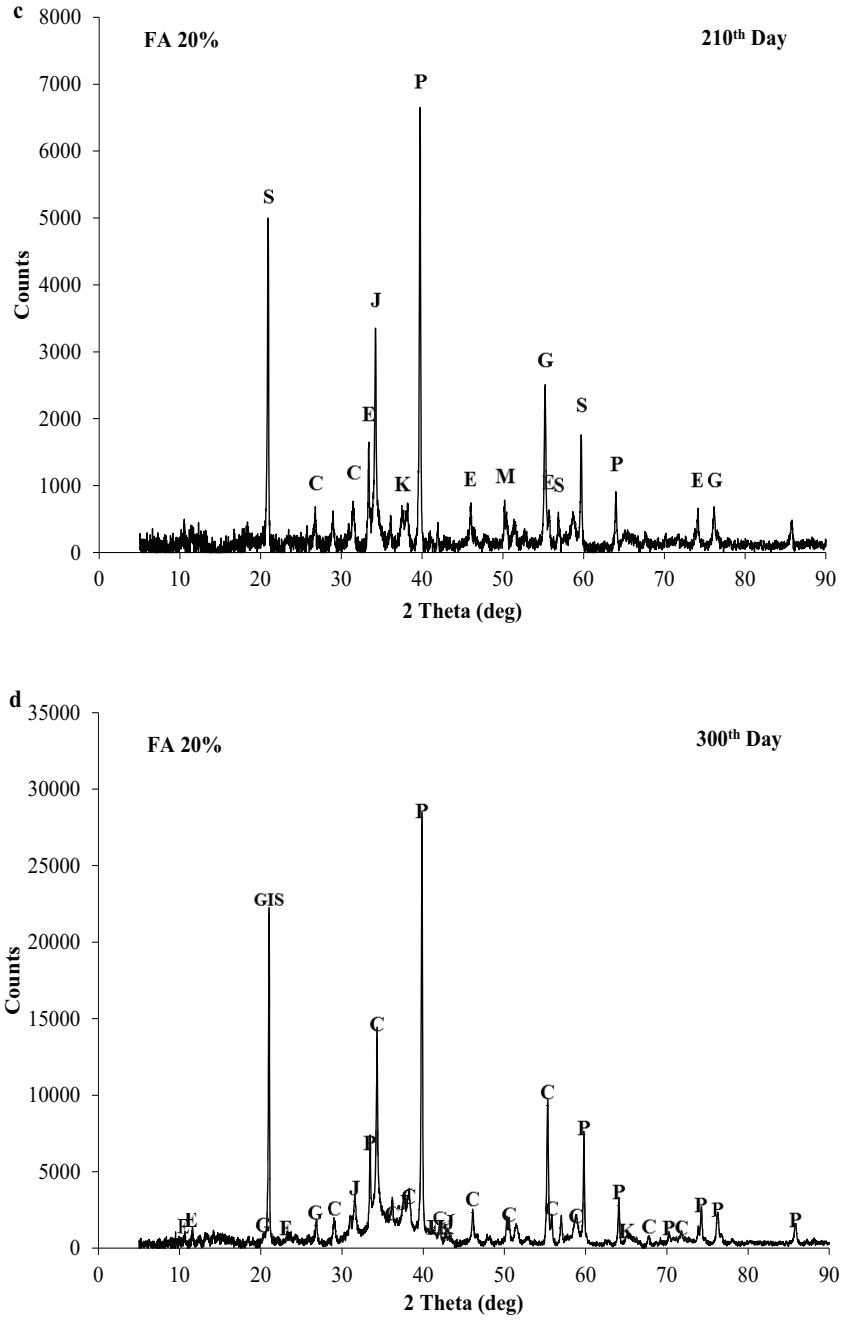

Figure 5.3: X-ray Diffraction Pattern for 20% Fly Ash mix; a) 60th day; b) 120th day; c) 210th day; d) 300th day.

5.2.2.2 Hydration of Cement with Silica Fume (SF)

Silica Fume normally contains 85-98% silica in the amorphous form and the miniscule crystalline may consists of quartz, cristobalite, silicon carbide (Siddique et al. 2011).

Figure 5.4 and 5.5 shows the XRD spectrum of 10 and 20% silica fume to binder ratio mixes for four hydration periods. It can be observed from Figure 5.4 that after 60^{th} day of hydration, the peaks of calcium hydroxide (CH), ettringite (E), calcite (C), tobermorite (T) and gehlenite (G) become prominent and traces of mullite (M), sillimanite (S) were also found. Even in the later stages same hydrated products were dominating except some of the portlandite peaks were replaced by strätlingite (S) and yeelemite (Y). This shows that the initial formation of CH gets consumed as the hydration time increases. It was also found that the intensity of occurrence of CH peaks in the presence of silica fume was lower as compared to the one in 0% reference mix. This clearly indicates about the ongoing pozzolanic activity.

In addition to this it was also noticed that the number of counts (frequency of occurrence) decreases as the time or the age of paste increase but again, this increases significantly by the end of 300^{th} day. This revels that the process of hydration is still ongoing and appearance of calcite peaks indicates the possibility of the reaction between any residual CH and atmospheric carbon dioxide to form more calcite.

From Figure 5.5, it can be noticed that the XRD spectrum for 20% silica fume to binder ratio mix does not significantly changes in comparison with 10% silica fume mix.

Same consumption of CH and formation of tobermorite (T) and gehlenite (G) strätlingite (S) and yeelemite (Y) was observed. Except that the peak values of CH were lower as compared to the 10% silica fume mix (see Appendix A).

Thus, it can be said that increased substitution of silica fume does not significantly alter the phases or component of the hydrated products but their peak intensities do decrease with the higher replacement. Also, an increase in the consumption of CH in case of silica fume indicates that the pozzolanic reaction is taking place.

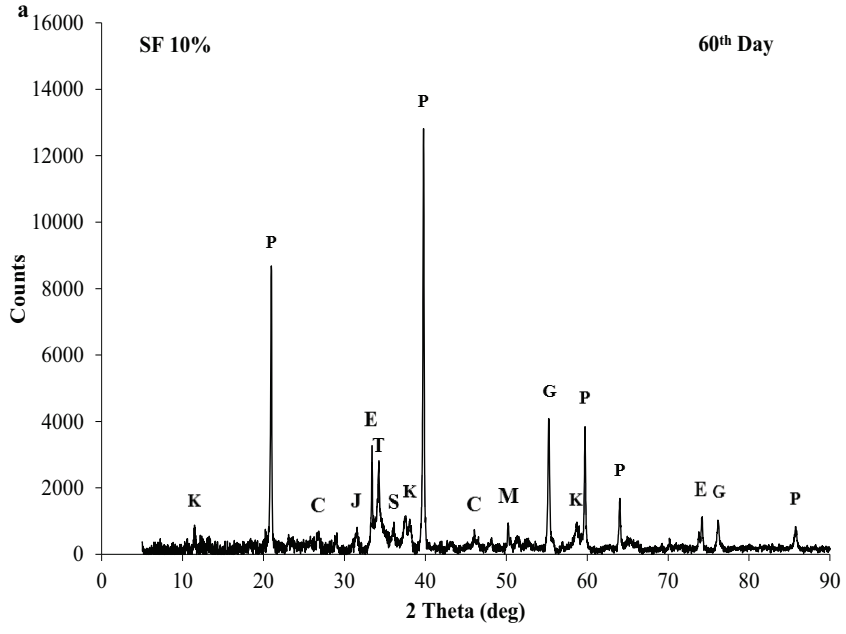
a
SF 10%
60th Day
Counts
2 Theta (deg)
P
K
C
J
E
T
S
M
G

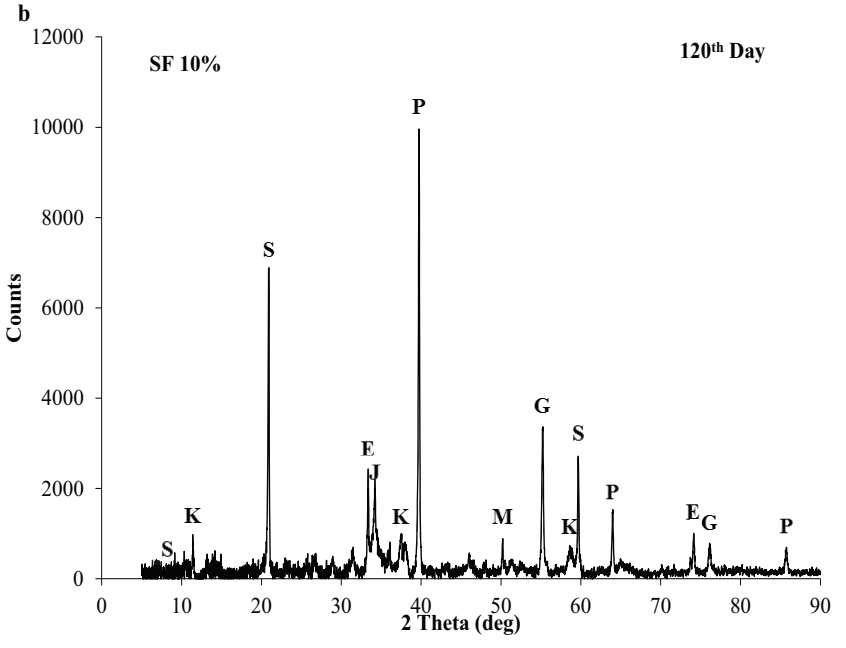
b
SF 10%
120th Day
Counts
2 Theta (deg)
P
S
K
E
J
G
M

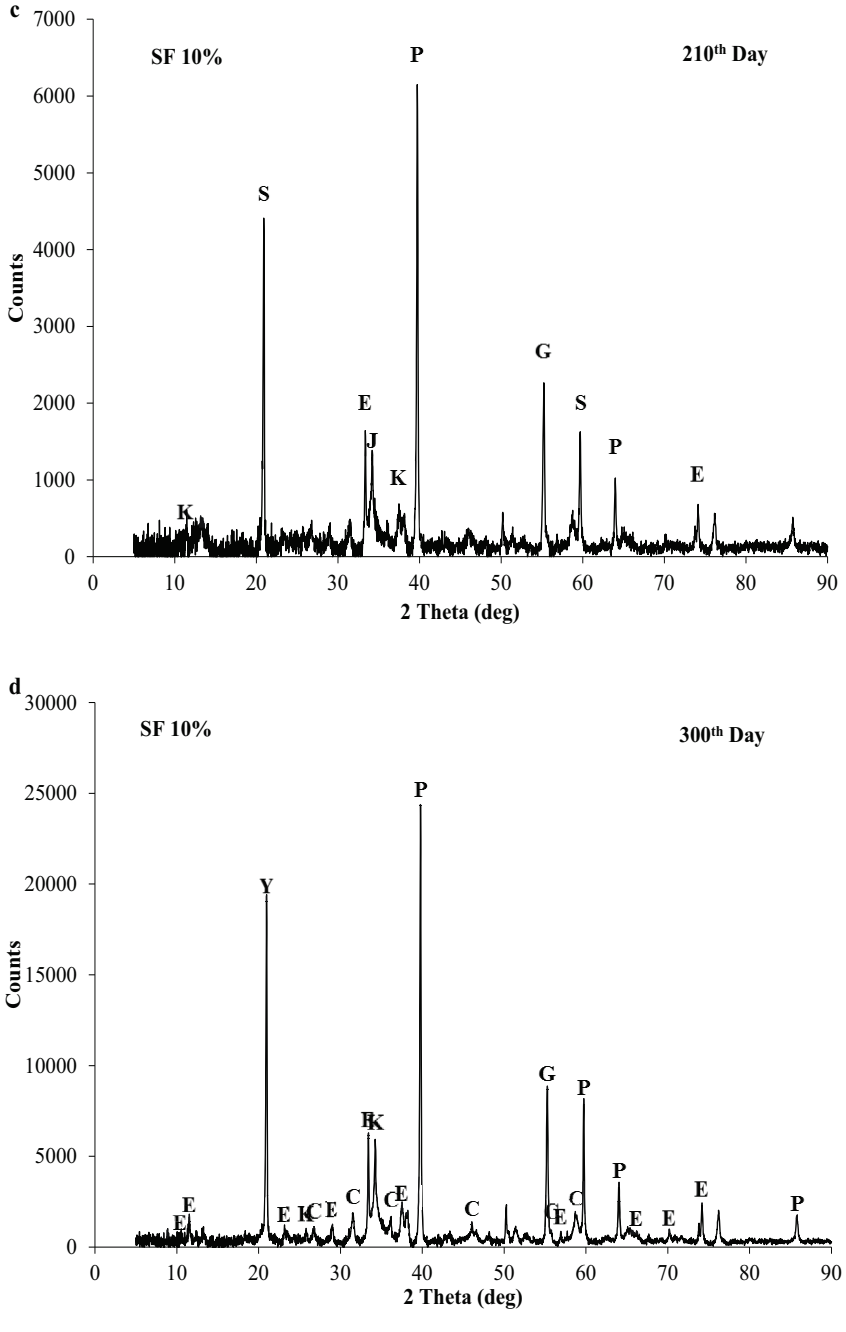

Figure 5.4: X-ray Diffraction Pattern for 10% Silica Fume mix; a) 60th day; b) 120th day; c) 210th day; d) 300th day.

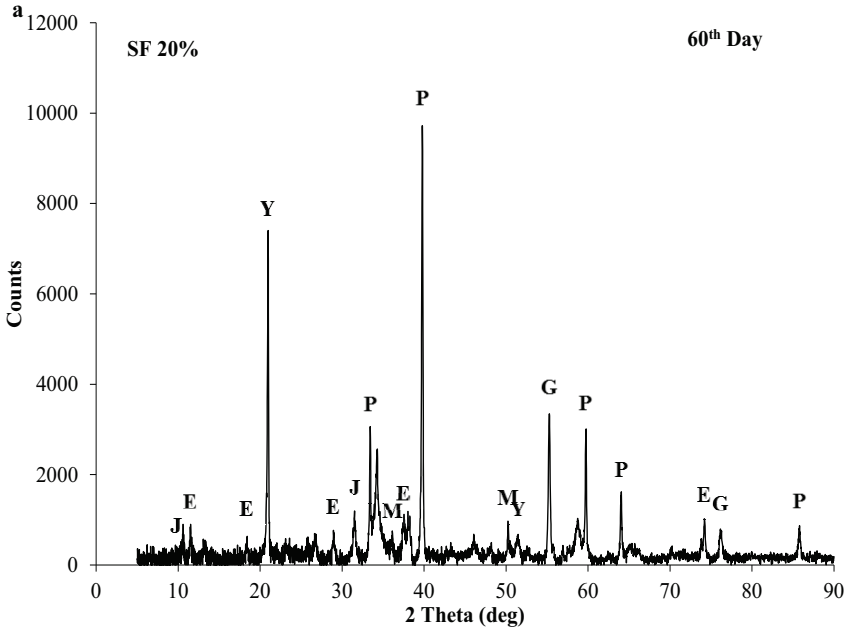
a
SF 20%
60th Day
Counts
2 Theta (deg)
P
Y
G
P
P
P
E
E
E
J
J
E
M
M
Y
E
G
P

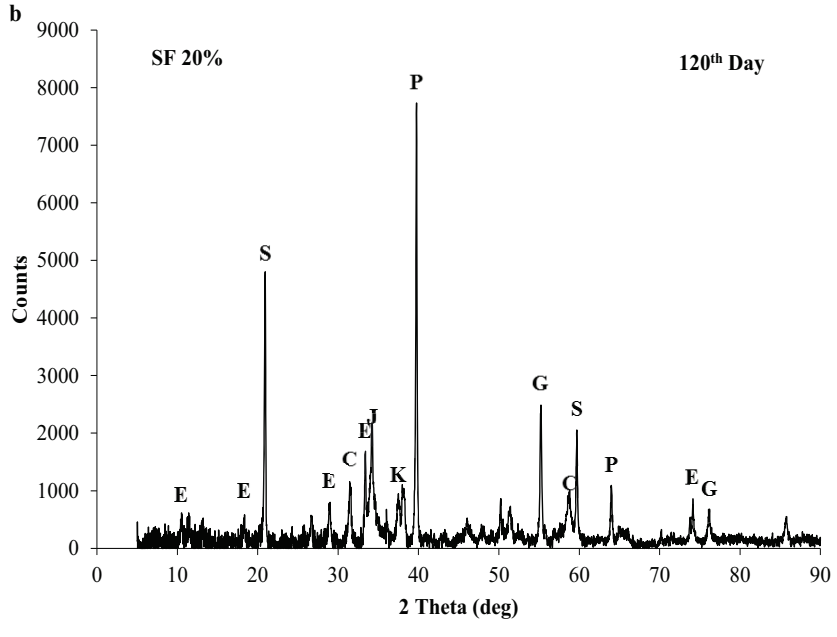
b
SF 20%
120th Day
Counts
2 Theta (deg)
P
S
G
S
J
E
C
E
E
K
C
P
E
G
E
E

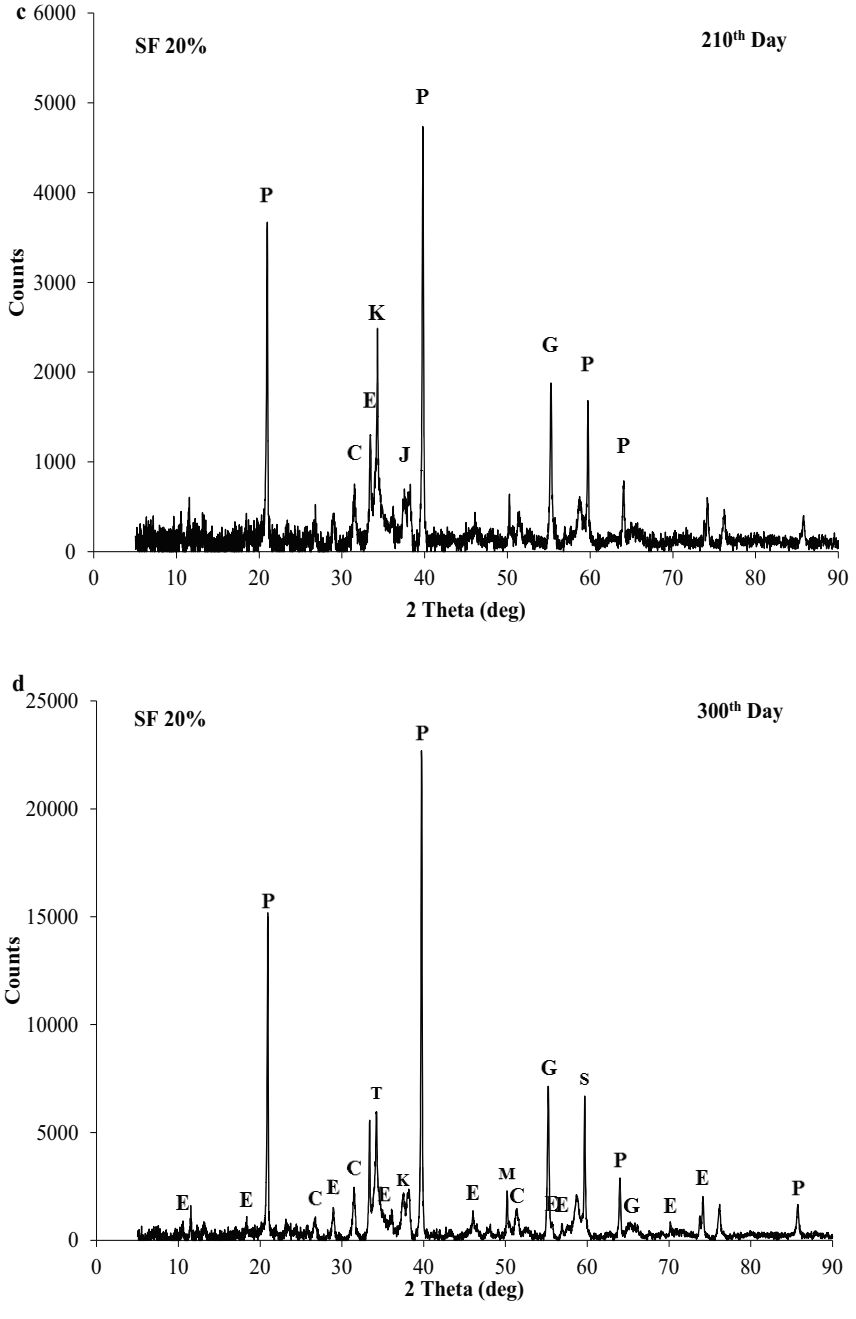

Figure 5.5: X-ray Diffraction Pattern for 20% Silica Fume mix; a) 60th day; b) 120th day; c) 210th day; d) 300th day.

5.2.2.3 Hydration of Cement with Metakaolin (MK)

Metakaolin mainly consist of silicon dioxide (SiO_2) and aluminum oxide (Al_2O_3) (Kosmatka et al. 2003, Shekarchi 2010, Siddique et al. 2011, Bapat 2013). In the presence of metakaolin the CH in hydrated cement paste reacts with these two oxides forming CSH gel and some other products like strätlingite (C_2ASH_8) and hydrogarnet (C_3AH_6) which are crystalline and contain alumina. Table 5.4 shows the crystalline phases of metakaolin powder.

Figure 5.6 and 5.7 illustrate the XRD patterns of 10% and 20% metakaolin mixes for four hydration periods. From Figure 5.6a which represents 60 days of hydration, it is seen that calcium hydroxide (CH) has significant intensity, although jennite (J) peaks are also visible. Jennite is a product of the reaction of CH and silica. Also seen are the beginnings of formation of phases like strätlingite (S) and kuzelite (K) which are due to the reaction of alumina in the metakaolin. In addition to this, small peaks of mullite (M), sllimanite (S), gehlenite (G), yeelemite (Y), all of which are rich in alumina and silica were also observed. Similar observations were recorded for other hydration periods, except that in the last two stages, CSH peaks were found. This implies that some part of CSH formed was of crystalline nature or maybe semi crystalline due to which it was detected by XRD.

Subsequently, same consumption of CH and formation of tobermorite (T) gehlenite (G) strätlingite (S) and yeelemite (Y) was found in 20% substitution metakaolin mix as shown in Figure 5.7. In addition to this it was also noticed that the XRD spectrum for 20% metakaolin mix does not significantly changes in comparison with 10% metakaolin mix (Figure A.6 Appendix A).

Interestingly, the peak of CH does not significantly decreases with the higher substitution ratios. As was noticed for other admixtures but in fact at some hydration stages rise was noticed in the peak, although the difference was not significant. On the other hand in the individual mixes decline was noticed in the CH peaks with the hydration time which confirms about the pozzolanic reaction.

Finally, it can be said that the addition of metakaolin consumes CH and forms silica and alumina related phases. However, a quantitative assessment is required to understand the influence of increased percentage of metakaolin on the consumption of CH and on the formation of other products as it is not apparent from these XRD traces. The following section deals with that subsequent quantitative analysis.

Table 5.4: Crystalline Phases of Metakaolin Powder (Siddique et al. 2011)

Notation	**Mineral Name**	**Chemical Composition**
Ka	Kaolinite	$Al_2Si_2O_5(OH)_4$
Al	Alunite	$KAl_3(SO_4)_2(OH)_6$
Q	Quartz	SiO_2
Ie	Illite	$K_{0.65}Al_{2.0}[Al_{0.65}Si_{3.35}O_{10}](OH)_2$

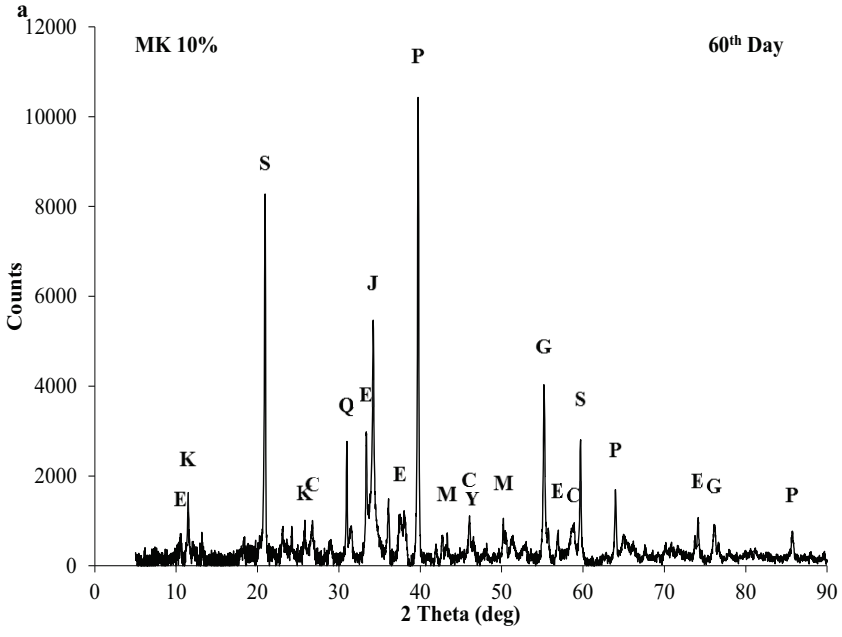
a
MK 10%
60th Day
Counts
2 Theta (deg)
P
S
J
G
Q
E
K
C
M
Y
S
P
E
G

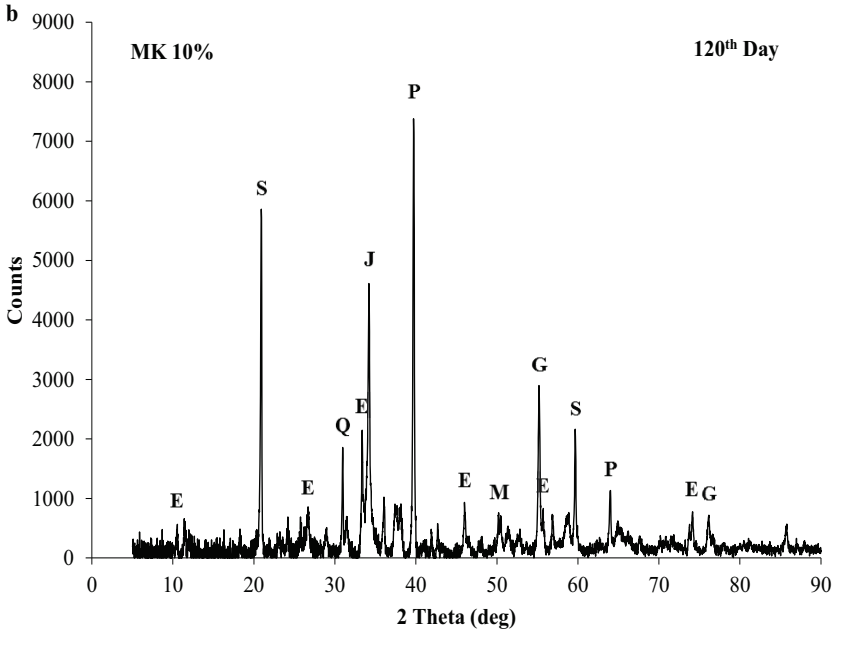
b
MK 10%
120th Day
Counts
2 Theta (deg)
P
S
J
G
Q
E
S
P
E
G
M

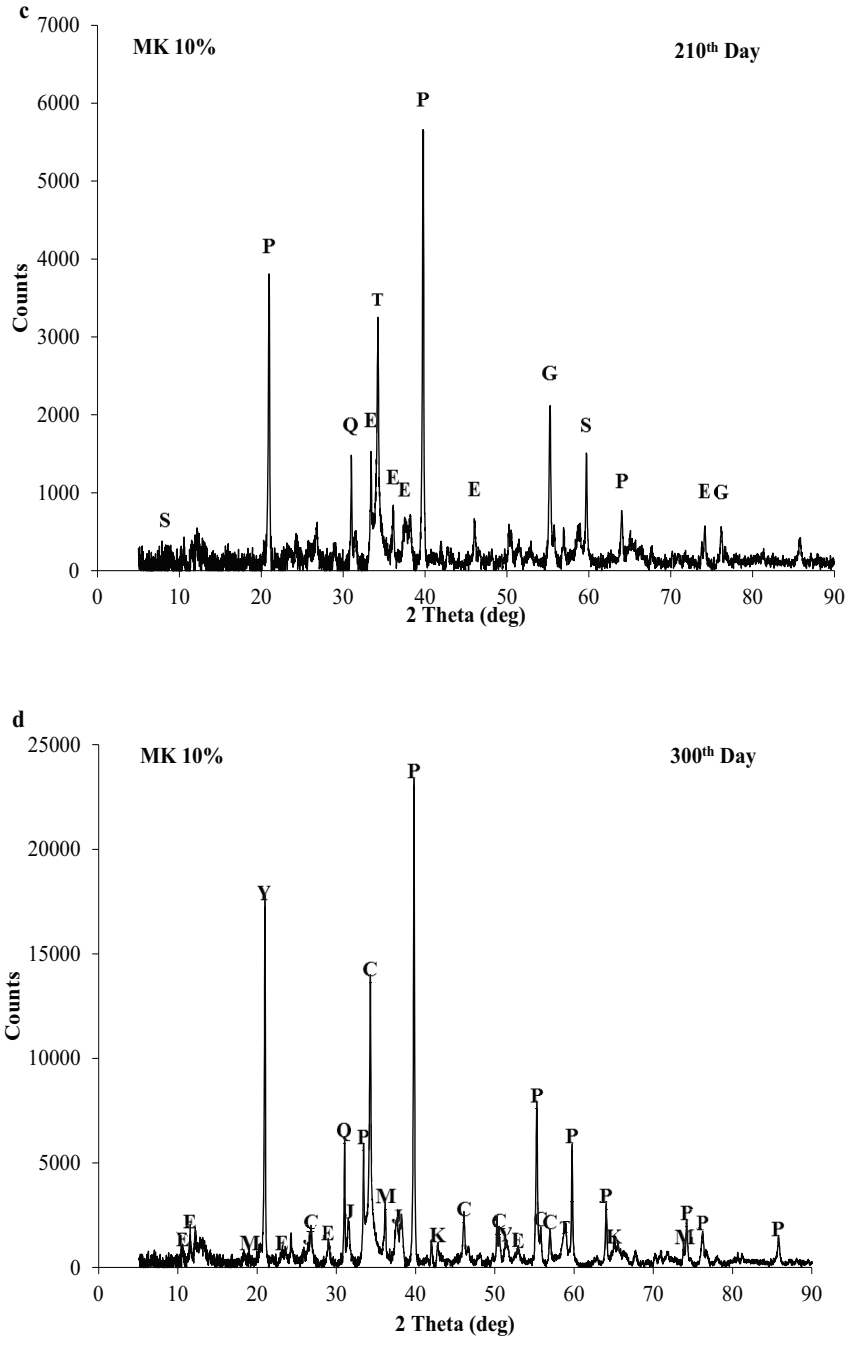

Figure 5.6: X-ray Diffraction Pattern for 10% Metakaolin mix; a) 60th day; b) 120th day; c) 210th day; d) 300th day.

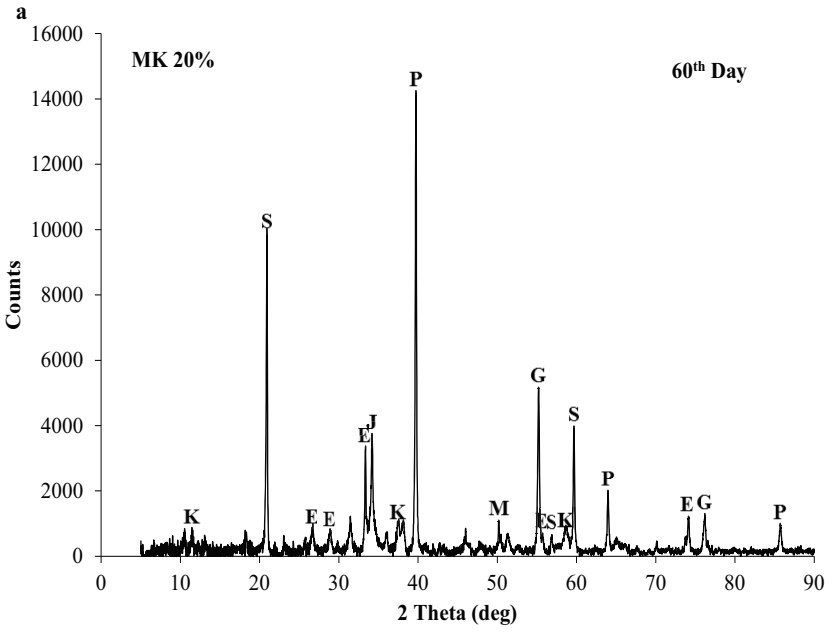
a
MK 20%
60th Day
Counts
2 Theta (deg)
P
S
G
S
J
E
P
K
E
E
K
M
E
S
K
E
G
P

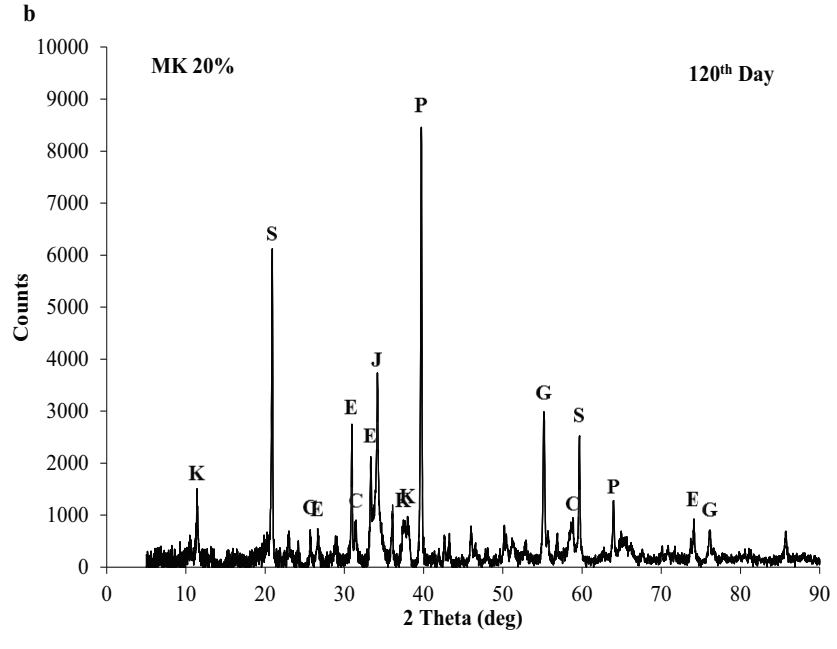
b
MK 20%
120th Day
Counts
2 Theta (deg)
P
S
J
E
E
G
S
K
P
E
G

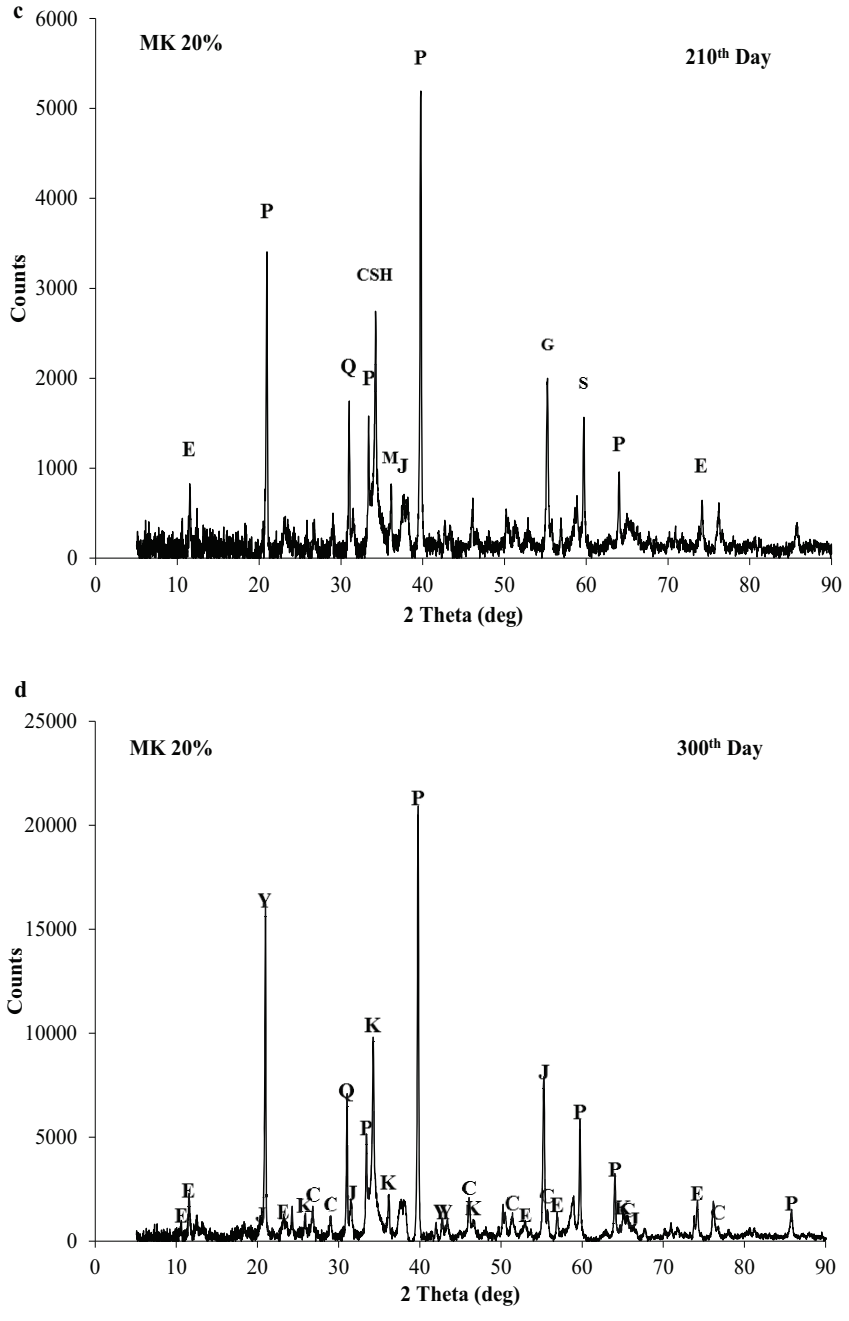

Figure 5.7: X-ray Diffraction Pattern for 20% Metakaolin mix; a) 60th day; b) 120th day; c) 210th day; d) 300th day.

5.3 Quantitative Analysis

Following the comprehensive identification of the crystalline phases as discussed above, their relative proportions were determined through Rietveld Quantitative X-ray Diffraction (RQXRD). The Rietveld method gives the sum of the phases fraction normalised to 100% crystalline phases, while the amorphous content is usually not included (Torre et al. 2003, Gualtieri et al. 2006). If amorphous phases are present and not included in the analysis then the weighted fraction of the crystalline phases estimated by the analysis will be higher than the true amounts present. This is also expected in the present analysis.

A publicly available software package (generalized structure analysis system) GSAS (Gualtieri et al. 2006) was used to perform the Rietveld refinement by using *pseudo-voigt peak shape function*. GSAS allows for a maximum of nine phases to be refined simultaneously and also requires structural models (CIF) for all the phases as an input, which were taken from the American Mineralogist Crystal Structure Database (AMCSD). The "Shifted Chebyschev Background Function" was used and the other parameters optimised includes: background coefficients, cell parameters, zero-shift error, peak shape parameters (GW,LY) and phase fractions. The "$Chi^{2"}$ factor which is the Rietveld Discrepancy Value and is one criterion for judging the goodness of fit should for the Rietveld plot be close to unity (Toby 2006). The Rietveld refinement plot for 60^{th} days of hydration on some mixes is presented in the (Figure A.7-A.9Appendix A) and the Chi^2 factor values for all the mixes are tabulated in Table 5.6.

Table 5.5: Chi^2 Factor values for Rietveld Plots

Mixes	Chi^2 value			
	60^{th} day	120^{th} day	210^{th} day	300^{th} day
0% Ref	3.150	2.852	3.415	9.206
FA 10%	3.037	3.048	3.185	4.935
FA 20%	3.126	3.278	2.292	6.150
SF 10%	2.224	3.449	2.209	9.968
SF 20%	2.183	3.133	3.758	2.392
MK 10%	3.599	2.352	2.093	4.228
MK 20%	7.068	3.248	1.900	2.855

5.3.1 CH and CSH Phases

Figure 5.8 shows the amount of CH in the reference mix measured by Rietveld method. It can be noticed from the Figure 5.8a that till 120^{th} day the portlandite was about 40% and afterward it start to reduce and at the end it was 20%. This mean the maximum formation of CH had occurred up till 120^{th} day or in other words, the C_3S and C_2S has been fully consumed by 120^{th} day. The reduction noticed in CH content in the later stages is likely due to the consumption by other hydrated products.

Here, it is worthwhile to discuss the findings of other researchers, who examined materials other than cement-based foams. For instance, Korpa et al. (2009) reported CH was about 15% in the cement paste (without aggregates) after 28 days of hydration. Jozić et al. (2010) cites 14.5% for the same parameter at 90 days, which changed only slightly to 14% at 310 days. Note that these authors had used the differential thermal analysis (DTA) and thermo gravimetric analysis (TGA) technique for measurement. Scrivener et al. (2004) reported the content of CH measured at 28^{th} day for ordinary Portland cement was 22% by weight and Mehta et al. (2006) has

given a figure of 20%–25% CH, for the hydrated cement paste of ordinary PC. In the present study, the corresponding value for CH content was 25% higher than the values cited above at 60 days and 11% higher for 300 days. This apparent difference is likely because the amorphous fractions are not accounted in QXRD, due to which the amounts of the crystalline phases estimated during the analysis gives higher values than the true amounts present.

On the other hand fly ash mixes shows decline in the weighted fraction of CH when compared with the reference mix except for the 300th day data. This reduction is due to the fact that the alumina and silica composition of fly ash consume CH of Portland cement to form more CSH and other products like strätlingite (S), hydrogarnet (C_3AH_6) and ettringite ($C_3A{\cdot}3CS{\cdot}H_{32}$). Furthermore, it was also noticed that the CH value decreases with the increased percentage of fly ash. This difference noticed was 6% for the measured hydration period which cannot be marked as significant.

It is worthwhile mentioning here that the CH content as found in this study was double of as reported by Jozić et al. (2010) for cement mortar with 20% of fly ash replaced by cement by mass. The latter reported CH content equals to 15.5% after 60 days of hydration, 16.5% at 90 days and 12% after 300 days.

From Figure 5.8b it is clear that the addition of silica fume reduces the amount of CH and can be noticed for the entire period of hydration. Silica fume is highly rich in silica and it react with calcium hydroxide CH of Portland cement to form CSH in larger quantity. This mean in the presence of silica fume the consumption of CH is more as compared to reference.

In addition of this it was also noticed that the addition of silica fume in higher substitution reduces the CH amount and the difference recorded was 6% but for 300th day the maximum difference of 10% was measured. This compares well with the findings of Cheng-yi et al. (1985) and Zhang et al. (1991), who have also reported 6% and 7.5% drop in CH values with higher silica fume content.

Furthermore, it can also be said that till 60th day the consumption rate of CH was slow for the both 10% and 20% SF (silica fume) mixes. As expected in both cases, the rate of CH consumption increased with hydration.

Figure 5.8c shows the weighted fraction for portlandite (CH) in the mixes containing metakaolin is shown as a function of hydration time. As compared with 0% reference it was noticed that calcium hydroxide, CH, drops significantly up to 120th day. The drop was in the range of 10-15% for 10% MK and 14-20% for 20% MK. Later at 210th days of hydration, a reversal of action that is, a rise in the CH values was noticed. However, the drop in CH content was once again seen. Siddique et al. (2011) explained this increase in calcium hydroxide (CH) content due to the Portland cement hydration, while the decrease later on is likely due to the dominance of the pozzolanic reaction. Moreover, it was also noticed that as the substitution ratio of metakaolin increases, the CH content decreases, similar observations were recorded for other pozzolanic admixture also. The maximum drop recorded between the two mixes was 10% at 210th day and for other hydration time period it was 6%. Wild et al. (1997) showed that higher substitution of metakaolin reduces the CH content significantly and observed that with the addition of 15% metakaolin, 50% reduction of CH content was found in the paste after one year of curing.

Furthermore, the CH level was almost constant for 20% MK mixes throughout the measured hydration period this implies that CH was consumed much earlier than 60^{th} day. Therefore, it can be said that metakaolin pozzolanic activity rate is quite fast as compared to other pozzolanic admixture; Siddique et al. (2011) also reported the same.

In studies by others (Kostuch et al. 1993, Ambroise et al. 1994), who investigated the influence of MK in concrete mixes, a significant reduction of CH was observed and in fact, at 20% dosage, all CH was removed and converted by 28 days. Frías et al. (2000) have reported that for 10% and 20% substitution of metakaolin, an inflexion point at 90 and 180 days was observed.

Beyond this point, the calcium hydroxide content remained constant or increases progressively. In addition to this it was further reported that level of CH recorded for 10% substitution was 15.5%, 14.8% and 16% respectively for hydration time of 60,100 and 365 days respectively. In the same study, for the 20% MK substitution, the corresponding values were 10%, 9% and 9%.

However, present study CH amounts recorded was two times more for 10% and three times more for 20% metakaolin mix for the same hydration time. Therefore, it can be said that present study CH is quite high as compared to other researchers finding and reason being overestimation by Rietveld method for not accounting the amorphous phases.

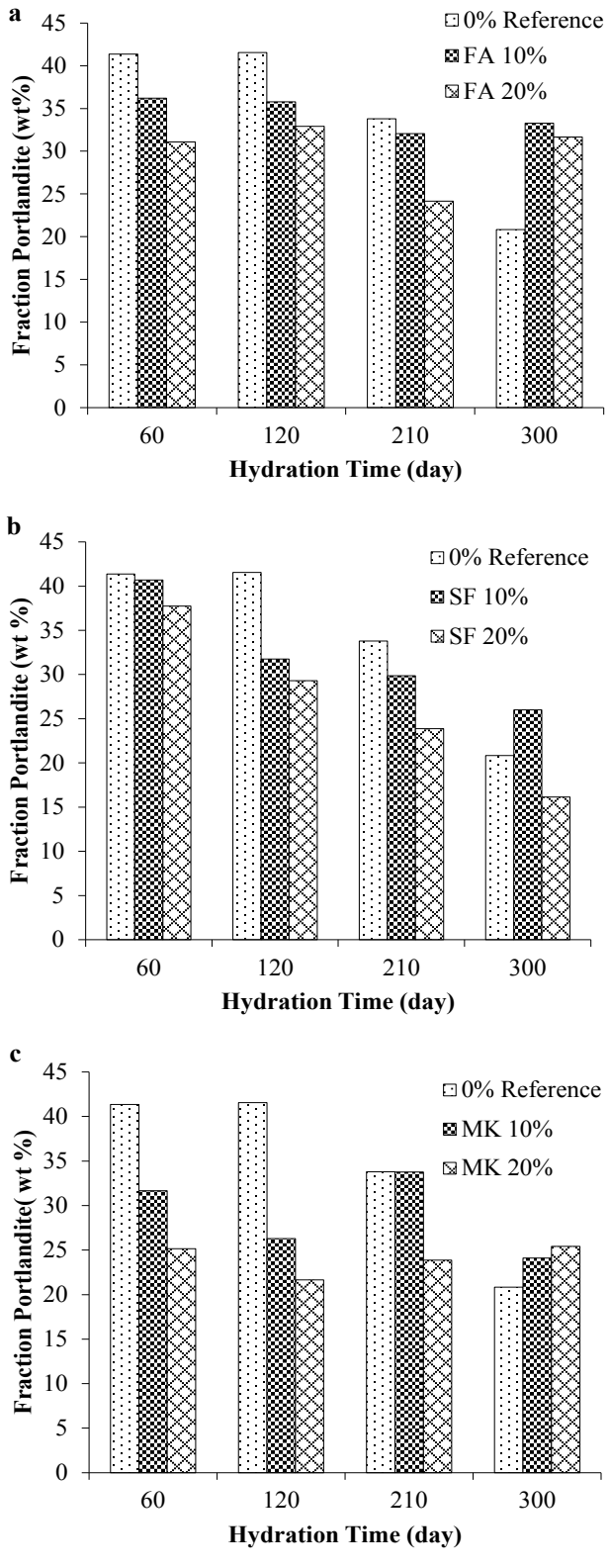

Figure 5.8: Time-dependent formation of portlandite (CH); a) Fly Ash mix; b) Silica Fume mix; c) Metakaolin mix.

As mentioned earlier, the quantitative evaluation of CSH from RQXRD is difficult because of its typically amorphous or semi crystalline nature. Thus, the quantities were evaluated indirectly employing the Rietveld method. The related hydrated products like tobermorite, jennite, clinotobermorite and xonolite which are related with CSH in chemical composition and are semi crystalline in nature were measured by Rietveld Quantitative X-ray diffraction (RQXRD) analysis and their sum is taken as calcium silicate hydrates (CSH) for all the mixes. The graphs plotted in Figure 5.9 shows the amount of CSH measured in the present study by Rietveld Quantitative X-ray Diffraction (RQXRD) analysis. It can be noticed for reference mix, the formation of CSH is a function of time, as the hydration time increase, the level of CSH increases. The maximum rise recorded between 120 to 210^{th} day was of 10% and the inflexion point was noticed at 210^{th} day beyond which formation of CSH becomes constant.

Recently, Soin et al.(2013) measured the CSH value (amorphous content included) on ordinary Portland cement paste alone and found the CSH equals to 62% by mass at the 56^{th} day of curing. However, the present study shows that the CSH values are almost low in comparison. It can be noticed from Figure 5.9a that the content of CSH increases with the addition of fly ash when compared with 0% reference mix and this increase was more pronounced with higher substitution. An inflexion point was noticed at 120^{th} day for 10% substitution with fly ash and after 300^{th} day for 20% substitution, thus indicating the end of pozzolanic activity.

Subsequently, when silica fume was added in the proportion of 10% and 20% it was found that higher substitution increases the level of CSH, this indicate the reaction between calcium hydroxide and amorphous silica in the SF. The percentage difference recorded in the content of CSH between

the two mixes was 13% with maximum on 210th hydration day. At the stage of 60th day the difference in the CSH level due the two mixes was not very pronounced but as the time increases the difference becomes significant. In addition to this the inflexion point was noticed at 210th day for 10% and 300th for 20% substitution. This shows that the consumption rate or reactivity becomes slow in the presence of silica fume but accelerates with time. Similar conclusion has been reached by Cheng-yi et al. (1985), Li et al. (1985), Siddique et al. (2011), Thomas (2013).

Figure 5.9c is for the cases of MK substitutions at 10% and 20%. Unlike in the above two cases with MK, the CSH amount increases significantly even at 60 days, compared to the reference mix. The difference compared to the correspondence values for the reference mix being as much as 20% after 210 days. There is a levelling off the CSH amount thereby indicating that the pozzolanic activity has ended.

Qualitatively speaking, the rise and fall of CH and CSH is in agreement with the findings of earlier research on regular paste or concrete, but quantitatively, the present study has shown higher amounts of CH and CSH compared to previous studies. This is due likely to the adoption of the XRD techniques which in this case is crystalline orientated analysis.

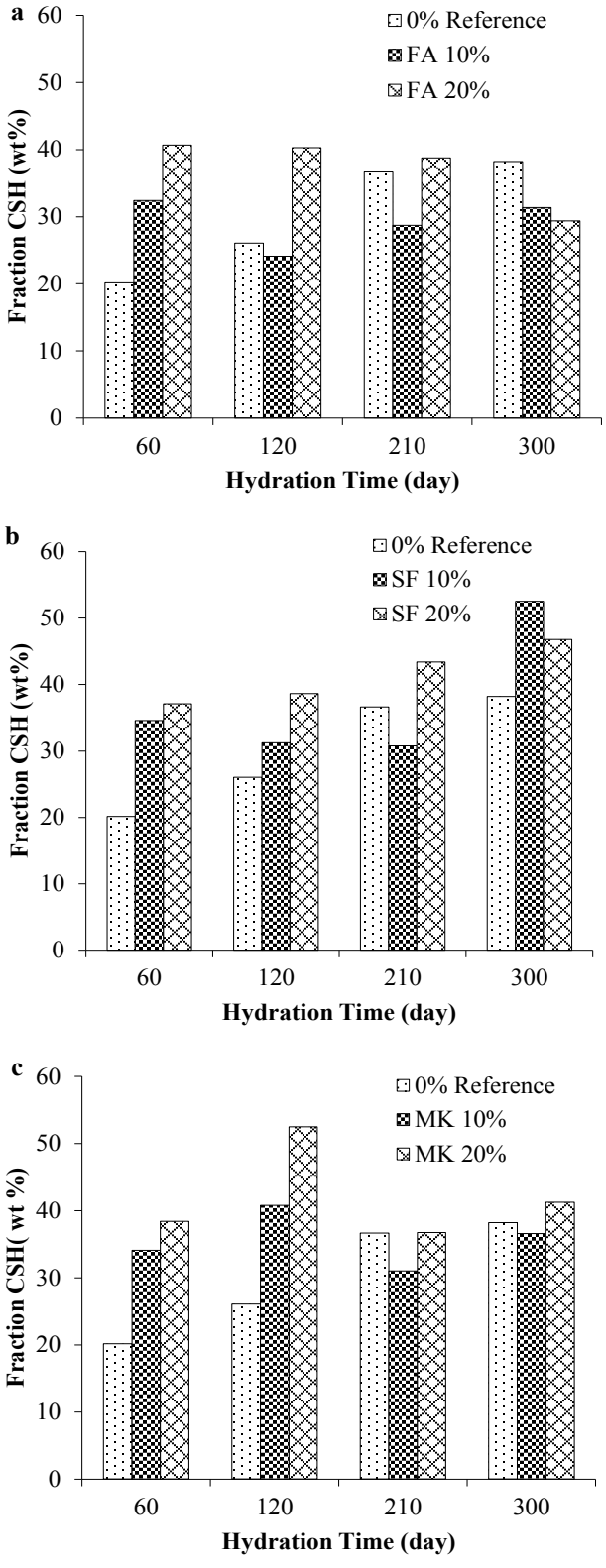

Figure 5.9: Time-dependent formation of calcium silicate hydrate (CSH); a) Fly Ash mix; b) Silica Fume mix; c) Metakaolin mix.

5.3.2 AFt and AFm Phases

The trisulfatehydrates ($C_6A\hat{S}_3H_{32}$) or ettringite (AFt) phase is formed due to the reaction of tricalcium aluminate phases (C_3A) of the clinker, water and calcium sulphate (gypsum). The monosulfate hydrate (AFm) phase is formed from AFt and additional tricalcium aluminate (C_3A) or calcium aluminate ferrite (C_4AF) or, in other words, trisulfate hydrate (AFt) or the ettringite gets converted to the monosulfate hydrate (AFm) in this period (Kosmatka et al.2003, Siddique et al.2011, Bapat 2013).

Figure 5.10 depicts the time dependent development of ettringite crystalline phases in mixes with and without pozzolanic admixture. It can be noticed from Figure 5.10a that there is a pronounced difference between the ettringite content of 0% reference and fly ash mixes. This difference can be anticipated due to the reaction between CH of portlandite, water, gypsum and non-crystalline alumina component of fly ash or in other word pozzolanic reaction. The general trend of decreases with the hydration time was noticed in the ettringite content for 0% reference and 10% fly ash mix decreases except at 120^{th} day when rise was noticed but of nominal percentage. Beside this 20% fly ash mix gradually increases with time this shows that the formation of ettringite gradually increases with higher substitution of fly ash.

Korpa et al. (2009) measured the amount of ettringite in regular Portland cement and found the level equal to 3.5% by weight after 28 days of hydration. Comparatively, the amount of ettringite noticed at 60^{th} days in the present study was less than 2%.This mean the amount of ettringite decreases with time, similar observations were reported by Siddique et al. (2011) also.

For mixes containing silica fume, it was noticed that the higher substitution of 20% gradually increases the ettringite contents up to 210th day and beyond that point it becomes constant. In the case of mix with 10% silica fume, the ettringite increases up to 120th day and afterwards decreases. It is important to note here that the formation of ettringite in the presence of silica fume is mainly due to the reaction of aluminate phases of the Portland cement clinker since the SF is high in silica and has only nominal amount of alumina. This is borne out by the fact that till the 120th day, the ettringite content for the both silica fume mixes and the reference mixes was almost same.

It is after this period that the difference in ettringite between the reference and SF mixes becomes visible because of the formation of other silica based products taumasite ($Ca_3Si(CO_3)(SO_4)(OH)_6 12(H_2O)$) and others which also belongs to AFt group and have silica present in their composition.

Figure 5.10c shows the picture of ettringite amounts at various periods and with different MK content. It can be noticed that, after 60 days, the ettringite content was more dominating in the case of mixes with metakaolin of both 10% and 20% substitution. This was as expected for metakaolin is highly rich in alumina, being almost 40%. In addition to this from the 120th day onwards, the ettringite content for both series of metakaolin percentages 10% and 20% remains mostly constant. It indicates thereby that full consumption of alumina has been reached.

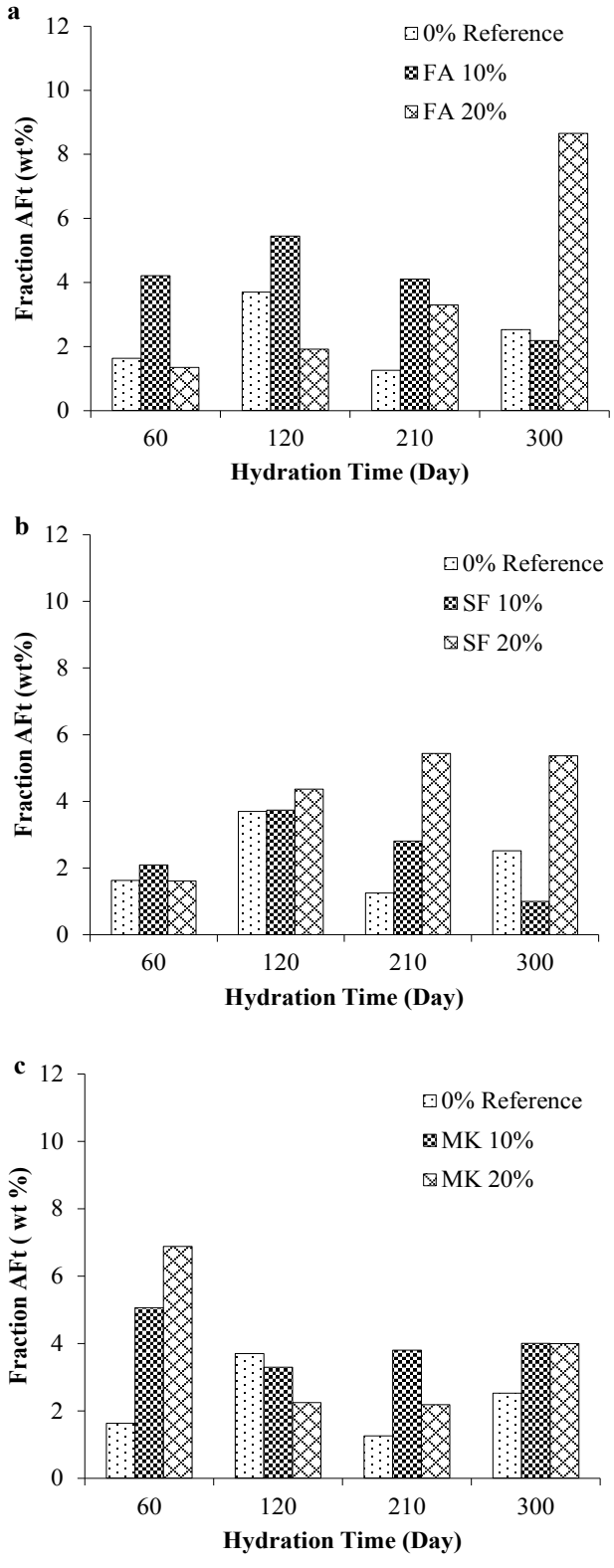

Figure 5.10: Time-dependent formation of Ettringite (AFt); a) Fly Ash mix; b) Silica Fume mix; c) Metakaolin mix.

Figure 5.11a depicts the time-dependent development of strätlingite (AFm) crystalline phases in the reference mix and the fly ash mix. It can be noticed that the strätlingite content in the reference and mix with 10% fly ash mix did not vary significantly over the period of time. Whereas, the mix with 20% fly ash substitution decreases during the period of 120 to 210th day and afterwards it increases. This dip indicates that the other hydrated products are also forming during the same period of time, for instance ettringites the rise in the content can be noticed in Figure 5.10a during the same period of time. From earlier research it is known that strätlingite is formed when all content of CH is consumed in the pozzolanic reactions or when a local deficiency of CH occurs (Snellings et al. 2012).

Following this, Figure 5.11b shows the measured contents of strätlingite (AFm) developed over the passage of time in the presence of silica fume. It is noticed that the content of strätlingite progressively increases with the passage of time except at 210th day where decline was noticed. Beside this, it was also observed that the 10% silica fume substitution resulted in higher content which could be due to quick consumption of CH. Simply, it can be said that formation of strätlingite in silica fume mix is the function of CH.

Similar findings were recorded when metakaoin was added in 10% and 20% ratio, strätlingite increases as the CH content decreases. According to Snellings et al. (2012) when metakaolin is added in the mix then the deficiency of Ca $(OH)_2$ and the recombination of alumina and silica with Ca_2^+ become the reason for the formation of strätlingite.

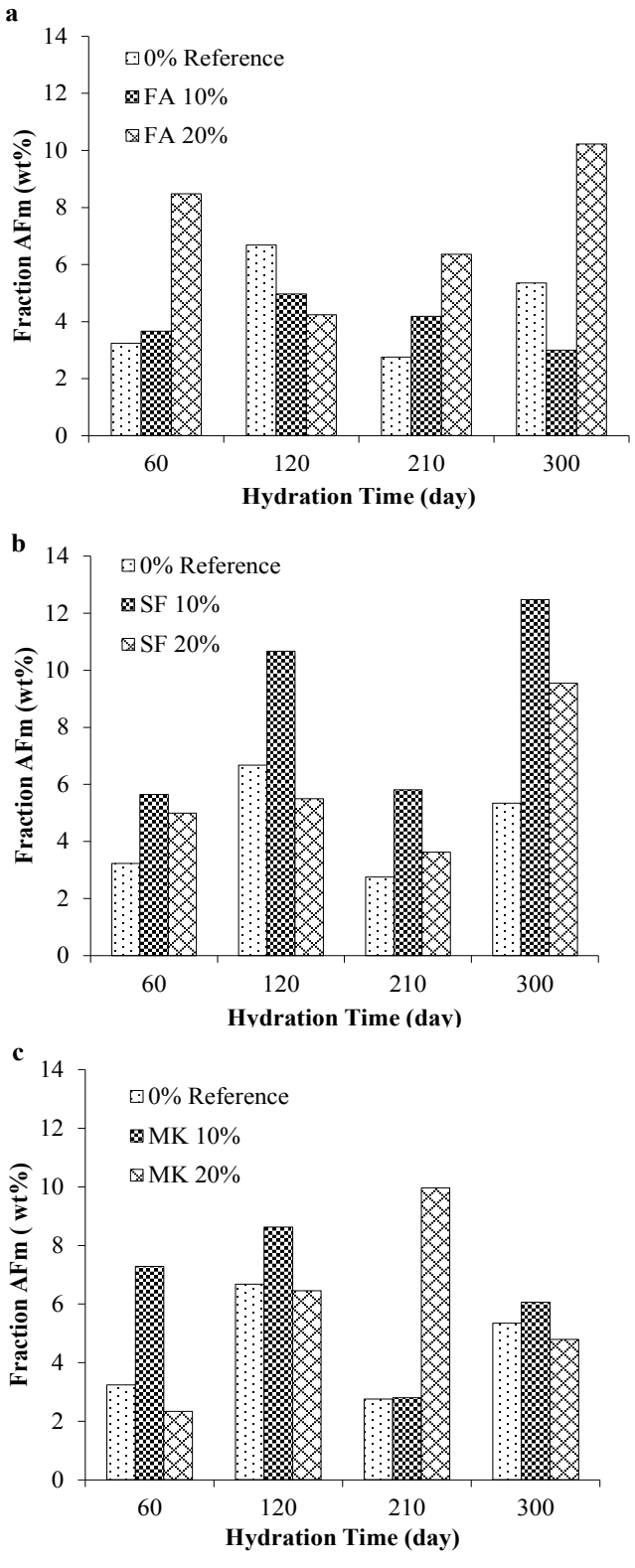

Figure 5.11: Time-dependent formation of Strätlingite (AFm); a) Fly Ash mix; b) Silica fume mix; c) Metakaolin mix.

5.3.3 Calcite Phases

Figure 5.12a shows the calcite phases evaluated during the analysis for the 0% and fly ash both mixes. Calcite is formed when CH reacts with the atmospheric carbon dioxide (Bapat 2013). It can be observed from the Figure that the content of calcite in the 0% reference did not differ significantly in fact it remained almost constant over the entire hydration time. Same was noticed for fly ash mixes except for 300^{th} day when rise in the content of calcite was noticed for 10% fly ash mix. A similar trend for calcite was noticed with mixes containing metakaolin as was recorded for fly ash at corresponding dosage of the pozzolanic admixture. However, in case of MK, there is a sudden rise in calcite content at 210^{th} days. That is, the rise occurred earlier than in case of the mixes with fly ash. Although it is difficult to explain this sudden rise in the calcite content at a specific time period, it is likely due to the fact that in the present study, the samples were left exposed to atmosphere.

As regards silica fume, no consistent or definable trend in the quantity of calcite formed is noticed. It can be seen that the calcite was low at 60^{th} days and 300^{th}days, but high at 120^{th} and 210^{th} days. During the (RQXRD) analysis, other phases like Gypsum, Quartz and Gismondine were also identified and the graph for these phases are presented in Figure A.10-A.12 (Appendix A).

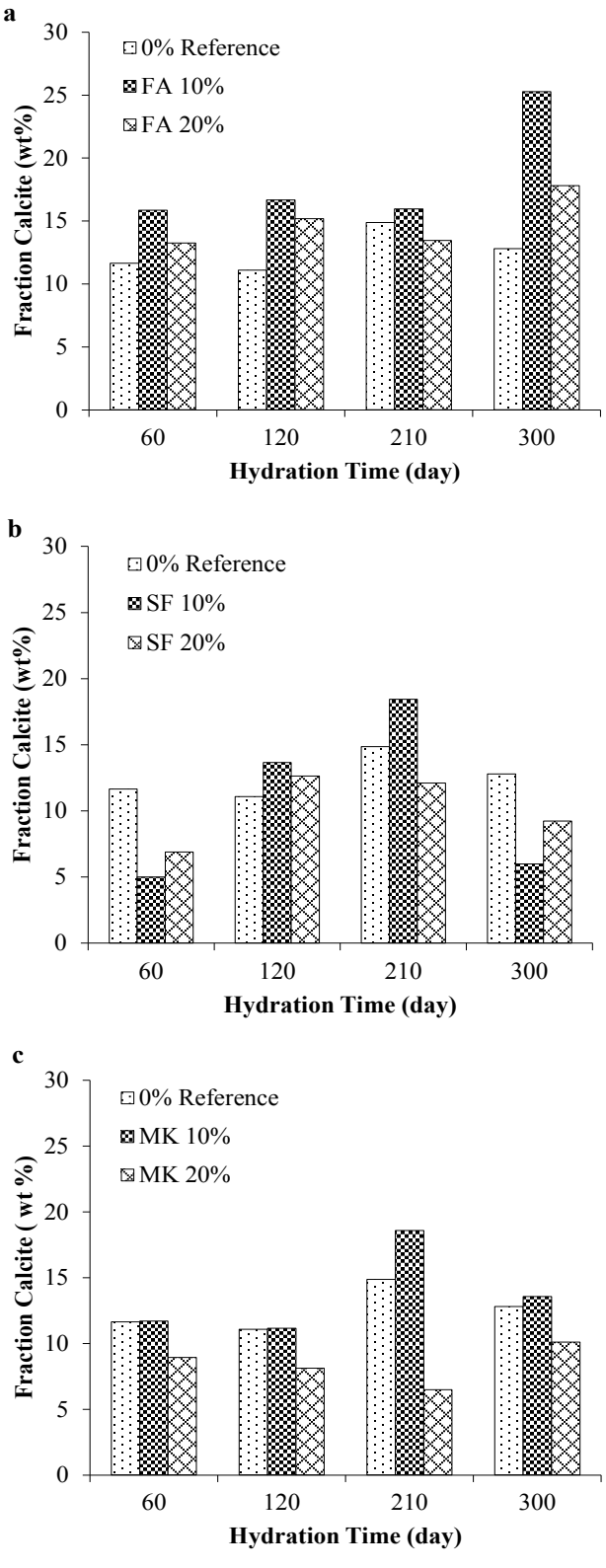

Figure 5.12: Time-dependent formation of Calcite; a) Fly Ash mix; b) Silica fume mix; c) Metakaolin mix.

Table 5.6: Details of Phases used for RQXRD

Phases	Identified in Mixes	Thermal Conductivity (w/m/k)	Mineral Group	Reference
Portlandite	All mixes	0.13	Brucite	http://www.brucite.cn/products_8.php
Ettringite	All mixes	0.17	Sulfate	http://www.engineering.com/Library/
Calcite	All mixes	2.6	Calcite	Straube et al. 2011
Gypsum	0% Ref, 10% FA, 20% FA	0.17	Sulfate	http://www.engineering.com/Library
Quartz	10% MK, 20% MK	0.15	Quartz	Hamdhan et al. 2010
Kuzelite	10% SF, 20% SF	0.10	Zeolite	Murashov et al. 2002
Stratlingite	All mixes	0.10	Zeolite	Murashov et al. 2002
Jennite	All mixes	0.18	Tobermorite	Straube et al. 2011
Tobermorite /Plombierite-14A	All mixes	0.18	Tobermorite	Straube et al. 2011
Clinotobermorite	All mixes	0.18	Tobermorite	Straube et al. 2011
Gismondine	All mixes	0.10	Zeolite	Murashov et al. 2002
Xonolite	0% Ref, 20% FA	0.18	Tobermorite	Straube et al. 2011

5.4 Model of Thermal Conductivity for Hydrated Products

The weighted fraction for CH, CSH, AFt, AFm and other phases were estimated in the foregoing Section 5.3. The values for these hydrated products fractions depend upon the hydration time and on the substitution ratio of the pozzolanic admixtures. Therefore, by using these weighted fractions, the thermal conductivity of hydrated products can be evaluated by using the following rule of mixture expressed in Equation 5.1.

$$K_{HP}(t) = K_{CH}W_{CH}(t) + K_{CSH}W_{CSH}(t) + K_{AFt}W_{AFt}(t) + K_{AFm}W_{AFm}(t) + K_{cal}W_{cal}(t) + K_{oth}W_{oth}(t) \quad \text{Eq 5.1}$$

Here, W_{CH}, W_{CSH} ,W_{AFt} ,W_{AFm} ,$W_{cal,}$ W_{oth} is the weighted fraction (%) for CH, CSH, AFt, AFm, calcite and other phases. In addition to this K_{CH}, K_{CSH} , K_{AFt} , K_{AFm} , $K_{cal,}$ K_{oth} (w/m/k) are the thermal conductivity for CH, CSH, AFt, AFm, calcite and other hydrated products, respectively, after hydration to age´ t ´. The thermal conductivity of hydrated products is tabulated in Table 5.5 respectively. This table was worked out by assigning to each product, a value of thermal conductivity taken from that of the mineral group to which it belongs. This became necessary since the actual conductivity of every hydrated product was not available from the literature. For instance brucite, which have similar structure and morphology as that of portlandite and belong to same mineral group. Similarly the conductivity of quartz is assumed to be the same as that of fine sand for which data is available.

5.4.1 Validation of Model

Figures 5.13 to 5.16 show the graphs comparing the values of thermal conductivity of the hydrated products as discussed above, using Equation 5.1.The thermal conductivity of the hydrated paste is tabulated in Table 7.1. Figure 5.13 shows the graph for the reference mix and as expected, at up to

120th days, the thermal conductivity of the paste evaluated experimentally is higher than the values obtained using Equation 5.1. This difference of almost 40% could be due to many reasons; the principal reason could be presence of moisture. As the moisture decreases at subsequent ages, the values tend to be the same as seen for 210th and 300th days.

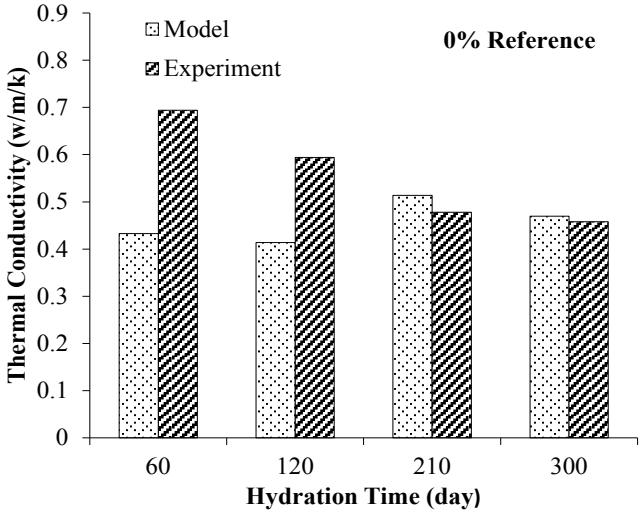

Figure 5.13: Comparison of conductivities between the present study results and model (Eq 5.1) for 0% reference mix.

On the contrary, as per Figure 5.14, with fly ash at both dosages, the thermal conductivities as derived from Equation 5.1 were close to the experimental values, especially at earlier age. On beyond 210th days, we do see a noticeable difference. Interestingly, with addition of fly ash, the values as derived from the Equation 5.1 are higher than the experimental data indicating the opposite trend with respect to the reference mix. This difference appears significant at 300 days. The reason for this apparently strange result could be that at 300 days, the calcite was formed in larger amount and the thermal conductivity of calcite is high among all the hydration products.

Therefore it can be said that calcite plays a major part in governing the thermal conductivity. Similarly, as portlandite and calcium silicate hydrate was found in higher percentage therefore it can be anticipated that these are also playing a major role in conductivity.

Figure 5.14 illustrate the comparison for the 10% and 20% fly ash respectively. It can be noticed for 10% fly ash that the both values were quite close to each other except for 300th day at which rule of mixture values was significantly high which look irrational and same was also noticed for 20% fly ash mix. The reason for this apparently strange result at 300 days could be due to the high amount of calcite formed which also (Figure 5.12a) has the highest thermal conductivity among all the products of hydration. Another reason for this difference could be due to measurement technique for instance, in experimental evaluation composite solid samples of cement paste were used whereas Equation 5.1 takes the individual thermal conductivity of the hydrated products.

Similarly Figure 5.15 shows the predicted and experimental values for the silica fume mixes. Values of thermal conductivity for both SF dosages are more or less the same at initial periods up to 120 days. The values from the experiment are higher than those as derived from Equation 5.1. Only in case of 10% SF at 210 days, there is a jump in the conductivity as derived from the rule of mixtures. Again, since at this period, the calcite level is significant, the mix conductivity is also high as can also be noticed in Figure 5.12b.

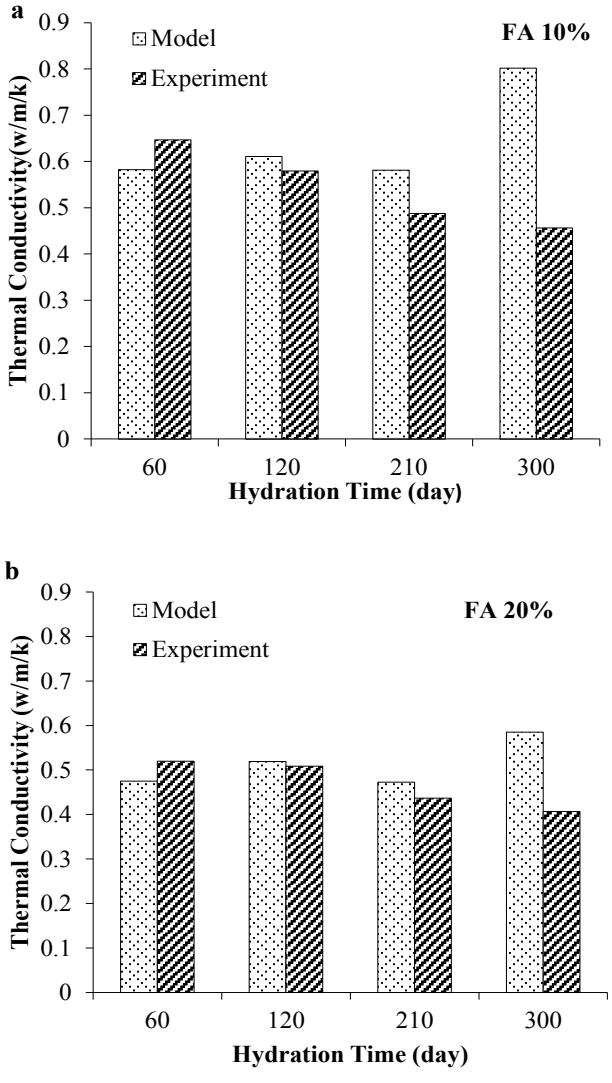

Figure 5.14: Comparison of conductivities between the present study results and model (Eq 5.1) for Fly ash mix; a) 10% FA mix; b) 20% FA mix.

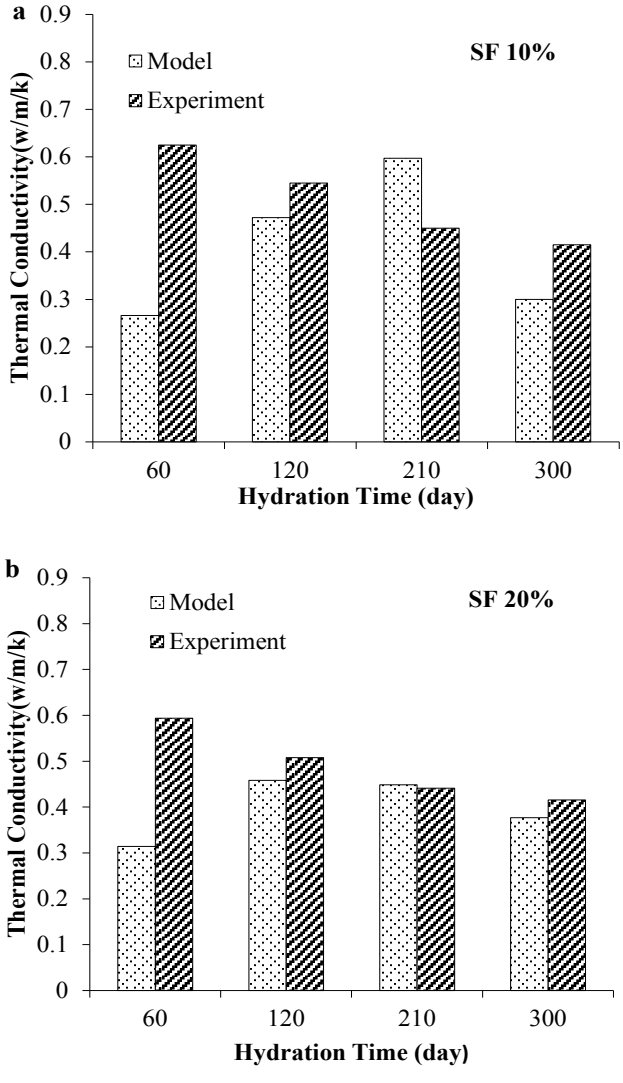

Figure 5.15: Comparison of conductivities between the present study results and model (Eq 5.1) for Silica Fume mix; a) 10% SF mix; b) 20% SF mix.

The conductivity of mixes with metakaolin are plotted in Figure 5.16.As in the previous cases with SF, here too it was noticed that experimental values are higher than or, almost equal to, those derived from Equation 5.1. However, for hydration period of 210 and 300 days in case of the mix with 10% metakaolin, the predicted values are higher. This is similar to the previous cases of mixes with SF and FA.

Overall, it can be concluded that the fraction (weight) of phases calculated by using the crystalline oriented analysis (RQXRD) was accurate. The Rule of Mixtures reveals that if the amorphous content were included in the analysis it will further drop the model values at 210^{th} and 300^{th} day which will result in better agreement with the experiment results. Further it was also noticed that the addition of pozzolanic admixture does not significantly reduces the thermal conductivity. These results have marked questions on previous findings and require further analysis that quantifies both the crystalline and amorphous phases together.

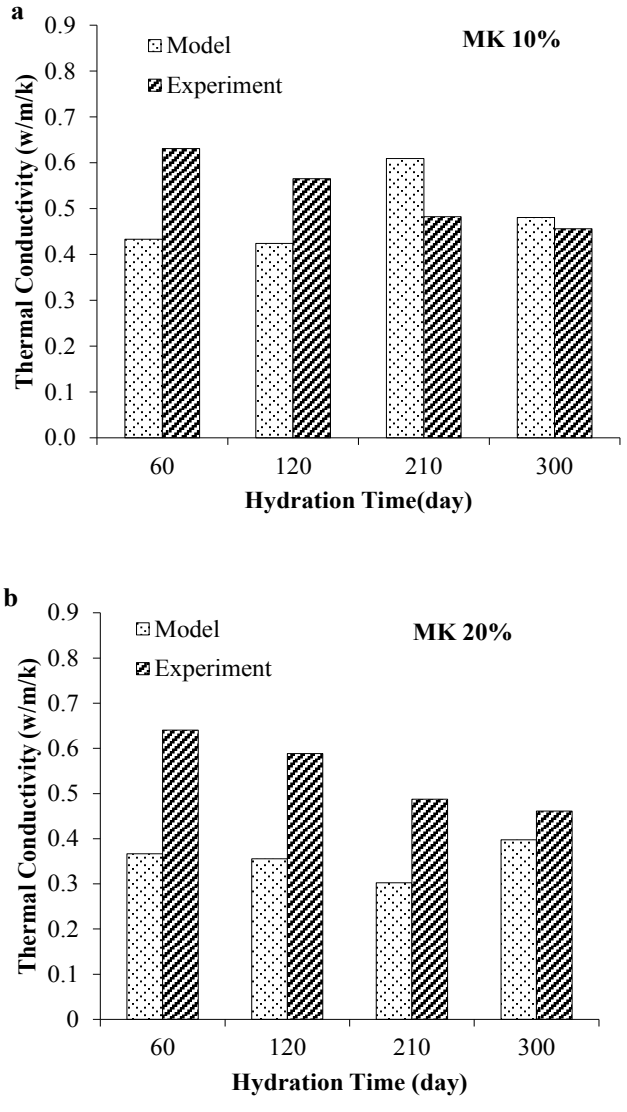

Figure 5.16: Comparison of conductivities between the present study results and model (Eq 5.1) for Metakaolin mix; a) 10% MK mix; b) 20% MK mix.

5.5 Conclusion

- The peak of portlandite (CH) dominates all the hydration periods in the 0% reference mix. The rate of formation of CH was quite fast initially and continued up to 120th day. However, in later hydration stages, other hydrated products appear.

- Formation of silica and alumina related phases were formed in the presence of these pozzolanic admixtures.

- The Rietveld quantitative X-ray diffraction (RQXRD) analysis performed reasonably in quantifying the hydrated product formed in all mixes. The changes and trend noticed in hydrated products in all mixes was in accordance with previous findings.

- The increased substitution ratio of three pozzolanic admixtures does not significantly affect the XRD pattern or the hydrated product, but the peak intensities do decrease/increase with higher replacement.

- The developed model gives reasonable results. The exception was for a few hydration periods when the predicted values were not in accordance with the experimentally evaluated value, which needs to be investigated further.

6. Air-Void Characterization of Cement-Based Foam

6.1 Introduction

The thermal conductivity of a porous material is greatly influenced by geometrical distribution of solid phase and the geometry of the pore structure. The microstructure of cement-based foam also comprises of two phases i.e. solid phase and void phase. Where the pore structure consists of air-voids deliberately introduced in the cement paste by artificial means.

In this chapter experimental result of pore structure parameters like air-void size distribution, air-void spacing and void shape factors with and without pozzolanic admixtures i.e. fly ash, silica fume and metakaolin are analysed and discussed in detail. The quantification of air-void parameters is also evaluated to understand their relationship with density, porosity and the thermal conductivity of the material under investigation. In addition to this the mathematical relationship between the quantified parameters and the density is also derived and presented here.

6.2 Air-Void Distribution of Synthetic Foam

Foam is mainly responsible for the formation of macropores (air-void network) in cement paste when blended together. The past researchers have stated that the foam is composed of bubbles structure (Aldridge 2005, Ramamurthy et al. 2009) and the size distribution is normally less than 1mm. As, no information is available regarding the bubble size of synthetic foam used in this study therefore, it was decided to investigate the foam structure.

In the present study, the synthetic pre-formed foam was viewed through a light microscope, which gave a magnification of 2.5, attached to a computer to get 150 resolutions on 2048 x 2048 pixels. The Figure 6.1 illustrates the bubbles structure of the foam used in this study. The foam samples prepared in the lab were immediately taken for image analysis because the bubbles start collapsing with the passage of time. Due to this difficulty it was decided to use light microscope. Even under this microscope it was hard to record the images, as collapses rate of bubble was too fast because of the heat emerging from the lens in form of light.

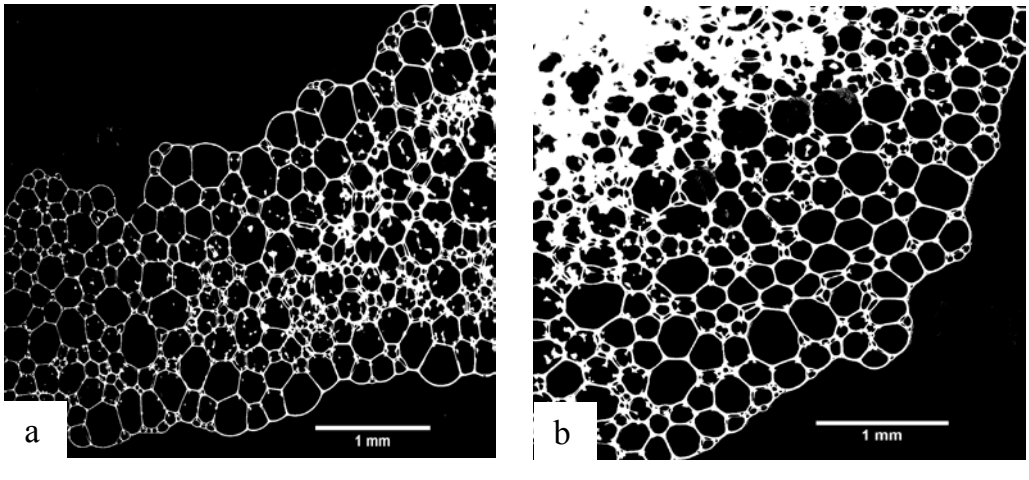

Figure 6.1: a) b) Bubble Structure of Foam

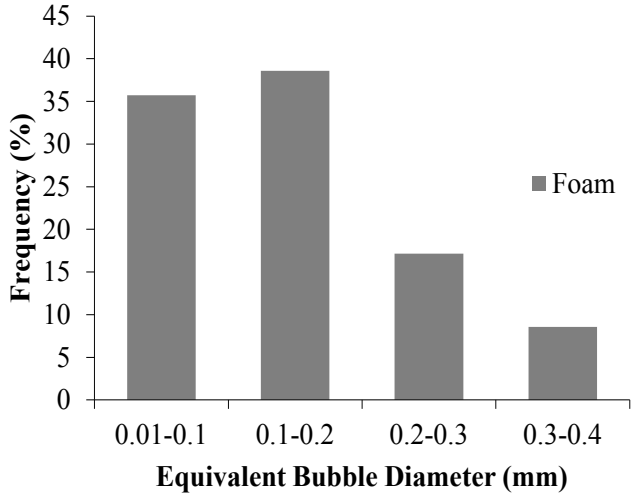

Figure 6.2: Histogram of bubble size distribution of foam.

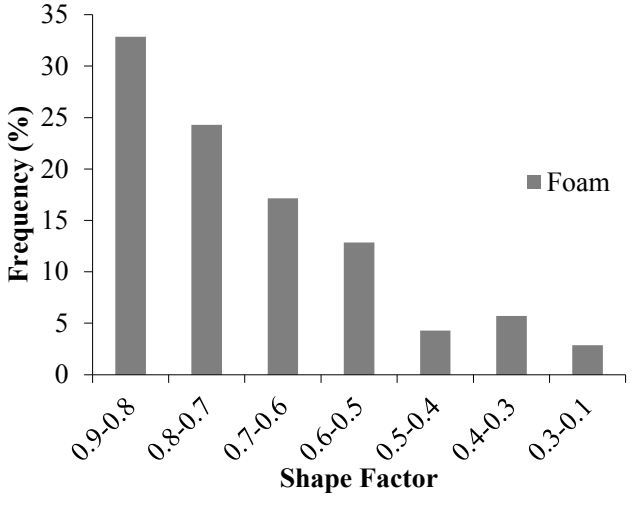

Figure 6.3: Shape Factor for foam bubble.

Afterward, for analysis purposes, six images for the foam samples were captured with the x10 object lens and a pixel representing 1.4 microns and each image covering an area of 1.46 mm x 1.46 mm. The image J Software was used for image analysis and results for area of void and circularity (shape factor) was stored in excel format. The measured bubble area was then analysed to calculate the equivalent circle diameter assuming that the bubbles are nearly perfect circle. Distribution of bubble sizes was determined by plotting a histogram of frequency as a function of bubble equivalent diameter as shown in Figure 6.2. It can be noticed that the 75% size of bubbles lies in the range of 0.01-0.2 mm diameter and remaining 25% lie in 0.2-0.4 mm. Moreover, the maximum equivalent bubble diameter recorded was less than 1 mm, this agrees with the findings of Aldridge (2005) and Ramamurthy et al. (2009) too.

6.2.1 Shape Factor of Synthetic Foam

The shape factor is a measure of how close the shape of the void is to a circle. Therefore, it is evident by the foregoing definition that the shape factor can vary between 1 on the upper limit and 0 on the lower limit. Here, a value of 1 indicates that the shape is a circle whereas a value of 0 indicates the shape as highly irregular. Aligizaki (2006) has expressed shape factor by Equation 6.1 as given below:

$$C = 4\pi A_p / P_p^2 \qquad \text{Eq 6.1}$$

Where P_p is the parameter of the void cross section and A_p is the cross-sectional area and C is the circularity. The Figure 6.3 shows the frequency distribution of shape factor (circularity) for the foam bubbles. From the graph it is evident that the maximum number of the bubbles has the circular shape or is close to one whereas around 10% (0.4-0.1) of the bubbles are irregular or reaching zero value. It is possible that this 10% irregularity in

the shape of the bubbles can be due to the mishandling of the samples. Therefore, it can be easily concluded that the foam used in this study have the bubble structure of almost circular shape.

6.3 Porosity of Cement-Based Foam

As mentioned earlier X-ray tomography technique was used to study the microstructure of cement-based foam and the XRT or CT scan images were collected from each cast density for each mix. The CT Analyser Software was used for 2D morphometry calculation of CT scan images and the results discussed here are based on the average value for 500 images (see chapter 3 for analysis procedure).

The pore system in hardened cement paste can be classified as micropores (1nm to 3nm), mesopores pores (2nm to 50nm), macropores (50µm to 1 mm) (Aligizaki 2006). Whereas, Mindess et al. (2002) has sub divided the last two classes into medium capillary pores (10nm to 50nm) and large capillary pores (3µm to 5µm) respectively. Similarly the pore structure of cement-based foam is also based on these categories whereas the air-voids (macropores) are artificially created by the introduction of foam. The parameter most commonly used to characterize the pore structure of cement-based material is the porosity. The total porosity is defined as a ratio between fractional volumes of pores to bulk volume of the material and is usually expressed in percentage (Aligizaki 2006).

In this study the CT images was able to identify the pores of size $\geq$ 10µm which according to convention may be classified as macropores. This means that other pores including even the largest of capillary pores were below the detection range of highest resolution scans obtained during this project. Therefore, the total porosity in this project explains only the air-

void (macropores) that were introduced primarily due to the presence of the foaming agent. At the age of 300th days the CT images were obtained for the cement-based foam samples for all the seven mixes. These images were analysed with the help of CT An software and the mean of total 2D porosity for 500 images is tabulated in Table 6.1.

The relationship between porosity and density for all the seven mixes of cement-based foam for 300 days is plotted in Figure 6.4. It can be observed that porosity has an inverse relationship with the density. Since the addition of foam reduces the density, one can conclude that the porosity has a direct relationship with foam content. In other words, more amount of foam in the cement mix more is the porosity. It can also be noticed that adding admixture in any cast densities resulted in increased porosity. When measured with respect to reference mix, but the difference was significant for higher densities.

Following this when the porosity of individual mix was compared for the density range of 800-400 kg/m^3. It was noticed that the higher substitution for fly ash increases the porosity and the rise of 5% was noticed between the two substitution ratios of fly ash. This, incidentally, is in agreement with the findings of Siddique et al. (2011) which reported that the higher percentages of fly ash ratios increase the porosity in the cement paste. Similar trend was noticed for both 10% and 20% metakaolin mixes and the increases recorded between the two mixes was 3%.

Siddique et al. (2011) reported that by adding 10% and 20% of metakaolin in cement paste resulted in 3% drop whereas, 3% increase was noticed in this study. However, with regards to silica fume mixes, the trend is consistently a reduction in porosity with more SF in the mix for all densities.

The reduction being 13% to 3% as the SF content increases from 10 to 20% this could be due to micro filling or pore refinement in these mixes. Similar conclusion has been reported by Khan (2003).

Previously, Kearsley et al. (2001a) reported 67% porosity for the cast density of 1000 kg/m^3 for foam concrete with fly ash as admixture. Which is higher as expected when compared with the two mixes of fly ash for 800 kg/m^3 cast density for the present study. Moreover, Awang et al. (2012) evaluated the porosity for light weighted foamed concrete after oven drying the samples for 600 kg/m^3 cast density with 15% and 30% fly ash substitution and reported 69% and 70% of porosity. In contrast, the present study report 71% and 73% porosity for 10% and 20% fly ash replacement which is 2% and 3% higher. Fine sand could be the reason for this small difference.

Finally, it can be concluded that the porosity is influenced by the addition of pozzolanic admixture especially for the higher densities, whereas for lower densities the effect was not significant.

Table 6.1: Measured 2D porosity for the cement-based foam

Mixes	Cast Density (kg/m^3)	2D Total Porosity (%) Mean	ST Dev	COV (%)
0% Ref	800	53.10	0.68	1.27
	600	65.77	0.76	1.15
	400	79.60	1.09	1.37
FA 10%	800	62.20	1.06	1.70
	600	71.40	0.33	0.46
	400	80.00	0.72	0.90
FA 20%	800	67.70	1.92	2.84
	600	73.50	0.37	0.50
	400	82.20	0.59	0.72
SF 10%	800	66.19	0.40	0.60
	600	74.53	0.52	0.70
	400	84.10	0.72	0.85
SF 20%	800	55.20	0.81	1.48
	600	69.14	0.85	1.23
	400	77.42	1.41	1.82
MK 10%	800	62.84	1.24	1.97
	600	71.19	0.86	1.20
	400	80.00	2.56	3.20
MK 20%	800	64.06	0.69	1.08
	600	73.44	2.20	3.00
	400	83.08	0.37	0.45

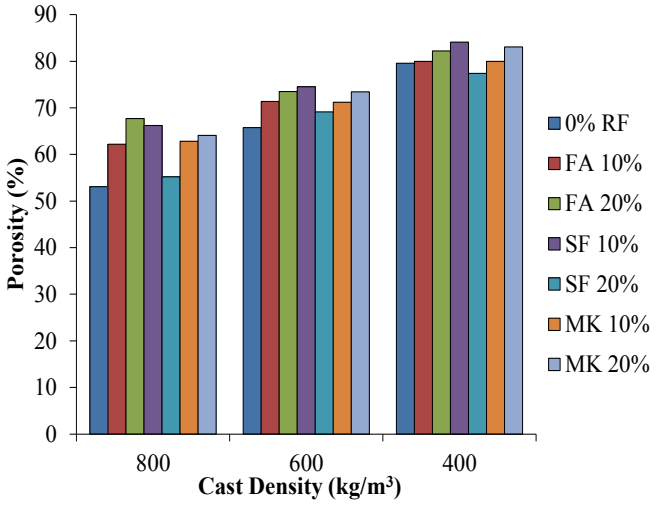

Figure 6.4: Relationship between the porosity and the cast density.

Equation 6.2 below is one way of theoretically calculating the porosity of porous materials as mentioned by Do et al. (2007) and Mydin (2010).While studying the porosity of building materials like hydrated calcium silicate board and lightweight foamed concrete.

$$P_p = (\rho_{solid} - \rho_{porous\ material})/\rho_{solid} \qquad \text{Eq 6.2}$$

where,

ρ_{solid} = density of solid part (kg/m^3)
$\rho_{porous\ material}$ = density of porous material (kg/m^3)
P_p = porosity (%)

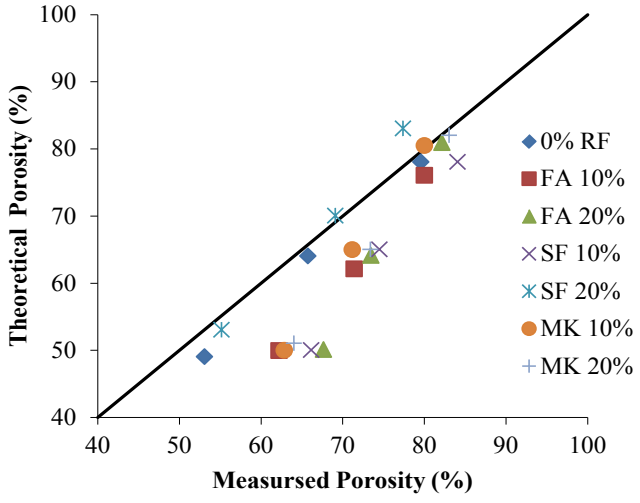

Figure 6.5: Comparison between the measured and the theoretical porosity (Eq 6.2).

The Equation 6.2 was applied on the present study porosity data and the comparison between measured and theoretical porosity is shown in Figure 6.5.It can be noticed that the equation predicts well for the higher porosities but for lower range of porosities, a significant difference was noticed. Comparatively, only the reference mix and the 20% silica fume mixes were found in good agreement for all the ranges of porosity with the predicted values. But, for other cases of admixtures, including the 10% SF series, the experimentally determined values differ widely from the theoretical prediction. Therefore, it can be said that the Equation 6.2 is not reliable enough to be applied for all cases of porosity or pozzolanic admixture examined here.

6.4 Scanning Electron Microscopic Image

Figures 6.6 to 6.12 show the SEM images for all the seven mixes. These images have been magnified x150 to bring out the clear picture of the microstructure of voids and solid phases in cement-based foam. In general, it can be easily noticed from all mixes that the higher densities have more uniform well defined pore structure with different size distribution as compared to lower densities. Actually, as the density decreases the number of pore increases resulting in more merging and overlapping of the pores. The picture of pore structure of cement-based foam with admixtures shows clearly that with addition of any of the pozzolanic admixtures, the shape, the number, uniformity and distribution of pores improved. This improvement is best seen in mixes of higher densities.

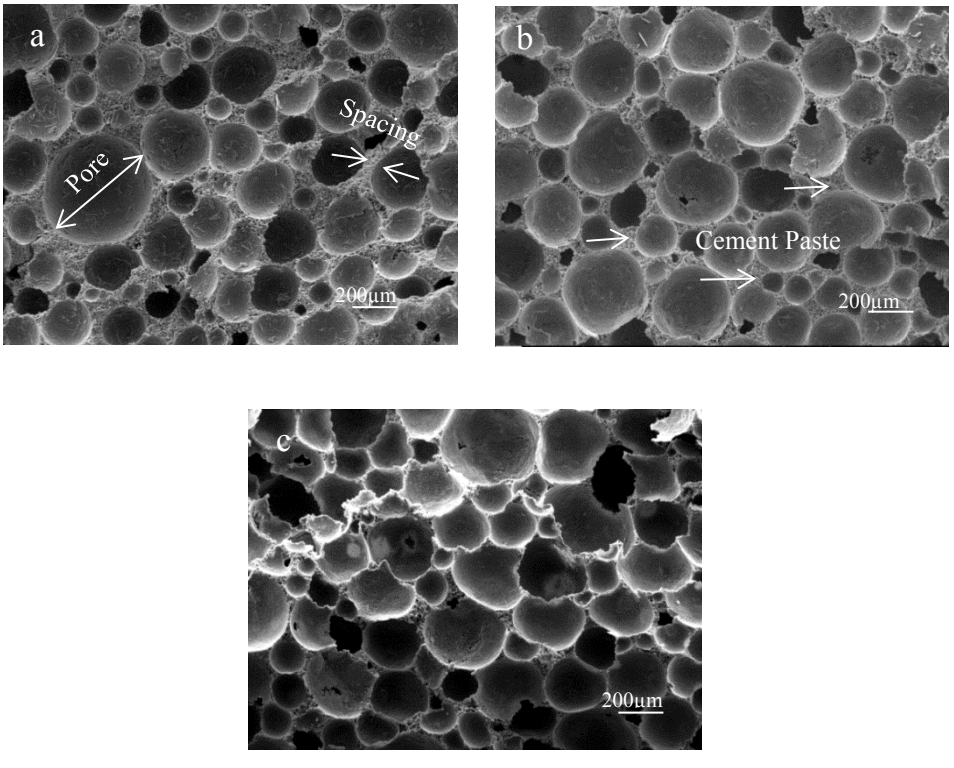

Figure 6.6: SEM images for 0% reference mix; a) 800 kg/m^3; b) 600 kg/m^3; c) 400 kg/m^3.

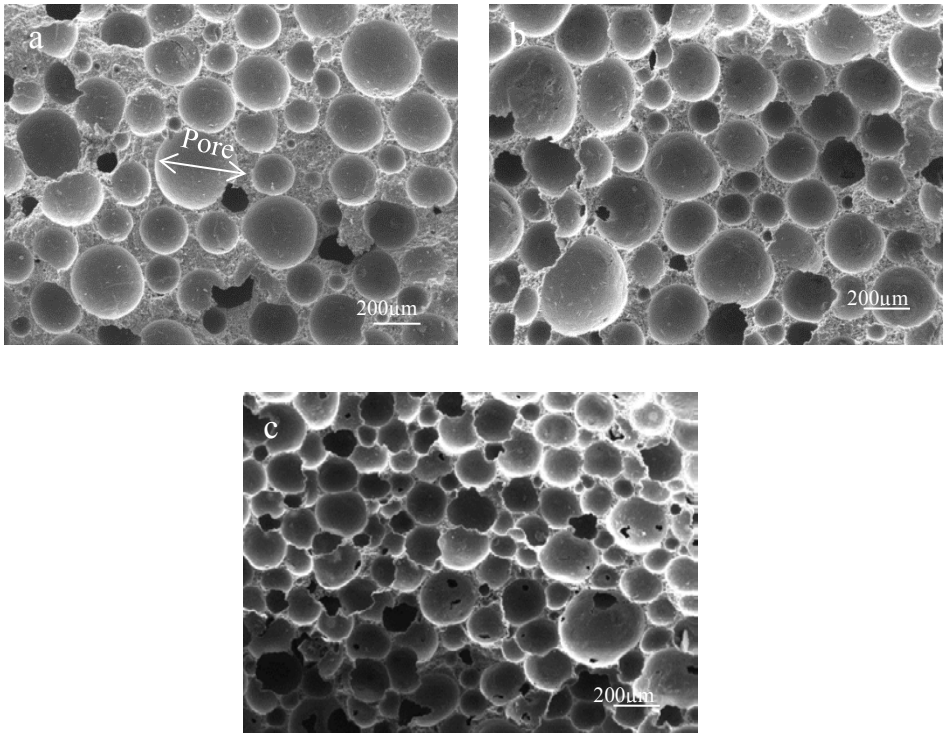

Figure 6.7: SEM images for 10% Fly Ash mix; a) 800 kg/m^3; b) 600 kg/m^3; c) 400 kg/m^3.

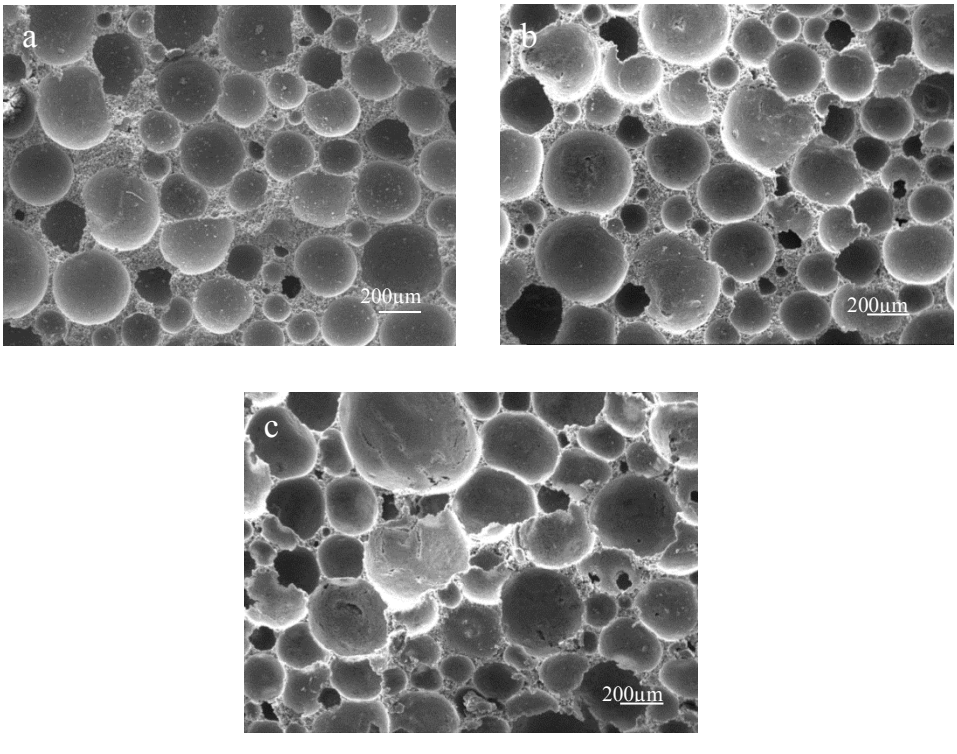

Figure 6.8: SEM images for 20% Fly Ash mix; a) 800 kg/m^3; b) 600 kg/m^3; c) 400 kg/m^3.

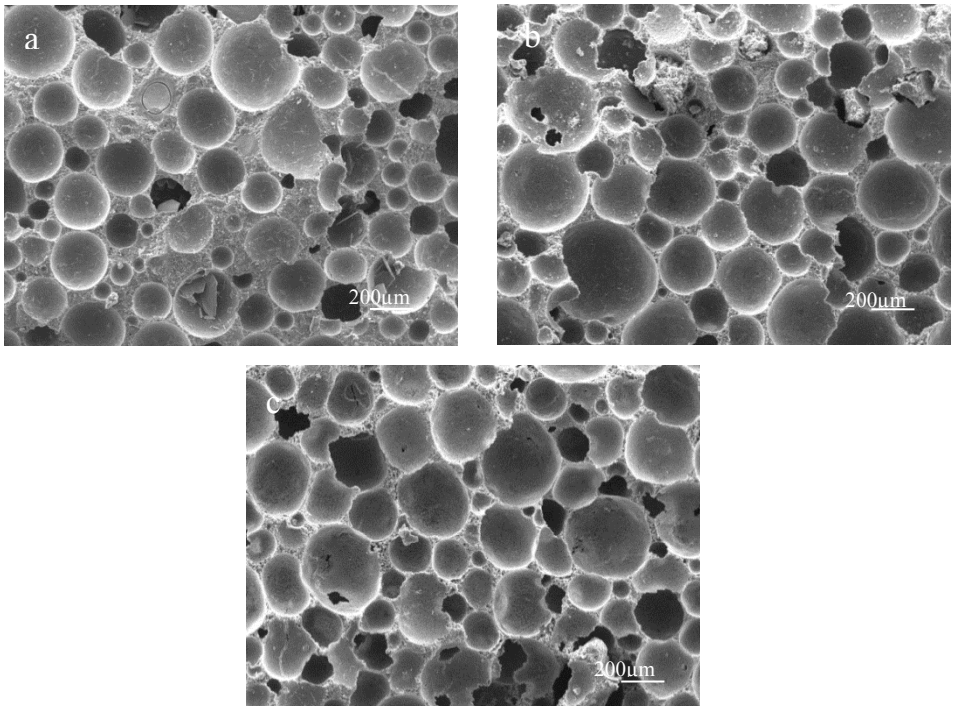

Figure 6.9: SEM images for 10% Silica Fume mix; a) 800 kg/m^3; b) 600 kg/m^3; c) 400 kg/m^3.

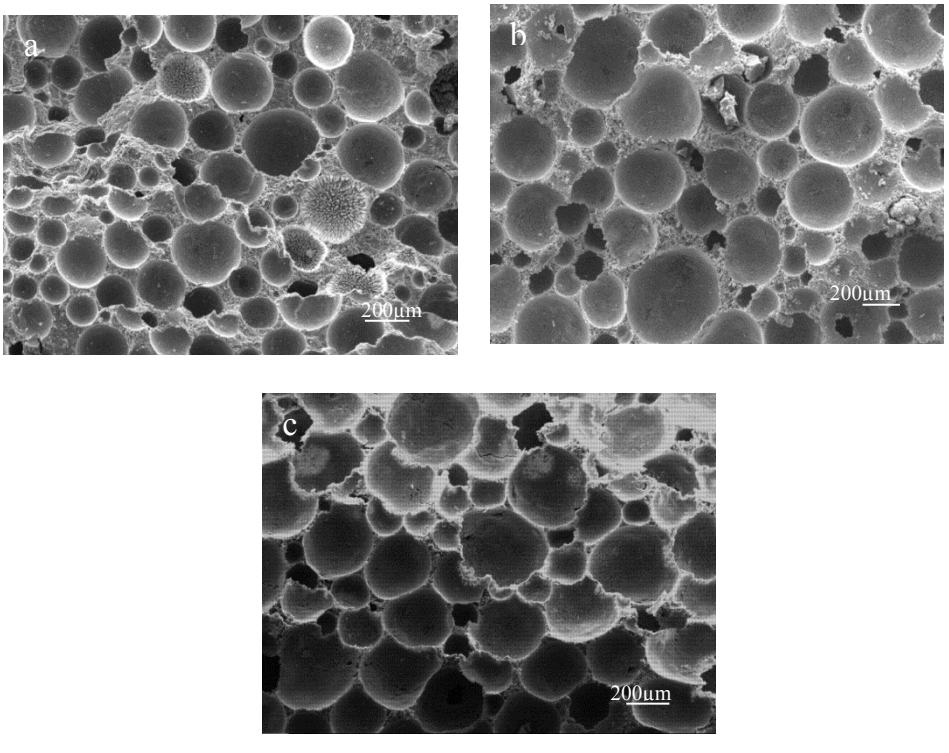

Figure 6.10: SEM images for 20% Silica Fume mix; a) 800 kg/m^3; b) 600 kg/m^3; c) 400 kg/m^3.

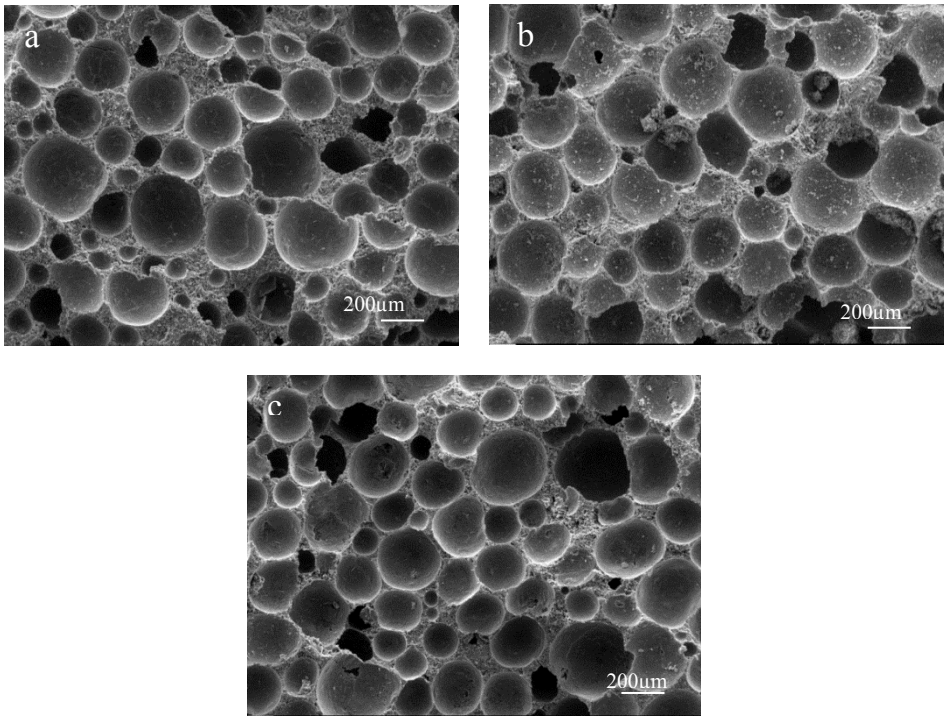

Figure 6.11: SEM images for 10% Metakaolin mix; a) 800 kg/m^3; b) 600 kg/m^3; c) 400 kg/m^3.

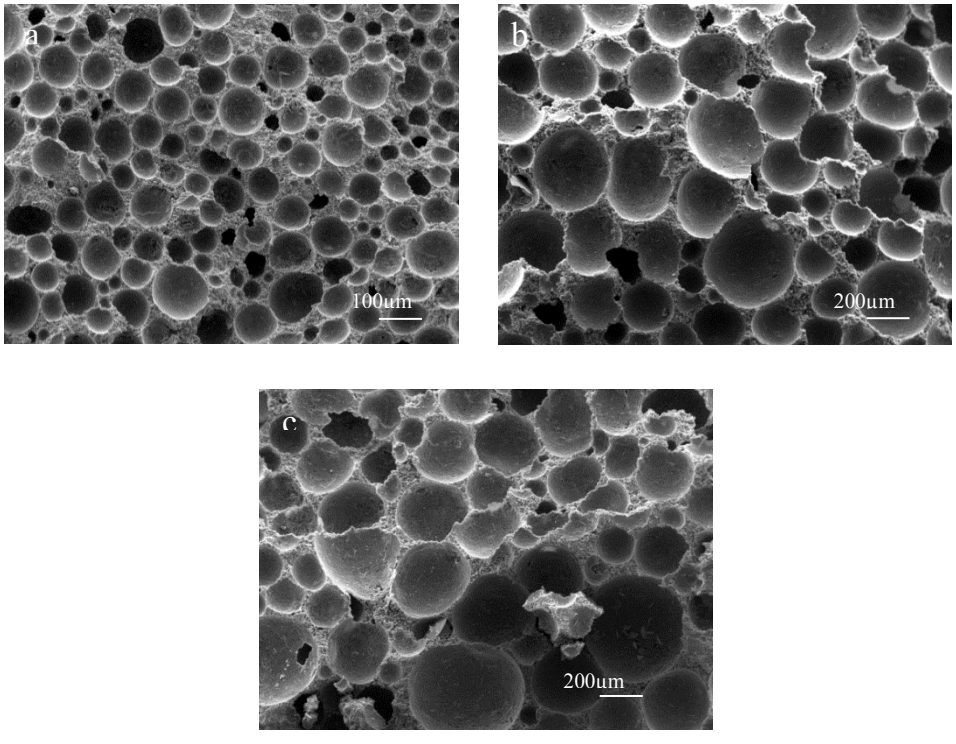

Figure 6.12: SEM images for 20% Metakaolin mix; a) 800 kg/m^3; b) 600 kg/m^3; c) 400 kg/m^3.

6.5 Air-Void Distribution of Cement-Based Foam

Figure 6.2 shows that the foam have different sizes of bubbles and when these bubbles are blended in cement paste, pore structure is formed in the cement matrix as noticed from SEM images in Figure 6.6 to 6.12. It was also noticed that this pore structure is influenced by density and admixture. These effects on air-void network of cement-based foam are investigated here. The CT Analyser Software directly measures the diameter of the void of CT scan images. The results discussed here are based on the average value for 500 images taken through CT scanning.

6.5.1 Effect of Density on Air-Void Size Distribution

The frequency histogram of air-voids distribution for reference mix is shown in Figure 6.13 for three cast densities. It can be noticed that for all the three densities the majority of the voids are of size 0.03 and 0.07 mm being almost 75%. Whereas, a few bigger sized voids of 4.40 and 8.81mm diameter were also found but the frequency of occurrence was too low due to which these diameters are not visible in the Figure 6.13. The coefficient of variance for these air-void sizes is given in table A-1 (Appendix A). These few larger sized pores could be due to merging and overlapping of the pores. In lower densities these irregularities happens due to increased volume of foam which dwindles the cement matrix. Due to which the pores starts to get closer and closer to each other eventually merging with each other and foaming a new pore of larger size which is evident from Figure 6.6c. Comparatively, in higher densities imperfection usually occurs due to over mixing or mishandling of the samples (Kearsley 1999).

In addition to this when the individual frequency histograms for the three cast densities were compared it was found that the number of pores

increases with decreased densities. Recently, Awang et al. (2012) investigated the microstructure of light weighted foamed concrete for 600 and 1000 kg/m^3 and reported that number of voids and the size of pore increases as the density decreases. Kearsley (1999) reported that the majority of pore sizes were less than 0.3 mm in the cast density of 700 to 1500 kg/m^3. In one more investigation Mydin (2010) found that the dominant pore size for 650 and 1000 kg/m^3 densities was 0.72 and 0.55 mm respectively whereas, in present study 0.03 to 0.07 mm are the prominent pore size for the three densities which is much smaller with other author findings. Furthermore, Hengst et al. (1983) investigated the pore sizes of cement-based foam for 720, 640 and 400 kg/m^3 densities respectively and reported the average pore size as 0.168, 0.335 and 0.430 mm which are high as compared to present finding.

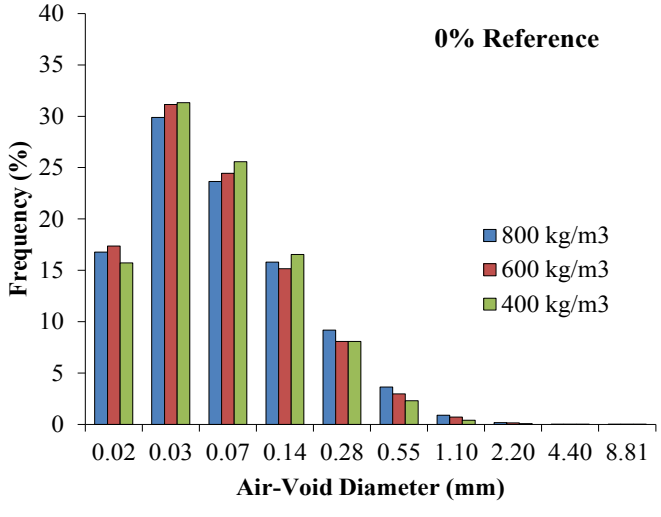

Figure 6.13: Air-void size distribution for 0% reference mix.

Figure 6.14, 6.15, 6.16 shows the frequency histograms of air-voids distribution for fly ash, silica fume and metakaolin mixes for the cast density of 800,600 and 400 kg/m^3. From these Figures it can be noticed that the majority of the voids are of size 0.03 and 0.07 mm (see table A-2 for COV value).However, when the frequency histogram of three cast densities

of Figure 6.14a for the 10% fly ash mix was compared it was found that the occurrence of pores size 0.02 to 0.03 mm and 1.10 to 2.20 mm was higher for the series with 800 kg/m^3 cast density which is different from 0% reference mix finding. In addition to this, 600 kg/m^3 cast density was higher for 0.55 mm and occurrence of pores for 400 kg/m^3 was higher for 0.07 to 0.28 mm and the difference noticed between the three cast densities for any pore size was 5%. Moreover, the frequency histogram for 20% fly ash mix as shown in Figure 6.14b was similar to mix with 10% fly ash except that the 400 kg/m^3 was slightly governing for the diameter of 0.02 mm.

From Figure 6.15a for 10% silica fume mix it can be noticed that pore sizes of 0.02,0.55,1.10 mm and 0.14,0.28 and 0.55 mm was leading in 800 kg/m^3 and 600 kg/m^3 whereas other pore sizes governs in 400 kg/m^3 cast density(refer to table A-3 for COV values in Appendix A). Comparatively when silica fume was added in the ratio of 20% as illustrated in Figure 6.15b the cast densities of 600 kg/m^3 and 400 kg/m^3 were dominating in pore size. Beside this, for 10% and 20% metakaolin mixes the frequency of occurrence as shown in Figure 6.16 of pore size 0.07, 0.14 and 0.28 mm was 3% higher in 400 kg/m^3 as compared to other densities.

Thus, it can be summarized that for three cast densities and for all the mixes the maximum frequency of occurrence is of 0.03 mm pore size. In addition to this the lower densities have more pores of larger size as compared to higher densities. Furthermore, this dataset generated here will be used for the quantification of air-void distribution.

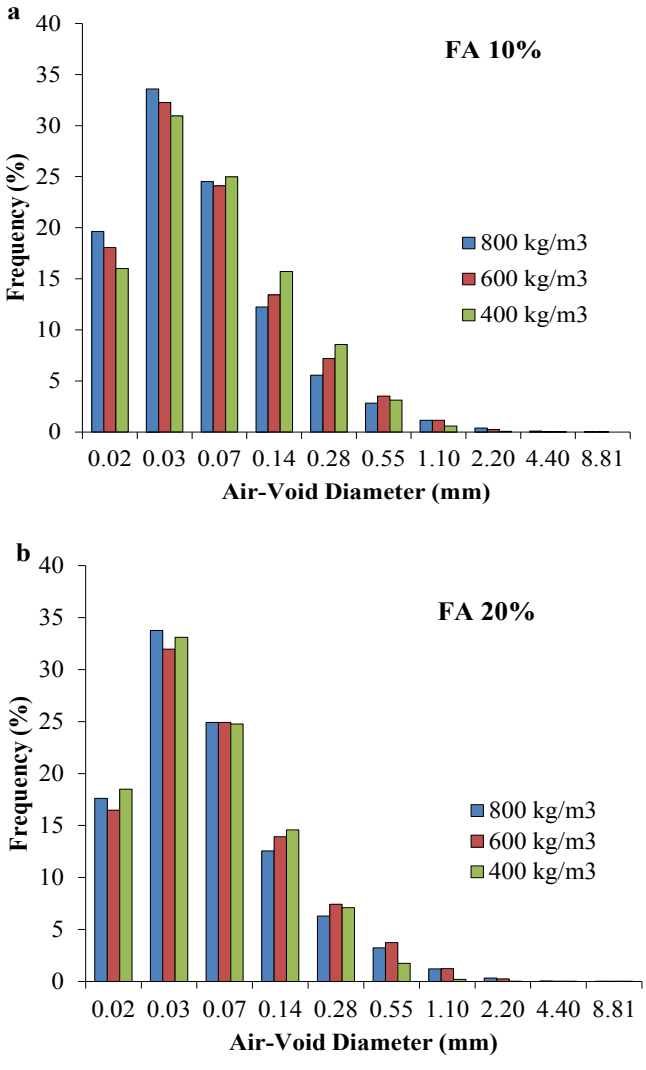

Figure 6.14: Air- void size distribution for Fly Ash mix; a) Mix with 10% Fly Ash; b) Mix with 20% Fly Ash.

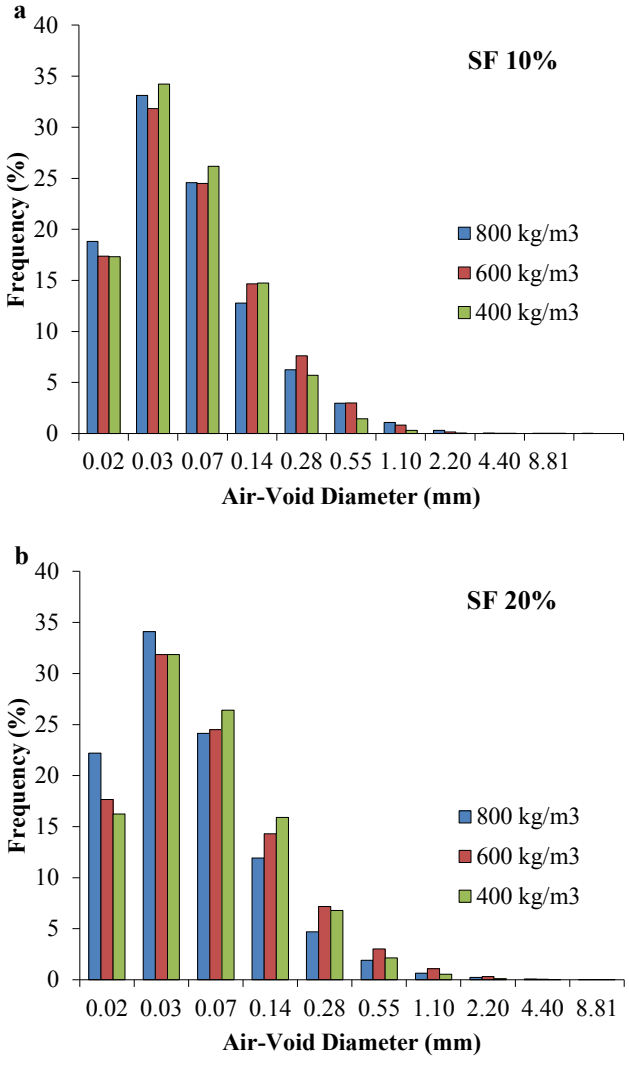

Figure 6.15: Air- void size distribution for Silica Fume mix; a) Mix with 10% Silica Fume; b) Mix with 20% Silica Fume.

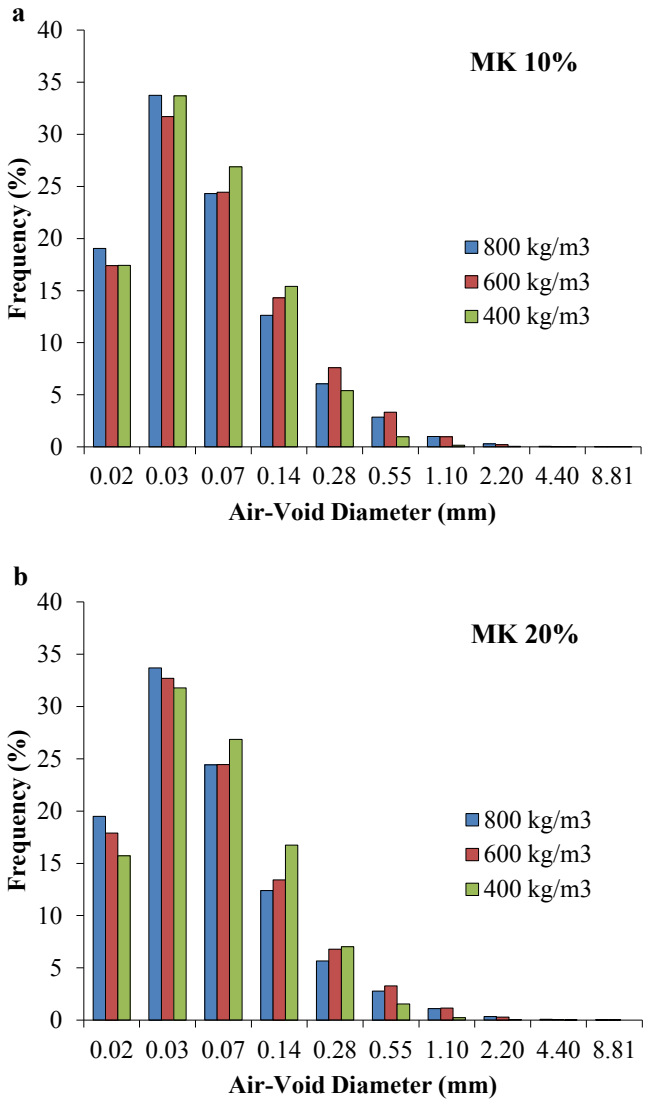

Figure 6.16: Air- void size distribution for Metakaolin mix; a) Mix with 10% Metakaolin; b) Mix with 20% Metakaolin.

6.5.2 Effect of Admixture Type and Content on Air-Void Size Distribution

Figure 6.17, 6.18 and 6.19 demonstrates the frequency of air-void size distribution of cement-based foam for 0% reference, fly ash, silica fume and metakaolin mixes for the cast density of 800,600 and 400 kg/m^3 respectively.

For the cast density of 800 kg/m^3 from Figure 6.17a, 6.17b, 6.17c it can be noticed that there is a reduction in frequency of occurrence as the pore size increases. For the reference mix, this reduction in frequency was 29% as the size of the pore increased from 0.03 to 2.2 mm. For mixes with FA, SF and MK, the reduction in frequency of occurrence for the same range of pore size increments is seen 32%, 33% and 32% respectively for 10% substitution. When the substitution is 20%, the corresponding reduction noted as 33, 34 and 33% respectively.

The comparison of mixes at different air-void size with respect to the reference mix was made and it was found that the frequency of occurrence for size 0.02, 0.03, 0.07 and 1.10 mm was 3%, 4%, 2% and 2% more in both fly ash mixes. Whereas, for 0.14, 0.28 and 0.55 mm size the percentage drop recorded was 3%, 4% and 2% respectively. However, the difference in frequency between the two (FA) ash/cement ratios for the entire air-void size distribution was almost 2%. This implies that presence of fly ash increase the number of smaller pores in this density but the higher substitution ratio for the fly ash does not significantly effect the number and sizes of pores.

Consequently, when same comparison was done for silica fume mixes it was found that the frequency of occurrence of pores was 6%, 5% and 2% higher for size 0.02, 0.03 and 0.07 mm. Whereas, for 0.14,0.28 and 0.55 mm size the reduction recorded in the number of pores due the presence of this admixture was 4%, 5% and 2% respectively. In addition to this the difference recorded between the (SF) ash/cement ratios for 0.02 mm was 5% and for remaining sizes was 2%. Therefore, it can be said that the presence of silica fume in higher substitution results in more formation of smaller pore size.

The air-void distribution trend for metakaolin mixes as shown in Figure 6.17c is quite similar to that of mixes with silica fume. Except the difference between the two ash/cement ratio which is 1% for all air-void sizes. Figure 6.18a, 6.18b, 6.18c illustrates that the air-void distribution for the mixes with the cast density of 600 kg/m^3. Interestingly, for all mixes same pore size 0.03 mm is in majority as was found in 800 kg/m^{3}density. From Figure 6.18a it was found that the frequency histogram of air-void distribution for fly ash mixes is very much similar to 800 kg/m^{3}density as illustrated in Figure 6.17a. The actual difference in the values between the two dosages levels of FA being only 1% and the difference with respect to the reference mix recorded was 2% for entire size of distribution. Subsequently, for silica fume (Figure 6.18b) mixes the pore size distribution histogram is similar to one shown in Figure 6.17b. Along with this significant difference (Figure 6.18b) was not noticed due to the different substitution ratio of silica fume. Surprisingly, the histogram trend noticed for the metakaolin mixes are very much similar to that of silica fume and difference between the two ash/cement ratios for MK recorded was almost 1%.

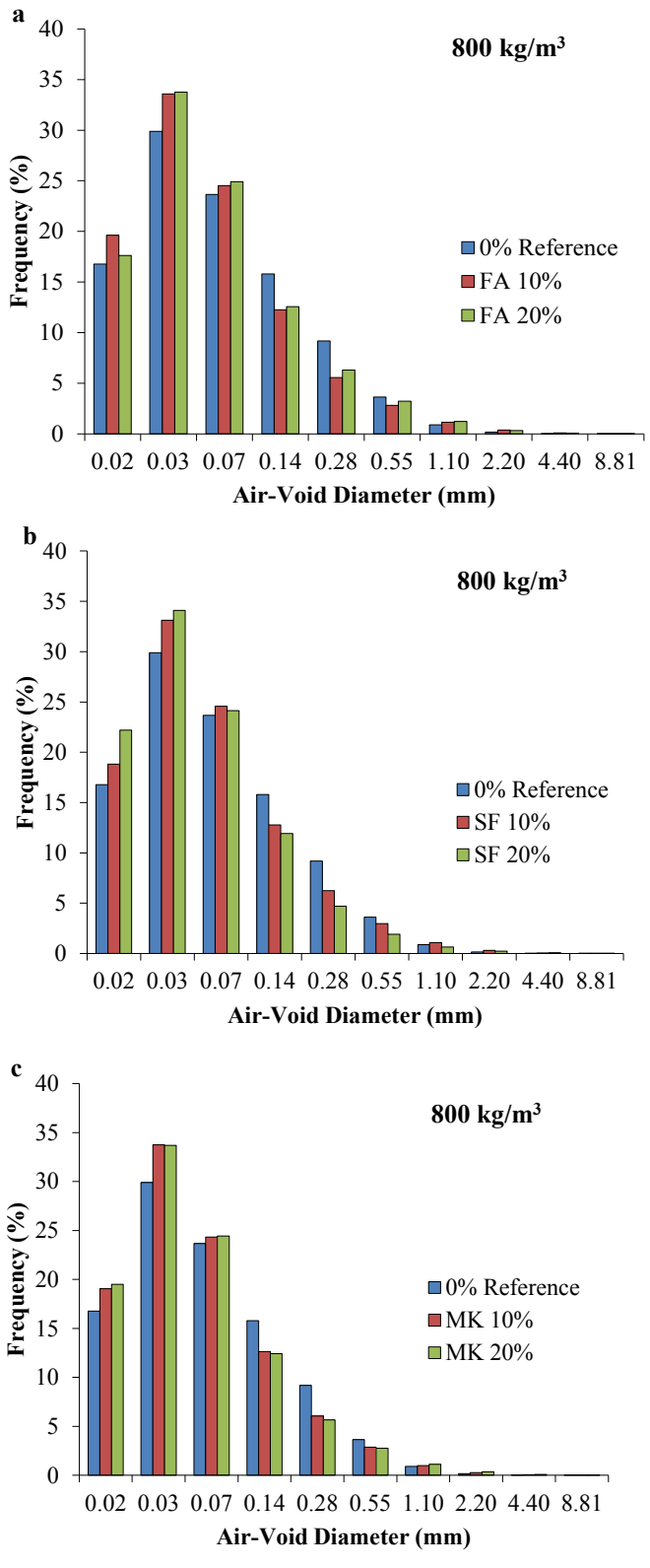

Figure 6.17: Air-void size distribution for 800 kg/m^3; a) Mix with Fly Ash; b) Mix with Silica Fume; c) Mix with Metakaolin.

The air-void size distribution for the mixes with the cast density of 400 kg/m^3 is demonstrated in Figure 6.19a, 6.19b, and 6.19c. It can be observed that the frequency of occurrence for the larger void size beyond 1.1 mm is much less for all the mixes. In addition to this, the void size of 0.03 mm remains the highest frequency size for this cast density also. From Figure 6.19a it can be noticed that the frequency of the fly ash mixes governs for sizes 0.02, 0.03 and 0.55 mm and the percentage of increase noticed with respect to the reference mix was within 3%.Whereas, the drop recorded for size 0.07, 0.14 and 0.28 was 1%, 3% and 4% respectively. Furthermore, a few numbers of voids were found of 1.10 mm size for instance only 0.5%.

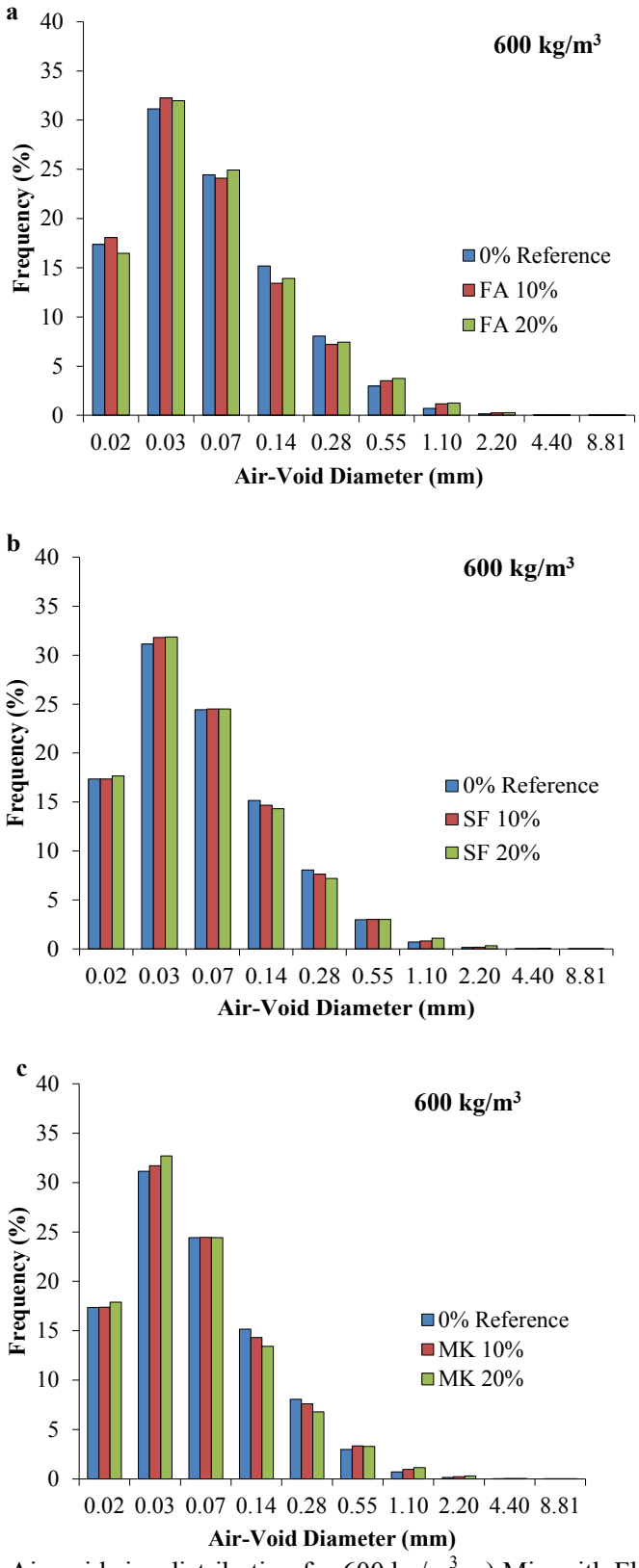

Figure 6.18: Air-void size distribution for 600 kg/m^3; a) Mix with Fly Ash; b) Mix with Silica Fume; c) Mix with Metakaolin.

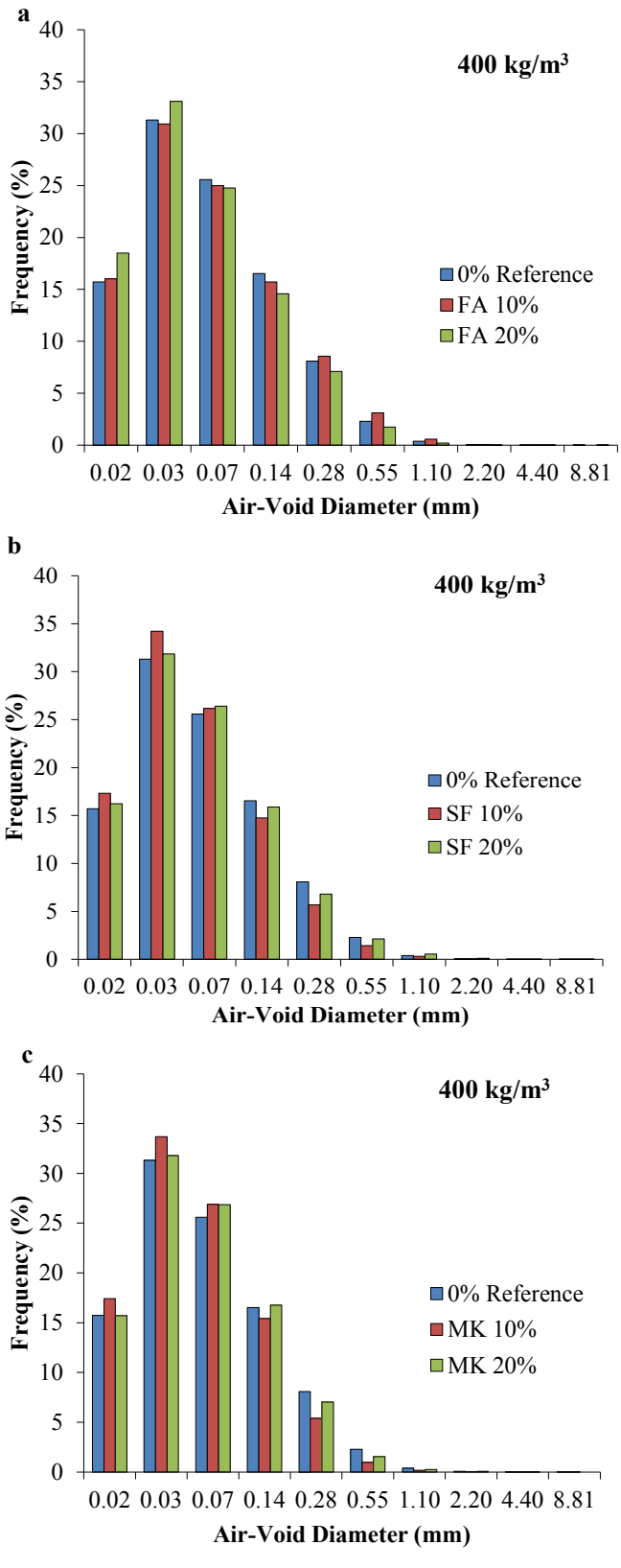

Figure 6.19: Air-void size distribution for 400 kg/m^3; a) Mix with Fly Ash; b) Mix with Silica Fume; c) Mix with Metakaolin.

Consequently, the frequency for silica fume and metakaolin mixes governs for the sizes 0.02, 0.03 and 0.07 mm and the rise notice as compared to reference mix was within 3% and 2% for two mixes. Importantly, the percentage of 10% silica fume was found 3% and 4% higher for sizes 0.02 and 0.03 mm whereas for 0.14,0.28 and 0.55 mm the reduction noticed was 2% when compared with 20% silica fume mix as shown in Figure 6.19b. Similarly, for 10% metakaolin mix for size 0.02 and 0.03 the rise noticed was 3% and the drop was 2% for 0.14, 0.28 and 0.55 mm in context of 20% metakaolin mix.

Finally, it can be concluded that the variation in the frequency of size distribution due to the addition of fly ash, silica fume and metakaolin is not very significant. However, the presence of these admixture increases the number of small pores in higher densities which could be due to coating of the bubbles resulting in less imperfection i.e. merging and broken pores. Furthermore, for 400 kg/m^{3}densities the higher substitution ratio of fly ash and lower ratio of silica fume and metakaolin increases the frequency of small size pore whereas the effect of ash/cement ratio was very nominal for 600 kg/m^3.

6.5.3 Quantification of Air-Void Size Distribution

Representing the pore size distributions of cement-based material (or for any other porous material) as a mathematical function remains a challenge for researchers. However, Gaussian and log-normal distribution functions are commonly used by past researchers (Aligizaki 2005, Chawla 2005, Diamond et al. 1971) to represent the pore size distribution of cement-based materials. When these distributions were applied on the data plotted in Figures 6.17, 6.18 and 6.19 it was found that the frequency histogram of air-void sizes of this study is also log-normal function.

In addition to this Kearsley (1999), Visagie (2000) also reported the same during their investigation on foamed concrete.

The integral of these distributions is cumulative distribution function which increases monotonically 0 to 100 from which 50^{th} and 90^{th} percentiles can be easily evaluated. Snyder (1998) used this approach for the quantification of air-void in concrete for freeze-thaw durability whereas Kearsley (1999), Visagie (2000), Petrov (1994) and Nambiar et al. (2007) used it for air-void pores in foamed concrete. The same approach of cumulative frequency is used in present study to quantify the 50^{th} and 90^{th} percentile of air-void size distribution for mixes of different cast densities.

Accordingly, the frequency histogram values as shown in Figure 6.17, 6.18 and 6.19 were used to plot the cumulative frequency distribution curves. A typical case is shown in Figure 6.20 and 6.21 (see Appendix A for other mixes) and then from these curves the values for D50 and D90 were evaluated which is tabulated in Table 6.2. The D50 is that size of voids below which 50% of void sizes occur. This is also the median void size and D90 is that size above which 10% void size occur. From Figure 6.22 it can be noticed that the value of D50 lies in the range of 0.025-0.040 mm, maximum was recoded for 400 kg/m^3 and minimum was recorded for 800 kg/m^3 cast density.

This implies that as the density increases the value of D50 decreases and it is irrespective of addition of pozzolanic admixture. In other words, as the density increases, number of smaller size pore increases. This is noticed for all cases irrespective of admixture type and content in Figure 6.22.

Table 6.2: Air-void Distribution Parameters

Mixes	Cast Density (kg/m^3)	D50 (mm)	D90 (mm)
0% Reference	800	0.025	0.200
	600	0.030	0.180
	400	0.040	0.170
FA10%	800	0.020	0.138
	600	0.025	0.175
	400	0.035	0.180
FA20%	800	0.029	0.168
	600	0.030	0.190
	400	0.035	0.140
SF10%	800	0.025	0.140
	600	0.028	0.160
	400	0.030	0.130
SF20%	800	0.028	0.125
	600	0.030	0.160
	400	0.035	0.150
MK10%	800	0.031	0.150
	600	0.032	0.180
	400	0.035	0.130
MK20%	800	0.028	0.15
	600	0.030	0.180
	400	0.040	0.140

Same was observed by Nambiar et al. (2007) the median value reported was 0.35mm for the density range of 600-1200 kg/m^3. This median value was reported for reference mix with sand which is 10 times more than the present findings. This difference in median values could be due to SEM and CT scan measurement techniques.

Kearsley (1999) and Nambiar et al. (2007) reported that as the density increases the value of D90 decreases but this is not true in the present findings. It can also be seen that in case of the reference mix, D90 is minimum for 400 kg/m^3 and maximum for 800 kg/m^3 which mean as the densities increases the range for 10% oversized pores reduces. This should be expected as the foam content increases the probability of occurrence of oversized pores increases. But, in the mixes with admixtures, as shown in Figure 6.23, the D90 values for 600 kg/m^3 and 800 kg/m^3 is lower.

Summarizing, the foregoing discussion, it can be said that D90 value is slightly higher when the density is higher and with the addition of pozzolanic admixture, the D90 values gets lower for the densities greater than or less than 600 kg/m^3. In addition to this not much difference was noticed in D90 values for the three cast densities.

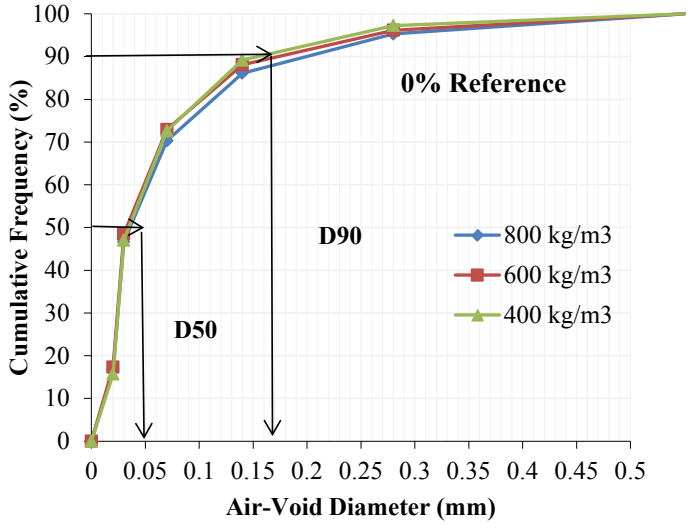

Figure 6.20: Cumulative frequency distribution of air-void size for 0% reference mix.

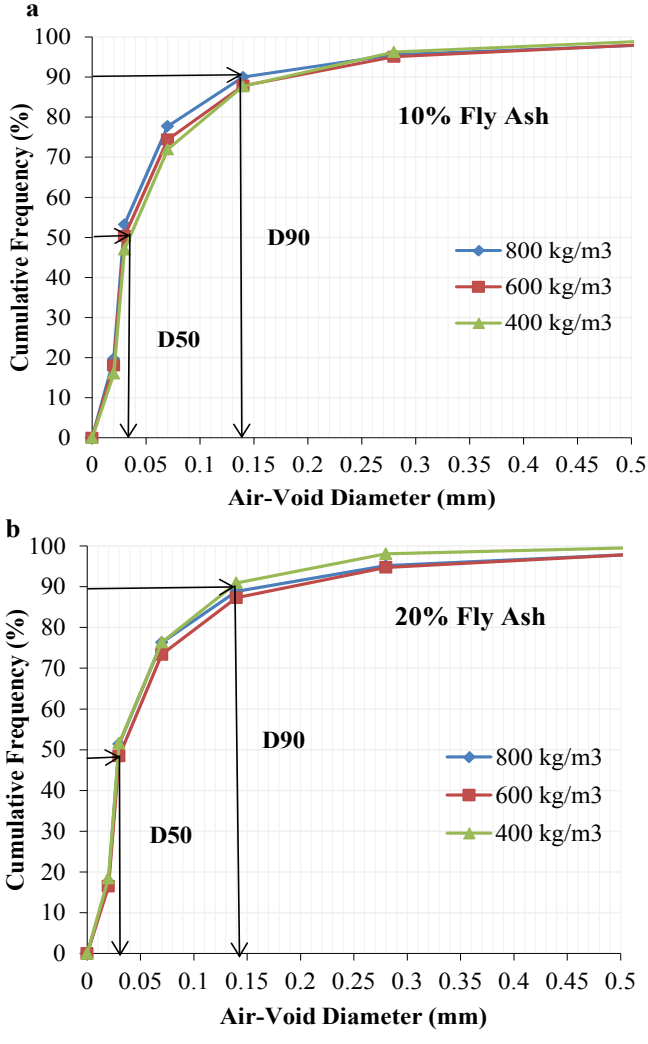

Figure 6.21: Cumulative frequency distribution of air-void size for three cast density; a) Mix with 10% Fly Ash; b) Mix with 20% Fly Ash.

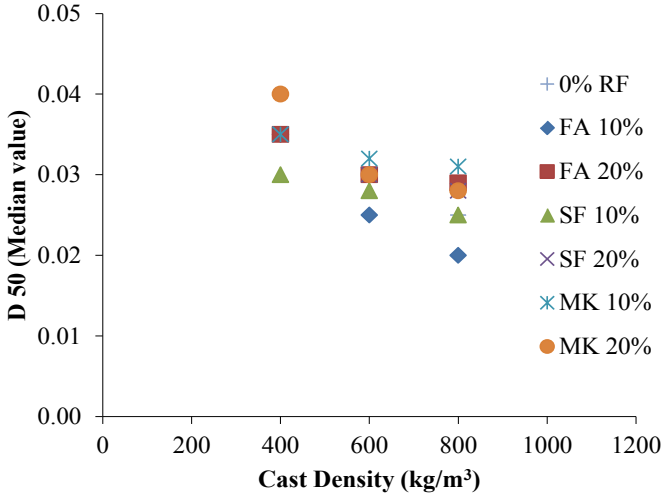

Figure 6.22: Relationship between D50 and cast density.

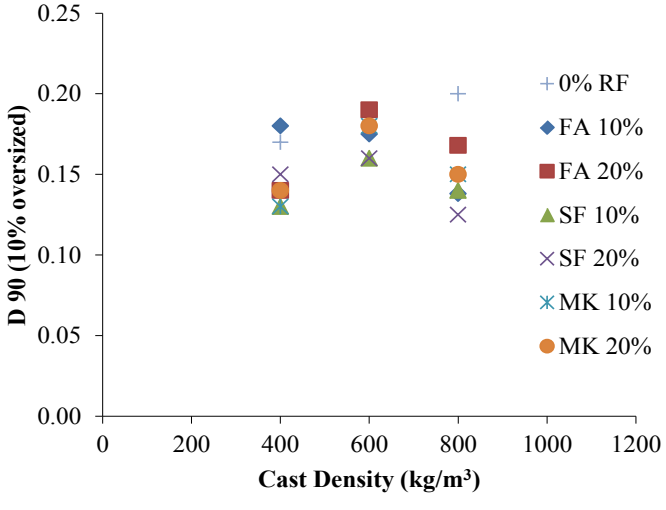

Figure 6.23: Relationship between D90 and the cast density.

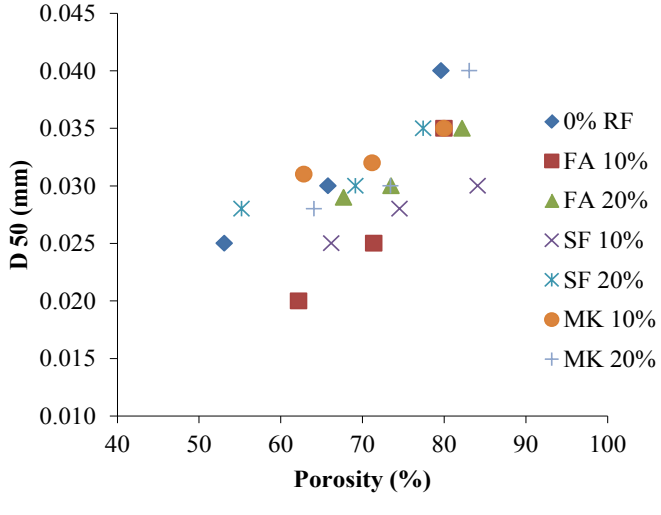

Figure 6.24: Relationship between D50 and the Porosity.

The relationship between the porosity and D50 of the cement-based foam for all the mix is plotted in Figure 6.24 and it can be seen that as the porosity increases the D50 increase. This is in accordance with Figure 6.22 findings. The SPSS software was used to fit the equation between the cast density and the D50 values for all the mixes. The fitted equation can calculate the D50 value for the cast density range of 800 to 400 kg/m^3.The respective Equations are tabulated in Table 6.3.

Table 6.3: Equations for D50 Air-Void Distribution Parameters

Mixes	Cast Density (Υ_d) (kg/m^3)	Fitted Equation for D50 Air-void distribution	Adjusted R^2
0% Reference	800	$D50=0.183\Upsilon_d^{(-0.278)}$	99.8%
	600		
	400		
FA 10%	800	$D50=4.442\Upsilon_d^{(-0.809)}$	99.8%
	600		
	400		
FA 20%	800	$D50=0.183\Upsilon_d^{(-0.278)}$	87.2%
	600		
	400		
SF 10%	800	$D50=0.141\Upsilon_d^{(-0.257)}$	88.7%
	600		
	400		
SF 20%	800	$D50=0.245\Upsilon_d^{(-0.326)}$	97.2%
	600		
	400		
MK 10%	800	$D50=0.101\Upsilon_d^{(-0.178)}$	94.2%
	600		
	400		
MK 20%	800	$D50=0.922\Upsilon_d^{(-0.527)}$	88.5%
	600		
	400		

6.6 Air-Void Spacing Distribution of Cement-Based Foam

In cement-based foams the voids are not uniformly distributed in the matrix. Due to which the spacing between voids varies considerably across the matrix (see Figure 6.6 to 6.12). This variation of distances was investigated by using CT analyser software which directly measures the distances between the outer surfaces of the voids.

6.6.1 Effect of Density on the Spacing of Voids

Figure 6.25, 6.26 and 6.27 demonstrate the frequency of air-void spacing distribution of cement-based foam for 0% reference, fly ash, silica fume and metakaolin mixes for the cast density of 800, 600 and 400 kg/m^3 respectively.

Figure 6.25a, 6.26a and 6.27a illustrates the reference mix. It can be noticed that the variation of frequency for the air-void spacing for 400 kg/m^3 cast density was higher for distance range of 0.02 to 0.28 mm whereas, 800 and 600 kg/m^3 cast density are prominent in the range of 0.55 to 8.81 mm (see Appendix A for individual mixes and Table A-5 for COV values). This implies that the air-void spacing or the distances between the voids is the function of the density. As the density increases the distances between the void gets larger. This finding is also supported by Kearsley (1999), Visagie (2000), Mydin (2010) and Nambiar et al. (2007) respectively. Same trend in the distance ranges was noticed for the both fly ash mixes. Except that the maximum difference in frequency recorded for the both fly ash mixes was for 400 kg/m^3 which was 17% higher when compared with other densities. Additionally, in 20% fly ash mix the frequency for 600 kg/m^3 densities was 6% high when compared with 800 kg/m^3 cast density.

Therefore, it can be said that as the density decreases the frequency of occurrences for individual spacing size increases. Similarly, from Figure 6.25b, 6.26b and 6.27b for silica fume mixes. It can be noticed that the range of distances in which frequency for 400 kg/m^3 is prominent was 0.02 to 0.14 for 10% silica fume and 0.28 to 2.20 for 20% silica fume whereas, other two densities were dominating in other remaining ranges.

This shows that the higher substitution ratio of silica fume increases the distance between the pores resulting in reduced number of pores for the same cast density i.e. 400 kg/m^3. In addition to this linear relationship was noticed between the frequency and the air-void spacing for the 800 kg/m^3 cast density. This trend was not noticed before in other mixes which could be due to the filler effect created by silica fume.

Additionally, the metakaolin mixes trend as shown in Figure 6.25c, 6.26c and 6.27c was very much similar to that of fly ash mixes. Thus, it can be concluded that even in the presence of admixture as the density increases the distance between the void of cement-based foam increases.

6.6.2 Effect of Admixture and its Content on Spacing

From Figure 6.25a, 6.25b and 6.25c for the cast density of 800 kg/m^3.It can be noticed that the variation of frequency for the air-void spacing for 0% reference mix was significantly high for a spacing of 0.03 to 0.55 mm and was low between 1.10 to 8.81 mm when compared with all other mixes. The rise noticed in the frequency of distances (spacing) for the size between 0.03 to 0.55 mm for 0% reference, 10% FA and 20% FA mixes was 20%, 11% and 16% and the reduction between 1.10 to 8.81 mm was 17%, 10% and 21% respectively (refer to Table A-6 in Appendix A for COV values).

Similarly for 10% silica fume the rise in frequency of occurrence of size range noticed was 18% between 0.03 to 2.20 mm. The 14% rise was noticed throughout the entire range for 20% silica fume. Along with this for 10% and 20% metakaolin mix the rise noticed was 16% and 13% and the decline was 16% and 12% respectively. The frequency of spacing in all mixes were analysed with respect to the reference mix. It can be noticed that the difference in the frequency for the range of 0.03 to 4.40 mm was 10% for 10% and 8% for 20% fly ash. However, the difference in frequency between the two ash/cement ratios (FA) for the entire air-void spacing distribution was 5%. Similarly for 10% and 20% silica fume with respect to reference mix the difference noticed was 10% and 15% for the given range of air-void spacing. However, the difference in frequency between the two ash/cement (SF) ratios was recorded to be 7%. In addition to this when binders containing 10% and 20% metakaolin are compared with the reference mix, the difference noticed was 8% and 10%. Moreover, the difference between the two dosages of 10% and 20% MK was 4%.

In conclusion, it can be said that for 800 kg/m^3 cast density series, the spacing size increases with the addition of pozzolanic admixture (FA, SF and MK) i.e. less imperfection in air-voids.

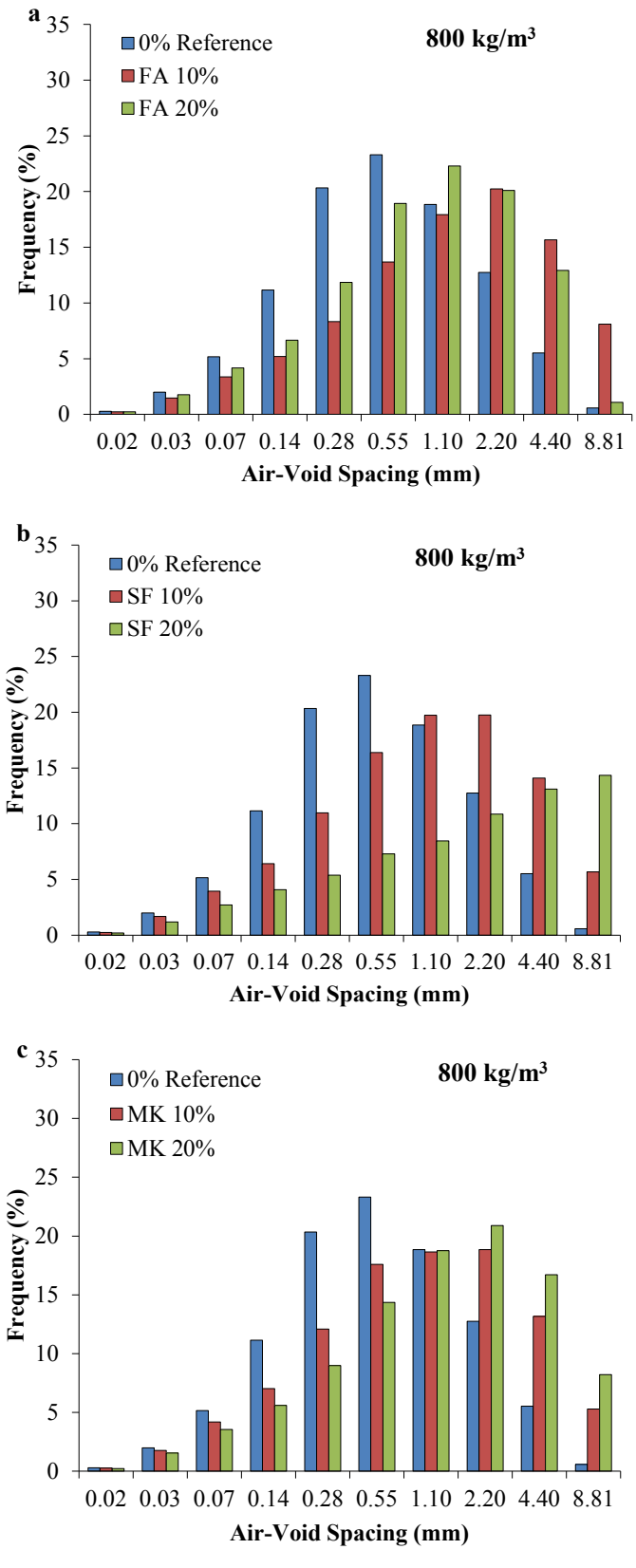

Figure 6.25: Air-void spacing for the 800 kg/m^3 cast density; a) Mix with Fly Ash; b) Mix with Silica Fume; c) Mix with Metakaolin.

For the cast density of 600 kg/m^3, it can be noticed from Figure 6.26a, 6.26b and 6.26c that the frequency of occurrence for the air-void spacing for 0% reference mix was high for distances range of 0.03 to 0.55 mm. The frequency was low between 1.10 to 8.81 mm when compared with all other mixes; same was noticed for 800 kg/m^3 (illustrated in Figure 6.25).

Similarly, the total variation noticed in the frequency of spacing for the size between 0.03 to 0.55 mm for 0% reference, 10% FA and 20% FA mixes was 20%, 20% and 21% and the reduction between 1.10 to 8.81 mm was 18%, 16% and 22% respectively. However, for 10% silica fume the rise noticed was 20% between 0.03 to 0.55 mm and drop recorded was 16% whereas for 20% silica fume rise of 19% was noticed for 0.03 to 1.11 and 18% between 1.11 to 8.81 mm. For 10% and 20% metakaolin the rise noticed was 19% and 20% and the decline was 13% for both mixes. So forth, when the frequency of mixes was compared with respect to the reference mix the difference recorded was 5% and 6% for 10% and 20% fly ash respectively for the spacing range of 0.03 to 4.40.

However, the difference in frequency between the two ash/cement ratios for the entire air-void spacing distribution was 2%. Then, for silica fume 10% and 20% with respect to reference mix the difference noticed was 2% and 5% whereas, the difference in frequency between the two ash/cement ratios was 5% for the entire spacing range.

Similarly, for 10% and 20% metakaolin mix with 0% mix being the reference the difference noticed was 4% and 3% whereas, the difference in frequency between the two ash/cement ratios was 4%.

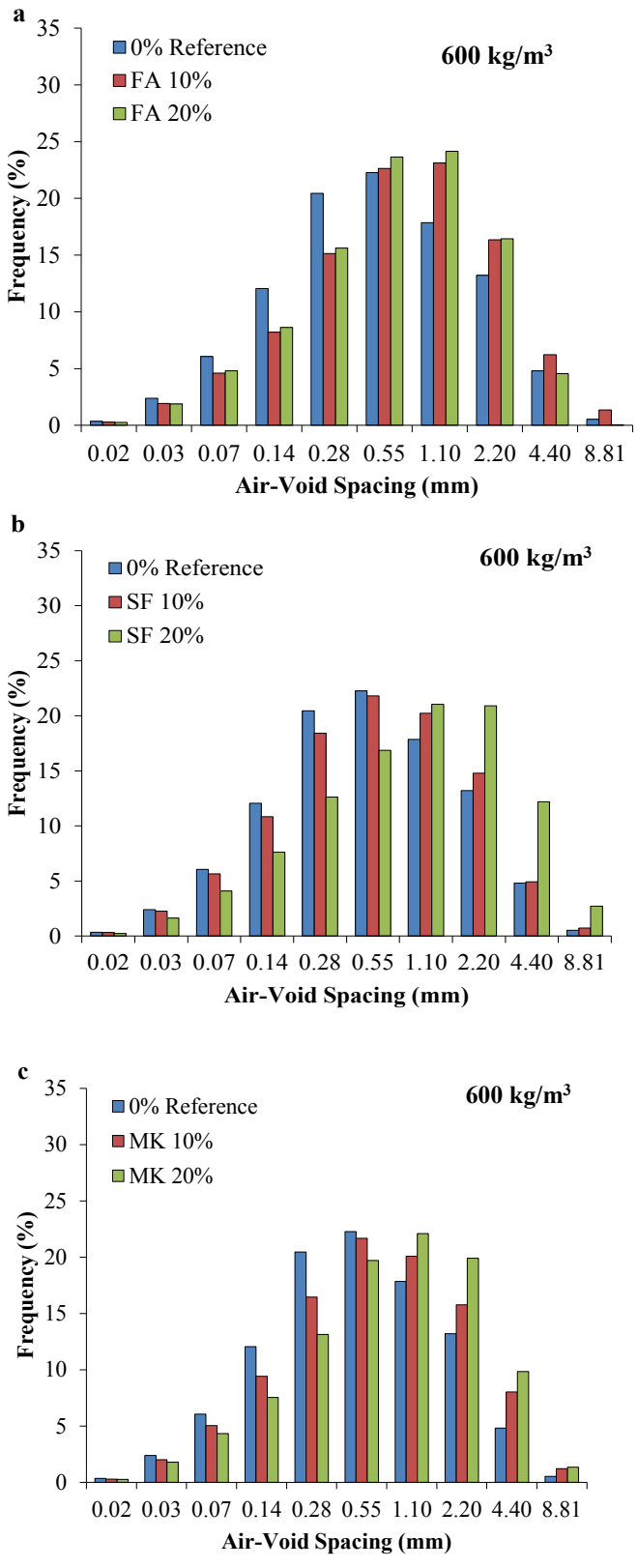

Figure 6.26: Air-void spacing for 600 kg/m^3 cast density; a) Mix with Fly Ash; b) Mix with Silica Fume; c) Mix with Metakaolin.

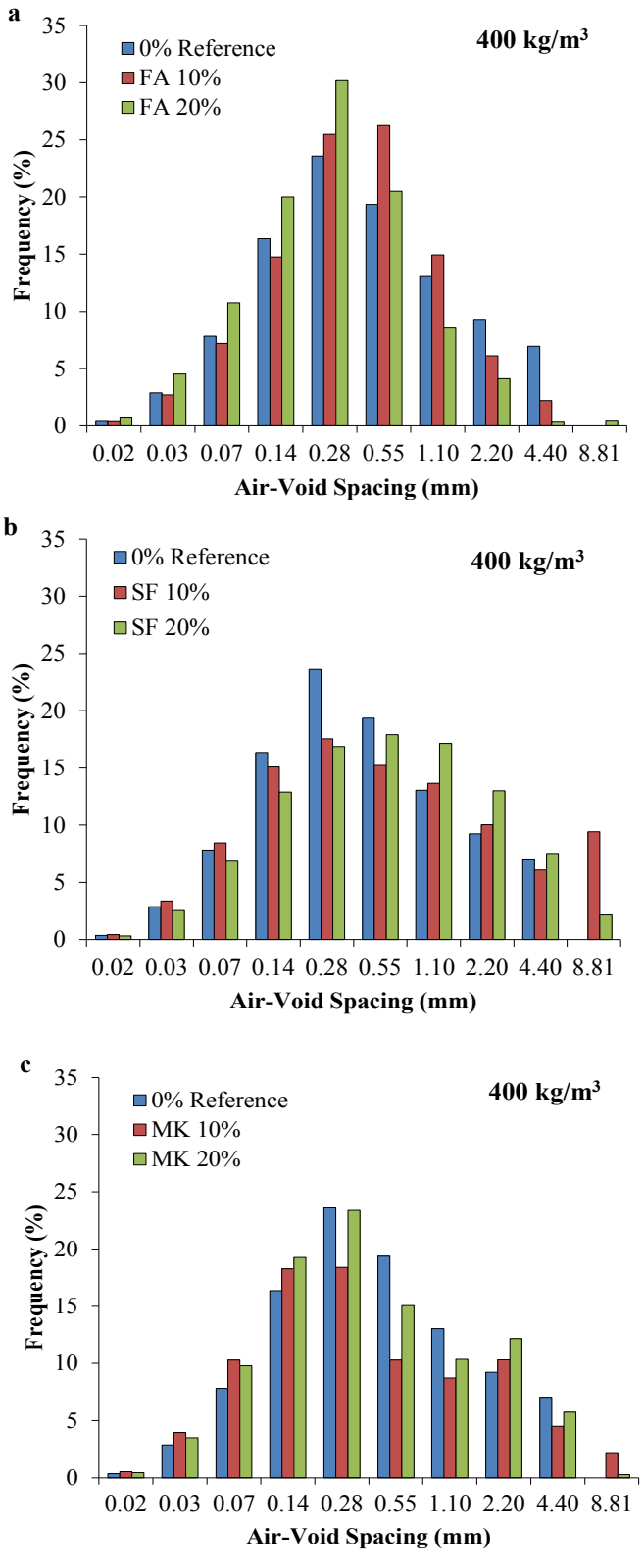

Figure 6.27: Air-void spacing for the 400 kg/m^3 cast density; a) Mix with Fly Ash; b) Mix with Silica Fume; c) Mix with Metakaolin.

From Figure 6.27a, 6.27b and 6.27c the frequency of occurrence for the air-void spacing for the cast density 400 kg/m^3 can be noticed. The frequency of occurrence noticed for individual mixes for distances between 0.03 to 0.28 mm for 0% reference, 10% FA and 20% FA mixes was 20%, 24% and 26% and the reduction between 0.55 to 8.81 mm was 17%, 24% and 10% respectively. However, for 10% and 20% silica fume the rise noticed was 14%,15% and drop recorded was 11%, 15%. Similarly, for 10% metakaolin mix the difference noticed was 15% and 20% for the distances ranges of 0.03 to 0.28 mm and 0.55 to 8.81 mm. Moreover, for 20% metakaolin mix the difference was 20% and 17% for the same spacing range.

Following this when the frequency of individual mix was compared with respect to the reference mix, the variation was 6% and 7% for 10% and 20% fly ash. However, the difference in frequency between the two (FA) ash/cement ratios for the entire air-void spacing distribution was 5%. For 10% and 20% silica fume mix the difference noticed was 5% and 7% whereas the difference in frequency between the two (SF) ash/cement ratios was 3%. Finally, for 10% and 20% metakaolin mix with 0% mix being the reference the difference noticed was 5% and 3% whereas, the difference in frequency between the two (MK) ash/cement ratios was 5%.

Overall, it can be concluded that the distances between the voids increases with the addition of pozzolanic admixture (FA, SF and MK). Especially in mixes with higher substitution the distances were found comparatively larger. However, the difference between the two ash/cement ratio was not significant i.e. 5%. It can be anticipated that the presence of these admixtures is refining the voids.

6.6.3 Quantification of Air-Void Spacing Distribution

The approach used in section 6.3.3 to quantify the air-void distribution is used here for the quantification of air-void spacing. For this purpose, the cumulative frequency distribution curves for reference and fly ash mixes shown in Figure 6.28 (see Appendix A, Figure A.20-A.21 for other mixes) were plotted by using the frequency histogram values of graphs in Figure 6.25, 6.26 and 6.27 respectively. From these cumulative frequency distribution curves the values for SP10, SP50 and SP90 were recorded and are tabulated in Table 6.4. Here, SP10 means spacing of the void below which 10% of spacing size occurred. Similarly, SP50 is the spacing value below which 50% of the spacing size lies and SP90 is defined in the same manner.

From Figure 6.29a it can be noticed that the value of SP10 lies in the range of 0.030-0.25 mm, a maximum was recoded for 800 kg/m^3 and minimum was recorded for 400 kg/m^3 cast density, respectively, in the reference mix series. This shows that as the density increases, the SP10 values increase. In other words, density has a bearing on the spacing of voids. The same was reported by Nambiar et al. (2007) in their investigation. It was further noticed that the addition of pozzolanic admixtures reduces the SP10 values for all cast densities when compared with reference mix. But as the density increases, the SP10 value also increases. That is, the addition of pozzolanic admixtures results in larger spacing of voids. The SP50 parameters also follow the same trends as above, with increases in the density resulting in larger spacing. The Figure 6.29b shows that the SP50 range between 0.20 to 1.20 mm. Except for SF 20% mix with cast density of 800 kg/m^3 value equal to 3.70 which was purposely not included in this dataset.

Apparently, there is no reason for this exception, may be some error occurred during the CT scan process. Following this for SP90 except for silica fume mixes and 10% metakaolin mixes it can be said that as the density increases the value for 90% increases as can be noticed in Figure 6.29c. Nambiar et al. (2007) reported SP10 and SP50 values for mixes without any pozzolanic admixture between 0-0.2 mm and 0.25-0.60 mm for the density range of 750-1500 kg/m^3. For the same cast density range but with 10% and 20% fly ash added in the mixture the SP10 value recorded was between 0.1 to 0.2 mm and for same proportion and for SP50 was 0.35 to 0.60 mm.

Kearsley (1999) reported that the minimum distances between the voids was found to be in range of 0.2 to 0.35 mm in foamed concrete, as the density increased from 1000 to 1500 kg/m^3.Therefore, it can be said that in the present study, the tends for SP10 and SP50 values are in agreement with findings from other researchers. Figure 6.30 shows the relationship between the D50 and SP50 for all the mixes. It was found that as the D50 increases, the value for SP50 decreases and this is true for all the mixes. This can be further explained as follow: As the value of D50 increases, the density decreases which means there are more pores at closer spacing. Kearsley (1999) also reported the same findings.

A plot of SP10 against the cast density will yield a curve to give a general equation for SP10 as a function of density. Such an equation can calculate the SP10 value for the cast density range of 800 to 400 kg/m^3.The equations are tabulated in Table 6.5.Similary, the equation those can calculate the SP50 values are tabulated in Table 6.6. The equations for SP90 were not generated due to non-linearity in the data.

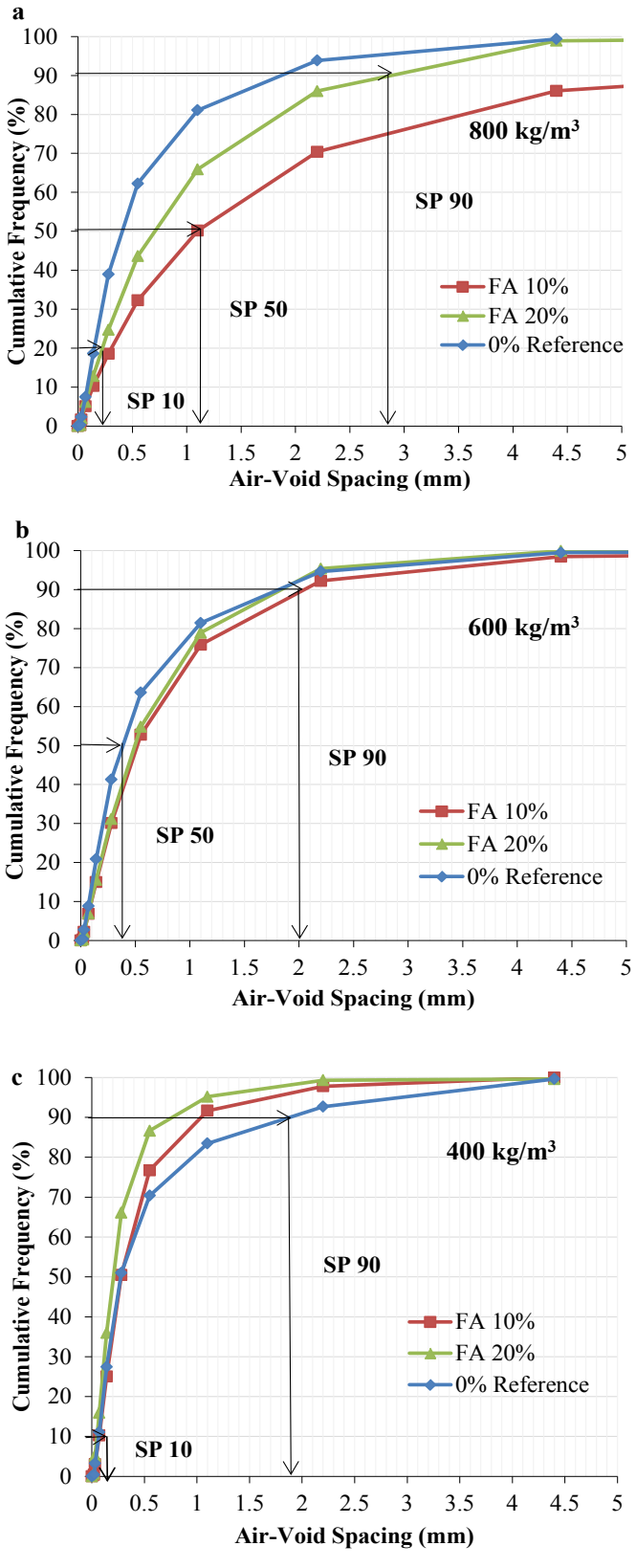

Figure 6.28: Cumulative frequency distribution of air-void spacing for three mixes; a) 800 kg/m^3; b) 600 kg/m^3; c) 400 kg/m^3.

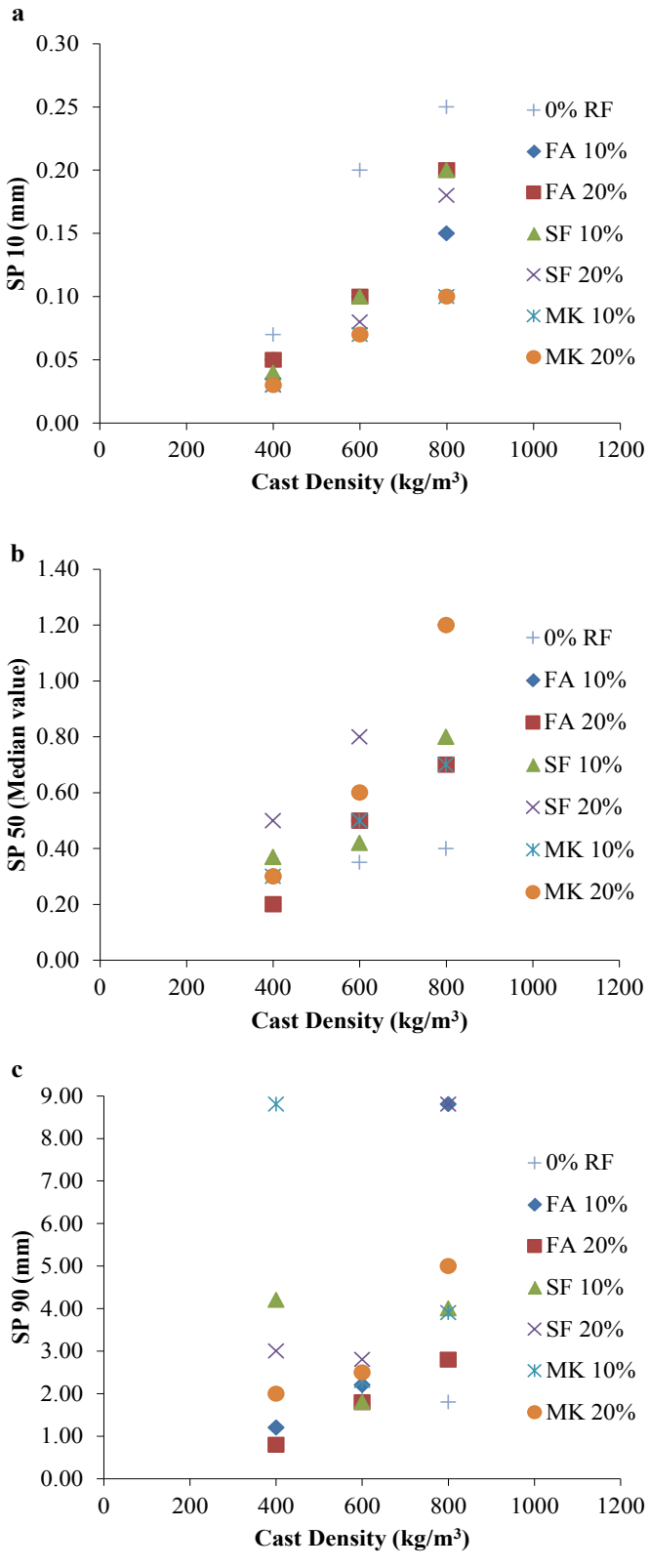

Figure 6.29: Relationship between air-void spacing parameters and the cast density; a) SP10; b) SP50; c) SP90.

Table 6.4: Air-Void Spacing Distribution Parameters

Mixes	Cast Density (kg/m^3)	SP10 (mm)	SP50 (mm)	SP90 (mm)
0% RF	800	0.25	0.40	1.80
	600	0.20	0.35	1.90
	400	0.07	0.30	2.00
FA 10%	800	0.15	1.20	8.80
	600	0.10	0.50	2.20
	400	0.05	0.30	1.20
FA 20%	800	0.20	0.70	2.80
	600	0.10	0.50	1.80
	400	0.05	0.20	0.80
SF 10%	800	0.20	0.80	4.00
	600	0.10	0.40	1.80
	400	0.04	0.37	4.20
SF 20%	800	0.18	3.70	8.80
	600	0.08	0.80	2.80
	400	0.03	0.50	3.00
MK 10%	800	0.10	0.70	3.90
	600	0.07	0.50	2.30
	400	0.03	0.30	8.80
MK 20%	800	0.10	1.20	5.00
	600	0.08	0.60	2.50
	400	0.04	0.30	2.00

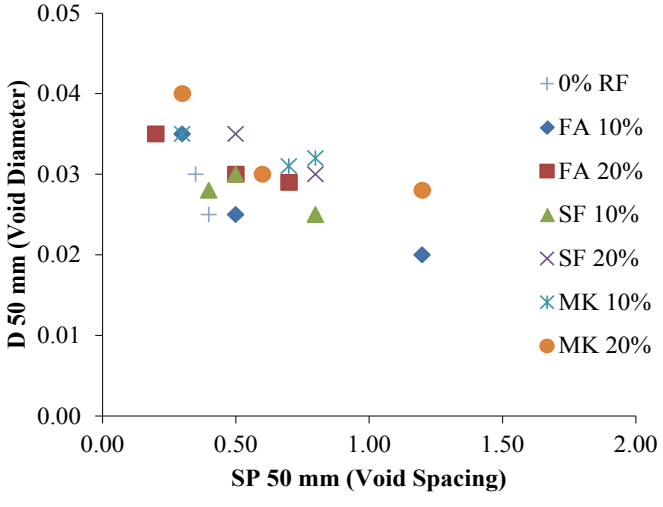

Figure 6.30: Relationship between the D50 and SP50.

Table 6.5: Equations for SP10 Air-Void Spacing Distribution Parameter

Mixes	Cast Density (Υ_d) (kg/m^3)	Fitted Equation for SP10 Air-Void Spacing	Adjusted R^2
0% Reference	800	$SP10=0.011Exp^{(0.003)\Upsilon_d}$	72.3%
	600		
	400		
FA 10%	800	$SP10=0.017Exp^{(0.003)\Upsilon_d}$	95.5%
	600		
	400		
FA 20%	800	$SP10=0.013Exp^{(0.003)\Upsilon_d}$	99.8%
	600		
	400		
SF 10%	800	$SP10=0.008Exp^{(0.004)\Upsilon_d}$	98.7%
	600		
	400		
SF 20%	800	$SP10=0.005Exp^{(0.004)\Upsilon_d}$	99.4%
	600		
	400		
MK 10%	800	$SP10=0.010Exp^{(0.003)\Upsilon_d}$	89.5%
	600		
	400		
MK 20%	800	$SP10=0.017Exp^{(0.002)\Upsilon_d}$	83.9%
	600		
	400		

Table 6.6: Equations for SP50 Air-Void Spacing Distribution Parameter

Mixes	Cast Density (Υ_d) (kg/m^3)	Fitted Equation for SP50 Air-Void Spacing	Adjusted R^2
0% Reference	800	$SP50=0.226Exp^{(0.001)\Upsilon_d}$	99.7%
	600		
	400		
FA 10%	800	$SP50=0.071Exp^{(0.003)\Upsilon_d}$	95.5%
	600		
	400		
FA 20%	800	$SP50=0.063Exp^{(0.003)\Upsilon_d}$	86.7%
	600		
	400		
SF 10%	800	$SP50=0.139Exp^{(0.002)\Upsilon_d}$	73.5%
	600		
	400		
SF 20%	800	$SP50=0.057Exp^{(0.005)\Upsilon_d}$	82.9%
	600		
	400		
MK 10%	800	$SP50=0.132Exp^{(0.002)\Upsilon_d}$	97.2%
	600		
	400		
MK 20%	800	$SP50=0.075Exp^{(0.003)\Upsilon_d}$	98.9%
	600		
	400		

6.7 Shape Factor of Cement-Based Foam

The circularity of an air-void inside the cement-based foam is known as the shape factor (Russ 2002), is a parameter which describes how close is the shape of any void as seen in 2D to a circle. In other words, the shape factor is a measure of the shape of the voids. If it is close to unity, then the shape is nearly circular. On the other extreme, a value close to zero indicates a highly elongated void (Aligizaki 2005). In present study, the circularity for

all the mixes was evaluated by using CT Analyser Software which has the built in facility to calculate this parameter.

6.7.1 Effect of Density on Shape Factor

Figure 6.31, 6.32 and 6.33 illustrates the frequency of shape factor for the cement-based foam for the reference mix against those with fly ash, silica fume and metakaolin, respectively across all three densities investigated here. From Figure 6.31, 6.32 and 6.33 it can be noticed as the density decreases, the frequency of occurrence of such voids that are circular or nearly so also decreases. In other words, as the density decreases, there is an increase in the irregularities in the void shape. This is to be expected as with lower densities the voids gets larger and this promotes coalescence and consequent irregularity. The same is applicable to the mixes having pozzolanic admixtures with different content.

6.7.2 Effect of Admixture and its Content on the Shape Factor

From Figure 6.31a for the cast density of 800 kg/m^3.It can be noticed that the frequency of occurrence of shape factor with numerical value of 0.9 to 1.0 reduces with the addition of fly ash and the difference with the reference mix was 10% when adding fly ash at 10% in binder and 18% when adding 20% fly ash in binder. That is with higher fly ash content, the frequency of occurrence of irregular pores increases thereby resulting in lower shape factor. However, for silica fume mixes as shown in 6.31b the difference noticed was 15% for 10% silica fume and 2% for 20% silica fume with respect to reference mix. This time higher substitution ratio of silica fume was resulting in more circular void and less irregularities whereas, lower substitution of silica fume was giving less perfect shape and more imperfection.

Similarly, both the metakaolin mixes were producing the same results and not any prominent difference was noticed between the two. Furthermore, the drop in the frequency noticed for the range of 0 to 0.9 due to addition of fly ash, silica fume and metakaolin mixes was 10%, 8% and 8% respectively. Figure 6.32a was investigated for fly ash mix for 600 kg/m^3 series. The addition of FA at both dosages shows a lower frequency occurrence of near circular pores (shape factor range 0.9 to 1.0) as compared to the reference mix. But, for the lower range of shape factor, the frequency increases as compared to the reference mix (i.e for shape factor < 0.8).

The same was noticed in Figure 6.32b and 6.32c with higher substitution of other admixture like SF and MK. It was found that these 20% silica fume and 20% metakaolin in the binder were comparatively less or equal to reference mix in the range of 0.9 to 1.0 shape factor whereas much higher in other shape factor ranges. In addition to this it was also noticed that the frequency reduction mean value for all the mixes when compared with the reference mix was 15%.With regard to mixes with 400 kg/m^3 cast density, a high shape factor is seen with any dosage of SF and also for MK at 10% in binder.

Thus, this discussion implies that the lower substitution of fly ash and metakaolin and higher ratio of silica fume improves the pore structure of 800 kg/m^3 but not very significantly whereas, other mixes shows less variation in shape factor in higher densities. However, for 600 kg/m^3 the higher ratio of admixture seems to be working effectively. For 400 kg/m^3 densities addition of silica fume in any ratio, fly ash and metakaolin in lower ratio significantly influences the frequency of shape factor.

Moreover, reduction for the range of 0-0.9 was found maximum for the 400 kg/m^3 cast density this indicates that the imperfection and irregularities are quite high for lower densities. Therefore, it can be concluded that the shape of the majority of the air-voids in all mixes was circular or spherical whereas the reduction in the of shape factor values in all mixes shows that some of the voids were irregular in shape which could be due to merging and overlapping of the voids but the probability of occurrence of extremely irregular shapes is very low. Kearsley (1999), Visagie (2000), and Nambiar et al. (2007) also noticed spherical shaped void with less irregularities in higher densities.

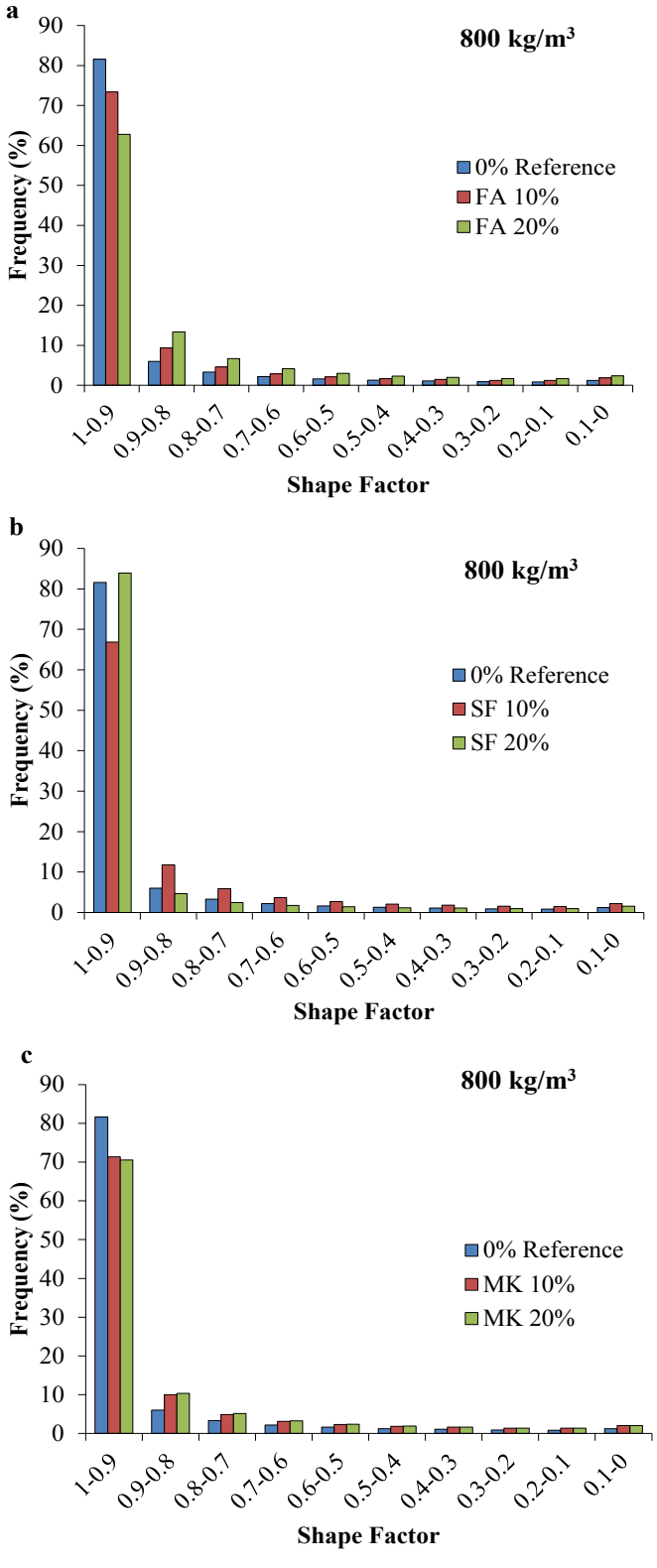

Figure 6.31: Shape Factor for the 800 kg/m^3 cast density; a) Mix with Fly Ash ;b) Mix with Silica Fume; c) Mix with Metakaolin.

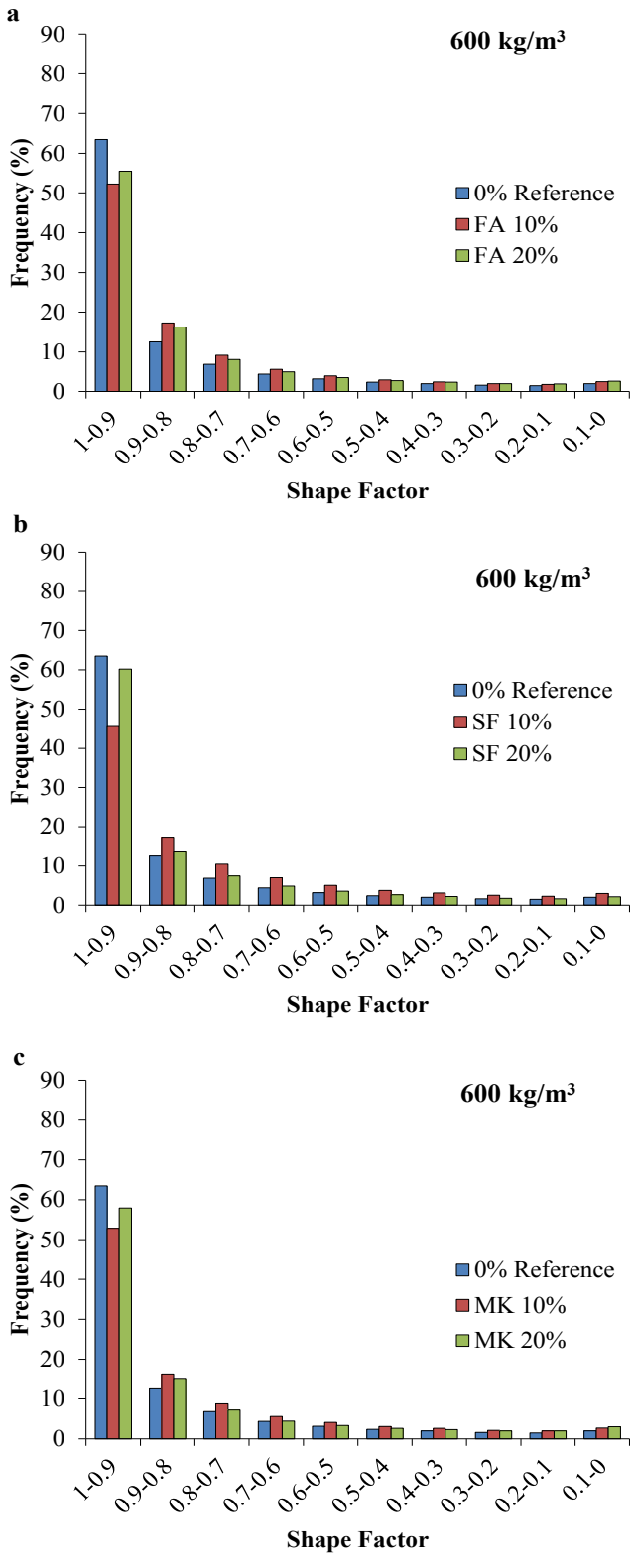

Figure 6.32: Shape Factor for the 600 kg/m^3 cast density; a) Mix with Fly Ash; b) Mix with Silica Fume; c) Mix with Metakaolin.

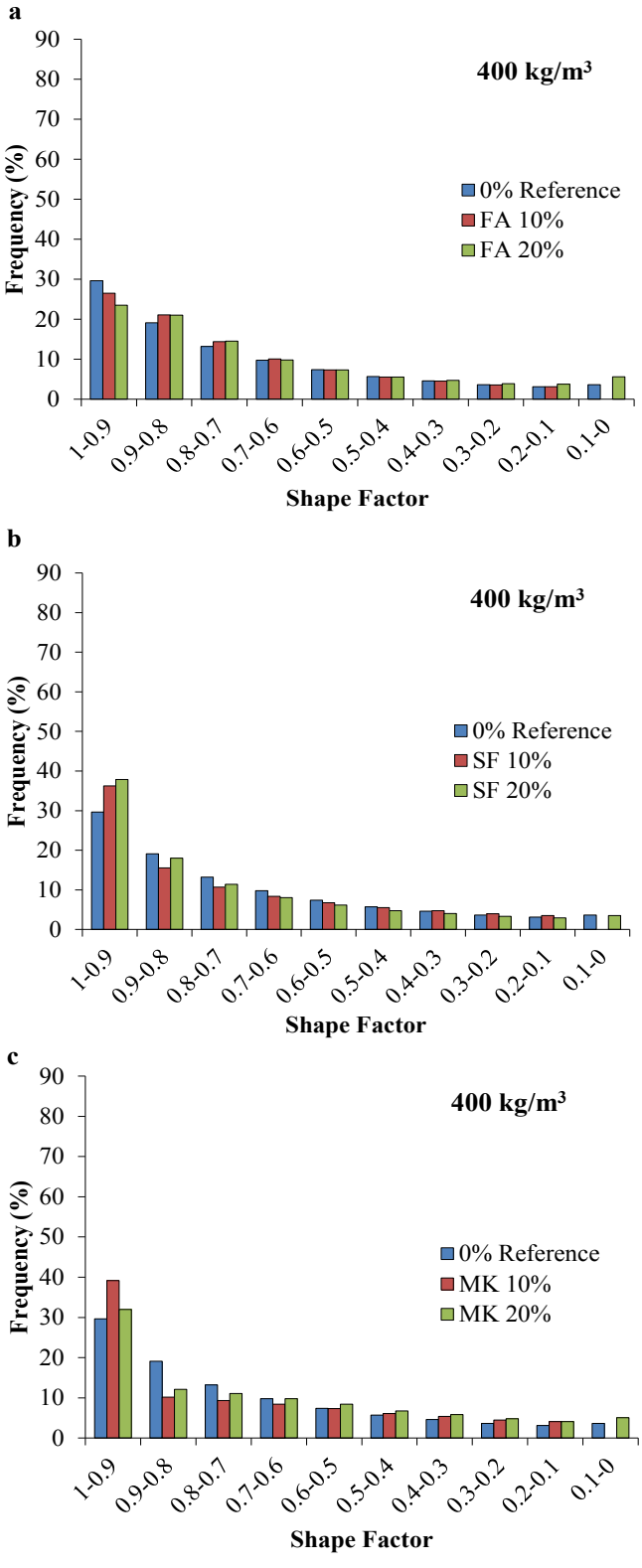

Figure 6.33: Shape Factor for the 400 kg/m^3 cast density; a) Mix with Fly Ash; b) Mix with Silica Fume; c) Mix with Metakaolin.

6.8 Conclusion

- The X-ray tomography (CT scan) images were able to identify the pores of with size ≥ 10 μm which, according to classification, fall under the macropores category.

- SEM showed that the higher densities have well-defined pore structure as compared to lower densities. With the addition of pozzolanic admixtures, the shape, number, uniformity and distribution of pores improves.

- Lower densities have more number of larger pores as compared with higher densities.

- The addition of fly ash increases the number of smaller pores, but the higher substitution ratio of fly ash does not significantly affect the number and size of pores. Similarly, silica fume in higher substitution leads to the formation of smaller pores. The same trend was noted for metakaolin.

- D50 is a function of porosity. As the D50 increases, the porosity increases linearly. Whereas, as the density increases, the value of D50 decreases for pore size, irrespective of the admixture type and content.

- The D90 value is slightly higher when the density is higher. The addition of the pozzolanic admixture lowers the value of D90 for densities greater than and less than 600 kg/m^3.

- As the density decreases, the frequency of occurrences for individual spacing size increases.

- As the density increases, the SP10 value increases. The maximum value in the range of 0.030-0.25 mm for 800 kg/m^3 and the minimum was recorded for 400 kg/m^3 cast density. The SP50 ranges between 0.20 and 1.20 mm.

- As D50 increases, the value for SP50 decreases. This is true for all the mixes.

7. Factors Influencing the Thermal Conductivity of Cement-Based Foam

7.1 Introduction

As mentioned earlier, cement-based foams are essentially combinations of phases namely, the paste and air-void. The thermal property of solid phase is dependent on the type of pozzolanic admixture, age of the mix and moisture content. Similarly, the void phase of the cement-based foam depend upon the foam content, mix density and the type of the binder.

This chapter presents in detail the analysis of the results from those experiments, highlighting the quantum and influences these various aforementioned parameters of solid and void phases have on the thermal conductivity. A relationship between the conductivity of cement-based foam and the factors on which it depends is also derived here.

7.2 Thermal Conductivity of Cement Paste (Solid Phase)

Specimens of cement paste were prepared with Portland cement and water without using sand or aggregate. The specimens were water cured for 28 days and after that air dried for further 30 days at room temperature. The thermal conductivity test was conducted on these samples by using the Transient Plane Heat Source and the results were extracted through the associated software as already explained in chapter 3. Values were recorded at the age of 60^{th}, 120^{th},210^{th} and 300^{th} day respectively. The mean thermal conductivity of hydrated cement paste tabulated in Table 7.1 is based on three data points.

Along with this, measured thermal conductivity of powder materials is given in Table 7.2. The thermal conductivity of the hydrated cement paste as a function of time is shown in Figure 7.1 and it was found that the conductivity of cement paste drops with its age. The present study has shown that this drop is significant up to 210 days and thereafter, it tends to stabilize. It can be seen that the conductivity drops is 15% between 60^{th} and 120^{th} days and 20% between 120^{th} to 210^{th} days and thereafter the change till 300^{th} day is nominal. This drop in conductivity as age advances is to be expected, since the free moisture in the specimen keeps reducing with age both due to hydration and due to evaporation. These findings are in agreement with those of Kim et al. (2003), Bentz (2007) and Milovanovic et al. (2011) respectively.

Figure 7.1 also plot the findings of Fu et al. (1999).It is clear that there was no change in conductivity over the entire period of their study. However, also note that they used air cured samples at a humidity of 40%. The conductivity at 28 days can be seen as 0.52 (w/m/k) much lower than those found in the present study whereas, the best comparison can be made of values for 120^{th} day and onwards which are quite close. This difference might be due to the rate of drying for samples which is much faster for air-drying than in the water cured samples examined here.

The findings of Demirboğa (2003) and Choktaweekarn et al. (2009) are also plotted as shown in Figure 7.1. It was observed that the oven dried thermal conductivity of hydrated cement paste containing sand was 1.18 (w/m/k) which is 61% times higher as compared to the present study value at 300^{th} day. This is probably due to the presence of sand which due to its crystalline silica nature leads to high thermal conductivity.

Table 7.1: Measured Thermal Conductivity of Hydrated Cement Paste

Thermal Conductivity	Testing Age(days)	0% Ref	FA 10%	FA 20%	SF 10%	SF 20%	MK 10%	MK 20%
Mean (w/m/k)	60	0.694	0.647	0.520	0.625	0.594	0.631	0.640
COV (%)		3.162	4.529	11.138	1.132	14.284	12.767	14.745
Mean (w/m/k)	120	0.594	0.581	0.509	0.545	0.508	0.565	0.588
COV (%)		13.313	1.656	4.743	0.908	14.809	7.717	5.277
Mean (w/m/k)	210	0.478	0.482	0.436	0.450	0.441	0.482	0.487
COV (%)		6.723	2.334	6.447	1.571	6.005	6.480	5.037
Mean (w/m/k)	300	0.458	0.458	0.407	0.415	0.416	0.456	0.461
COV (%)		1.467	2.457	0.800	1.704	4.645	2.993	10.553

Table 7.2: Measured Thermal Conductivity of Powder Material for Present Study

Material	Thermal Conductivity (w/m/k)
Portland Cement (HE)	0.169
Fly Ash (FA)	0.119
Silica Fume (SF)	0.092
Metakaolin (MK)	0.093
Water	0.600

Table 7.3: Measured Moisture Content of Hydrated Cement Paste containing Pozzolanic Admixture

Moisture Content (%)	Testing Age(days)	0% Ref	FA 10%	FA 20%	SF 10%	SF 20%	MK 10%	MK 20%
Mean	60	15.175	14.250	13.065	13.185	12.080	13.954	13.215
	120	11.691	13.502	11.834	12.105	11.043	12.339	11.463
	210	6.026	6.183	6.094	6.137	5.275	7.382	5.400
	300	5.245	5.450	4.500	3.085	3.200	5.285	4.275

Demirboğa et al. (2007) reported that the thermal conductivity of crystalline silica is 15 times of amorphous silica. In another study, Choktaweekarn et al. (2009) investigated cement paste with crushed limestone as fine aggregates. The specimens were kept under sealed curing conditions and reported the conductivity to be 0.96 (w/m/k) at 30th day. In addition to this Kim et al. (2003) reported the conductivity of paste (water and cement) at the age of 28 days to be 1.15 (w/m/k), the samples were moist cured and fully saturated at the time of testing.

It is interesting to mention here that Milovanovic et al. (2011) have reported thermal conductivity of cement paste at seven day of casting with w/c=0.6 and cured under 90% relative humidity conditions to be 1.45 (w/m/k). The present findings at 60th day were reported around 0.69 (w/m/k). It can be said that almost 50% of the conductivity values was reduced between 7 to 60 days. Although, the values are different (attributed to different water-to-binder ratio), the nature of drop is consistent with this present study.

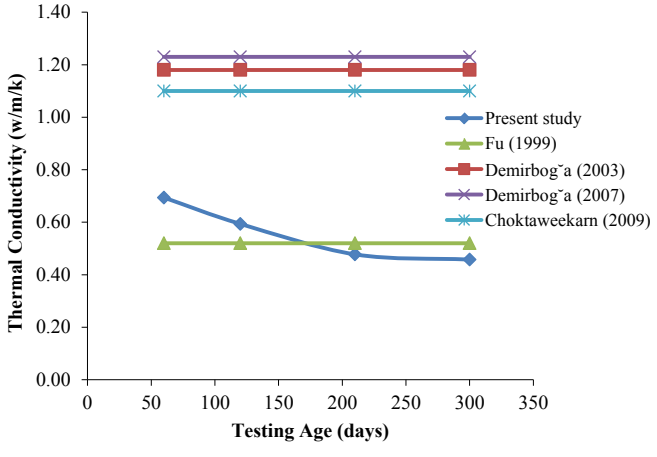

Figure 7.1: Thermal conductivity of hydrated cement paste as a function of time.

7.2.1 Effect of Pozzolanic Admixtures and Content

As mentioned in earlier chapters, specimens were made with three pozzolanic admixtures like fly ash (FA), silica fume (SF) and metakaolin (MK). In this case the substitution was 10% and 20% by weight of cement. The results are tabulated in Table 7.1 and shown in Figure 7.2. One infers that the addition of pozzolana reduces the conductivity at every age of maturity when compared to the reference mix with cement only. However, the quantum of drop due to any pozzolanic admixture is significant at the earlier ages and progressively insignificant at later age. Considering the quantitative variation in each case with respect to reference mix, it is seen in Figure 7.2a that the fly ash at 10% of binder caused a drop in conductivity of 7% at 60 days, reducing to 2% and 0.8% at 120 days and 210 days and only 0.06% at 300 days. With 20% substitution of cement with fly ash, the corresponding drop is 28% at 60 days, 15% at 120 days whereas, 9% and 12% for 210 and 300 days. Further, the results indicate that as far as the changes in conductivity between using 10% FA or 20% FA in binder are concerned, the increases in FA content results in a maximum drop of 22% when measured at 60 days, but this difference drops to 11% at 300 days. Clearly, due to the higher moisture demand at earlier age during ongoing hydration, the presence of FA is more significant.

Previous researchers Kim et al. (2003), Demirboğa et al. (2003), Demirboğa (2007), Demirboğa et al. (2007) and Bentz et al. (2011) have also noticed drop in conductivity, varies with an increase in the pozzolana content. However, as seen in Figure 7.1 these values remain unaltered through all ages, presumably due to the specimens in those studies being significantly drier.

Demirboğa (2003) investigated the thermal conductivity of mortar with 10% and 20% of fly ash replaced by weight of Portland cement. The samples were over dried at the time of testing and 1:2 was the binder: sand ratio. The author observed that the presence of fly ash and especially in higher substitution effectively reduces the conductivity. For example the author reported that the 10% of fly ash reduces the conductivity up to 15% with respect to the reference mix whereas 20% was responsible for 29% reduction these difference are higher as compared to present study finding. Comparatively, the reduction between the two ratios noticed was 15% which is close to present study findings.

The behavior of mixes with SF (Figure 7.2b) is the same as the foregoing observation for FA. For mixes with 10% SF/cement ratio, the drop in conductivity was 11% at 60 days and 10% at 300 days. For mixes with 20% SF/cement ratio, the corresponding drop was 16% at 60 days and 10% at 300 days. Further, the drops between the two dosages were even smaller in this case compared to FA as admixture.Demirboğa (2003) also investigated the thermal conductivity of mortar containing 10% and 20% of silica fume replaced by cement weight and observed that there was a reduction in conductivity at 17% and 31% relatively, when compared with the reference mix. This drop is primarily due to the reduction in the density (or higher porosity) of mortar with the addition of silica fume, as well as partly due to amorphous contents which results in the creation of amorphous hydration products. Note that the thermal conductivity of amorphous silica is lower than that of crystalline silica.

In another study on lightweight concrete made with pumice stone aggregates and oven dried samples, the silica fume was added in the replacement of cement in the ratio of 10%, 20% and 30% by weight.

Demirboğa et al. (2003) reported that the conductivity of concrete was reduced by 43% with SF as admixture and also observed that the fly ash to be more effective than silica fume for reducing the conductivity. Figure 7.3 summarizes the comparison of thermal conductivity of hydrated cement paste containing fly ash and silica fume recorded by Demirboğa (2003) and in the present study. It can be seen that Demirboğa (2003) values are higher as compared to this study which can be anticipated due to different mixtures i.e. lightweight concrete and cement-based foam.

With regard to use of MK as admixture, although there is a drop in comparison with the reference mix, Figure 7.2c illustrates how increasing the dosages does not cause any appreciable drop in the thermal conductivity at any age. The actual reduction when compared over the reference mixes was 8.5% at 60 days and 0.4% at 300 days when considering the 10% MK/cement ratio The corresponding values are 10% and 0.6% for the 20% MK/cement ratio. The maximum fallout was at the initial age which is similar with the fly ash and silica fume mixes. In addition to this the conductivity reduction between the two dosages was smaller, being 1.5% at 60 day and 1% at 300 days. Therefore it can be said that higher metakaolin (MK) dosages do not significantly effective the thermal conductivity which is opposite to fly ash and silica fume findings.

Overall, it can be concluded that the addition of pozzolanic admixture does not significantly reduces the thermal conductivity. In comparison, addition of silica fume resulted in more reduction which could be due formation of CSH in higher amount and due to pore filling. However, significant reduction in slurry density with the addition of fly ash could be the reason for conductivity reduction. For metakolain higher water absorptive property may be the reason.

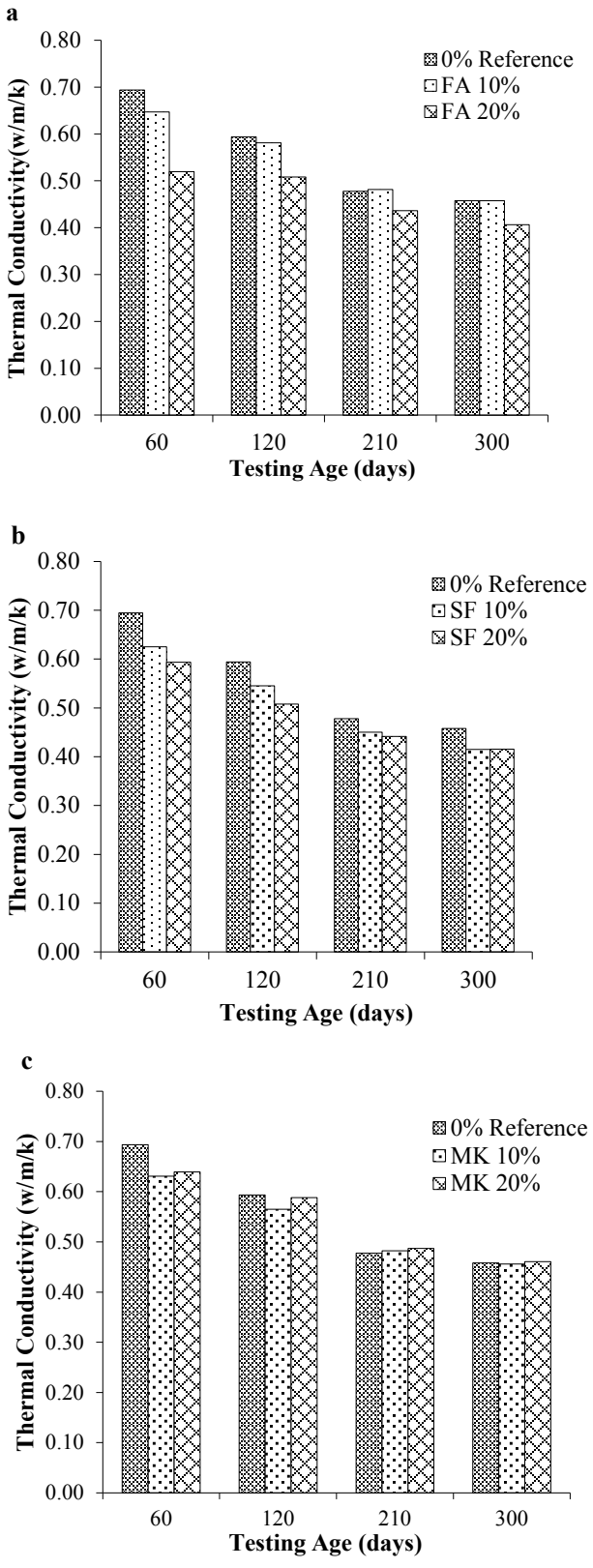

Figure 7.2: Thermal conductivity of cement paste (solid phase) as a function of time; a) Mix with Fly Ash; b) Mix with Silica Fume; c) Mix with Metakaolin.

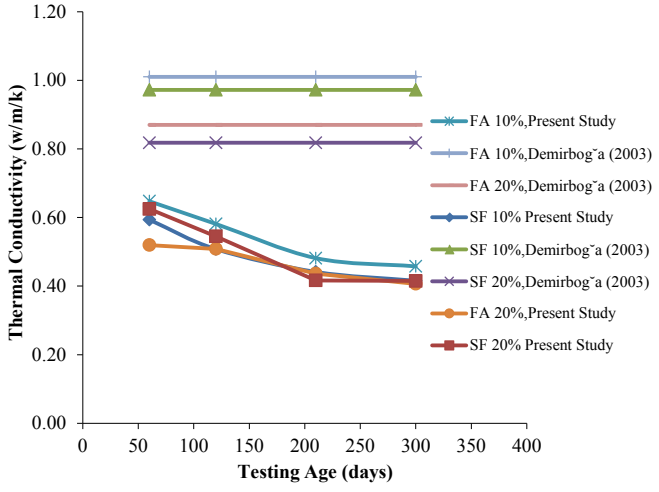

Figure 7.3: Thermal conductivity of hydrated cement paste according to other researchers.

7.2.2 Effect of Moisture Content

Water in cement paste can be present in three different forms namely, i) the chemically bound water which is non-evaporable; ii) the physically bound water which can be lost on oven drying and iii) the free water, also evaporable on air-drying (Aligizaki 2005). In the following discussion, the moisture refers to that is left after loss of water through air-drying of samples at the time of test. Moisture content of three samples from each mix after oven drying was calculated by weight using Equation 3.4 (chapter 3) for different period of time. The moisture content values of hydrated cement paste containing admixture is tabulated in Table 7.3.

Figure 7.4 illustrates the mean moisture content of cement paste containing fly ash, silica fume and metakaolin as a function of time. It can be seen that addition of higher admixture to binder resulted in reduction of the moisture content and interestingly, same trend was observed for all the three mixes. This implies that cement replacement by weight with other admixtures

reduces the moisture content at a particular age, and this drop could be due to the higher water demand by Portland cement for hydration.

Moreover, it can also be noticed from Figure 7.4 that maximum drop in moisture content occurred between the age of 120 to 210 days. This is basically due to loss of evaporable water from the paste. After 210 days most of the free moisture and the physically bound water evaporates, only the chemical bound remains. In the present study, the mean drop in moisture content for all four case namely, the reference mix was 64% and those with each of the three admixtures (FA,SF,MK) at two specific dosages of 10% and 20% was 74%,65%,50% and 64%,70%, and 71% for the period of 120 to 210 days respectively.

As regards the variation of thermal conductivity with moisture, since water has high conductivity, it should be expected that thermal conductivity will drops significantly. The moisture in the specimens reduces over a period due to loss on drying and due to conversion of moisture in the mix into chemically bound water of hydration. Figure 7.5 below illustrates this point clearly. The conductivity is plotted against an increase in the moisture content and one can see the trend in all cases of the three admixtures. In case of FA, the variation is 0.4 (w/m/k) to 0.65 (w/m/k). For mixes with SF too, the values lie in this range. But in case of MK, the minimum noted was 0.48 (w/m/k) and the maximum was 0.62 (w/m/k) and there was nominal change with MK dosage. Similar conclusions have been drawn by other researchers like Khan (2002) and Choktaweekarn et al. (2009). A study carried out by Kim et al. (2003) observed 24% increases in conductivity of the hydrated cement paste due to the presence of moisture.

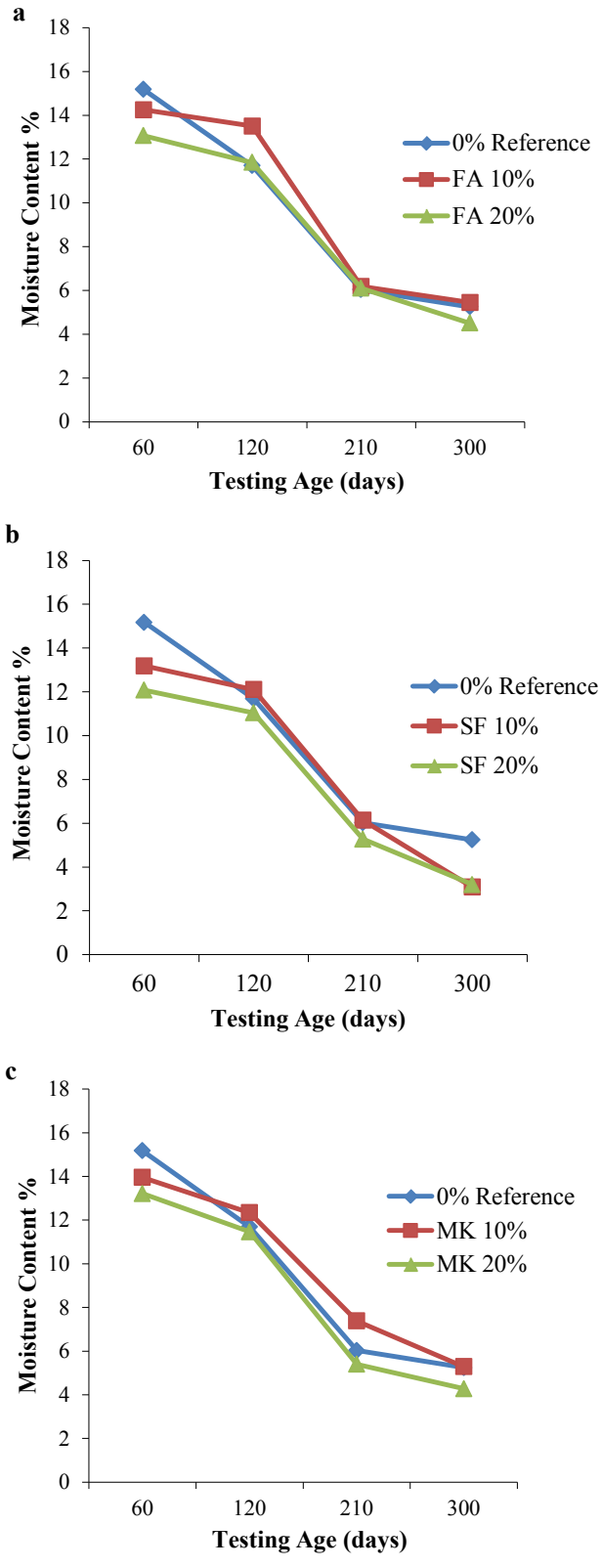

Figure 7.4: Moisture Content as a function of time of hydrated cement paste (slurry); a) Mix with Fly Ash; b) Mix with Silica Fume; c) Mix with Metakaolin.

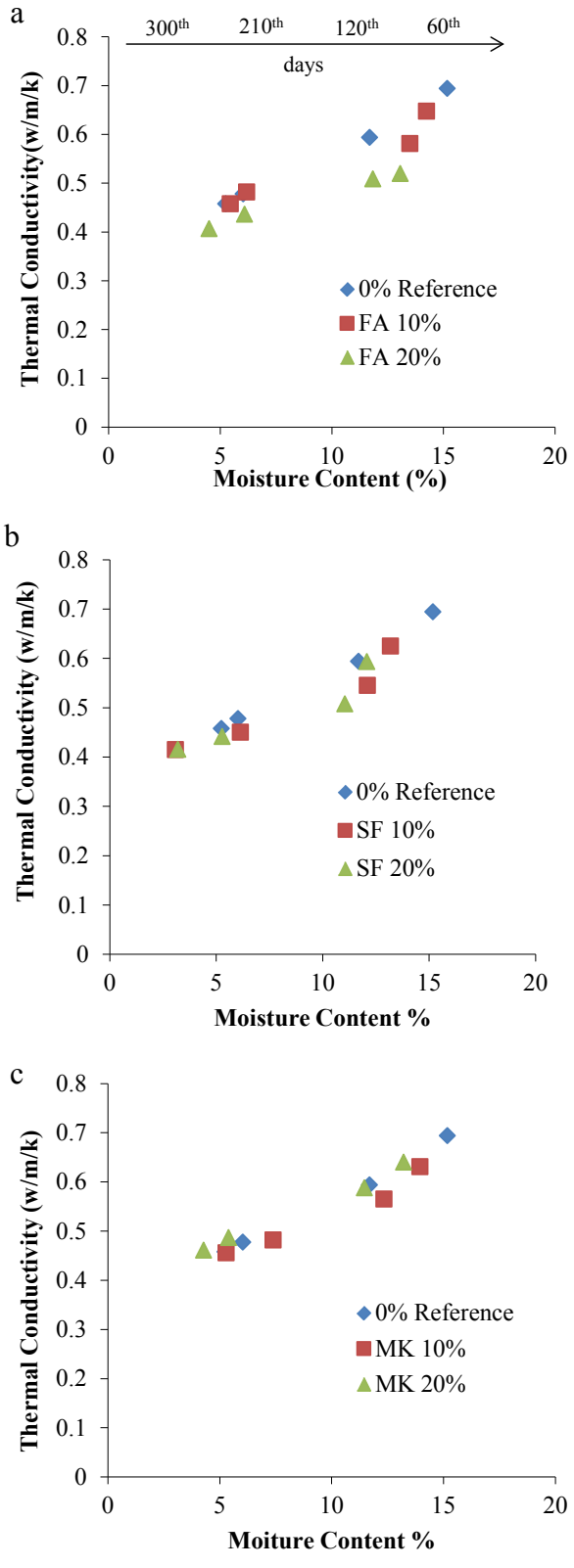

Figure 7.5: Relationship of thermal conductivity of hydrated cement paste (slurry) with moisture content; a) Mix with Fly Ash; b) Mix with Silica Fume; c) Mix with Metakaolin.

7.3 Thermal Conductivity of Cement-Based Foams

As already mentioned in the earlier chapters, a total of 18 specimens for each mix and six specimens for each cast density were tested for conductivity. The mean measured thermal conductivity for six data points from each mix is tabulated in Table 7.4, 7.5 and 7.6.

Figure 7.6, 7.7 and 7.8 respectively show the variations in conductivity with the cast densities. As already stated in this study, three distinct densities namely 800,600 and 400 kg/m^3 were chosen for the lightweight foams. Each of these figures has three separate plots to highlight the effect of different densities on the conductivity for the ages from 60-300 days. It can be noticed in Figure 7.6a, 7.7a and 7.8a that the measured thermal conductivity of 0% reference mix decreases with the passage of time and the reduction noticed between 60 to 300 days of testing period was 33%, 28% and 31% respectively for the three cast densities. Interestingly, after 210th days the conductivity becomes more or less constant and this is true for all the three densities.

ACI 523.1(2006) reported the thermal conductivity values for the oven dried cellular concrete using lightweight aggregates as 0.20, 0.16 and 0.13 (w/m/k) for 800, 640 and 480 kg/m^3 respectively. As it can be noticed that ACI 523.1(2006) reported values are 11%, 28% and 4% higher when compared with values at 300th day which is considered to be in most dry state. Thus, this difference could be due to presence of lightweight aggregate in ACI 523.1(2006) samples which is resulting in higher values.

7.3.1 Effect of Admixture Type and Content

Figure 7.6, 7.7 and 7.8 bring out the fact that the thermal conductivity values of cement-based foam decreases with the addition of admixture of all types. The conductivity again further decreases with the advancing age of testing. This trend was also noticed by many researchers working with other building materials (Khan 2002, Kim et al. 2003, Bentz 2007 Choktaweekarn et al. 2009) even in section 7.2.1, dealing with cement paste, the same trend was observed. For the cast density of 800 kg/m^{3}from Figure 7.6a, 7.6b, 7.6c it can be noticed that on 60th day the thermal conductivity for all the mixes is in the range of 0.200-0.250 (w/m/k). Whereas, after 300 days, the drop is in the range of 0.166-0.183 (w/m/k) which means the total reduction over this period is in the range of 20-36% respectively this also includes the moisture effect.

The analysis of the effect of the type of pozzolana on the conductivity reveals that silica fume drops the conductivity most among all the three types of admixtures discussed in this study. Considering the values at the 60th day and taking reference mix as a measuring mix, it can be seen that with 10% SF, the drop in conductivity is about 10% and with 20% SF in binder, the drop is about 16%. As opposed to this, when FA was used, the corresponding drops were only 2% and 7%, respectively.

However, metakaolin shows a different trend. At 10% MK in binder, there was a drop of 2% with respect to the reference mix. But, when the dosage is 20% MK in binder, instead of a further drop as with the other two admixtures, the thermal conductivity rose. The Figures 7.6 also reveals that as age of the specimen's increases to 300 days, there is only a slight drop in the thermal conductivity with respect to the reference mix.

Table 7.4: Measured Thermal Conductivity of Cement-Based Foam containing Fly Ash

Thermal Conductivity	Testing Age (days)	Cast Density								
		800kg/m^3			600kg/m^3			400kg/m^3		
		0% RF	FA 10%	FA 20%	0% RF	FA 10%	FA 20%	0% RF	FA 10%	FA 20 %
Mean(w/m/k)	60	0.240	0.237	0.223	0.160	0.163	0.152	0.100	0.108	0.088
COV %		3.247	2.462	1.112	1.568	1.724	1.851	2.501	3.207	3.550
Mean(w/m/k)	120	0.220	0.219	0.214	0.150	0.158	0.144	0.090	0.101	0.082
COV %		5.161	2.720	3.558	5.645	0.732	1.366	3.660	2.765	2.133
Mean(w/m/k)	210	0.190	0.182	0.184	0.130	0.141	0.129	0.080	0.088	0.078
COV %		5.629	6.209	2.299	7.556	1.554	1.214	3.134	2.882	3.735
Mean(w/m/k)	300	0.180	0.183	0.182	0.125	0.136	0.122	0.076	0.081	0.074
COV %		3.368	2.465	3.869	5.983	3.563	1.902	5.931	8.693	2.423

Note:RF stands for reference

Table 7.5: Measured Thermal Conductivity of Cement-Based Foam containing Silica Fume

Thermal Conductivity	Testing Age (days)	Cast Density					
		800kg/m^3		600kg/m^3		400kg/m^3	
		SF 10%	SF 20%	SF 10%	SF 20%	SF 10%	SF 20%
Mean (w/m/k)	60	0.218	0.203	0.140	0.123	0.097	0.090
COV %		2.518	3.075	1.945	2.881	1.965	1.858
Mean (w/m/k)	120	0.196	0.187	0.128	0.115	0.088	0.080
COV %		5.351	1.672	4.268	2.811	3.323	3.265
Mean (w/m/k)	210	0.173	0.161	0.113	0.101	0.079	0.070
COV %		3.031	1.531	3.653	2.444	4.298	2.102
Mean (w/m/k)	300	0.173	0.166	0.111	0.100	0.079	0.071
COV %		3.831	3.849	3.944	4.372	6.042	3.777

Table 7.6: Measured Thermal Conductivity of Cement-Based Foam containing Metakaolin

Thermal Conductivity	Testing Age(days)	Cast Density					
		800kg/m^3		600kg/m^3		400kg/m^3	
		MK 10%	MK 20%	MK 10%	MK 20%	MK 10%	MK 20%
Mean(w/m/k)	60	0.236	0.250	0.151	0.168	0.095	0.097
COV%		1.707	4.951	1.827	5.522	2.390	3.076
Mean(w/m/k)	120	0.214	0.220	0.137	0.142	0.083	0.085
COV%		3.968	2.823	1.837	6.371	2.726	2.012
Mean(w/m/k)	210	0.180	0.182	0.120	0.124	0.074	0.076
COV%		3.934	4.128	3.903	3.160	2.940	4.302
Mean(w/m/k)	300	0.176	0.179	0.119	0.121	0.074	0.074
COV%		6.972	2.856	3.853	4.441	3.279	2.139

A comparison with the case of the cementitious paste (i.e. simulating the solid phase) shows that a similar trend was obtained (see Figure 7.2). The Figure 7.7a, 7.7b, 7.7c illustrate the thermal conductivity for the mixes with the cast density of 600 kg/m^3.It can be noticed that the conductivity is in the range of 0.123-0.168 (w/m/k) at 60th day (ageing time) for all the mixes. Moreover, as age approaches to 300 days the conductivity drops further and the range noticed was of 0.100-0.136 (w/m/k).Thus, the drop for entire period lies in the range of 23%-24%. For 60th day and with regard to reference mix here again, SF shows the maximum drop: At 10% dosages of SF, it is 13% and at 20% SF in binder, it drops to 25% of the reference mix. The effect of FA is not much at this density, it leading only to a drop of 2% and 5% respectively for 10% and 20% dosages.

Similarly, in case of metakaolin, the corresponding drops are 6% and 5%. In other words, in case of MK at 20% binder, there was a rise in conductivity over the mix with 10% MK in binder, which was contrary to other admixtures. This is at variance with the normal trend seen in cases of the other two admixtures. Further, as the age approaches 300th day the reduction in conductivity values are 9% and 3%, for mixes with FA, 11% and 25% for mixes with SF and 5% and 3% for mixes with MK, respectively. Awang et al. (2012) investigated the thermal conductivity of lightweight foamed concrete. For the cast density of 600 kg/m^3, after oven drying the samples with 15% and 30% substitution of fly ash along with sand, reported that the conductivity was equals to 0.17 and 0.16 (w/m/k). However, the present study measured 0.136 and 0.122 (w/m/k) for 10% and 20% fly ash for the same density. This difference can be anticipated due to the presence of the fine sand, which has the thermal conductivity of 0.15 (w/m/k).

The Figures 7.8a, 7.8b and 7.8c show the behaviour of conductivity when the mix density is 400 kg/m^3.At the outset it is evident that as this density is lowest so is the conductivity in all cases including the reference mix. The actual values are only in the range of 0.09–0.18 w/m/k at 60 days age. At 300th day, the values dropped to 0.071–0.074 w/m/k. The total drop is between 26% and 45%, depending on the type of pozzolana over the entire period of examination. In other words, at 400 kg/m^3, the drop in conductivity due to addition of pozzolanic admixture is significant, compared to higher densities.

To conclude this discussion, the 300th day results are compared to exclude the influence of moisture. It can be safely assumed that by this age the hydration is significantly progressed and also that free moisture has evaporated. So, any influence on conductivity can be taken due to admixtures only. At the higher density of 800 kg/m^3, the difference in drops in conductivity between FA dosage of 10% and 20% was merely 1%. However, at lower densities this value was significant at over 10%. This clearly shows that at higher densities, an increase in the dosage of fly ash does not ensure a correspondingly noticeable reduction in the conductivity but for lower densities, an increase in admixture brings down the conductivity considerably.

With SF mixes, it is seen that at higher density of 800 kg/m^3, an increase in dosage from 10 to 20% resulted in a drop in conductivity of only 5%. Consequently, for lightweight densities in this study, the corresponding value is 10% between the two dosages. That is, a case similar to the FA case discussed already above. As far metakaolin in the mix, it is already reported in the foregoing paragraph that 20% dosage results in an increase in conductivity compared to mixes with 10% MK.

The results reveal that for high density of 800 kg/m^3, this difference is 2% and for the lower densities in this study, the corresponding difference was 3%. In other words, with the metakaolin mixes, there is certainly a drop in conductivity with regard to the reference mix. However, increasing the dosage does not significantly change the conductivity. The foregoing conclusion is only as far as the choice of pozzolanic admixtures examined. The fact that the overall conductivity depends quite significantly on the moisture content and on the porosity in the mixes, therefore it should be taken into account.

So, it may be suggested that when mix density is at 800 kg/m^3, it is best to choose silica fume as the pozzolanic admixture at 20% of binder. For lighter mixes (400 kg/m^3), both FA and SF are suitable to achieve similar reductions in conductivity at 20% of binder. On the other hand when metakaolin is the admixture, it is likely best to keep the dosage limited to 10%, which does indeed result in a lower conductivity.

Finally, it can be concluded that the reduction in thermal conductivity in presence of fly ash is mainly due to hydrated products (CH and CSH), porosity and less water absorptive property. Same can be reported for silica fume except that higher silica content also contributes in further reduction. Whereas, for metakaolin along with hydrated products and porosity, its high water absorptive property plays the vital role.

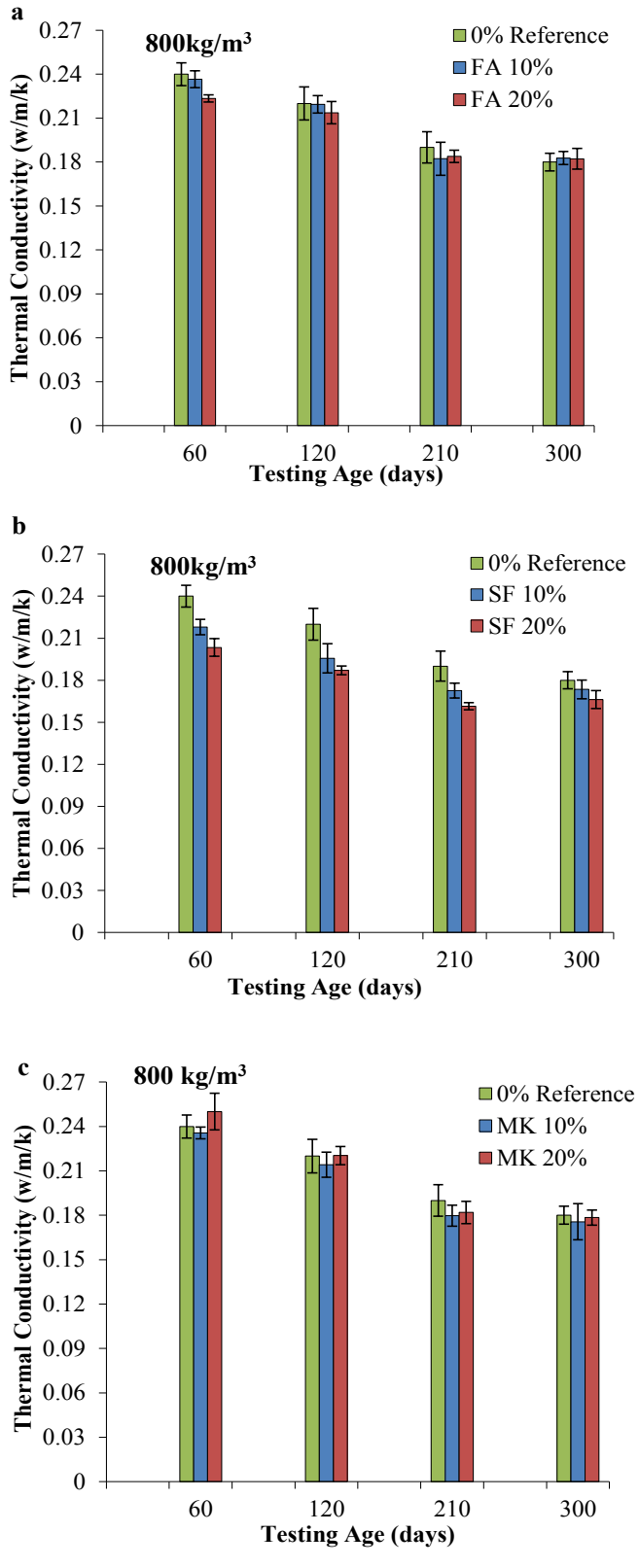

Figure 7.6: Thermal Conductivity of cement-based foam as a function of time for the 800 kg/m^3 cast density; a) Mix with Fly Ash; b) Mix with Silica Fume; c) Mix with Metakaolin. The error bars indicates the standard deviation for six data points.

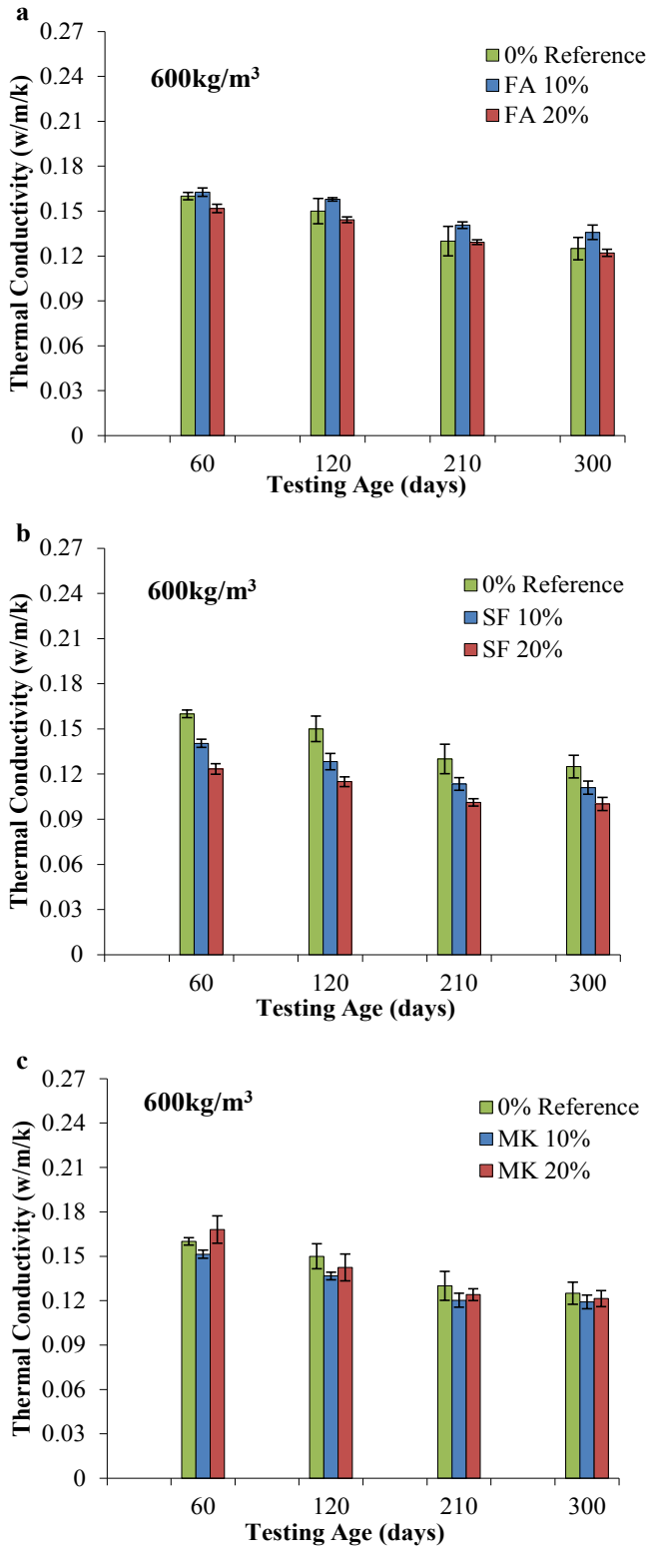

Figure 7.7: Thermal Conductivity of cement-based foam as a function of time for the 600 kg/m^3 cast density; a) Mix with Fly Ash; b) Mix with Silica Fume; c) Mix with Metakaolin. The error bars indicates the standard deviation for six data points.

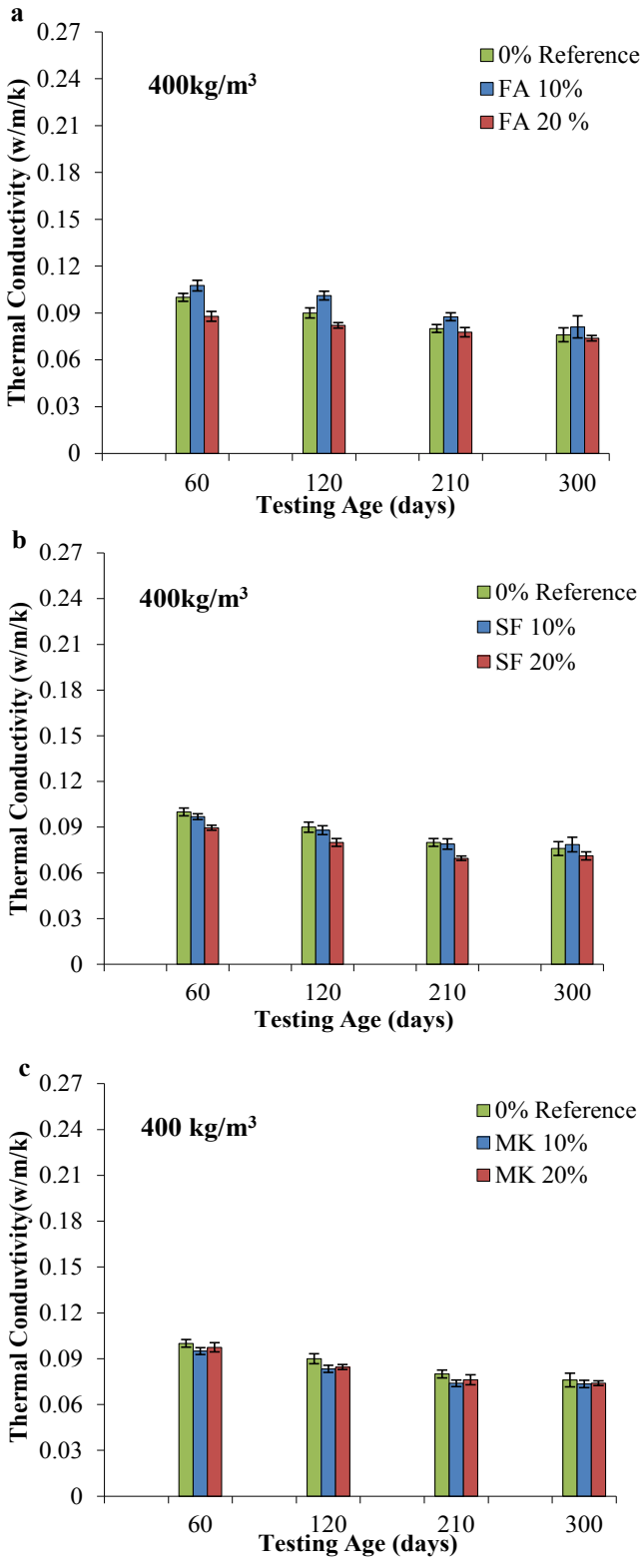

Figure 7.8: Thermal Conductivity of cement-based foam as a function of time for the 400 kg/m^3 cast density; a) Mix with Fly Ash; b) Mix with Silica Fume; c) Mix with Metakaolin. The error bars indicates the standard deviation for six data points.

7.3.2 Effect of Density

As mentioned earlier the required cast density is achieved by adding foam into the cement paste at the time of mixing. The addition of foam creates an air-void network within the cement paste thus reducing the density. Higher the foam content, lower is the density. Pozzolanic addition also results in the reduction of the density. The relationship of thermal conductivity with mean density for the mixes with and without pozzolanic admixture is plotted in Figure 7.9, 7.10 and 7.11. The Figures illustrates the relationship between the conductivity and the density-at-test for 60^{th} and 300^{th} day. These two dates are chosen because while at the 60^{th} day, the specimens are still partially wet, at 300^{th} day, they may safely be assumed to be dry. The mean density recorded at test for all the mixes at different period of time along with coefficient of variance are tabulated in Table 7.7, 7.8 and 7.9 respectively.

In order to make a quantitative analysis, the extent of variation in conductivity at two ranges of densities have been examined for 300^{th} day, i.e in the range of 800-600 kg/m^{3}and 600-400 kg/m^3.The conductivity of the reference mix noticed was about 36% and 48% for these respective density ranges (Figure 7.9). Similarly for 10% fly ash in binder, it was 30% and 50% respectively. When the fly ash dosage was 20% in binder, the reduction noticed was 39% and 49% for the said density ranges. As regards mixes with silica fume, Figure 7.10 gives values against different densities. The corresponding values of drop for the two ranges of density with 10% SF in binder, they were 43% and 34%. Again, when the SF dosage was raised to 20% of binder, the corresponding values for reduction in conductivity was 50% and 34%, respectively. With mixes containing MK, the corresponding values were respectively, 38% and 47%: (10% MK in binder), 38% and 48% (at 20% MK in binder).

It can be said that the change in density significantly reduces the conductivity and this reduction was around 35% for 800-600 kg/m^3 and 46% for 600-400 kg/m^3 densities range. However, further 5% reduction in the conductivity, for the both densities range was noticed due the addition of pozzolanic admixtures. Thus, it can be concluded that as compared to pozzolanic admixture the reduction in the thermal conductivity of cement-based foam is greatly influence by the change in density.

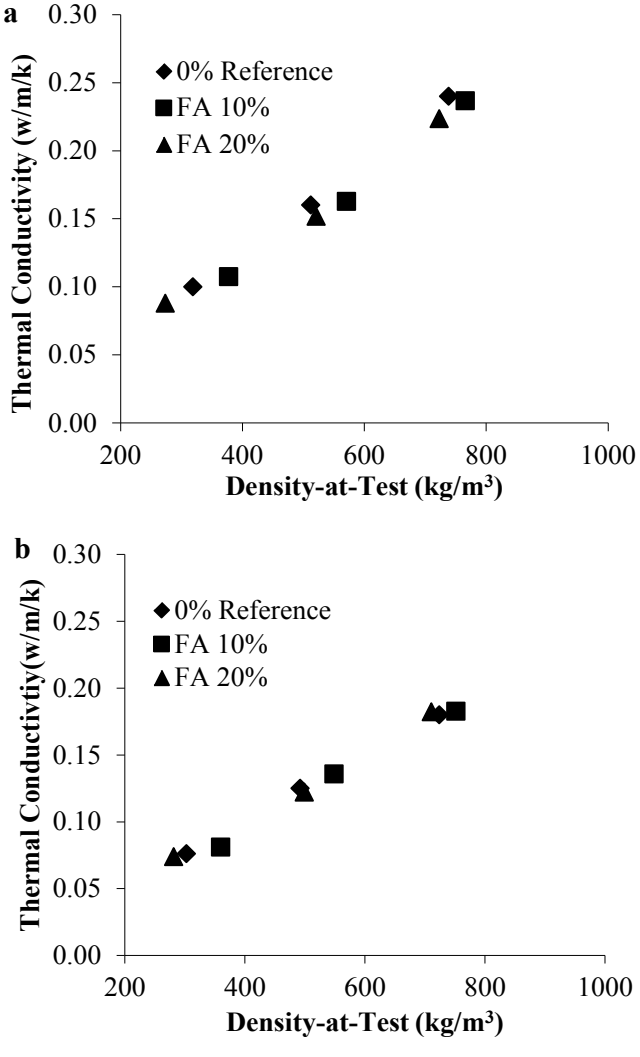

Figure 7.9: Thermal Conductivity of cement-based foam as a function of density for Fly Ash mix; a) 60th day; b) 300th day.

Table 7.7: Measured Density-at-test of Cement-Based Foam containing Fly ash.

Density-at-Test	Testing Age (days)	Cast Density 800 kg/m^3			Cast Density 600 kg/m^3			Cast Density 400 kg/m^3		
		0% RF	FA 10%	FA 20%	0% RF	FA 10%	FA 20%	0% RF	FA 10%	FA 20 %
Mean (kg/m^3)	60	738.19	766.01	723.10	512.05	570.90	521.29	318.55	377.58	281.39
COV %		2.23	3.11	0.89	2.32	2.78	1.68	5.86	5.50	7.98
Mean (kg/m^3)	120	728.76	759.88	717.06	505.83	568.63	516.77	309.49	369.66	275.17
COV %		2.26	3.628	1.12	2.55	2.66	1.64	5.52	2.10	8.06
Mean (kg/m^3)	210	730.74	737.43	715.93	507.26	557.88	515.26	307.23	352.68	274.04
COV %		2.21	3.48	1.14	2.57	5.12	1.58	6.19	7.69	8.01
Mean (kg/m^3)	300	723.67	751.39	710.46	492.06	548.64	499.23	302.70	359.66	273.47
COV %		1.75	2.79	1.12	2.40	2.36	1.51	2.29	5.44	8.11

Table 7.8: Measured Density-at-test of Cement-Based Foam containing Silica Fume.

Density-at-Test	Testing Age(days)	Cast Density 800kg/m^3		Cast Density 600kg/m^3		Cast Density 400kg/m^3	
		SF 10%	SF 20%	SF 10%	SF 20%	SF 10%	SF 20%
Mean (kg/m^3)	60	771.01	772.33	508.29	490.27	331.94	286.98
COV %		4.97	1.53	2.73	2.98	3.36	3.77
Mean (kg/m^3)	120	762.90	764.03	492.82	483.39	325.15	288.11
COV %		3.81	1.75	2.91	3.31	3.23	3.04
Mean (kg/m^3)	210	758.00	752.71	499.61	475.66	326.28	268.95
COV %		4.41	1.52	2.82	3.45	2.87	7.67
Mean (kg/m^3)	300	755.17	750.07	498.67	473.58	319.87	270.46
COV %		4.30	1.55	2.92	3.42	4.58	2.58

Table 7.9: Measured Density-at-test of Cement-Based Foam containing Metakaolin.

Density-at-Test	Testing Age(days)	Cast Density 800 kg/m^3		Cast Density 600 kg/m^3		Cast Density 400 kg/m^3	
		MK 10%	MK 20%	MK 10%	MK 20%	MK 10%	MK 20%
Mean(kg/m^3)	60	779.50	779.12	537.33	547.89	307.23	291.58
COV %		2.49	1.03	3.14	2.31	3.79	4.05
Mean(kg/m^3)	120	771.39	787.98	521.49	544.31	300.07	286.87
COV %		2.55	1.57	3.30	1.73	2.78	2.31
Mean(kg/m^3)	210	763.65	762.71	529.41	537.14	296.86	281.21
COV %		2.18	1.03	3.44	2.24	3.16	3.69
Mean(kg/m^3)	300	759.13	755.92	528.92	533.18	295.35	275.89
COV %		2.41	2.23	3.59	2.28	2.99	3.59

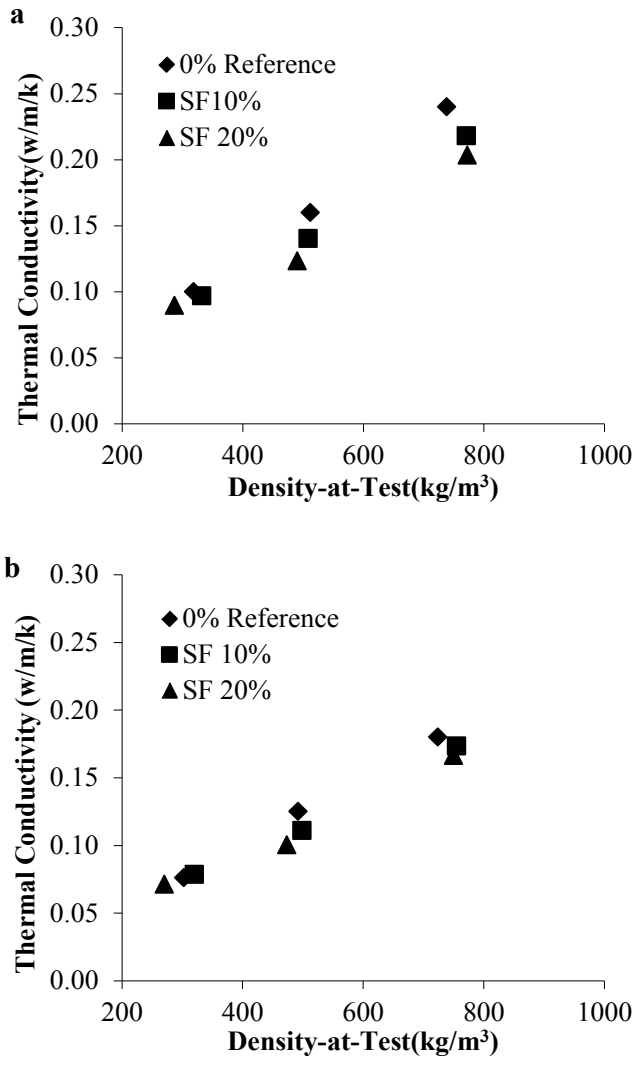

Figure 7.10: Thermal Conductivity of cement-based foam as a function of density for Silica Fume mix; a) 60th day; b) 300th day.

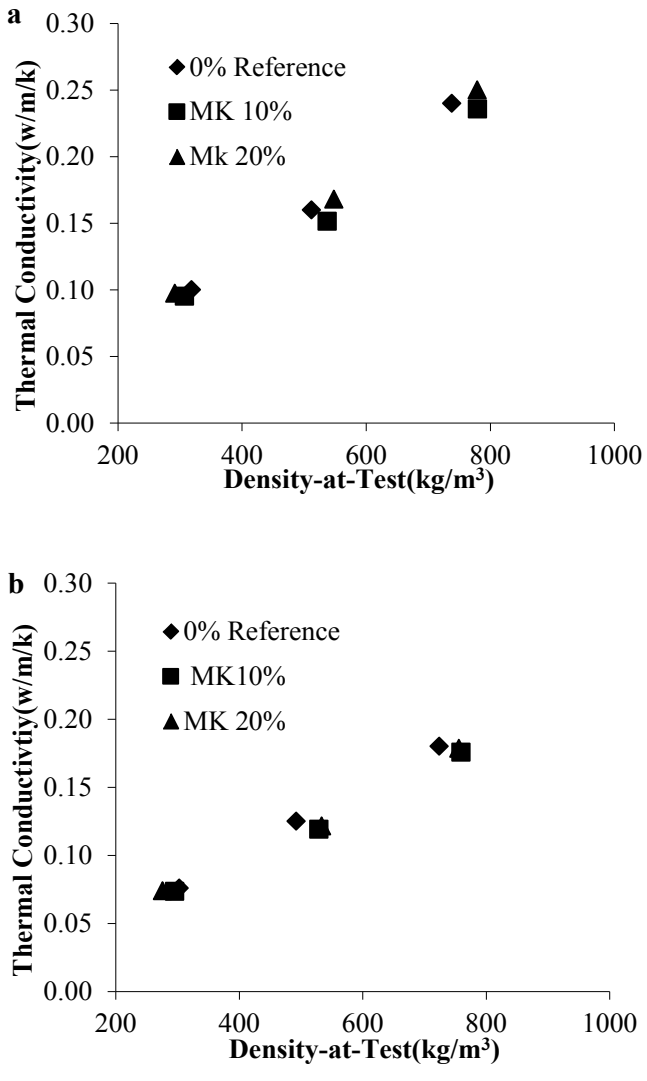

Figure 7.11: Thermal Conductivity of cement-based foam as a function of density for Metakaolin mix; a) 60th day; b) 300th day.

7.3.3 Effect of Porosity (Void)

In this study porosity is based on only air-voids (macropores) other pores were not included nor investigated as they are out of scope. The porosity for all the seven mixes was evaluated through CT scan at 300th days as discussed in chapter 6 (section 6.3) and the mean porosity is tabulated in Table 6.1. The porosity was evaluated at 300th days due to the fact that the samples were almost dried and the porosity has matured enough by then.

It is worthwhile to recollect discussions from the previous chapters wherein the inter-relationship between porosity, density and the foam quantity has been established (section 6.2&6.3). It was found that, as expected the porosity has inverse variation with density and varies directly with foam quantity. Figure 7.12 shows this relation between the density and the porosity for all the seven mixes for 300th days. It can be seen that the variation in porosity is more at higher cast densities. Also, it can be seen that for a density, the higher dosages of admixture results in higher porosity variations. Except for higher substitution of silica fume mix which reduces the porosity, which could be due the filler effect.

Moreover, it was also noticed that the porosity is influenced by density, type of admixture and content (section 6.3) same findings were reported by Kearsley et al. (2001). The relationship between the porosity and the thermal conductivity for the fly ash mixes is illustrated in Figure 7.13. It can be noticed that porosity is the exponential function of conductivity. As the porosity increases conductivity decreases and is also true for mixes in Figure 7.14 and Figure 7.15. For same mixes but for 50% porosity range the difference in the thermal conductivity recorded was only 1.5% and 1% respectively. Beside, this as the porosity increases the variation between the fly ash mixes decreases.

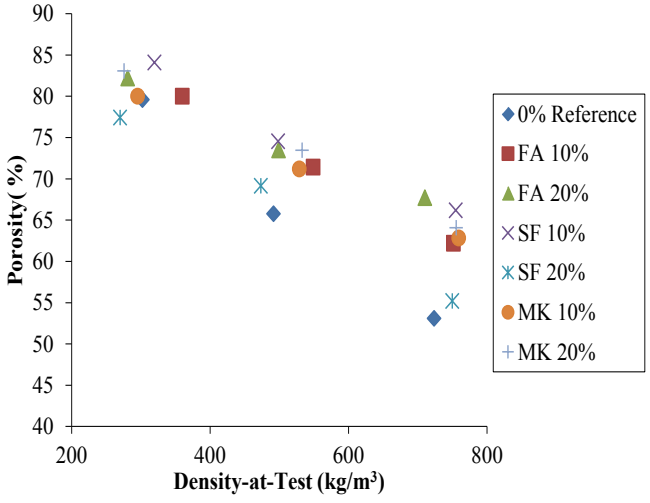

Figure 7.12: Porosity as a function of density.

For instance, the difference was 2% for 80% porosity range but thermal conductivity recorded was in the range of 5%. This influence leads to the conclusion that for lower porosities cases cement paste (solid phase) plays a vital role in thermal conductivity whereas for higher porosities the air-void leads. Therefore, it can be said that this 5% difference of thermal conductivity for higher porosities could be due to imperfection in air-void network (see chapter 6 for detail).

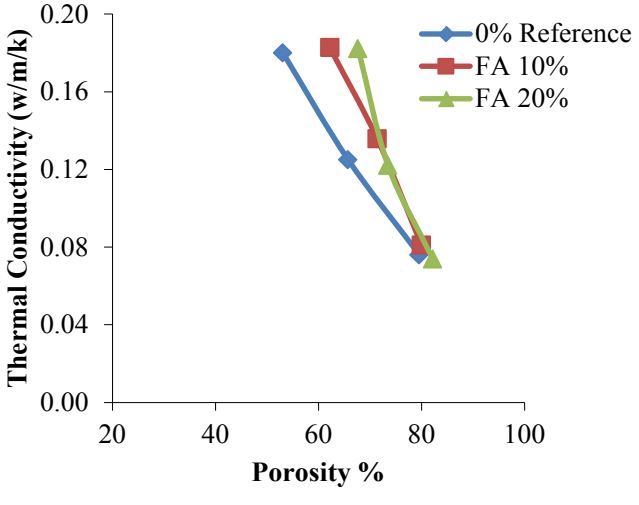

Figure 7.13: Relationship of Thermal Conductivity of cement-based foam with porosity for Fly Ash mix.

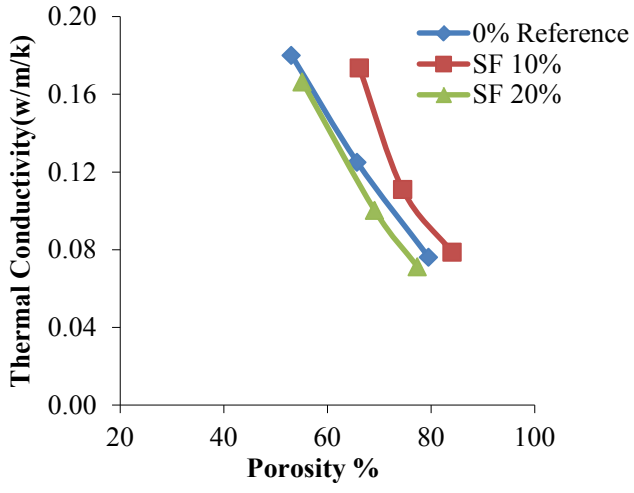

Figure 7.14: Relationship of Thermal Conductivity of cement-based foam with porosity for Silica Fume mix.

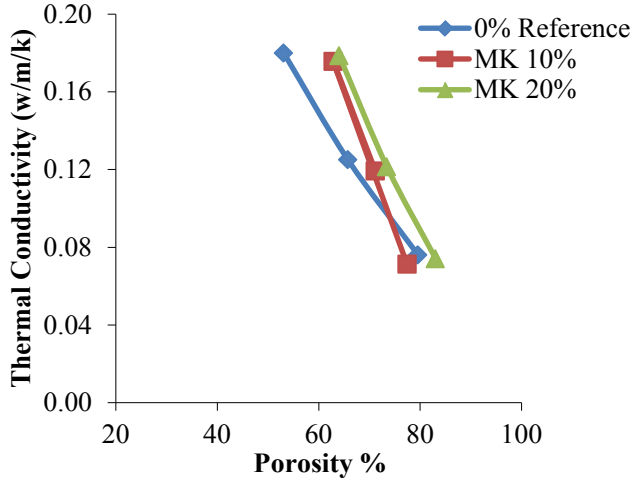

Figure 7.15: Relationship of Thermal Conductivity of cement-based foam with porosity for Metakaolin mix.

The silica fume mixes (10% & 20%) exhibit the difference of 24% and 4% for 50% porosity range when compared with the reference mix (Figure 7.14). Whereas, the difference in the thermal conductivity recorded was 4% and 8% respectively. The 10% silica fume mix variation is quite high as compared to 10% fly ash mix. On the other hand for 80% porosity range the difference was 5% and the conductivity was 7% which is also higher as

compared with fly ash mixes. Conversely, the mix with 20% silica fume exhibit lower when compared with other mixes which is obviously due to the filler effect as silica fume particle are very fine.

Similarly for metakaolin mixes (10% & 20%) the difference recorded was 18% and 20% for the 50% porosity range and the conductivity was 2%. For 80% porosity range the variation was 5% and conductivity difference was 3% respectively (Figure 7.15). Nevertheless, it can be stated that the variation of the porosities between the different admixture mixes was significantly high but the conductivity was not greatly influenced in fact was marginally varied. Thus, the variation of porosity due to addition of admixture and its effect on the thermal conductivity is clear from the above discussion.

In order to understand the respective contribution from the solid phase and the void phase to the overall thermal conductivity, Figure 7.16 was developed. It is a plot of normalized conductivity against the porosity. The normalized conductivity, (Tc/Tc_p) is defined here as the ratio of the conductivity of the cement-based foam (Tc) to that of cements paste alone (Tc_p). These values are taken from Table 7.1, 7.4, 7.5 and 7.6 for four periods of testing ages and for three cast densities. From the Figure 7.16 the reduction noticed in the normalized conductivity for 55-70% porosity range was 55% and for 70-85% porosity range it was almost 37%. This clearly indicates that the porosity is greatly influenced by the conductivity and so does the density.

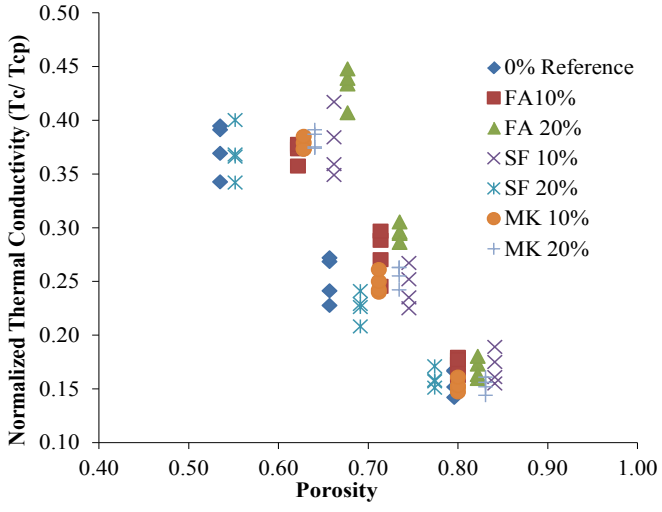

Figure 7.16: Normalized thermal conductivity versus porosity of cement-based foam.

7.3.4 Effect of Moisture Content

The measured moisture content value of cement-based foam containing admixture is tabulated in Table 7.10, 7.11 and 7.12. Moisture content by weight was calculated using Equation 3.4 as explained in chapter 3. Figure 7.17a, 7.17b, 7.17c illustrates the relationship between the moisture content of cement-based foam respectively for 800, 600 and 400 kg/m^3 cast densities as a function of time. The reduction trend observed in Figure 7.17 is similar as noticed in Figure 7.4. In Figure 7.4 on initial testing age it was observed for cement paste that the addition of pozzolanic admixture and higher admixture/cement ratio drops the moisture content and was true for all three admixtures. However, a reverse trend is noticed for cement-based foam in Figure 7.17 here the addition of pozzolanic admixture was resulting in higher moisture content for 60th day of testing age the reason being addition of admixture results in higher porosity variations. Except for SF 20% mixes whose moisture content was lower when measured for 600 and 400 kg/m^3 cast densities.

Awang et al. (2012) reported 12% moisture for light weighted foam concrete at 60th day with the cast density of 600 kg/m^3.The mixes were prepared by replacing 15% and 30% of cement by fly ash and also adding fine sand in to it. However, in this study the moisture for 10% and 20% fly ash mixes for 600 kg/m^{3}cast density and at 60th aging period was found to be 9% and 8% which is approximately 5% less than reported by Awang et al. (2012), the reason for this difference could be due to presence of fine sand. For 60th day in Figure 7.17a which is the 800 kg/m^3 it can be observed that the mix with 10% silica fume and 20% metakaolin retained the maximum moisture whereas, the reference mix bears the minimum.

This is also true for 600 and 400 kg/m^3 mixes as shown in Figure 7.17b and 7.17c. In contrast at 300th days for all cast densities the control and metakaolin both mixes holds the maximum moisture, this reveals that these mixes have the capability to hold the non-evaporable water for longer period of time.

In addition to this it is also evident that for theses mixes the moisture reduction rate decreases after a 210th day which was also observed in Figure 7.4. Along with these findings the maximum reduction was observed during the testing period of 120 to 210 days and same was observed for the cement paste in Figure 7.4.The drop noticed for this period for the 800 kg/m^3 cast density for all the mixes was within 65% as shown in Figure 7.17a. Similarly for 600 kg/m^3 and 400 kg/m^3 cast densities the drop noticed for all mixes was 55% ± 5 which is bit higher when compared with the cement paste. However, this difference can be anticipated due to presence of water in the voids of cement-based foam.

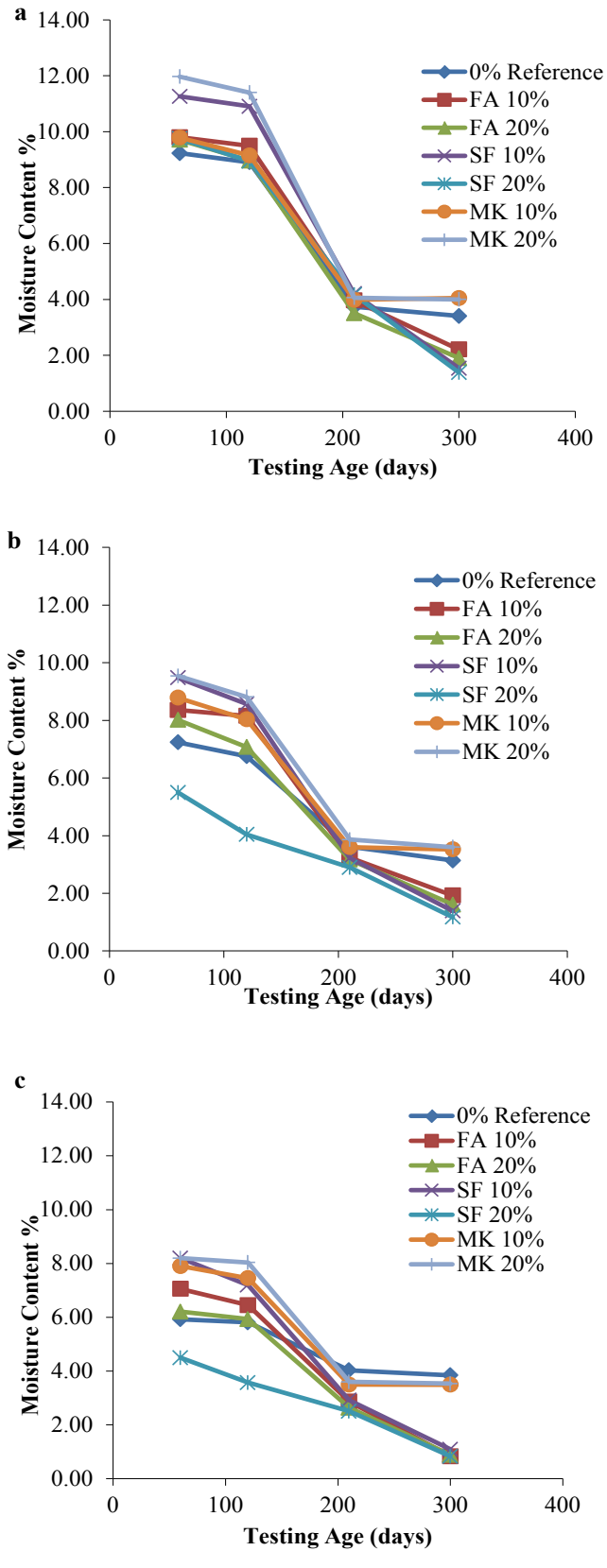

Figure 7.17: Moisture Content as a function of time for different cast densities; a) 800 kg/m^3; b) 600 kg/m^3; c) 400 kg/m^3.

The variation of measured mean thermal conductivity of cement-based foam with fly ash, silica fume and metakaolin is plotted in Figure 7.18, 7.19 and 7.20, against the moisture content for the three cast densities. The moisture content values plotted on x-axis is in the descending order i.e. measured at 300^{th}, 210^{th}, 120^{th}, 60^{th} days respectively.

From Figure 7.18, it can be noticed that the presence of moisture influences the thermal conductivity results and a linear relationship was found between them. In other words, it can be said that as the moisture content increases, conductivity increases. This conductivity difference is quite significant in higher densities mixes whereas, as the density decreases the rise in the conductivity becomes less significant (Figure 7.19 & 7.20). In addition to this, it is also evident from all Figures (7.18, 7.19, 7.20) that the presence of admixture, even in higher proportion does not change this trend i.e. moisture content and conductivity.

Furthermore, among the three admixtures, silica fume mixes, shows a steady trend for the moisture content, which is not surprising as the water demand for silica fume is quite high as compared to other.

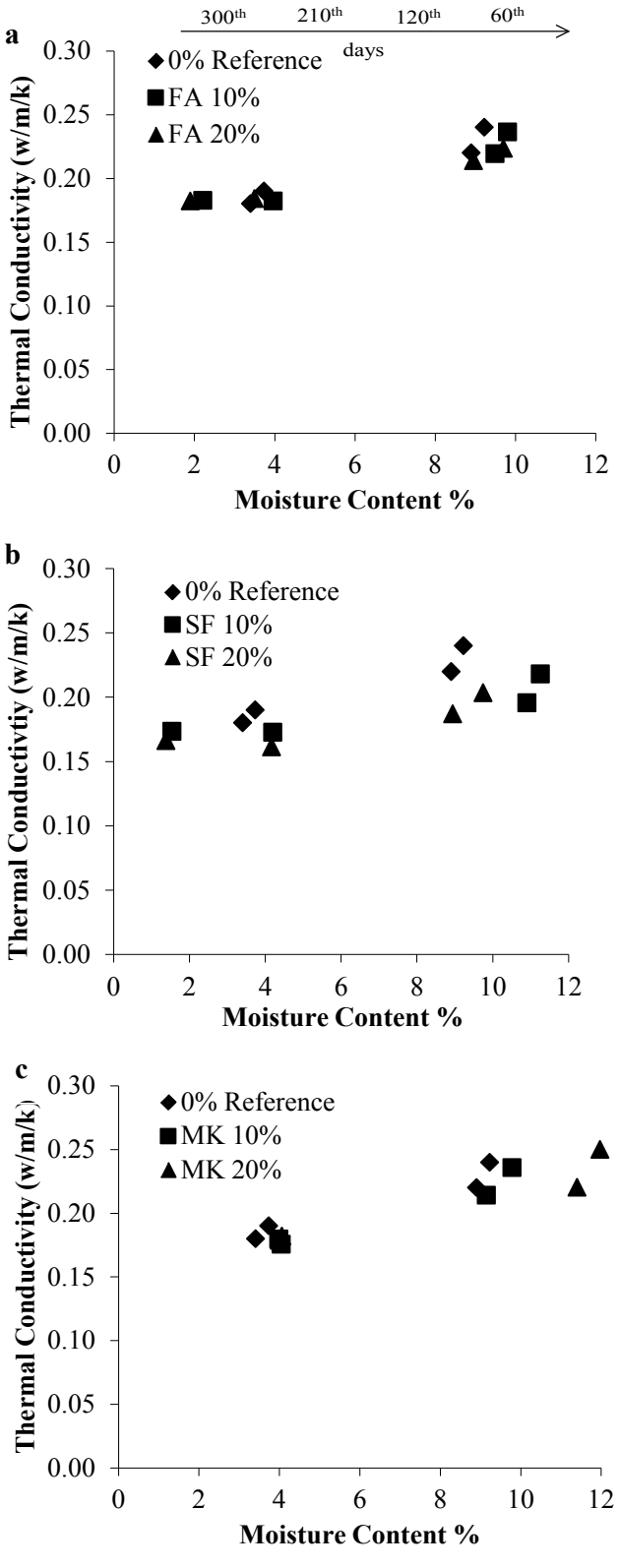

Figure 7.18: Relationship of Thermal Conductivity of cement-based foam with moisture content for 800 kg/m^3 cast density; a) Mix with Fly Ash; b) Mix with Silica Fume; c) Mix with Metakaolin.

Table 7.10: Measured Moisture Content for Cement-Based Foam containing Fly ash.

Moisture Content (%)	Testing Age (days)	Cast Density								
		800 kg/m^3			600 kg/m^3			400 kg/m^3		
		0% RF	FA 10%	FA 20%	0% RF	FA 10%	FA 20%	0% RF	FA 10%	FA 20 %
Mean	60	9.23	9.80	9.71	7.24	8.36	8.02	5.93	7.06	6.21
	120	8.90	9.49	8.97	6.76	8.15	7.08	5.81	6.45	5.93
	210	3.74	3.96	3.50	3.62	3.24	3.17	4.03	2.87	2.64
	300	3.41	2.21	1.90	3.14	1.92	1.61	3.85	0.83	0.89

Table 7.11: Measured Moisture Content for Cement-Based Foam containing Silica fume.

Moisture Content (%)	Testing Age (days)	Cast Density								
		800 kg/m^3			600 kg/m^3			400 kg/m^3		
		0% RF	SF 10%	SF 20%	0% RF	SF 10%	SF 20%	0% RF	SF 10%	SF 20%
Mean	60	9.23	11.26	9.75	7.24	9.48	5.50	5.93	8.20	4.50
	120	8.90	10.90	8.95	6.76	8.57	4.04	5.81	7.19	3.57
	210	3.74	4.20	4.17	3.62	3.23	2.90	4.03	2.92	2.51
	300	3.41	1.54	1.38	3.14	1.39	1.17	3.85	1.09	0.83

Table 7.12: Measured Moisture Content for Cement-Based Foam containing Metakaolin.

Moisture Content (%)	Testing Age (days)	Cast Density								
		800 kg/m^3			600 kg/m^3			400 kg/m^3		
		0% RF	MK 10%	MK 20%	0% RF	MK 10%	MK 20%	0% RF	MK 10%	MK 20 %
Mean	60	9.23	9.79	11.97	7.24	8.79	9.54	5.93	7.90	8.20
	120	8.90	9.15	11.40	6.76	8.04	8.81	5.81	7.45	8.04
	210	3.74	3.99	4.06	3.62	3.60	3.86	4.03	3.50	3.60
	300	3.41	4.05	4.00	3.14	3.52	3.60	3.85	3.49	3.54

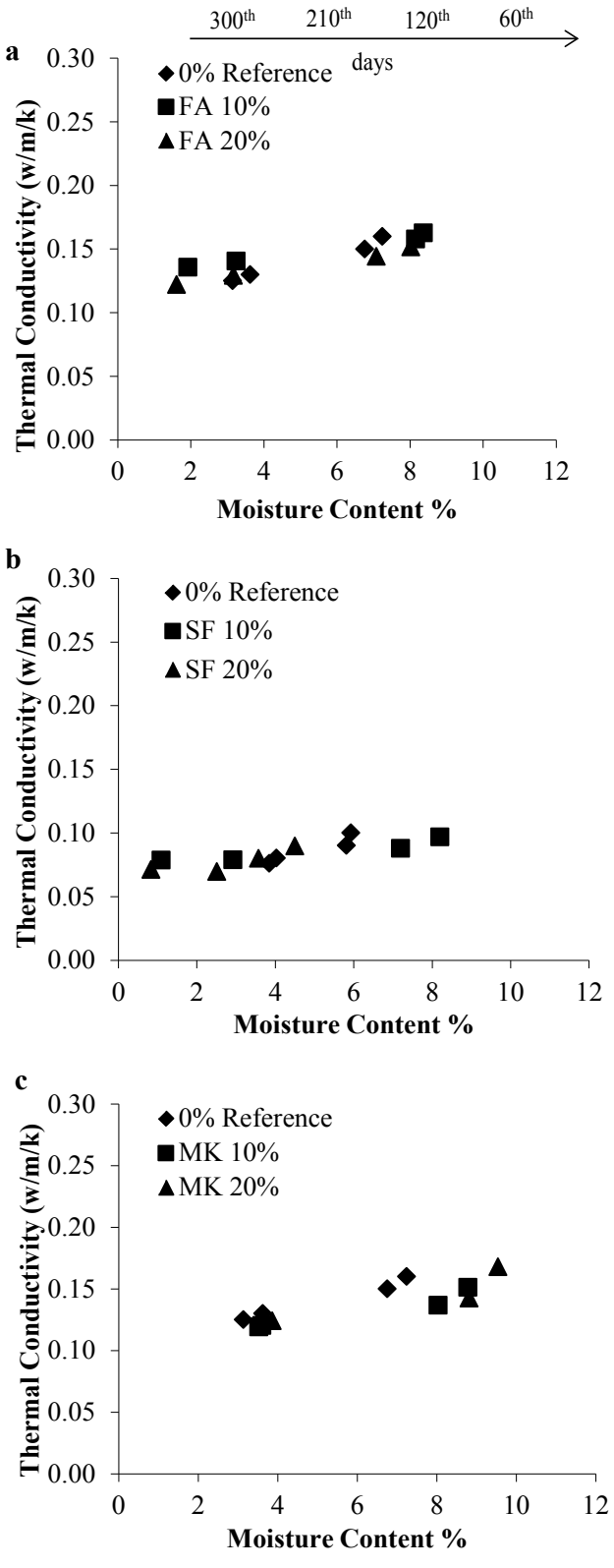

Figure 7.19: Relationship of Thermal Conductivity of cement-based foam with moisture content for 600 kg/m^3 cast density; a) Mix with Fly Ash; b) Mix with Silica Fume; c) Mix with Metakaolin.

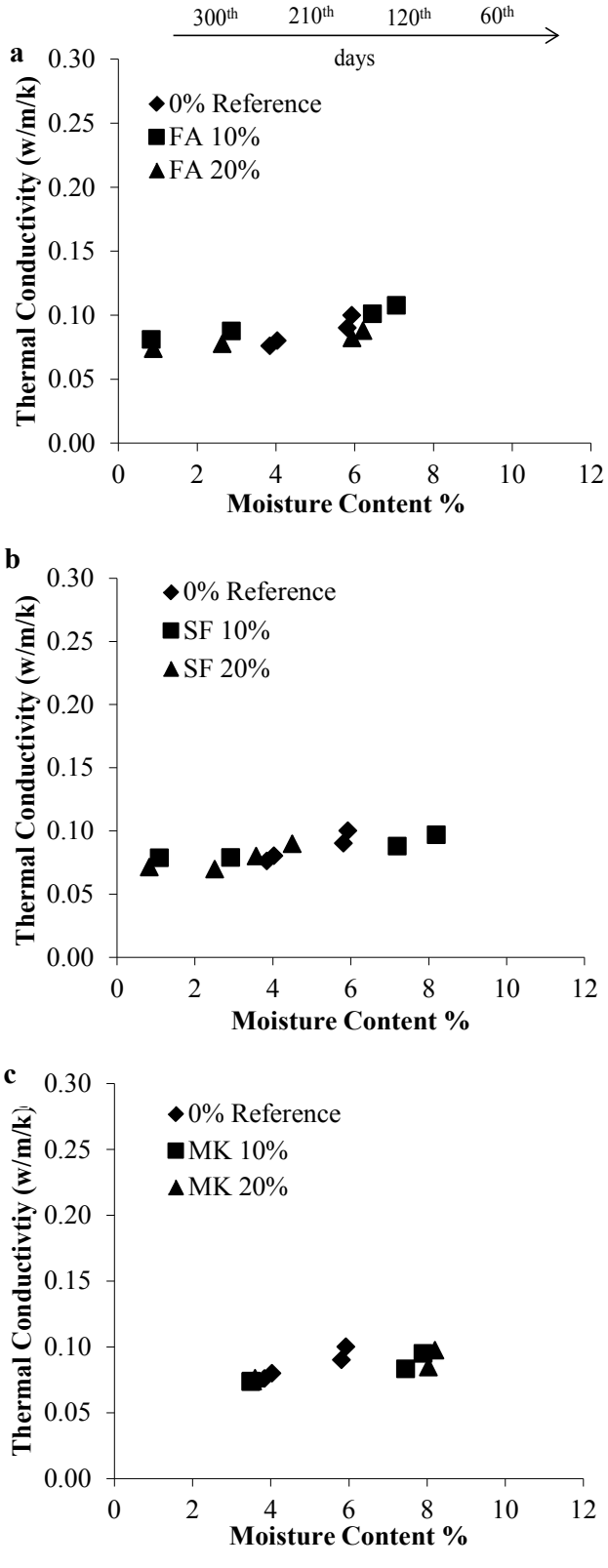

Figure 7.20: Relationship of Thermal Conductivity of cement-based foam with moisture content for 400 kg/m^3 cast density; a) Mix with Fly Ash; b) Mix with Silica Fume; c) Mix with Metakaolin.

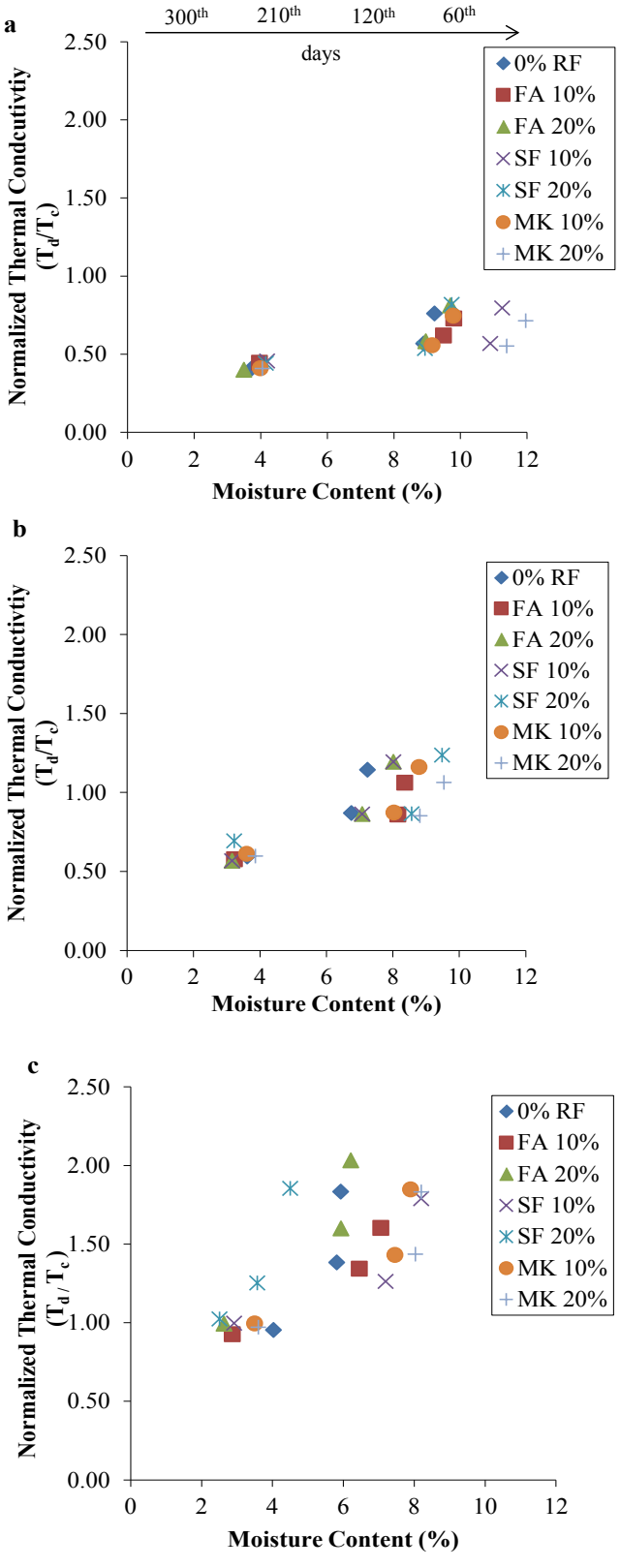

Figure 7.21: Normalized Thermal Conductivity verses moisture content for all mixes; a) 800 kg/m^3; b) 600 kg/m^3; c) 400 kg/m^3.Note RF is for reference mix.

The plot of normalized thermal conductivity (T_d /T_c) verses moisture content for the three cast densities is shown in Figure 7.21. The moisture content values plotted on x-axis is in the descending order i.e. measured at 300^{th}, 210^{th}, 120^{th}, 60^{th} days respectively. Here, T_d stands for thermal conductivity of cement-based foam at 300^{th} day at this time samples were considered to be dried this can also be noticed in Figure 7.17 which illustrates that the moisture content was minimum at 300^{th} day of aging and was true for all mixes and for three cast densities. However, Tc is for thermal conductivity of cement-based foam. Therefore, it was decided to use (T_d /T_c) ratio to investigate the moisture effect on conductivity for 60^{th}, 120^{th} and 210^{th} days. For that a graph was plotted in Figure 7.21 which shows the relationship between the normalized thermal conductivity (T_d /T_c) and the moisture content measured at different aging period.

The Figure 7.21 clearly indicates that the normalized thermal conductivity increases with increasing moisture and therefore with decreasing density. In addition to this for all the cast densities and for 2-4% moisture range (at 210^{th} day) the normalized value is practically same for all the cases of density and type of pozzolanic admixture. This is in accordance with the discussion in the sections (7.3.2&7.3.4).

7.3.5 Effect of Air-Void Size Parameters

Figure 7.22 shows the relationship between the thermal conductivity of cement-based foam for all the mixes and air-void parameters. These D50 and D90 parameters were evaluated in chapter 6 (section 6.5). It can be noticed from Figure 7.22 that an increase in median diameter value (D50) leads to reduction in thermal conductivity. It can be said that that mixes with a narrower range of air-void size distribution showed higher conductivity whereas, at lower density larger size of voids and wider distribution of voids were formed resulting in reduced conductivity. The D50 correlates better than D90 for thermal conductivity of all the mixes, showing that compared to bigger pore it is smaller pores that influence the conductivity. Moreover, this correlation does not get affect due to the presence of pozzolanic admixture.

7.3.6 Effect of Air-Void Spacing Parameters

The relationship between the thermal conductivity and the air-void spacing is illustrated in Figure 7.23. It can be noticed that an increase in the air-void spacing value (SP10 & SP50) leads to increase in the thermal conductivity value, both the SP10 and SP50 values correlate well, even in the presence of pozzolanic admixtures. This implies that for the higher densities (larger spacing), the thermal conductivity is more governed by smaller void size as compared to bigger size. Comparatively, in lower densities the larger size and number of voids plays a vital role.

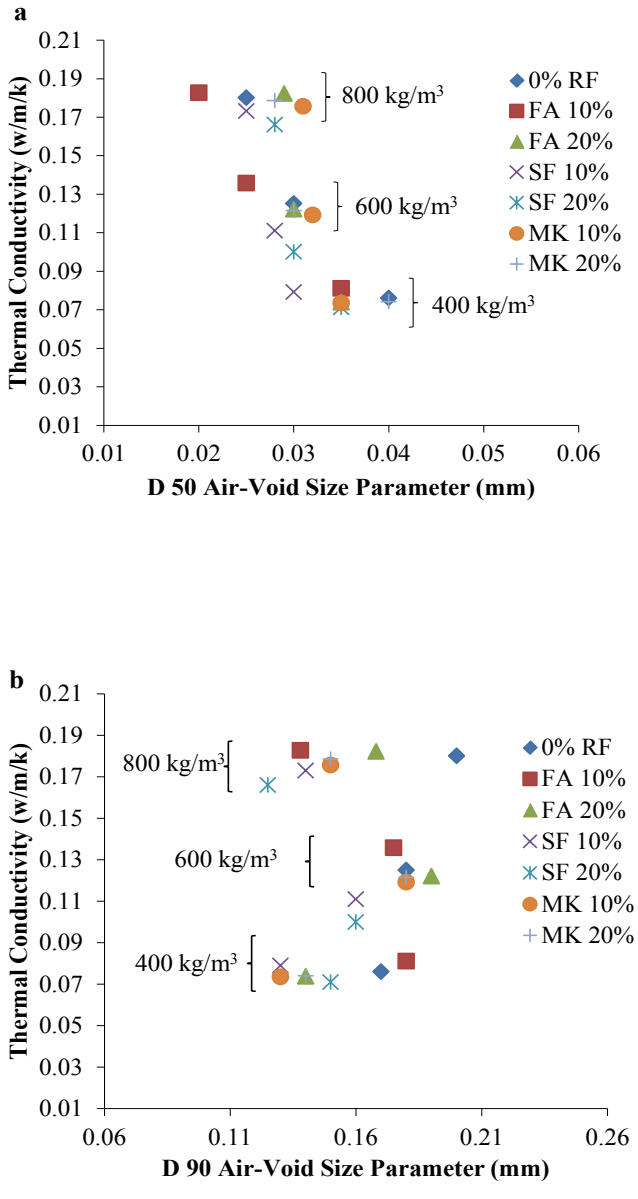

Figure 7.22: Relationship between the Thermal Conductivity and the Air-void Size parameters; a) D50; b) D90. Note RF is for reference mix

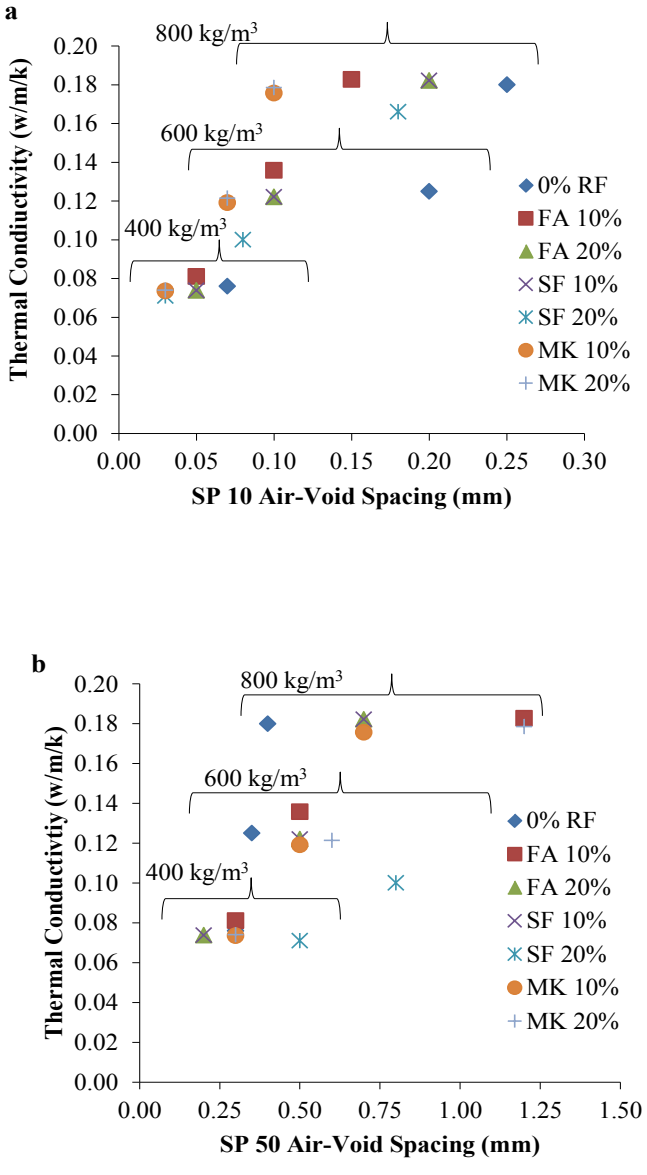

Figure 7.23: Relationship between the Thermal Conductivity and the Air-void Spacing parameters; a) D50; b) D90. Note RF is for reference mix.

7.4 Conclusion

- The drop in thermal conductivity due to the addition of any pozzolanic admixture in the cement paste is significant at the earlier stages, i.e., 60th day, but becomes progressively insignificant at later stages (i.e, 300th day). However, the higher substitution ratio (20%) of fly ash in the cement paste effectively reduces the conductivity as compared to silica fume and metakaolin.

- Adding fly ash and silica fume in cement paste decreases the thermal conductivity. This trend was reversed in the case of metakaolin.

- The thermal conductivity of the cement paste is the linear function of moisture content, which means that conductivity increases as the moisture content increases. In the mixes with the pozzolanic admixture, the conductivity variation noted was 0.65 (w/m/k) to 0.4 (w/m/k) between the period beginning with the 60th day through to the 300th day.

- The higher dosages of admixture result in higher porosity variations for a density, except for the higher substitution of silica fume mix, which reduces the porosity.

- For cement-based foam, the adding of the pozzolanic admixture resulted in higher moisture content for the 60th day of the testing age. The exception was for the SF 20% mixes, whose moisture content was lower when measured for 600 and 400 kg/m^3 cast densities.

8. Mathematical Modeling

8.1 Introduction

In this chapter, two mathematical models have been developed for evaluating the thermal conductivity of cement-based foam. Statistical analysis is done and the models generated are based on the results of twenty one different mixes casted with varying admixture ratio, densities and age of paste. The first model is based on the three constituent phases of cement-based foam; solid phase, void phase and moisture phase i.e. water saturation as discussed in chapter 7. However, the second model is simpler and is based on void phase (porosity), substitution ratio of pozzolanic admixture and age of the paste.

The proposed model is then compared with the existing model for evaluating and for validation the developed model is further investigated against the available database.

In addition to this, the model for predicting the thermal conductivity of cement hydrated paste containing pozzolanic admixture was also developed. As density greatly influences the thermal conductivity therefore, its correlation with porosity and moisture content is also established.

8.2 Modeling of Thermal Conductivity of Hydrated Cement Paste

The relationship of thermal conductivity of hydrated cement paste as a function of time was plotted in Figure 7.1. It was noticed that the thermal conductivity drops with the age of the paste and after certain age, the drop become very nominal. In order to generate regression model, the analysis requires the inputs values of dependent and independent variables. Therefore, the time period (60 to 300 days) was taken as the independent variable and the value of conductivity, tabulated in Table 7.1, was taken as dependent variable. A simple linear regression model formulated by using IBM SPSS statistics version 21.0 is expressed in Equation 8.1.

$$Tc_p = 1.340 - 0.158\ln(t) \qquad \text{Eq 8.1}$$

where,

Tc_p = thermal conductivity of cement paste (w/m/k)

t = age of the paste since the day of casting but air- dried after 28 days of water curing (days) (table 7.1)

The 84.6% of variability in the thermal conductivity of the cement paste was recorded which was explain by R-squared statistic (N=12) also known as coefficient of determination. The adjusted R-squared was 82.9% and the standard error of estimation which shows the standard deviation of the residuals was 0.044. The addition of natural logarithm of age in the above equation increases the correlation to 92.0%.

The dash line fitted using Equation 8.1 for different ages is shown in Figure 8.1. It can be noticed that the model predict quite well for the earlier ages. However, the maximum difference recorded was 3% and 4% for 210 and 300 days which is acceptable as it in within 5% limit. Figure 8.2 shows the comparison of the Equation 8.1 results with the other researcher´s test results for cement paste thermal conductivity. The Kim et al. (2003) samples were moist cured with w/b=0.4 and fully saturated at the time of testing whereas, the Bentz (2007) samples were cured under sealed conditions. It can be noticed that Kim et al. (2003) results were different from the values predicted by Equation 8.1 even at initial ages. While the results of Bentz (2007) samples were slightly different in the initial ages but the difference increased considerably as the age approached 30 day. This difference is due to the fact that Equation 8.1 can incorporate only the time period between 60 to 300 days. Therefore, it also be said that this model (Eq 8.1) is limited only for this time period.

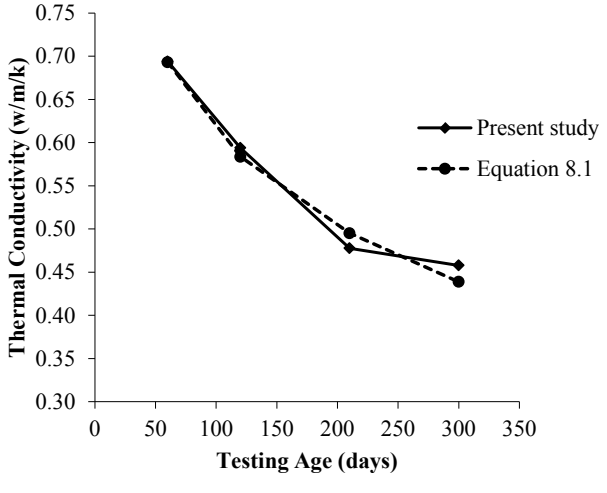

Figure 8.1: Comparison between the present study results and Tc_p model of cement paste.

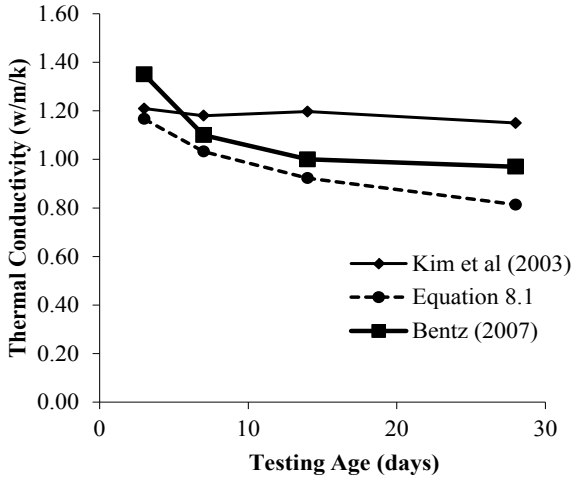

Figure 8.2: Comparison between the Kim et al. (2003) test results, Bentz (2007) test results and model of cement paste.

8.2.1 Modeling of Conductivity of Hydrated Cement Paste Containing Pozzolanic Admixture

The thermal conductivity for the cement paste containing pozzolanic admixtures like fly ash, silica fume and metakaolin is plotted in Figure 7.2 (chapter 7). It was concluded that the addition of admixture resulted in the reduction of thermal conductivity and factors influencing are admixture content, age and moisture content. It may be mentioned here that even though in chapter 7 the influence of porosity has been clearly brought out in case of cement-based foam. As far as cement paste is concerned the porosity is quite low and hence, can be ignored as a factor influencing the conductivity while developing this model. Remaining is the effect of moisture content, which is already included, as the measurements were taken at the different time period.

A multiple linear regression model is used to describe the relationship between the thermal conductivity of cement hydrated paste and two

independent variables; age and admixture content. The range of the age which this regression model can take as an input is between 60 to 300 days and admixture ratio range lies from 10% to 20% respectively. Altogether 12 data points for each mix were used for the formulation of this model (Table 7.1). Finally, the model predicting the thermal conductivity of cement paste containing pozzolanic admixture is expressed in Equation 8.2.

$$Tc_{pa} = \beta_o + \beta_1 \ln(t) + \beta_2 (ratio) \qquad \text{Eq 8.2}$$

where,

Tc_{pa} = conductivity of cement paste containing admixture (w/m/k)

β_o = constant (table 8.1)

β_1, β_2 = regression coefficient (table 8.1)

t = age of the paste (days)

ratio = admixture/cement ratio (by weight)(fraction)

Table 8.1: Constants for Equation 8.2

Constant	Fly Ash	Silica Fume	Metakaolin
β_o	1.112	1.151	1.101
β_1	-0.099	-0.125	-0.116
β_2	-0.762	-0.215	0.108

8.2.1.1 Interpreting Regression Coefficients of Model for Mixes with Fly Ash (Eq 8.2)

The R-squared statistics (N=12) indicate that the fly ash predictive model as fitted explains 83.4% of variability in the thermal conductivity of the cement paste. The adjusted R-square statistics in the model summary was 81.6% which mean this percentage of the variation in the thermal conductivity can be attributed to these two variables namely, age and admixture/cement ratio. Although the enter command was used for the whole regression analysis but on one stage stepwise regression was done to check the individual R-square value and it was found that 58.6% of the variation in thermal conductivity of hydrated cement paste is controlled by natural logarithm of time variable. Along with this the standard error of estimation shows the standard deviation of the residuals to be 0.033 (w/m/k). The pearson correlation coefficient of time and ratio variables with thermal conductivity was 76.6% and 49.7% respectively. The acronym for analysis of variance (ANOVA) table from the SPSS output indicates that the p-value for the regression model F-test is 0.000 which shows that model is highly significant. Therefore, it can be concluded that these two independent variables together predict the thermal conductivity of cement paste but to understand the individual role of each variable it is equally important to investigate the regression coefficients. Thus, the ratio variable relationship is statistically significant (Sig.=0.000) but the regression coefficient is negative (-0.762) which mean higher the fly ash/cement ratio lower is the thermal conductivity. This inverse relation between admixture/cement ratio and conductivity has been found while analysing as reported in the chapter 7. In addition to this the regression coefficient for days is also negative (-.099) but the statistical relationship is significant (Sig.=0.000) which mean as the age of the paste increases thermal conductivity decreases.

Figure 8.3 illustrates the comparison between the measured mean thermal conductivity values and those predicted by using Equation 8.2. It was found that the equation predicts quite reasonable for the later ages but the difference for the early period between the predicted and observed values are clear for the both mixes.

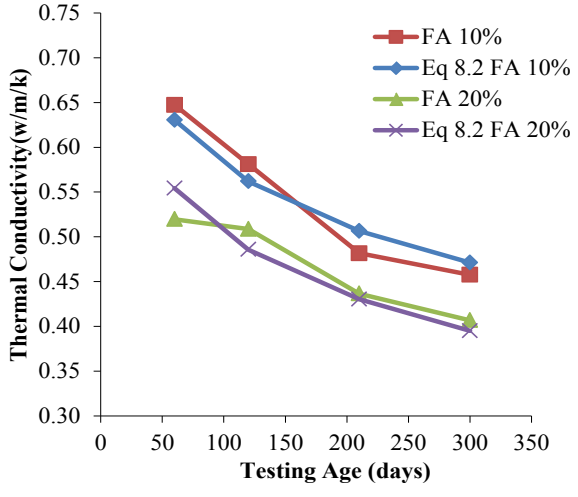

Figure 8.3: Comparison between the present study results and Tc_{pa} model of cement paste containing fly ash (Eq 8.2).

8.2.1.2 Interpreting Regression Coefficients of Model for Mixes with Silica Fume (Eq 8.2)

In the model summary output it was noted that the R-square value (N=12) for cement paste containing silica fume was 78.5%. The strength and goodness of the model can be evaluated by the adjusted R-square value and in this multiple linear regression model the value was 76.3% which mean this percentage of the variation of the dependent variable which is thermal conductivity can be attributed to two independent variables which are age and time. Along with this the standard error of estimation shows the standard deviation of the residuals to be 0.042 (w/m/k). The pearson correlation coefficient of time and ratio variables with thermal conductivity

was 87.7% and 12.4% respectively but with negative sign. The ANOVA table illustrate the p-value for F-test was 0.000 which mean model is significant. The both regression coefficients are negative which indicate as the age and ratio increases thermal conductivity drops, same result was concluded in chapter 7. Figure 8.4 shows the comparison of measured thermal conductivity of cement paste containing silica fume and that predicted by using Equation 8.2. It can be concluded that the observed and the predicted thermal conductivity values are quite close to each other.

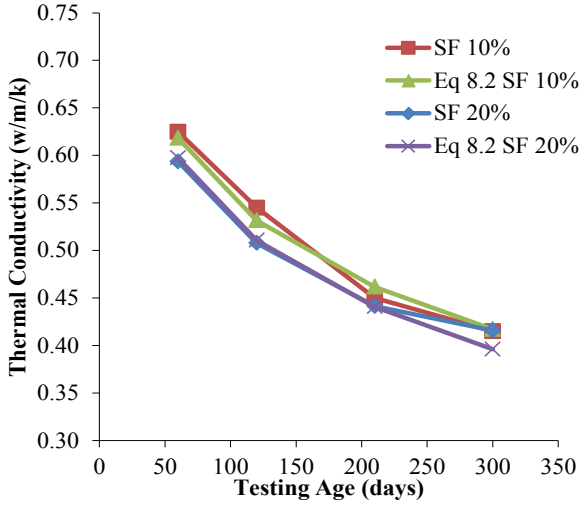

Figure 8.4: Comparison between the present study results and Tc_{pa} model of cement paste containing silica fume (Eq 8.2).

8.2.1.3 Interpreting Regression Coefficients of Model for Mixes with Metakaolin (Eq 8.2)

The observed and predicted thermal conductivity of cement paste mixes containing metakaolin are expressed in Figure 8.5. Equation 8.2 was used to predict the thermal conductivity of the paste and it can be noticed that this model performed quite reasonable. This model was formulated by applying the multiple linear regression analysis in a similar way as done before for other mixes. First the model strength was checked and it was found that the

model summary indicate the R-square statistics (N=12) as 70% and adjusted R-square as 66.8%, which shows that this percentage of the variation in the thermal conductivity can be attributed because of two variables namely age and admixture ratios. Moreover, the standard error of estimation shows the value of 0.048 (w/m/k) which is actually standard deviation of the residuals. Next the relationship between the variables was investigated and the pearson correlation coefficient of time and ratio variables with thermal conductivity was found to be 83.4% and 6.5% respectively showing a strong tie with time variable. The p-value for F-test was Sig.= 0.000 which explain that the model is highly significant and these two independent variables together predict the conductivity but it is equally important to the check the individual variable significance. Therefore, coefficient tables explains that the time variable is statistically significant (Sig.= 0.000). Along with negative sign which mean the conductivity drops as the age of this paste increase which is in accordance with the pervious finding. However, the relationship of ratio variable is statistically not significant (Sig.= 0.609) the recommendations are this value should be less than 0.05.The positive sign means ratio is directly proportional with the thermal conductivity which is also in agreement. Overall, it can be concluded that the model expressed in Equation 8.2 is adequate and stable for all pozzolanic mixes disused here.

Moreover, Figure 8.4 shows the comparison of measured thermal conductivity of cement paste containing metakaolin and that predicted by using Equation 8.2. It was found that the predicted results by Equation 8.2 were quite close to measured test results.

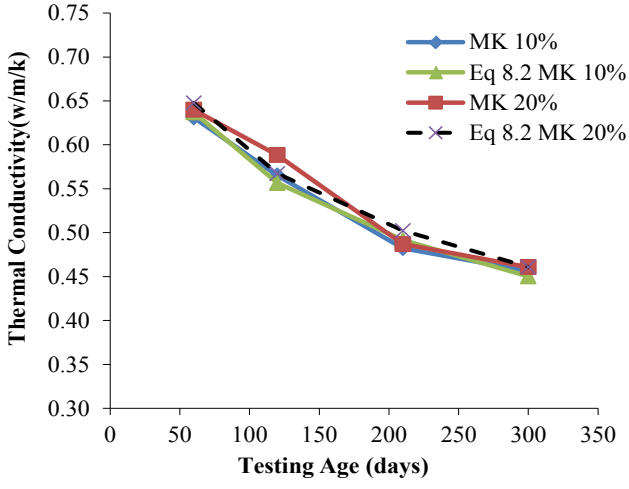

Figure 8.5: Comparison between the present study results and Tc_{pa} model of cement paste containing metakaolin.

8.2.1.4 Validation of Model

To examine the validity of the model developed in section 8.2, the predicted values from Equation 8.2 are compared with those of experimentally measured values by other researchers like Demirbog˘a (2003) and Batool et al. (2013). These researchers used cement paste with admixtures fly ash (FA), silica Fume (SF) and metakaolin (MK) in their works. The comparison is shown in Figure 8.6 and it is clear that the model developed in the present study (T_{cpa}) has shown an excellent agreement with the experimental values by both the researchers, even though Demirbog˘a (2003) specimens were oven dried with sand.

In the case of oven dried samples the value of ln (t) in the proposed model was taken between 1-10 days, the reason being samples used in the regression analysis was air dried and measured at the age of 60^{th} day. However, for Batool et al. (2013) samples the actual age of 35 days was used and the maximum range of error of the model note was within 5%.

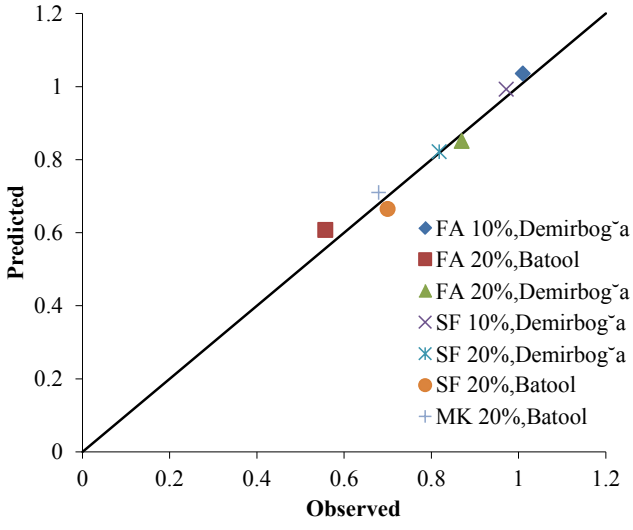

Figure 8.6: Comparison between the Demirbog˘a (2003) test results, Batool et al. (2013) test results and predicted results of cement paste model (Eq 8.2).

8.3 Regression Modeling for Cement-Based Foam

8.3.1 Modeling the *Porosity-Density* Relationship

In cement-based foams there is considerable porosity which is generated by the addition of foam. It was concluded in chapter 7 that the porosity has an inverse relationship with density, type and content of admixture.

Normally, the cement-based foam sample gets dried with time therefore it was decided to take the density value of 300th day for modeling this relationship. It is expected that by this time all the evaporable water has been evaporated and the air-void network also becomes stable.

The simple regression with one independent density variable was done by using SPSS and eleven different models were applied to find the best fitted equation on eleven mixes as shown in Figure 8.7. The data for the porosity and density-at-test can be found in Table 6.1, 7.7, 7.8, 7.9. Thus, the model

which fits best was linear one. Therefore, the relationship of porosity with the dry density of different pozzolanic admixture can be expressed as follow

$$þ = 93.267 - 0.042\Upsilon_d \qquad \text{Eq 8.3}$$

where,

þ = porosity (%)

Υ_d = dry density (kg/m^3) (air dried @ 300 days)

The model summary indicates the R-square value (N=21) as 80.2% and adjusted R-square equal to 79.2%.The ANOVA table from the SPSS output indicates that the p-value for the regression model and F-test is 0.000. This shows that model is highly significant and the density independent variable in the coefficient column illustrate it is statistically significant.

Although the above model 8.3 developed satisfy all the regression analysis requirements, with regard to silica fume mixes the values deviate considerably especially at a dosage of 20% silica fume (SF), and at higher range of densities (Figure 8.7).

Similar deviation, from observed values is noticed with regard to the reference mix, with no pozzolanic admixture. The reason behind is porosity decreases with the increased substitution of silica fume admixture, as discussed in chapter 7 (section 7.3.3). Therefore, it was decided to carry out regression analysis on the model having ratio and density as an independent variable. Hence, different models were tired and their adjusted R-square values were compared and finally, multiple linear regression model expressed in Equation 8.4 was formulated.

$$\text{þ} = \lambda_o - \lambda_1 (\Upsilon_d) + \lambda_2 (\text{ratio}) \qquad \text{Eq 8.4}$$

where,

þ = porosity (%)

Υ_d = dry density (kg/m^3) (air dried@ 300 days)

λ_o = constants (table 8.2)

λ_1, λ_2 = regression coefficient (table 8.2)

ratio = admixture/cement ratio (by weight)(fraction)

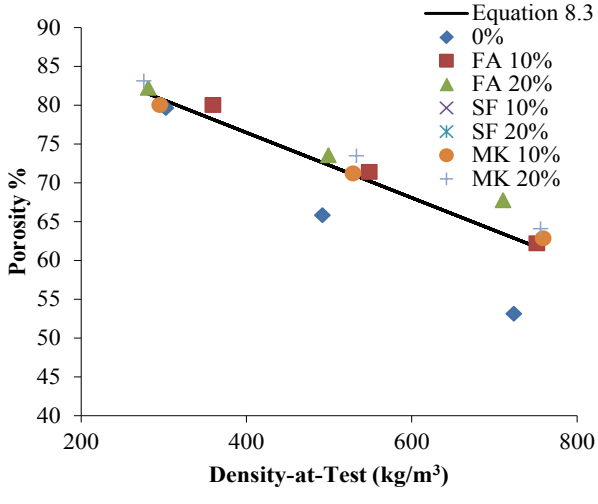

Figure 8.7: Porosity as a function of density-at-test.

Table 8.2: Constants for Equation 8.4

Constant	0%(Reference)	Fly Ash(FA)	Silica Fume(SF)	Metakaolin(MK)
λ_o	89.099	89.099	106.789	89.099
λ_1	0.042	0.042	0.044	0.042
λ_2	36.187	36.187	-88.498	36.187

The predicted results obtained for porosity by using Equation 8.4 are plotted in Figure 8.8 against the experimentally recorded values. Hence, it was found that the model can predict the porosity of cement-based foam with reasonable accuracy. Regarding the model analysis, the regression coefficient for reference, fly ash and metakaolin model indicate the R-square value as 92.9% (N=15) and adjusted R-square as 91.7% which is higher as compared with the model in Equation 8.3.This rise in value also explains the influence and the role of admixture /cement ratio porosity. In addition to this the standard error of estimation shows the value of 2.517 (%) which is actually standard deviation of the residuals.

Overall, the models (reference, fly ash, metakaolin) and individual independent variables were found to be statistically highly significant. With density variable having negative sign which mean as the porosity increase density reduces. Similarly, the regression coefficient for silica fume model was investigated and it was found that R-square was 99.4% (N=6) and adjusted R-square 98% which shows the variation is strong. In addition to this the standard error of estimation was 1.41 (%). Furthermore, the ANOVA and coefficient table shows statistically significant model.

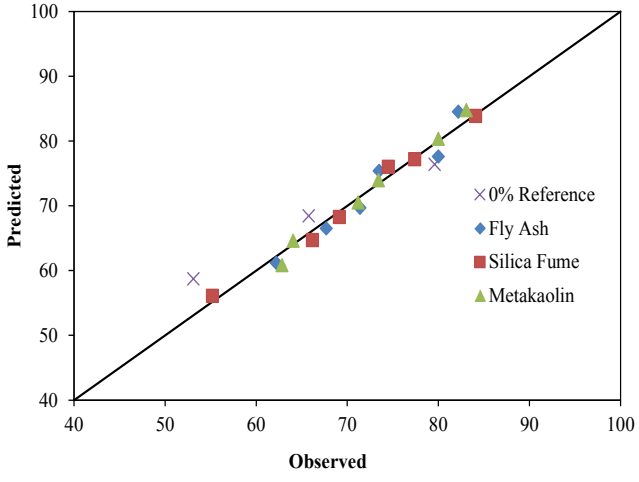

Figure 8.8: Comparison between the predicted values by using equation 8.4 and tested values for porosity.

8.3.2 Modeling the *Moisture Content – Density* Relationship

In chapter 7 it was found that moisture content of cement-based foam depend upon density, type of admixture, % of substitution and age of paste. The most effecting factor among these is the density, as it changes, the percentages of paste and void changes. These are the two constituent phases which hold the moisture. Then, with time as the hydration process continues the free water evaporates leaving non-evaporable behind. With these inferences it was decided to generate a predicted model with density, age and ratio as independent variables.

Numbers of trials were made to get the best predicted model and it was found that the model with density and age as independent variables was having the highest adjusted R-square value. Therefore, this multiple linear regression model was selected for predicting the moisture content of cement-based foam and also for explaining the relationship with density and age.

The model expressed in Equation 8.5 can predict the moisture content for cement-based foam containing fly ash, silica fume and metakaolin as pozzolanic admixture for dry density range of 400 to 800 kg/m^3 and age between 60 to 300 days respectively.

$$M_c = \alpha_o + \alpha_1 (\Upsilon_d) - \alpha_2 \ln (t) \qquad \text{Eq 8.5}$$

where,

M_c = moisture content (%)

Υ_d = dry density at the age of paste (kg/m^3)

α_o = constants (table 8.3)

α_1, α_2 = regression coefficient (table 8.3)

t = age of the paste (days)

Table 8.3: Constants for Equation 8.5

Constant	0%(Reference)	Fly Ash (FA)	Silica Fume (SF)	Metakaolin (MK)
α_o	17.726	24.243	23.443	24.686
α_1	0.003	0.005	0.006	0.003
α_2	2.798	4.353	4.348	4.028

Figure 8.9 illustrate the predicted results of moisture content for mixes containing pozzolanic admixture these predication are based on Equation 8.5. The maximum range of error of the model is 12% for reference, 21% for fly ash, 25% for silica fume and 14% for metakaolin mixes respectively at higher density range but the range of error is much smaller in the case of lower densities for example ≤ 600 kg/m^3.The difference in error is of great concern but it is equally important to check the adequacy of the model.

Therefore, the model summary for fly ash mix indicates R-square value as 86.5% (N=24), and adjusted R-square as 85.5%. Moreover, the standard deviation of the residuals was equal to 1.166 (%). Similarly, for reference, silica fume and metakaolin mixes the R-square value noted was 70.0% (N=12), 76.4% (N=24), 80.0% (N=24) and adjusted R-square was 69.4%74.2%,78.9% with standard error of estimation as 1.20% ,1.73% and 1.33% respectively.

Furthermore, the ANOVA and coefficient tables for reference, fly ash, silica fume and metakaolin mixes shows that all the four models and their independent variables both were statistically significant with values less than 0.05. It can be summarized that all the four models are statically adequate and stable. However, the percentage of error between the tested and predicted noted for all the model is greater than 5%.

a

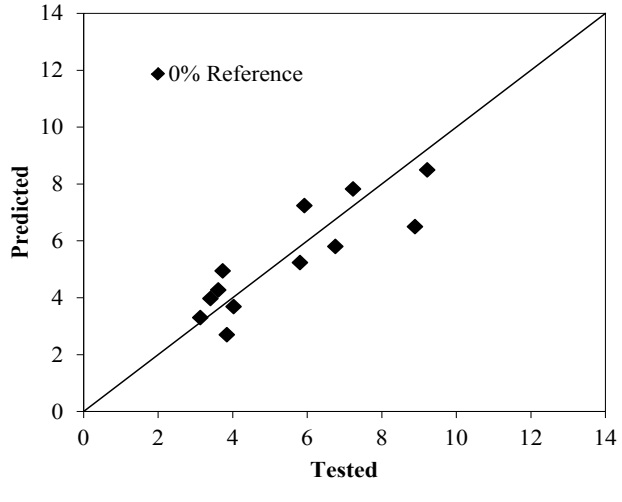

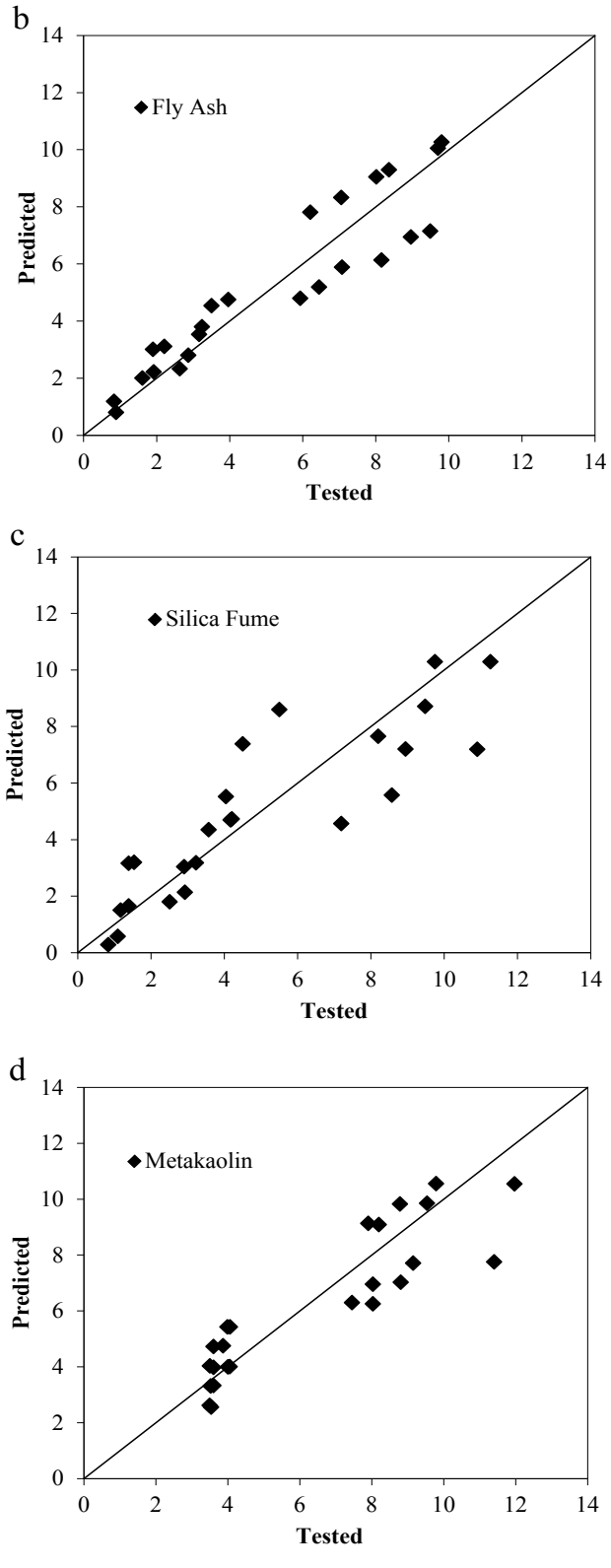

Figure 8.9: Comparison between the predicted values using equation 8.5 and tested values for moisture content a) 0% Reference Mix; b) Fly Ash Mix; c) Silica Fume Mix; d) Metakaolin Mix.

8.3.3 Validation of Model (Eq 8.5)

This model is verified by the test results of light weight of foamed concrete conducted by Awang et al. (2012). In that study, the samples were prepared with cement, sand, water, foam and pozzolanic admixture fly ash. The moisture content was measured at 7^{th}, 14^{th} and 60^{th} day in dry state condition. In this study samples were prepared without sand and moisture content was recorded at 60^{th}, 120^{th}, 210^{th} and 300^{th} days.

The comparison between the measured test results reported by Awang et al. (2012) and the corresponding prediction by applying Equation 8.5 is shown in Figure 8.10. It can be seen that the predicted results of 0% reference mix at 7^{th} day and of mixes with fly ash with 15% and 30% at 60^{th} day were fairly close to the test results. But the remaining values predicted were wide off the mark. This showed that while predictive model as per Equation 8.5 is statistically adequate but its applicability is limited.

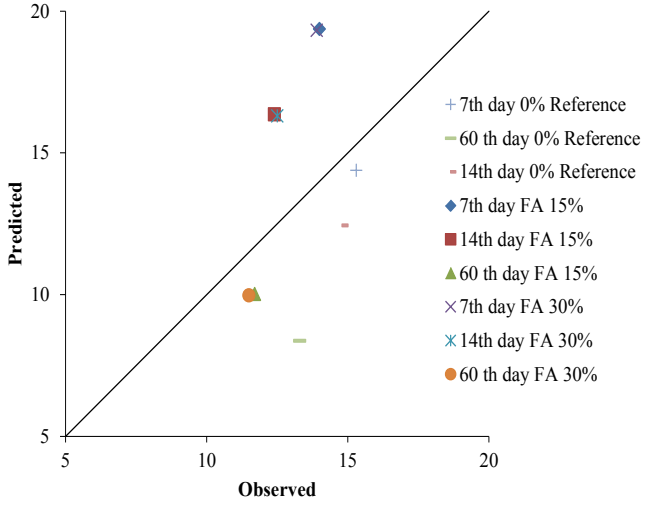

Figure 8.10: Comparison between the tested values by Awang et al. (2012) and predicted values using equation 8.5.

8.4 Modeling of Thermal Conductivity of Cement-Based Foam

8.4.1 Development of a *Conductivity-Moisture* Based Model

From the discussion of results in chapter 7, it has been summarized that the thermal conductivity of cement-based foam is not only the function of time, admixture content and moisture content but is significantly influenced by properties of constituent phases i.e void and solid phase which is explained as porosity and hydrated cement paste. Figure 7.13, 7.14, 7.15 shows that cement-based foam samples contain 50 to 80% of the porosity which is only air-void and 50 to 20% is the cement paste. As a result, the porosity and the hydrated cement paste become two important variables. Among the other remaining factors moisture content is the most prominent and time dependent factor. As the evaporable water disappears air gets filled in the voids varying the conductivity significantly because water has a high 0.6 (w/m/k) whereas, air has the lower conductivity of 0.026 (w/m/k). On another hand non-evaporable or chemically bound water stays in cement paste for longer period of time. Thus, this leads to the conclusion that cement-based foam act as three-phase porous medium having air, water and solid at same time especially when not completely dried or fully saturated. Hence, a predictive model for conductivity of cement-based foam should take into effect the influence of all the above three phases.

Therefore, it was decided to use multiple linear regression models as these models are capable of operating many variables at a time and on another hand these variables either function independently, or in concert with one another, to explain variation in the dependent variable.

After doing number of trials with different independent variables, the multiple linear regression model expressed in Equation 8.6 was found to be the best model for cement-based foam with and without pozzolanic admixture like fly ash, silica fume and metakaolin. Following is the Equation 8.6

$$Tc = \beta_o + \beta_1 Tc_p (1- þ) + \beta_2 Tc_v (þ- M_c) + \beta_3 Tc_w (M_c) \quad \text{Eq 8.6}$$

where,

Tc = thermal conductivity of cement-based foam (w/m/k)

Tc_p = thermal conductivity of cement paste (w/m/k)

Tc_v = thermal conductivity of air in pores (air-void) (w/m/k)

Tc_w = thermal conductivity of water (w/m/k)

M_c = moisture content (fraction)

$þ$ = porosity (fraction)

β_o = constant (table 8.4)

$\beta_1, \beta_2, \beta_3$ = regression coefficient (table 8.4)

Here, in Equation 8.6 the $Tc_p (1- þ)$ and $Tc_w (M_c)$ variables explain the contribution of thermal conductivity due to paste and water. On another hand the influence due to amount of thermal conductivity of the air can be represent by $Tc_v (þ- M_c)$. It can be noticed that age and ratio variables were not included in Equation 8.6 because they are already present in Equation 8.1, 8.2, 8.4 and 8.5 and these same Equations can be used for calculating the value of Tc_p, $þ$ and M_c respectively.

Table 8.4: Constant for Equation 8.6

Constant	0% (Reference)	Fly Ash (FA)	Silica Fume (SF)	Metakaolin (MK)
β_o	0.254	0.720	0.386	0.022
β_1	0.264	-0.300	-0.073	1.120
β_2	-10.625	-29.926	-15.219	-2.168
β_3	0.233	-2.498	0.514	-0.261

8.4.1.1 Interpreting Regression Coefficients for *Conductivity-Moisture* Based Model

The descriptive statistics tables in the output section for fly ash, silica fume, metakaolin models shows that 144 data point were used for regression analysis whereas for reference mix model 72 data point were investigated. All the models contain three independent variables and one dependent variable which is thermal conductivity of cement-based foam. Forced entry method was selected for all the mixes as in this method all the predictors are forced into the model simultaneously. Secondly, this method relies on theoretical reasoning for adding the selected independent variables (Field 2013).

The model summary table (sample table in Appendix B) in output section describes the overall adequacy of the model. For instance, the R-squared statistics (N=144) indicate that the fly ash predictive model as fitted explains 97.4% of variability in the thermal conductivity of the cement-based foam. In addition to this the adjusted R-square is a very important parameter in term of strength and goodness of the model and increases only if the contribution of the variables is significant towards the model. Therefore, for fly ash model this value was 94.7% which mean this percentage of the variation in the thermal conductivity of cement-based

foam can be attributed due to those three independent variables. Along with this the standard error of estimation shows the standard deviation of the residuals to be 0.011 (w/m/k). Moreover Durbin-Watson value was 0.476 less than 2 which mean the residuals are positively correlated, as this test explains the residuals correlation (Field 2013).

The ANOVA table from the SPSS output (sample table in appendix B) indicates that the p-value for the regression model F-test is 0.000 which is less than the recommended value of 0.05 indicating that the model is highly significant. However, it is equally important to investigate the t-test and the regression coefficient for all the independent variables. Thus, the three independent variable relationship was found to be statistically significant (Sig. = 0.000<0.05) but the regression coefficients were having negative sign. Here, the negative sign with Tc_v (þ- M_c) indicates that as the thermal conductivity increases this variable decreases. This can be explained by the fact that the porosity decreases the density and also the conductivity.

Negative sign with remaining two variables can be explained due to the ratio and age factor which influences the thermal conductivity of cement paste and moisture content. In this model all the predictor were having very tight confidence intervals explaining that the current model is the true representative of 95% value, none of them crossing zero value. The negative sign explains about the direction of the relationship between the independent variables and the outcome results.

Finally the correlation matrix was investigated and it was found that 94.7% multicollinearity exist two independent variables $Tc_p (1- þ)$ and $Tc_v (þ- M_c)$. Presence of multicollinearity make is difficult to understand the individual role of the independent variables therefore it was necessary to check the tolerance and VIF coefficients. As a result it was found that tolerance values were within limits i.e. greater than 0.2 whereas VIF coefficients values were close to 10 which is of great concern. The normality test for standardized residual was done and it was found that the Kolmogorov-Smirnov significance value was greater than 0.05 whereas Shapiro-Wilk test was not significant as it was less than 0.05. The skewness value was found to be 0.146 which lies between -1 to +1 therefore no transformation was required.

Similarly the output of model summaries for silica fume, metakoalin and reference predicted models were investigated. The R-square and adjusted R-square values recorded was 80.8% (N=144), 95.0% (N=144), 97.3% (N=72) and 80.4%, 94.9%, 97.2% respectively. In addition to this the Durbin-Watson value for silica fume model was 0.229 for metakaolin and reference was 0.594 and 1.593 in all cases it was less than 2 which mean residuals are positively correlated. The ANOVA table (see sample table in Appendix B) generated after the analysis indicates that the F-test and t-test value for three models is 0.000. This means a high significance of prediction but in case of metakaolin, silica fume and reference mixes, the values of independent variables $Tc_v (þ- M_c)$, $Tc_w (M_c)$ and $Tc_p (1- þ)$ were greater than 0.05.

The negative sign with the outcome of independent variable; $Tc_p (1- þ)$ and $Tc_v (þ- M_c)$ for the silica fume model can be explained as inversely related with the thermal conductivity of cement based.

This sign with Tc_p (1- þ) variable is not clear which might be due to age or ratio factors. Whereas, the positive sign with third variable indicate that as the moisture content drops thermal conductivity also drops or vice versa. Same findings are reported in chapter 7.

As far as the models for mixes with metakaolin admixture and the reference mix are concerned, all the regression coefficients with either positive or negative sign indicate the true relationships between the variables and conductivity. Expect for the negative sign with Tc_w (M_c) independent variable in metakaolin model which indicate the presence multicollinearity (Field 2013). Moreover, a very strong correlation (89-95%) exist between Tc_p (1- þ) and Tc_v (þ- M_c) variables in these models as a result VIF value was noted to be greater 10 and the tolerance value below 0.1 indicating a large inflation of standard errors of regression coefficients due to these variables.

Therefore, it can be said that all these models are statistically significant but the presence of multicollinearity restrict their applicability.

8.4.1.2 Validation of *Conductivity-Moisture* Model

Figures 8.11 shows the comparison between the predicted thermal conductivity using the model expressed in Equation 8.6 and the experimentally observed values for cement-based foam with and without pozzolanic admixture. Overall, it can be noticed that the model expressed in Equation 8.6 performed quite well in predicting the thermal conductivity. Expect for lower densities the predicted conductivity seems to be slightly underestimating and at higher densities this condition is very prominent for silica fume case.

Beside, this if higher densities is not of great concern and the input parameters like age of cement, substitution ratio and dry density are known this model can be used to evaluate the thermal conductivity of cement-based foam. After the comparison, the maximum range of error found for model is 7% for reference, 8% for fly ash, 15% for silica fume and 10% for metakaolin respectively.

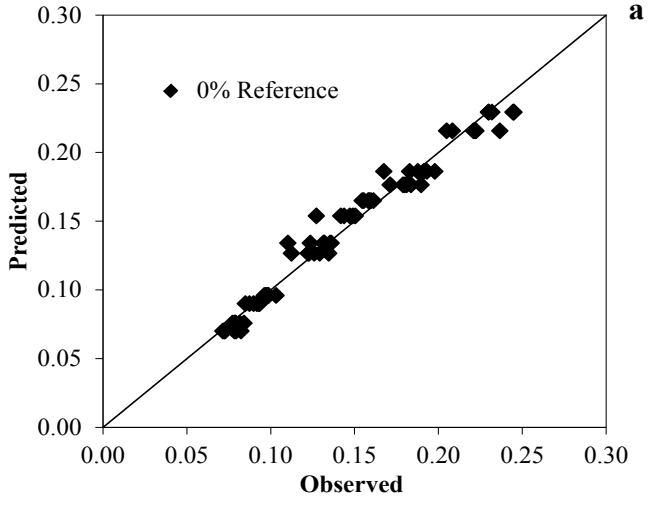

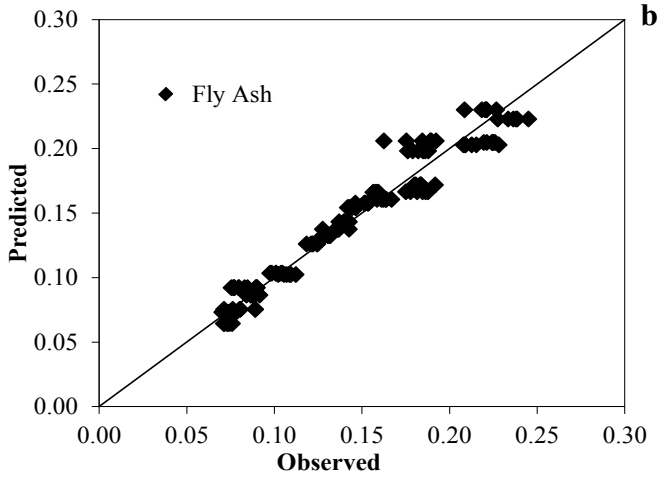

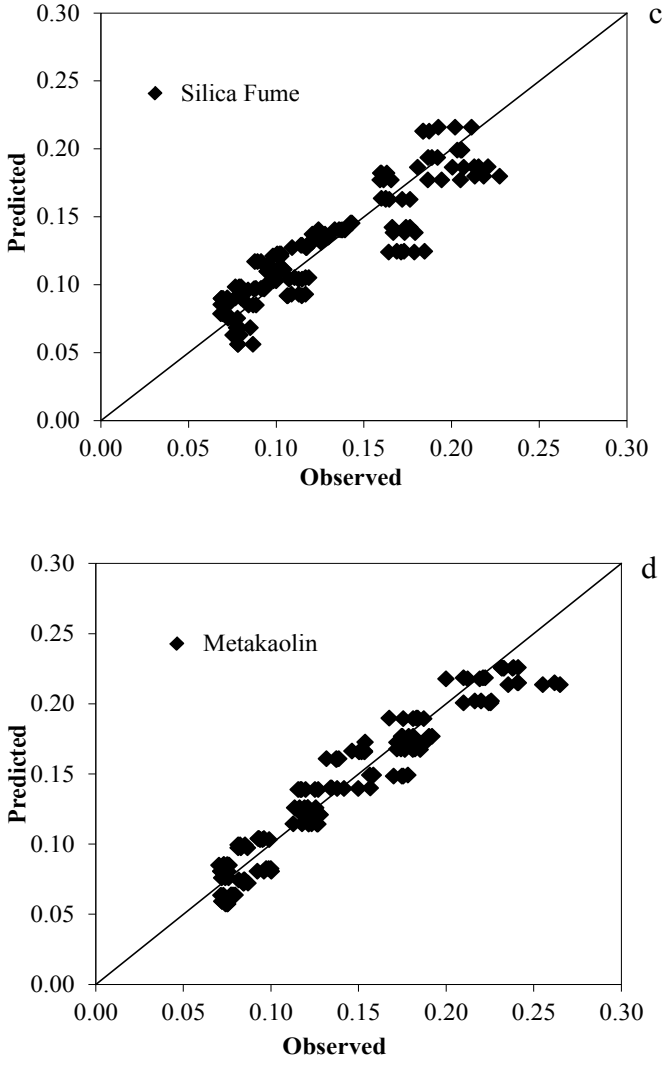

Figure 8.11: Comparison between the predicted values using equation 8.6 and tested values; a) 0% Reference Mix; b) Fly Ash Mix; c) Silica Fume Mix; d) Metakaolin Mix.

8.4.2 Development of a *Conductivity-Porosity* Based Model

The conductivity-moisture based model (Eq8.6) can predict quite accurately the conductivity for lower density cases <= 600 kg/m^3, but for higher densities than 600 kg/m^3 the model predicts less than observed values. In addition to this, the presence of multicollinearity is also of great concern. However, another equation that best describe the correlation between the thermal conductivity of cement-based foam and the porosity (void phase)

was worked out. This is based on a similar approach used by Kearsley (1999). She first evaluated the best equation that expresses the relationship between the compressive strength and total porosity of their dataset for the foamed concrete. Afterward, includes the age and admixture/cement ratio variables in the same relationship with the help of regression analysis and finally, developed a model capable of predicting the compressive strength of the foamed concrete. Following the same approach, different normalized thermal conductivity ratio was plotted against porosity. Therefore, it was found that the graph shown in Figure 7.16, illustrates the best relationship between the normalized thermal conductivity (Tc/Tc_p) and the measured porosity for all the mixes.

The curve fitting was done through SPSS on all different normalized thermal conductivity ratios-porosity graph and it was found that the (Tc/Tc_p) ratio-porosity equation fitted best using an linear function as shown in Figure 8.12.The adjusted R-square and R-square values as 71.8% (N=84) and 72.1% respectively and the linear function is expressed as follow in Equation 8.7.

$$\Psi = 0.923\text{-}0.919\ þ \qquad \text{Eq 8.7}$$

where,

Ψ= ratio (Tc / Tc_p)

þ = porosity (fraction)

Multiple linear regression analysis was carried out by using the measured thermal conductivity data of cement-based foam with and without pozzolanic admixture for three cast densities 800,600,400 kg/m^3 tested for 60 to 300 days.

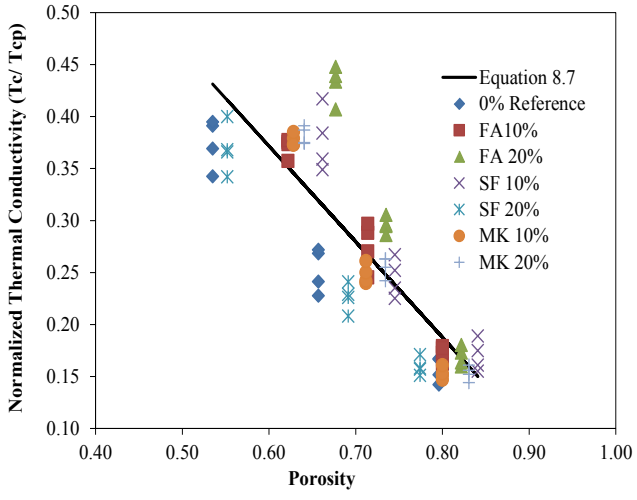

Figure 8.12: Normalized Thermal Conductivity with Porosity of all mixes. Solid line indicates predicted results by equation 8.7.

After doing number of trials three variables Ψ (Eq 8.7), time and (admixture /cement) ratio were selected as independent along with thermal conductivity as dependent variable. As a result the predicted model for thermal conductivity of cement-based foam for 0% reference, fly ash, silica fume and metakaolin is expressed in Equation 8.8.

$$Tc = \beta_o + \beta_1 (0.923 - 0.919þ) + \beta_2 \ln (t) + \beta_3 (ratio) \qquad \text{Eq 8.8}$$

where,

Tc = thermal conductivity of cement-based foam (w/m/k)

þ = porosity (fraction)

t = age of the paste (days)

ratio = admixture/cement ratio (by weight)(fraction)

β_o = constant (table 8.5)

$\beta_1, \beta_2, \beta_3$ = regression coefficient (table 8.5)

8.4.2.1 Limitations of Proposed Model (Eq 8.8)

The proposed conductivity-porosity model in this section is limited to the following conditions:

- Cement-based foam without aggregates.
- Porosity range of $0.50 \leq p \leq 0.85$.
- Age of paste for $60 \leq t \leq 300$ range.
- Admixture/Cement ratio range of $0 \leq ratio \leq 0.2$.
- Fly Ash, Silica Fume and Metakaolin.

Table 8.5: Constant for Equation 8.8

Constant	0% (Reference)	Fly Ash (FA)	Silica Fume (SF)	Metakaolin (MK)
β_o	0.110	0.038	0.149	0.062
β_1	0.498	0.770	0.552	0.734
β_2	-0.025	-0.021	-0.019	-0.028
β_3	0.000	0.121	-0.495	0.198

8.4.2.2 Interpreting Regression Coefficients for *Conductivity-Porosity* Based Model

The 144 data points were used for regression analysis for fly ash, silica fume and metakaolin models whereas for 0% reference model 72 data points were investigated. This dataset is based on the measured thermal conductivity of cement-based foam with and without pozzolanic admixture for three cast densities 800,600,400 kg/m^3 tested for 60 to 300 days. All the models are based on three independent variables porosity, time and (admixture/cement) ratio and dependent variable of thermal conductivity of cement-based foam. Whereas, the method selected was forced entry method for all the mixes.

The output section (Figure B.8 Appendix B) for fly ash model indicates that the R-squared statistics (N=144) explains 94.8% of variability in the thermal conductivity of the cement-based foam. Whereas, the adjusted R-square was 94.7% which mean this percentage of the variation in the thermal conductivity of cement-based foam can be attributed due to these three independent variables i.e. porosity, time and ratio. The standard error of estimation which shows the standard deviation of the residuals recorded was 0.014 (w/m/k), a value quite close to zero. This establishes that the model performs satisfactorily. Further, when tested according to the Durbin-Watson test a value of 0.522 is obtained. This being less than 2 therefore, this reveals that the residuals are positively correlated.

The Pearson correlation coefficient of porosity, time and ratio variables with thermal conductivity was 93%, 25.9%, and 10.9% respectively. The ANOVA table from the SPSS output (Figure B.8 Appendix B) indicates that the F-test and t-test is 0.000 which shows that model is highly

significant. Therefore, it can be said that these three independent variables together predict the thermal conductivity of cement-based foam. All the independent variable relationship is statistically significant (Sig.=0.000) but the negative sign with the time regression coefficient means that as the time increases conductivity decreases (Figure B.8 Appendix B).

In this model all the predictors were having very close confidence intervals none of them crossing zero value therefore, indicating significant correlation. After this multicollinearity was checked and it was found that none of the independent variable has strongly correlation. In addition to this tolerance and VIF limits were also checked and they were also found to be in acceptable limits.

As a further check, the normality test for the standardized residual was done and it was found that the Kolmogorov-Smirnov test value was 0.200 and the Shapiro-Wilk test value was 0.183 greater than 0.05 which indicate that this performed test is statistically significant. Moreover, the Skewness and Kurtosis value was found to be -0.374 to 0.616 respectively. This is well within the range of -1 to +1 and therefore, no transformation is deemed necessary. In the same the way the output summaries for silica fume, metakaolin and reference predicted models were investigated.

The R-square and adjusted R-square values recorded was 94.8% (N=144), 95.8% (N=144), 95.8% (N=72) and 94.7%, 95.7%, 95.7% respectively. Moreover, the model summary indicates that the Durbin-Watson value for silica fume model was 0.568 for metakaolin and reference was 0.773 and 1.189 respectively. For all cases it was less than 2 which mean residuals are positively correlated.

The F-test and t-test value for three models (silica fume, metakaolin, reference) is 0.000 which is highly significant and the negative sign with coefficient of time variable is present in all models which reflect the inverse relationship with conductivity. However, strong correlation does not exist between any independent variables which mean multicollinearity is not present at all in any predicted model.

Regarding, the standardized residual normality test the reference and the metakaolin model passes the test whereas, silica fume model significance value was slightly less than 0.05. As per requirement it has to be greater than 0.05. On another hand the skewness and kurtosis values for all the three models lie within the acceptable range of -1 to +1.

8.4.2.3 Validation of *Conductivity-Porosity* Model Results

The predicted thermal conductivity of cement-based foam is plotted against the measured conductivity in Figure 8.13. It can be noticed that model expressed in Equation 8.8 is reasonable good in predicting the thermal conductivity of cement-based foam for 800 to 400 kg/m^3 cast densities with pozzolanic admixture. Except the predicted conductivity seem to be slightly underestimating at higher density. In addition to this the maximum overall error in the model was of 7% for reference, 4% for fly ash, 5% for silica fume and 6% for metakaolin respectively. In contrast this model is much better than the conductivity-moisture model in all aspect. It can be concluded based on the foregoing rigorous analysis and validation proceedings that this model can be used to predict quite reliably the thermal conductivity of cement-based foams containing pozzolanic admixture.

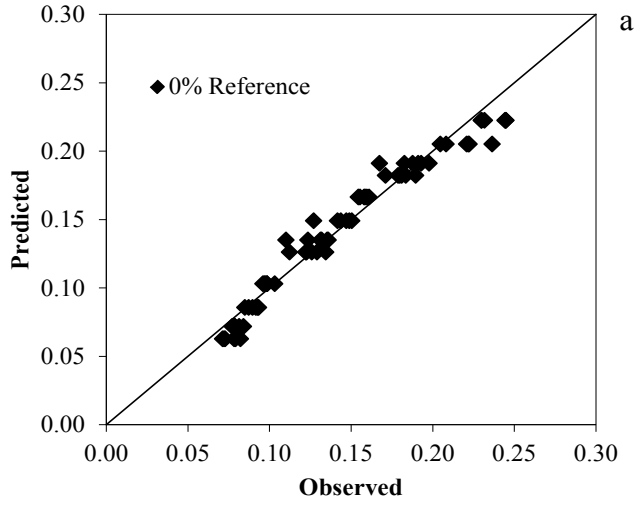
a
0% Reference
Predicted
Observed
0.00
0.05
0.10
0.15
0.20
0.25
0.30

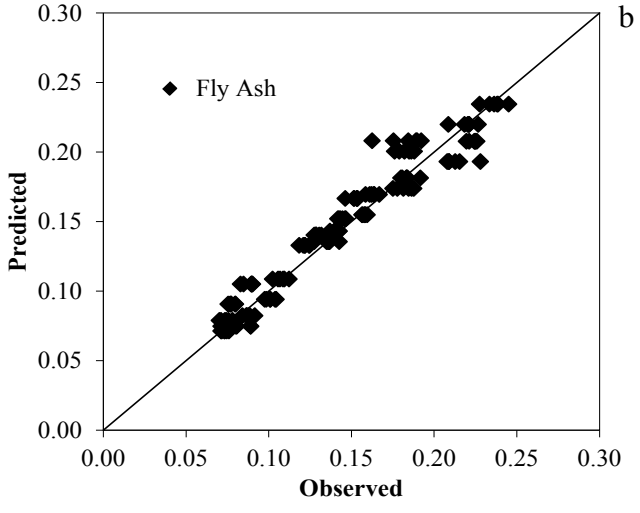
b
Fly Ash
Predicted
Observed
0.00
0.05
0.10
0.15
0.20
0.25
0.30

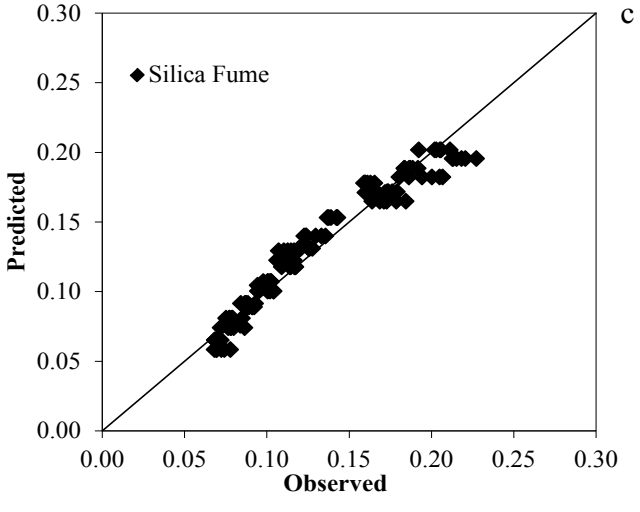
c
Silica Fume
Predicted
Observed
0.00
0.05
0.10
0.15
0.20
0.25
0.30

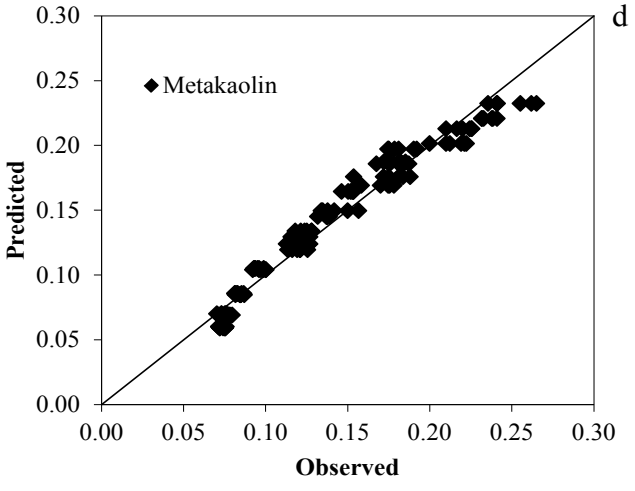

Figure 8.13: Comparison between the predicted values using equation 8.8 and tested values; a) 0% Reference Mix; b) Fly Ash Mix; c) Silica Fume Mix; d) Metakaolin Mix.

8.5 Comparison of Proposed Model with Existing Thermal Conductivity Models

As already mentioned in chapter two, there exist several mathematical models to predict the conductivity of porous cementitious materials. The popular models which are quite extensively used by others while dealing with the thermal conductivity of similar porous building materials are those of Maxwell (Eq 2.7), Frey (Eq 2.9), Russell (Eq 2.8), Series (Eq 2.11) and Parallel (Eq 2.10). These models take the parameters of porosity, thermal conductivity of solid which is actually conductivity of cement paste and air as an input. In this regards the porosity values were taken from Table 6.1,conductivity of cement paste from Table 7.1 and air was taken as 0.026 (w/m/k). For comparison, Equation 8.6 and 8.8 were also added along with the five models.

The comparison between the experimental evaluated mean thermal conductivity of cement-based foam and as predicted by analytical models for 60 and 300 days is summarized in Figure 8.14 to 8.20. Whereas, the remaining graph for 120 and 210 days for all mixes is given in Appendix B (Figure B1-B7).

As already discussed in the previous chapters the parallel approach model and the series model define the upper and lower bound values of conductivity respectively. The values predicted by the three classic models of Maxwell, Frey and Russell as well as those by the present study Equations 8.6 and 8.8, all lie within these two bounds. Therefore, it can be concluded that the models developed here in this study are following the principles of heat transfer. However, the accuracy has some doubts as it is evident from all the mixes that these existing models predicted well for density less than 600 kg/m^3 and is true for all mixes. Therefore, for case in which thermal conductivity is controlled by solid phase or for density greater than 600 kg/m^3 these three models over predict the conductivity for reference mix and under predict for remaining three mixes with pozzolanic admixture.

This trend remains similar at all testing day i.e. 60,120,210 and 300 days. For example in case of reference mix, at 60th day, the maximum percentage of over prediction predicted by Russell was approximately 20% and for 300th day was 7%. It can also be noticed that as compared with existing five analytical models, the Equation 8.6 and 8.8 seem to quite accurately and closely predicting the thermal conductivity of cement-based foam. It can be said that the proposed model (Equation 8.8) as also noticed from the following Figures (8.14-8.20) is the efficient and reasonably accurate model.

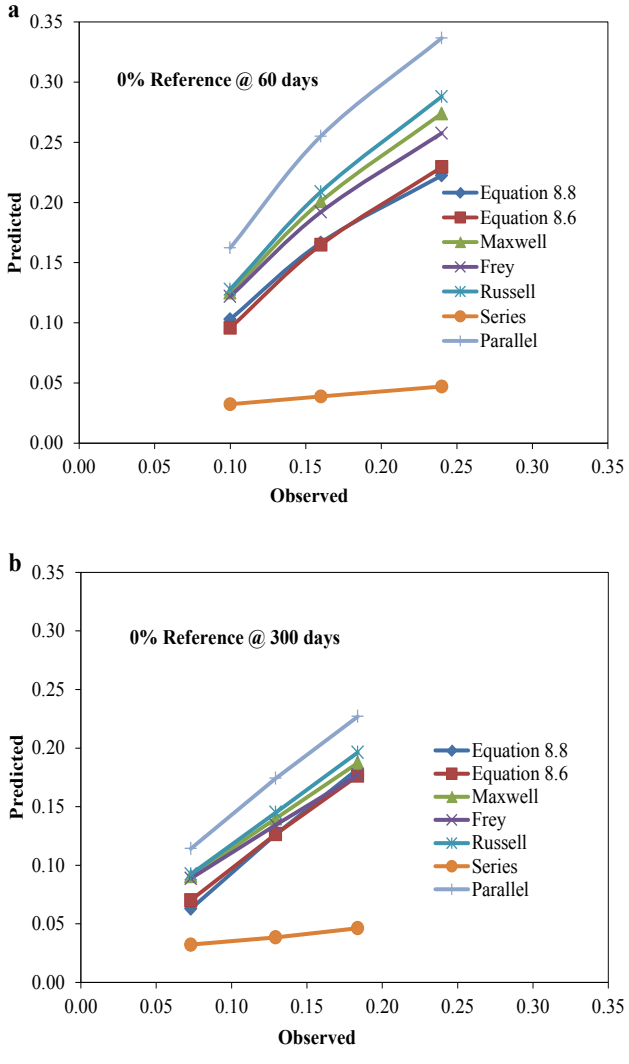

Figure 8.14: Comparison between the predicted and the tested values of conductivity measured by the current authors' and other researchers; 0% reference mix; a) 60th day; b) 300th day.

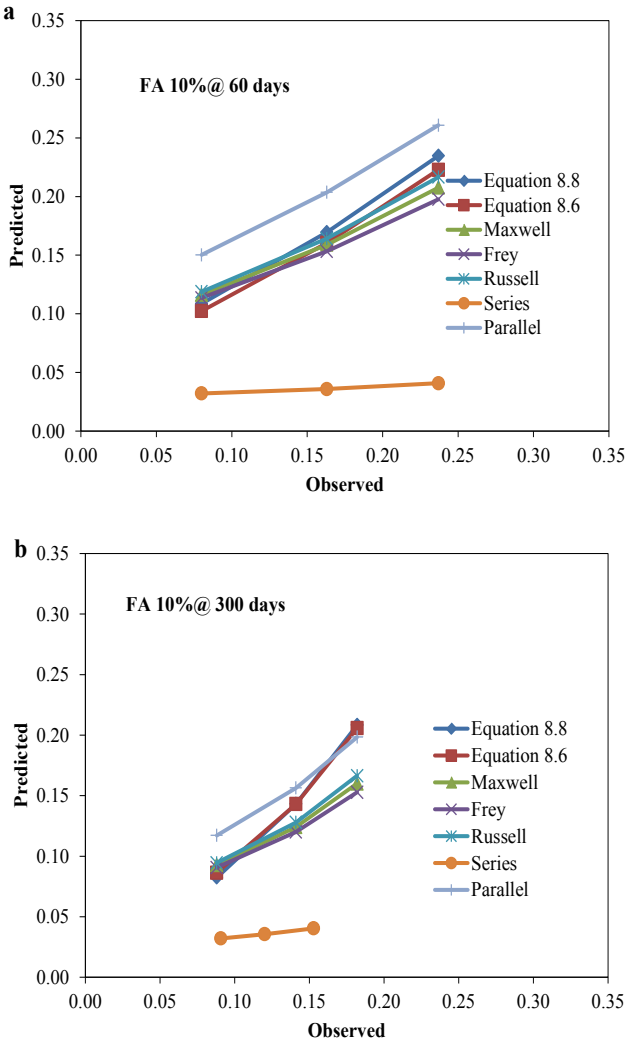

Figure 8.15: Comparison between the predicted and the tested values of conductivity measured by the current authors' and other researchers; 10% fly ash mix; a) 60th day; b) 300th day.

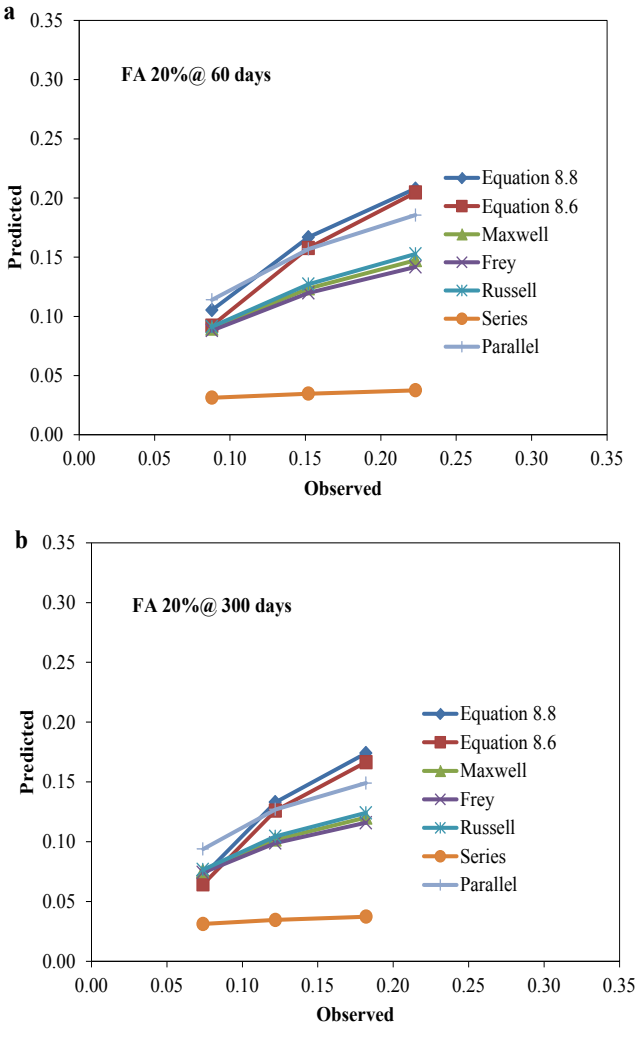

Figure 8.16: Comparison between the predicted and the tested values of conductivity measured by the current authors' and other researchers; 20% fly ash mix; a) 60th day; b) 300th day.

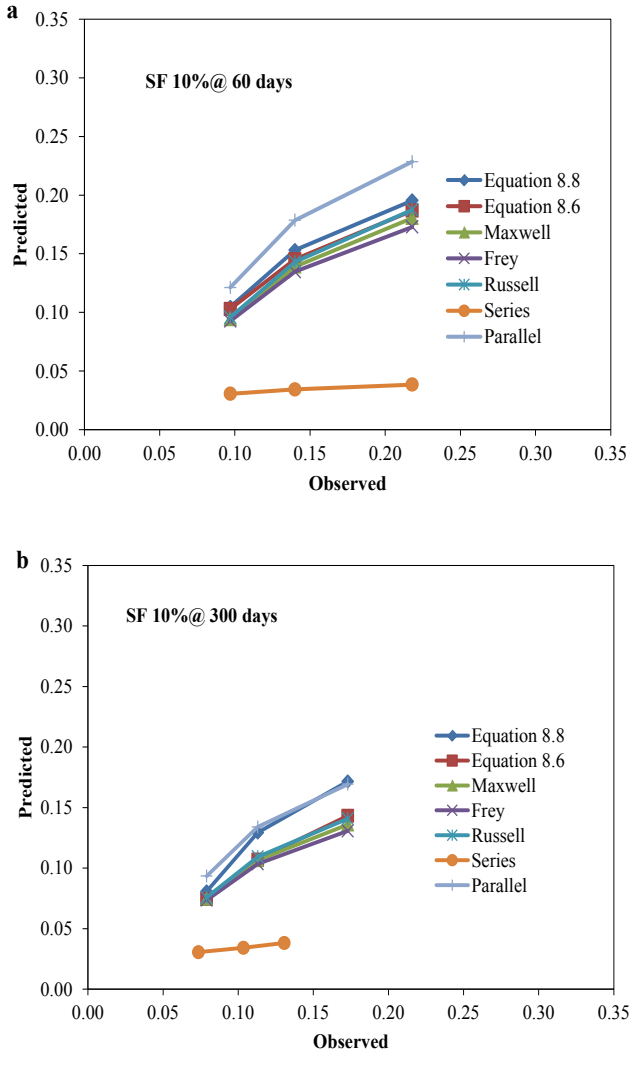

Figure 8.17: Comparison between the predicted and the tested values of conductivity measured by the current authors' and other researchers; 10% silica fume mix; a) 60th day; b) 300th day.

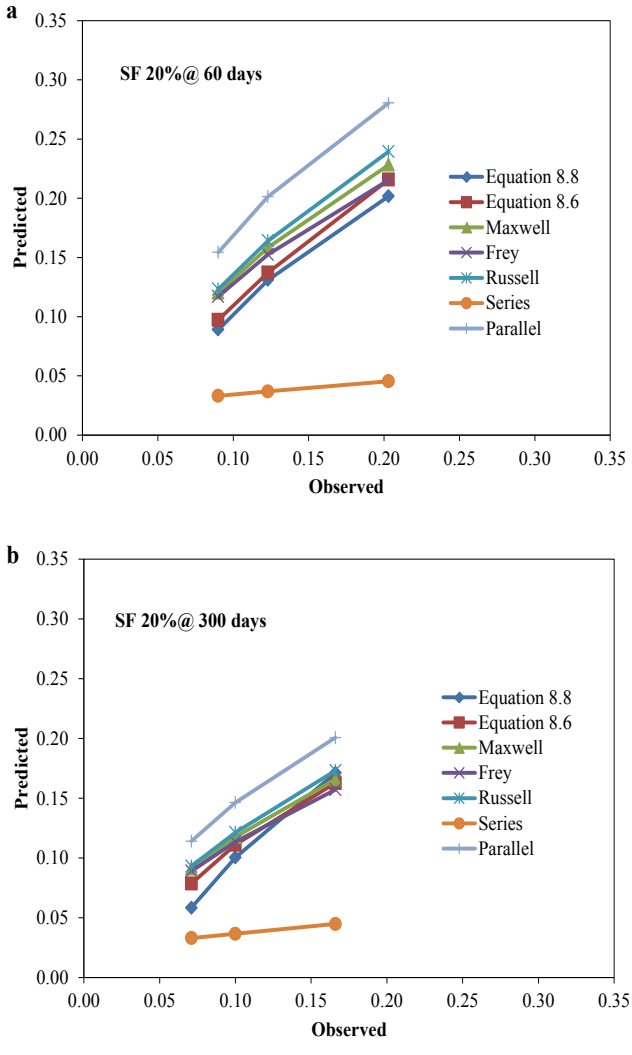

Figure 8.18: Comparison between the predicted and the tested values of conductivity measured by the current authors' and other researchers; 20% silica fume mix; a) 60th day; b) 300th day.

.

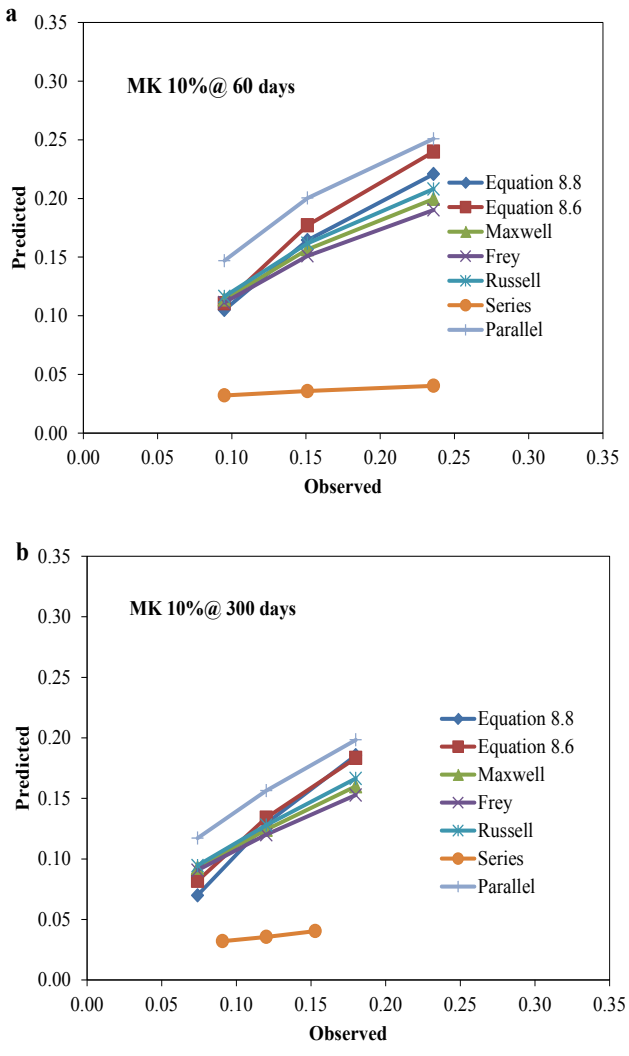

Figure 8.19: Comparison between the predicted and the tested values of conductivity measured by the current authors' and other researchers; 10% metakaolin mix; a) 60th day; b) 300th day.

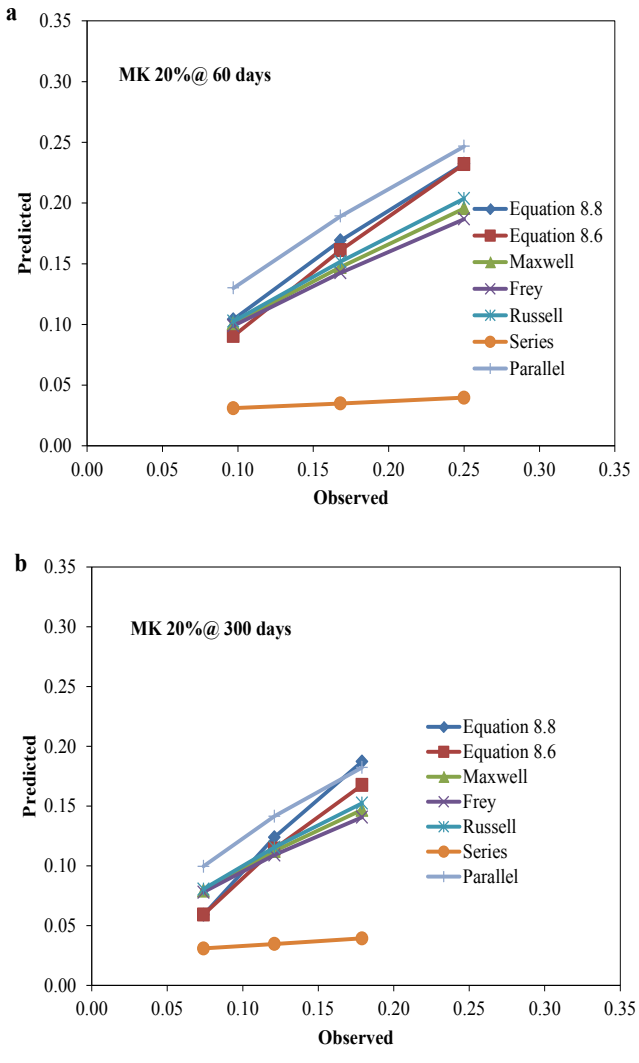

Figure 8.20: Comparison between the predicted and the tested values of conductivity measured by the current authors' and other researchers; 20% metakaolin mix; a) 60th day; b) 300th day.

8.6 Applicability of Proposed Model (Eq 8.8)

8.6.1 Comparison with CEMATRIX™ Dataset

In addition to cement-based foam specimens tested in the current study in section 8.4.2.1, database for eight mixes of cement-based foam supplied by CEMATRIX™ was use for the validation of proposed model (Eq 8.8). The specimens were made of Type HS Portland cement with 0.48 w/c ratio, pozzolanic admixture and provoton foaming agent. The thermal conductivity of these samples was measured, using a transient plane source (TPS) in civil engineering laboratory at the University of Alberta. Total 24 specimens were validated against Equation 8.8.

Figure 8.21 summarizes the comparison between experimental evaluated thermal conductivity of cement-based foam of dataset tabulated in Table 8.6 and as predicted by proposed model 8.8. For the evaluation of thermal conductivity Equation 8.8 takes value of porosity, time and ratio as an input. However for this dataset, age of paste, ratio and the density-at-test was known and the porosity was not known therefore, Equation 8.4 was used to calculate the porosity for all these eight mixes. It can be noticed in Figure 8.21 that the Equation 8.4 and Equation 8.8 together performed quite accurately. Except for mix C and mix E which was 5% over and 9% under predicted. Further, this proposed model Equation (8.8) was used to predict the thermal conductivity of mixes F, G, H which contain 40% slag as pozzolanic admixture. Since in the present study slag as admixture is not included it was decided to use the model applicable to mixes containing fly ash instead since the pozzolanic characteristics of slag are closer to those of fly ash than to silica fume or metakaolin.

Interestingly, it was found from the plot in Figure 8.21 that the proposed model predicts the conductivity for mixes with 40% slag quite accurately.

Although the model is design for admixture/cement ratio ≤ 20% but it performed reasonably for ratios greater than 20% i.e. mixes with 40% slag.

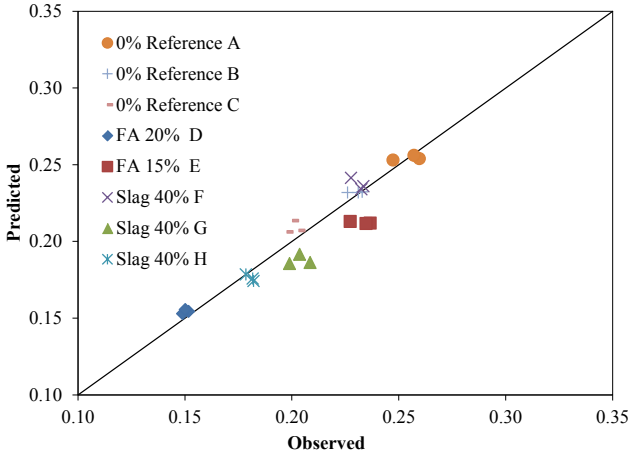

Figure 8.21: Comparison between the Cematrix database test results and as predicted by conductivity-porosity model (Eq 8.8).

Table 8.6: Comparing the accuracy of proposed model (Eq 8.8) with cematrix database

Database	Mix	Specimen Id	Observed TC (w/m/k)	Cast density kg/m^3	Dry density kg/m^3	Porosity (Eq 8.4) (%)	Predicted TC (Eq 8.8) TC (w/m/k)	Mean TC	STDEV TC	COV (%) TC
Cematrix	0% Reference	A	0.260	650	688	54	0.254	0.254	0.0016	0.617
			0.257		699	54	0.256			
			0.247		683	54	0.253			
		B	0.226	550	573	66	0.232	0.232	0.0003	0.108
			0.231		573	66	0.232			
			0.233		575	66	0.232			
		C	0.200	475	568	80	0.214	0.207	0.0040	1.952
			0.203		534	80	0.207			
			0.198		530	80	0.206			
	FA 20%	D	0.152	467	458	77	0.154	0.153	0.0013	0.883
			0.149		453	77	0.153			
			0.150		462	77	0.155			
	FA 15%	E	0.227	545	612	69	0.213	0.212	0.0007	0.330
			0.237		609	69	0.212			
			0.235		608	69	0.212			
	Slag 40%	F	0.228	650	758	72	0.241	0.236	0.0038	1.622
			0.234		740	72	0.236			
			0.233		733	73	0.234			
	Slag 40%	G	0.199	550	570	80	0.185	0.186	0.0033	1.783
			0.209		573	80	0.186			
			0.204		591	79	0.191			
	Slag 40%	H	0.182	475	538	81	0.176	0.174	0.0022	1.268
			0.182		532	81	0.174			
			0.179		547	81	0.178			

8.6.2 Comparison with Batool et al. (2013) Dataset

Batool et al. (2013) recently recorded the thermal conductivity values for cement-based foams for different mix with and without pozzolanic admixture. As this dataset was not the part of the data used in the development of the model (Eq 8.8) therefore, Batool et al. (2013) data was used here to check the applicability of the proposed model. In their study, type GU cement was used with a w/b ratio of 0.56 and synthetic foaming agent was used to generate the foam. The Equation 8.4 of the present study was used to get the values of porosity and density-at-test to be inputs to the Equation 8.8. Batool et al. (2013) conducted their tests for conductivity at age 35 days on specimens which were first water cured for 28 days after casting and thereafter air dried for seven more days. The details of those dataset and the prediction through the present model 8.8 applied to those data are tabulated in Table 8.7. The comparison between observed and predicted values is presented in Figure 8.22. The prediction is found to be quite good for lower densities less than 600 kg/m^3. For specimens of higher densities the prediction deviated from the experimentally observed values slightly. The deviation recorded being 8%, 10%, 19% and 3% for reference, FA 20%, SF 20% and MK 20% respectively.

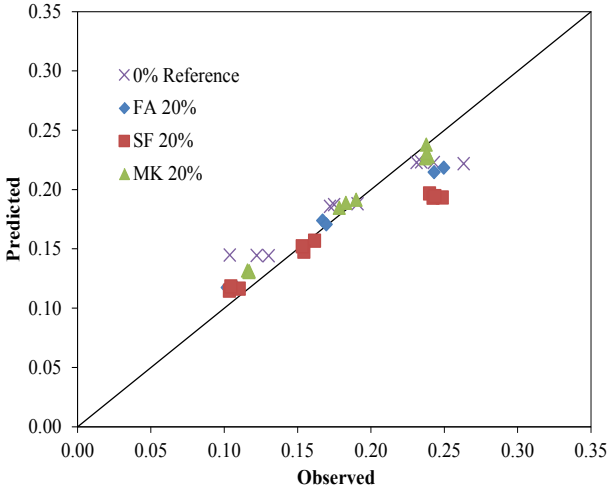

Figure 8.22: Comparison between the Batool database test results and as predicted by conductivity-porosity model (Eq 8.8).

Table 8.7: Comparing the Accuracy of Proposed Model (Eq 8.8) with Batool Database

Database	Mix	Specimen Id	Observed TC (w/k/m)	Dry Density kg/m^3	Dry Density kg/m^3	Porosity (Eq 8.4) (%)	Predicted TC (Eq 8.8) TC (w/m/k)	Mean TC	STDEV TC	COV (%) TC
Batool et al(2013)	0% Reference	A	0.234		782	54	0.223	0.223	0.001	0.349
			0.231		779	54	0.223			
			0.263	800	774	54	0.222			
		B	0.175		594	66	0.187	0.187	0.001	0.628
			0.191		598	66	0.188			
			0.172	600	586	66	0.186			
		C	0.104		373	80	0.145	0.144	0.000	0.203
			0.122		371	80	0.144			
			0.130	400	370	80	0.144			
	FA 20%	A	0.232		666	68	0.215	0.218	0.003	1.385
			0.243		679	68	0.218			
			0.250	800	686	68	0.220			
		B	0.170		529	74	0.174	0.172	0.002	1.013
			0.167		518	75	0.171			
			0.170	600	520	74	0.171			
		C	0.108		340	82	0.118	0.122	0.008	6.535
			0.108		339	82	0.117			
			0.102	400	386	80	0.131			
	SF 20%	A	0.240		721	59	0.197	0.194	0.002	1.021
			0.242		704	59	0.193			
			0.249	800	705	59	0.193			
		B	0.162		534	67	0.157	0.152	0.005	3.019
			0.154		491	68	0.148			
			0.153	600	512	68	0.152			
		C	0.104		336	75	0.115	0.116	0.002	1.529
			0.110		344	75	0.116			
			0.105	400	353	74	0.118			
	MK 20%	A	0.239		684	68	0.228	0.231	0.006	2.708
			0.238		719	66	0.238			
			0.237	800	679	68	0.226			
		B	0.179		531	74	0.185	0.188	0.003	1.810
			0.183		546	73	0.189			
			0.190	600	555	73	0.191			
		C	0.116		344	82	0.132	0.131	0.001	0.444
			0.117		342	82	0.131			
			0.117	400	340	82	0.130			

8.6.3 Comparison with Awang et al. (2012) & Mydin (2011) Database

Database of light weight foamed concrete summarized by Awang et al. (2012) and formcrete by Mydin (2011) was validated by using the proposed Equation 8.8. This database was selected in order to see if the presence of sand in their investigations makes any significant impact on the predictability of 8.8 which is based on cement-based foams without sand. Awang's tests were on oven dried specimens which correspond to a case of free moisture. This condition in the present study can be assumed at an age of 350 days as input to the Equation 8.8. In other words the time `t` in the factor ln (t) appearing in the Equation is taken to mean 350 days. Awang et al. (2012) used 1:1.5 cement sand ratio whereas, the corresponding ratio of cement to sand was 1:2 in the samples prepared by Mydin (2011) and the conductivity test was performed after 14 days of casting. The detail is tabulated in Table 8.8. For densities higher than 600 kg/m^3 the predicted values are lower than measured. But in case of samples having density 1000 kg/m^3 the model prediction was very much different from the observed. This is to be expected because this model Eq 8.8 has been developed with a density range of 400 to 800 kg/m^3 only.

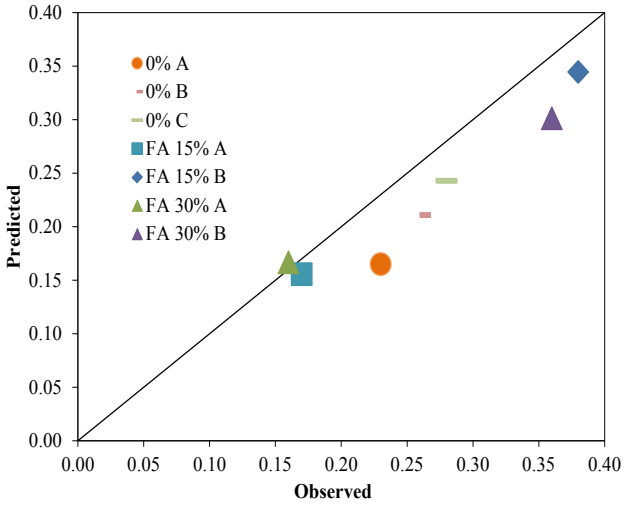

Figure 8.23: Comparison between the Mydin and Awang database test results and as predicted by conductivity-porosity model (Eq 8.8).

8.7 Robustness of Proposed Model (Eq 8.8)

The proposed conductivity-porosity model in this section has the ability to provide accurate and precise results under these additional conditions:

- Slag as admixture.
- GU type cement.
- Provoton foaming agent.
- Age of paste for $14 \leq t \leq 350$ range.
- Fly ash/Cement ratio range of $0 \leq \text{ratio} \leq 0.3$.

Table 8.8: Comparing the Accuracy of Proposed Model (Eq 8.8) with Mydin and Awang Database

Database	Mix	Specimen	Observed TC (w/k/m)	Cast Density (kg/m^3)	Porosity (%)	Predicted TC (Eq 8.8) TC (w/m/k)	Error (%)
Mydin (2011)	**0% Reference**	**A**	0.230	650	74	0.165	28
		B	0.260	800	64	0.211	19
		C	0.280	900	57	0.243	13
Awang et al. (2012)	**FA 15%**	**A**	0.170	600	69	0.156	8
		B	0.380	1000	50	0.344	9
	FA 30%	**A**	0.160	600	70	0.167	4
		B	0.360	1000	51	0.301	16

9. Conclusions and Recommendations

9.1 Summary

The research presented herein focused on the influence of air-void parameters and hydrated cement paste on the conductivity of cement-based foam by varying the density and binder types. In order to fulfill the objectives of this research, both experimental and analytical work were carried out as described in the preceding chapters.

During the experimental phase, three series of cement-based foams were prepared with cast densities of 800 kg/m^3, 600 kg/m^3 and 400 kg/m^3 respectively. The reference mix in each series was made with Portland cement as the sole component of the binder whereas fly ash, silica fume and metakaolin were added to the binder at up to 10% and 20% by cement mass respectively. Thus, three pairs of specimens of slurry mix (without any foam added yet) and six pairs of cement-based foam specimens for each density from the seven mixes were prepared. Testing was carried out at room temperature and at four different ages i.e. when the specimen was at 60th, 120th, 210th and 300th days of maturity.

The consistency for the fresh cement-based foam mix is measured in term of spreadability and flowability. The Marsh Cone test is used here to measure the flowability of the cement paste and the Flow Cone test used for a mixture with foam to measure the spreadability. These tests indicate the quality of the mixes and suitability of the process used to design the mixes.

The X-ray diffraction technique was used to identify the phases in the cement paste and later Rietveld refinement (RQXRD) was adopted to estimate the fraction by weight for the hydrated products. In this manner, the thermal conductivity of each significant hydrated product was extended to compute that of the composite by using the rule of mixtures.

The X-ray tomography technique (CAT Scan) was used to investigate the pore structure by evaluating parameters including: air-void size distribution, air-void spacing and void shape factors. This exercise was performed for both mixes with and without pozzolanic admixtures. In all, 21 samples of size 35 mm x 35 mm with height of 20 mm were examined. The image resolution in the instrument was limited to 9 μm. The 2D quantitative analyses of all the cement-based foam specimens were done by using the Skyscan CT-analyzer software provided to this author by the Department of Pharmacy, University of Alberta. This quantification of air-void parameters helped understand their relationship with density, porosity and in turn, the thermal conductivity of the material under investigation.

The Transient Plane Source (TPS) technique was used for the experimental evaluation of thermal conductivity. In all, 21 pairs of specimens for the hydrated cement paste and 126 pairs for the cement-based foam were examined to evaluate their thermal parameters. In order to quantify the effect of moisture on the thermal conductivity in the cement-based foam samples, the moisture content was evaluated by oven drying at four different ages. This thesis reports the influence of density, porosity, admixture type, moisture content and air-void parameters on the measured conductivity.

Once the experimental data was obtained, a mathematical model was developed to express the thermal conductivity of cement-based foam by performing statistical analysis. In this, the author utilized the SPSS software. The result of twenty one different mixes was used to generate the model presented here (conductivity-porosity) and is based on porosity, substitution ratio of pozzolanic admixture and the age of the paste variables. The proposed model was then compared with the existing models for other porous materials. This model was further investigated against the available database of cement-based foams, independent of this thesis. It was found that the proposed model is capable of predicting the thermal conductivity with accuracy.

9.2 Conclusions

9.2.1 Fresh State Properties

The following are the significant findings in regard to the fresh properties of cement-based foam, with particular emphasis on the substitution of Portland cement with pozzolanic admixtures at different ratios.

1. The addition of pozzolanic admixtures makes the mixes more viscous due to which the flow time increases as compared to the reference mix (Portland cement only). This increase in viscosity is mainly due to the fineness of the pozzolanic admixture and resultant higher water demand.

2. Adding fly ash and silica fume in the cement-based foam increases the spread in comparison with the reference mix, whereas mixes with metakaolin had smaller spread.

This implies that among the three pozzolanic admixtures examined, metakaolin imparts cohesive ability.

3. Adding fly ash necessitated an average increase in foam content by 14% for the cast density of 800-400 kg/m^3. Similarly, when silica fume was added, there was a 7% increase. On the other hand, for metakaolin there was a reduction in foam demand by 7% and 24% for the two substitution ratios. The increase with fly ash may be attributed to the inherent high residual carbon. For silica fume, the increase is likely due to the very fine particle size. Metakolin possesses relatively higher water absorption, which explains the drop in foam demand.

9.2.2 Quantification of Hydrated Products

This study established the following conclusion regarding the phase identification and quantification of hydrated products in cement paste.

1. The addition of the pozzolanic admixtures resulted in the consumption of CH as compared to the reference mix, which is mainly due to the presence of silica and alumina.

2. Qualitatively, the weighted fractions for phases detected are in agreement with the findings of earlier research. But, quantitatively the crystalline phases were higher as reported here. However, the Rule of Mixtures reveals that even though the amorphous content was included in the analysis it will not significantly affect the thermal conductivity.

3. Portlandite (CH), Calcium Silicate Hydrate (CSH) and Calcite governs the thermal conductivity of the hydrated products as they are most predominant.

9.2.3 Air-Void Characterization

The following are the significant findings related to the air-void network in the microstructure of cement-based foam. Recall that mixes with and without pozzolanic admixture were investigated in this study.

1. Seventy five percent of the foam bubble lies in the range of 0.01-0.2 mm diameter. The remaining 25% is in the 0.2-0.4 mm diameter range.

2. The porosity is influenced by the density, type of admixture and content. Adding admixture to any cast densities increases the porosity compared to the reference mix with Portland cement only, whereas the higher substitution ratio of the silica fume reduces the porosity significantly which is mainly due to pore filling.

3. Due to the 10% and 20% substitution of fly ash and metakaolin, the increases in porosity was 5%. For silica fume, a 10% reduction was noted as the content increased from 10% to 20%.

4. The maximum frequency of occurrence is of 0.03 mm pore size diameter across all the mixes in this study.

5. Adding fly ash, silica fume and metakaolin does not significantly influence the frequency of air-void size distribution. However, these admixtures increase the number of small pores in higher densities.

This is due to coating of the bubbles resulting in less imperfection i.e. merging and broken pores.

6. Distances between the voids increases with the addition of pozzolanic admixture especially in mixes with a higher admixture substitution ratios. Spacing size 0.55 mm and 1.10 mm was predominant for 800 kg/m^3, 0.55 for 600 kg/m^3 and 0.28 mm for 400 kg/m^3.

7. For all mixes, D50 lies in the range of 0.025-0.040 mm, the maximum was recorded for 400 kg/m^3 and the minimum was recorded for 800 kg/m^3 cast density.

8. The D50 value for void spacing is the function of SP50 (spacing below which 50% of the spacing lies) values and this relationship is not affected by adding the pozzolanic admixture.

9. The shape of the majority of the air voids in all mixes was circular in 2D (or spherical in reality).

9.2.4 Thermal Conductivity

A. Cement Paste

1. The 20% substitution ratio of fly ash and silica fume effectively reduces the conductivity of the cement paste around 12% and 10% at the 300th day when measured with regard to the reference mix. The changes in the ratio between 10% FA and 20% FA in the binder results in a maximum drop of 11%. However, for silica fume and metakaolin, this drop was nominal. Formation of CSH in higher

amount, reduction in slurry density and higher water absorptive property are the main underlying reasons.

2. The addition of three pozzolanic admixtures reduces the moisture content significantly in the cement paste. Overall, the drop recorded for the reference mix was 64%. The drop for admixtures (FA, SF, MK) at two specific dosages of 10% and 20% was 74%, 65%, 50% and 64%, 70%, and 71%, respectively (period 60^{th} to 300^{th} day).

B. Cement-Based Foam

3. The change in density significantly reduces the thermal conductivity of cement-based foam. The drop recorded was 35% for the 800-600 kg/m^3 and 46% for the 600-400 kg/m^3 densities ranges at the 300^{th} day. However, a further 6% reduction in conductivity for the both density ranges was seen after the pozzolanic admixtures were added.

4. With the substitution of fly ash and metakaolin, the average reduction noticed in conductivity for all density ranges was 5%, whereas for 20% metakaolin addition, an increase of 3% was noticed. For silica fume it was 8% for 600 kg/m^3 cast density and 15% for 400 kg/m^3 cast density. These values were recorded at the 300^{th} day to eliminate the effect of moisture.

5. The reduction in thermal conductivity in presence of fly ash is mainly due to formation of hydrated products (CH and CSH) and less water absorptive property. Same can be reported for silica fume except that higher silica content also contributes in further reduction. Whereas, for metakaolin along with above mentioned factors its high water absorptive property plays the vital role in reversing the trend.

6. For all the mixes, the average conductivity drop recorded due to the moisture content, for the cast density of 800,600,400 kg/m^3 was 8%,16%, and 13% respectively. These values were recorded at the 300^{th} day.

7. The relationship of median diameter (D50) values to thermal conductivity reveals that smaller size of pores influences conductivity. However, the drop in thermal conductivity in lower densities is mainly due to more number of air voids.

8. The air-void spacing parameters SP10 and SP50 increase as thermal conductivity increases.

9.2.5 Regression Modeling

1. A mathematical model (Eq 8.4) was developed relating porosity with density and the substitution ratio of the pozzolanic admixture. This model was used to predict the porosity value of cement-based foam for three pozzolanic admixtures. Another model which was developed was used to predict the moisture content related to the dry density and the age of the paste. For validation, these models' predicted values were compared with the experimental results and reasonable accuracy was obtained.

2. The conductivity-porosity model (Eq 8.8) which was developed by relating porosity, age of the paste and the substitution ratio of the pozzolanic admixture was used to predict the thermal conductivity of cement-based foam. The model shows accuracy when compared with the experimental results. The maximum total error recorded

between the observed and predicted values for reference model was 7%. For mixes with fly ash it was 4%. For those with silica fume it was 5% and for metakaolin mixes it was 6%. The applicability of this model was compared with database from other researcher or data generated by this author independent from the present study. A close agreement was found in all cases between the predicted and experimental values.

9.3 Recommendations for Future Research

Based on the findings, conclusion and discussion from this study, following recommendations are made for future investigation.

- The present study used only two replacement ratios by mass of cement, 10% and 20%, for the pozzolanic admixture. Future work is necessary to look into more and different substitution ratios and their influence on thermal conductivity to promote a low carbon footprint in construction industry.

- This research was executed at room temperature. Future investigations into thermal conductivity of cement-based foam should be carried out under elevated temperatures and at sub-zero temperatures to examine the insulation potential.

- The RQXRD analysis was performed evaluating only the crystalline phases, whereas amorphous phases are also present in hydrated cement paste. A complete investigation should be carried out to estimate the amorphous phases as well.

- The addition of fibre to the cement-based foam significantly improves the mechanical and physical properties. Therefore, future studies should investigate its effect on the thermal conductivity.

- This investigation was carried out with closed cell cement-based foam. For closed cell foam, it was found that the thermal conductivity is simulated by parallel approach as illustrated in chapter 8 (section 8.5). Assuming, that thermal conduction in open cell foam samples is largely through the air-void, thermal conductivity in open cell cement-based foam is likely to be simulated by the series approach. This implies that for identical cast density, the open cell cement-based foam likely result in lower thermal conductivity and therefore performs better as thermal insulation. It is recommended that further studies should be carried out with suitable foaming agent that will result in open cell cement-based foam in order to explore more thermal insulating options.

References

ACI 523.1R, (2006). Guide for cast in Place Low density Cellular Concrete. American Concrete Institute, Farmington Hills, MI.

ACI 523.2R, (1996). Guide for Precast Cellular Concrete, Floor, Roof, and Wall Units. American Concrete Institute, Farmington Hills, MI.

ACI 116R, (2000). Cement and concrete terminology. American Concrete Institute, Farmington Hills, MI.

ACI 234 R., (2006). Guide for the Use of Silica Fume in Concrete. Reported by ACI Committee 234.

ACI 523.3R., (2014). Guide for Cellular Concretes Above 50 pcf. Reported by ACI Committee 523.

ACI 232.2R., (2003). Use of Fly Ash in Concrete. Reported by ACI Committee 523.

Agarwal, S. K., (2006). Pozzolanic activity of various siliceous materials. Cement and Concrete Research, (36), 1735– 1739.

Agulló1, L., Toralles-Carbonari, B., Gettu1, R. and Aguado, A., (1999). Fluidity of cement pastes with mineral admixtures and superplasticizer - A study based on the Marsh cone test. Materials and Structures,(32), 479-485.

Aldridge, D., (2005). Introduction to Foamed Concrete: What, Why, How?. Proceedings of the International Conference on the Use of Foamed Concrete in Construction. University of Dundee, Scotland, (5), 1-14.

Aligizaki, K.K.,(2006).Pore Structures of Cement-Based Materials: Testing, interpretation and requirements. 1st Taylors and Francis.

Ambroise, J., Maximilien, S. and Pera, J., (1994). Properties of metakaolin blended cements. Advanced Cement Based Materials, (1), 161–168.

Aranda, M.A.G., De la, T. A.G., León-Reina, L.,(2012). Rietveld quantitative phase analysis of OPC clinkers, cements and hydration products. Reviews in Mineralogy & Geochemistry,(74),169-209.

Arthur, L.L.,(1954).Thermal Conductivity: VIII, A Theory of Thermal Conductivity of Porous Materials. Journal of the American Ceramic Society,(37),(2).

ASTM C 457 (2010).Standard Test Method for Microscopical Determination of Parameters of the Air-Void System in Hardened Concrete. ASTM International, West Conshohocken, PA.

ASTM C150/C150M.,(2012).Standard Specification for Portland Cement. ASTM International, West Conshohocken, PA.

ASTM C566., (2013). Standard Test Method for Total Evaporable Moisture Content of Aggregate by Drying. ASTM International, West Conshohocken, PA.

ASTM C939., (2010). Standard Test Method for Flow of Grout for Preplaced-Aggregate Concrete (Flow Cone Method). ASTM International, West Conshohocken, PA.

ASTM C230., (2008). Standard Specification for Flow Table for Use in Tests of Hydraulic Cement. ASTM International, West Conshohocken, PA.

ASTM C618., (2012a). Standard Specification for Coal Fly Ash and Raw or Calcined Natural Pozzolan for Use in Concrete. ASTM International, West Conshohocken, PA.

ASTM C1240., (2012). Standard Specification for Silica Fume Used in Cementitious Mixtures. ASTM International, West Conshohocken, (2012), PA.

ASTM C869., (2011). Standard Specification for Foaming Agents Used in Making Preformed Foam for Cellular Concrete. ASTM International, West Conshohocken, PA.

ASTM C796 (2012). Standard test method for foaming agents for use in producing cellular concrete using preformed foam. ASTM International, West Conshohocken, PA.

ASTM C618 (2012). Standard specification for coal fly ash and raw or calcined natural pozzolan for use in concrete. ASTM International, West Conshohocken, PA.

ASTM C1043 (2010). Standard Practice for Guarded-Hot-Plate Design Using Circular Line-Heat Sources. ASTM International, West Conshohocken, PA.

ASTM D6574 (2013). Standard Test Method for Determining the (In-Plane) Hydraulic Transmissivity of a Geosynthetic by Radial Flow. ASTM International, West Conshohocken, PA.

Awang, H., Mydin, M. A. O. and Roslan, A. F., (2012). Effect of additives on mechanical and thermal properties of lightweight foamed concrete. Pelagia Research Library Advances in Applied Science Research, (3), (5), 3326-3338.

Bragg W.L.,(1975).The Development of X-ray Analysis. Bell & Sons, London.

Bapat J. D., (2013).Mineral Admixtures in Cement and Concrete. 1st edition, Taylor & Francis Group.

Batool, F. and Bindiganavile, V., (2013). Thermal conductivity of cement based foams and applicability of predictive models. Conference, CONSEC13, Nanjing, China, September 23-25.

Bave,G.,(1980). Aerated light weight concrete-current technology. In: Proceedings of the Second International Symposium on Lightweight Concretes. London.

Bentz, D.P., Peltz, M.A., Durán-Herrera, A.,Valdez, P. and Juárez, C.A., (2011).Thermal Properties of High-Volume Fly Ash Mortars and Concretes. Journal of Building Physics, (34), 263-275.

Bentz, D.P., Quenard, D.A., Kunzel, H.M., Baruchel, J., Peyrin, F., Martys, N.S., Garboczi, E.J., (2000). Microstructure and transport properties of porous building materials: Three dimensional X-ray tomographic studies. Materials and Structures, (33), 147–153.

Bentz, D.P., (2007).Transient plane source measurements of the thermal properties of hydrating cement pastes. Materials and Structures,(40),1073–1080.

Bindiganavile, V. and Hoseini, M., (2008). Foamed concrete. In mindess, S., ed., Developments in the formulation and reinforcement of concrete. CRC Press, Cambridge, England.

Borisov, S. V. and Podberezskaya, N. V., (2012). X-ray Diffraction Analysis: a Brief History and Achievements of the First Century. Journal of Structural Chemistry, (53), S1-S3.

Brady, K.C., Watts, G.R.A. and Jones, M.R., (2001).Specification for foamed concrete. Prepared for Quality Services, Civil Engineering, Highways Agency.

British Cement Association (1994).Foamed concrete: Compositions and Properties. Cambery,UK.

Bruggeman, D., Dielectric., (1935). Constant and Conductivity of Mixtures of Isotropic Materials. Annalen Der Physik, (24),(7).

Burgers, H. C., (1919).Physik Z,(20),(73).

CAN/CSA A3000., (2013). Cementitious Materials Compendium`,Canadian Standards Association Mississauga, Ontario, Canada.

Carson, J., Lovatt, J., Tanner, D. and Cleland, A., (2005). Thermal conductivity bounds for isotropic porous materials. International Journal of Heat and Mass Transfer, (48), 2150–2158.

Cheung, A. K. F., Zhu, H. G. Leung, C. K. Y. and Lin, M. S. W., (2012). High Performance Cementitious Materials with Thermal Insulation Property. 11th International Conference on Concrete Engineering and Technology. CONCET, Putrajaya, Malaysia.

Chancey, R. T., Stutzman, P., Maria, C.G.J., Fowler, D. W., (2010). Comprehensive phase characterization of crystalline and amorphous phases of a Class F fly ash. Cement and Concrete Research,(40),146–156.

Chawla, N, and Deng, X., (2005). Microstructure and Mechanical Behavior of Porous Sintered Steels. Materials Science and Engineering, (390), 98–112.

Cheng-yi, H. and Feldman, R. F., (1985). Influence of Silica Fume on the Microstructural development in cement mortars. Cement and Concrete Research, (15), 285-294.

Chotard, T.J., Boncoeur-Martel, M. P., Smith, A., Dupuy, J. P., and Gault, C., (2003). Application of X-ray computed tomography to characterise the early hydration of calcium aluminate cement. Cement and Concrete Composites, (25),(1), 145-152.

Choktaweekarn, P., Saengsoy, W, and Tangfermsirikul, S., (2009). A model for predicting the specific heat capacity of fly-ash concrete. Science Asia, (35), 178–182.

Chaudhary, D. R. and Bhandari, R.C., (1968). Heat transfer through a three-phase porous Medium. J. Applied Physics, (2), (1).

Cnudde, V., Cwirzen, A., Masschaele, B., Jacobs, P.J.S., (2009).Porosity and microstructure characterization of building stones and concretes. Engineering Geology, (103), 76–83.

David, L., Bish., Jeffrey, E.,(1993). Post Quantitative mineralogical analysis using the Rietvetd full-pattern fitting method. American Mineralogist,(78), 932-940.

Demirbog˘a, R., (2003). Influence of mineral admixtures on thermal conductivity and compressive strength of mortar. Energy and Buildings, (35),189–92.

Demirbog˘a, R. and Gul, R., (2003). The effects of expanded perlite aggregate, silica fume and fly ash on the thermal conductivity of lightweight concrete.Cement and Concrete Research, (33),(5),723–7.

Demirbog˘a, R., Turkmen, I. and Karakoc, M.B., (2007). Thermo-mechanical properties of concrete containing high-volume mineral admixtures. Building and Environment,(42), 349–354.

Demirbog˘a, R., (2007). Thermal conductivity and compressive strength of concrete incorporation with mineral admixtures. Building and Environment, (42), 2467-2471.

Deschner, F., Winnefeld, F., Lothenbach, B., Seufert, S., Schwesig, P., Dittrich, S., Goetz-Neunhoeffer, F., and Neubauer, J., (2012). Hydration of Portland cement with high replacement by siliceous fly ash. Cement and Concrete Research,(42),(10),1389-1400.

DeVries, D.A.,(1952).The Thermal Conductivity of Soil. Mededelingen van de Landbouwhogeschool te Wageningen,(52),(1),1-73. Translated by Building Research Station (Library communication No. 759),England.

Diamond, S. and Dolch, W.I., (1971). Generalized Log-Normal Distribution of Pore Sizes in Hydrated Cement. Journal of Colloid and Interface Science, (38),(1).

Dinnebier, Robert E., and Karen F., (1999).Modern XRD methods in mineralogy. Max-Planck-Institute for Solid State Research, Stuttgart, FRG.

Dittrich, S., Neubauer, J. and Goetz-Neunhoeffer, F.,(2014). The influence of fly ash on the hydration of OPC within the first 44 h-A quantitative in situ XRD and heat flow calorimetry study. Cement and Concrete Research, (56), 129-138.

Do, C. T., Bentz, D. P. and Stutzman, P. E., (2007). Microstructure and Thermal Conductivity of Hydrated Calcium Silicate Board Materials. Journal of Building Physics. Journal of building Physics, (31), 55-67.

Esteves, L. P., (2011). On the hydration of water-entrained cement–silica systems: Combined SEM, XRD and thermal analysis in cement pastes. Thermochimica Acta, (518), (1–2), 27–35.

Fang, Y., Wen, Q. and Dai, P., (2011).Investigation on the Property and Air Void Structure of Foamed Cement-Fly Ash–Steel Slag Concrete. Advanced Materials Research, (150-151), 1457-1461.

Feng-qing, Z., Jun-qin, L., Qian, L., Hao, L., (2011). Study of Foamed Concrete from Activated Ash/slag Blended Cement Advanced Materials Research,(160-162), 821-826.

Ferna´ndez-Jimeneza, A., Torreb, A.G., Palomoa, A., Lo´pez-Olmob, G., Alonsoa, M.M. and Aranda, M.A.G., (2006). Quantitative determination of phases in the alkali activation of fly ash. Part I. Potential ash reactivity. Fuel, (85), 625–634.

Field, A., (2013). Discovering Statistics using IBM SPSS Statistics. Sage Publications.

Flannery, B. P., Deckman, H. W., Roberge, W. G. and D'amico, K. L.,(1987). Three-dimensional X-ray microtomography. Science, (237),1439.

Francl, J. and Kingerywd., (1954).Thermal Conductivity: IX, Experimental Investigation of Effect of Porosity on Thermal Conductivity. Journal of the American Ceramic Society, 18(1), (37).

Frey,S.,(1932).Uber Die Elektrische Leitfahigkeit Binarer Aggregate. Zeitschrift Fur Elektrochemie,(38),260-274.

Friedrich, W., Knipping, P. and Laue, M., (1912). Sitzungsberichte der mathematisch-physikalischen klasse der koeniglich bayerischen akademie der wissenschaften zu muenchen. Proc Bavarian Acad Science, 303-322.

Fricke, H., (1924). Physics Revision, (24), 575.

Frías, M. and Cabrera, J., (2000). Pore size distribution and degree of hydration of MK-cement pastes. Cement and Concrete Research, (30),(4), 561–569.

Fu, X, and Chung, D. D. L., (1999). Effect of Admixtures on Thermal and Thermomechanical Behavior of Cement Paste. ACI Materials Journal,(96), July-August,455-461.

Gallucci, E., Scrivener, K., Groso, A., Stampanoni., M. and Margaritondo., G.,(2007). 3D experimental investigation of the microstructure of cement pastes using synchrotron X-ray microtomography ([mu] CT). Cement Concrete Research, (37), 360-368.

Gard, J. A. and Taylor, H.F.W. and EMENT., (1976). Calcium Silicate Hydrate II ("C-S-H.(II)"). Concrete Research, (6), 667-678.

Goual, M. S., Bali, A. and Qu´eneudec, M., (1999). Effective thermal conductivity of clayey aerated concretein the dry state: experimental results and modelling. Journal of Physics D: Applied Physics, (32), 3041–3046.

Gualtieria, A. F., Viania, T. A. and Montanarib, C., (2006). Quantitative phase analysis of hydraulic limes using the Rietveld method. Cement and Concrete Research,(36),401-406.

Gustafsson, S.E., (1991). Transient plane source techniques for thermal conductivity and thermal diffusivity measurements of solid materials. Review of Scientific Instruments, (62), 797-804.

Hamdhan, I. N. and Clarke, B. G., (2010). Determination of Thermal Conductivity of Coarse and Fine Sand Soils. Proceedings World Geothermal Congress Bali, Indonesia, 25-29.

Harris, W. and White, N.,(2007). Methods of Soil Analysis. Part 5. Mineralogical Methods University of Florida, Gainesville SSSA Book Series, no. 5.

Helfen, L., Dehn, F., Mikulik, P. and Baumbach, T., (2004).Synchrotron-radiation X-ray tomography: a method for the 3D verification of cement microstructure and its evolution during hydration. In: Bartos PJM, Hughes JJ, Trtik P, Zhu W (eds) Nanotechnology in construction. Royal Society of Chemistry, Cambridge, 89-100.

Hengst, R.R. and Tressler, R.E.,(1983). Fracture of Foamed Portland Cement. Cement and Concrete Research,(13), 127-134.

He, Y., (2005). Rapid thermal conductivity measurement with a hot disk sensor: Part 1. Theoretical considerations. Thermochimica Acta, (436),122-129.

Hoseini, M., (2013). Effect of Compressive Loading on Transport Properties of Cement-Based Materials. Phd thesis, Universiy of Alberta.

Ibáñez, J., Font, O., Moreno, N., Elvira, J.J., Alvarez, S. and Querol, X., (2013). Quantitative Rietveld analysis of the crystalline and amorphous phases in coal fly ashes. Fuel, (105), 314-317.

ISO, International Standards, (2008),ISO/DIS 22007-2.2.

Jähne, B., (2005). Digital image processing Bernd Jähne. Springer-Verlag, Berlin Heidelberg.

Jones, M. R., McCarthy, M. J. and McCarthy, A., (2003). Moving fly ash utilization in concrete forward: A UK perspective. Proc., Int. Ash Utilization Symp, Center for Applied Energy research, University of Kentucky, 20–22.

Jones, M.R., Dhir, R.K. and McCarthy, A., (2004). Development of foamed concrete insulating foundations for buildings and pilot demonstration project. DETR Contract 39/03/621 (CC2046), Concrete Technology Unit, University of Dundee.

Jones, M.R. and McCarthy, A., (2005a). Utilising unprocessed low-lime coal fly ash in foamed concrete. Fuel, (84), 1398-1409.

Jones, M.R. and McCarthy, A., (2005b). Behaviour and assessment of foamed concrete for construction applications. In Dhir, R. K., Newlands, M. D., McCarthy, A., Editors; Use of foamed concrete in construction, Thomas, London, 61-88.

Jones, M.R. and McCarthy, A., (2006). Heat of hydration in foamed concrete: effect of mix constituents and plastic density. Cement and Concrete Research, (36), (6), 1032–1041.

Jozić, D., Zelić, J, and Janjatović, I., (2010).Influence of the coarse fly ash on the mechanical properties of the cement mortars. Ceramics- Silikáty, (54), (2), 144-151.

Jumate, E. and Manea, D.L., (2011). X-ray Diffraction Study of Hydration Processes in the Portland Cement. Journal of Applied Engineering Sciences, (1),(14), 79-86.

Jumate, E. and Manea, D.L., (2012). Application of X-ray Diffraction (XRD) and Scanning Electron Microscopy (SEM) methods to the Portland Cement Hydration Processes. Journal of Applied Engineering Sciences, (2),(15),(1), 35-42.

Just, and Middendorfv., (2009). Microstructure of high-strength foam concrete. Materials Characterization, (60), 741-748.

Kar, A., Ray, I., Unnikrishnan, A. and Davalos, J. F., (2012).Microanalysis and optimization-based estimation of C–S–H contents of cementitious systems containing fly ash and silica fume. Cement and Concrete Composites, (34), (3), 419–429.

Kaviany, M., (1995). Principles of heat transfer in porous media. Second edition, Springer.

Kearsley, E.P., (1996). The use of foamed concrete for affordable development in third world countries. In Dhir R.K., McCarthy M.J., editors, Appropriate concrete technology, London E&FN Spon, 233–243.

Kearsley, E.P., (1999). The Effect of High Volumes of Ungraded Fly Ash on the Properties of Foamed Concrete. Ph.d Thesis. The University of Leeds.

Kearsley, E. P. and Visagie, M.,(1999).Micro-properties of Foamed Concrete.Specialist Techniques and Materials for Concrete Construction, Proceedings of the International Conference, R. K. Dhir, ed., Scotland, 173-184.

Kearsley, E. P. and Wainwright P. J., (2001).The effect of high fly ash content on the compressive strength of foamed concrete. Cement Concrete and Research, (31), 105-112.

Kearsley, E. P. and Wainwright P. J., (2001a). Porosity and permeability of foamed concrete. Cement Concrete and Research, (31), 805-812.

Kearsley, E.P. and Wainwright, P.J., (2002). Ash Content for Optimum Strength of Foamed Concrete. Cement and Concrete Research, (32),(2), 241–246.

Kearsley, E.P. and Mostert, H.F., (2005).The use of Foamed Concrete in Refractories. Proceedings of the International Conference on the Use of Foamed Concrete in Construction, University of Dundee, Scotland,(5), 89-96.

Kearsley, E.P. and Mostert, H.F., (2005a). Designing mix composition of foamed concrete with high fly ash contents. Proceedings of the International Conference on the Use of Foamed Concrete in Construction, University of Dundee, Scotland, (5), 89-96.

Kim, K. H., Jeon, S. E., Kim, J. K. and Yang, S., (2003). An experimental study on thermal conductivity of concrete. Cement and Concrete Research, (33),(3), 363–371.

Khan, M. I., (2002). Factors affecting the thermal properties of concrete and applicability of its prediction models. Building and Environment,(37),(6), 607–614.

Khan, M. I., (2003). Isoresponses for strength, permeability and porosity of high performance mortar. Building and Environment, (38), 1051-1056.

Korpa,T., Kowald, R., Trettin.,(2009). Phase development in normal and ultra-high performance cementitious systems by quantitative X-ray analysis and thermoanalytical methods. Cement and Concrete Research,(39), 69–76.

Kodur, V. and Khaliq, W., (2011). Effect of Temperature on Thermal Properties of Different Types of High Strength Concrete. ASCE Journal of Materials in Civil Engineering, (23), (6), 793-781.

Kosmatka, S. H., Kerkhoff, B., and Panarese, W. C. (2003). Design and control of concrete mixtures, (14th ed.), Portland Cement Association.

Kostuch, J.A., Walters, G.V. and Jones, T.R., (1993). High Performance Concrete Incorporating Metakaolin - A review. Concrete 2000, University of Dundee, 1799–1811.

Kramar, D. and Bindiganavile, V. (2011).Mechanical properties and size effects in lightweight mortars containing expanded perlite aggregate. Materials and Structures, (44),(4),735–748.

Lavina, B., Dera, P, and Downs, R., T., (2014). Modern X-ray Diffraction Methods in Mineralogy and Geosciences. Reviews in Mineralogy & Geochemistry, (78), 1-31.

Lee, H. K., Lee, K. M. and Kim, B. G., (2003). Autogenous Shrinkage of High-Performance Concrete Containing Fly Ash. Magazine of Concrete Research, (55),(6), 507-515.

Li, S., Roy, D., Mand, and Kumar, A., (1985).Quantitative Determination of Pozzolanas in Hydrated Systems of Cement or Ca $(OH)_2$ with fly ash or silica fume. Cement and Concrete Research, (15), 1079-1086.

Liu, W. V., Apel, D. B. and Bindiganavile, V., (2011). Thermal character-isation of a lightweight mortar containing expanded perlite for underground insulation. International Journal of Mining and Mineral Engineering, (3),(1).

Lu, S., Landis, E. N., Keane, D. T.,(2006). X-ray microtomographic studies of pore structure and permeability in Portland cement concrete. Materials and Structures, (39), 611–620.

Madsen, I.C. and Scarlett, N.V.I., (2008). Quantitative Phase Analysis. *In:* Powder Diffraction Theory and Practice. Dinnebier RE, Billinge SJL (eds). Royal Society of Chemistry Publishing, Cambridge, 298-331.

Madsen, I.C., Scarlett, N.V.I., Cranswick, L.M.D. and Lwin, T., (2001). Outcomes of the International Union of Crystallography Commission on powder diffraction round robin on quantitative phase analysis: samples 1a to 1h. Journal of Applied Crystallography,(34),409-426.

Madsen, I.C., Scarlett, N.V.I., (2000). Cement: Quantitative Phase Analysis of Portland Cement Clinker. *In:* Industrial Applications of X-Ray Diffraction. Chung FH, Smith DK (eds) Taylor & Francis, 415-440.

Maire, E., Fazekas, A., Salvo, L., Dendievel, R., Youssef, S., Cloetens, P. and Letang, J., (2003). X-Ray Tomography Applied To the Characterization of Cellular Materials. Related Finite Element Modeling Problems. Composite Science and Technology, (63), (16), 2431-2443.

Mamun M., (2010), Loading Rate Effects and Sulphate Resistance of Fibre Reinforced Cement-based Foams. Phd thesis, University of Alberta.

Martz, H. E., Scheberk, D. J., Roberson G. P. and Monteiro, P. J. M.,(1993) "Computerized tomography analysis of reinforced concrete, ACI Material Journal,(90).

Marshall, L., (1972). The Thermal Properties of Concrete. Build Science, (7), 167-174, Pergamon Press,Printed in Great Britain.

Masad, E., Jandhyala, V.K., Dasgupta, N., Somadevan, N. and Shashidhar, N., (2002). Characterization of air void distribution in asphalt mixes using x-ray computed tomography. Journal Material Civil Engineering,(14),122-130.

Matiašovský, P., Koronthályová, O., (2005).Thermal Conductivity of Mortars and Fractal Properties of their Microstructure. In Proceedings of Thermophysics, Bratislava, 38-45.

Matiašovský, P., Koronthályová, O., (2008). Analysis and modelling of effective thermal conductivity of dry porous building materials. In Proceedings of Nordic Symposium on Building Physics.

Manual TPS (2010). Hot Disk Thermal Constants Analyser Instruction manual.

Maxwell, J. C., (1904). A Treatise of Electricity and Magnetism. 3rd edition, Clarendon, Oxford.

McCormick, F.C.,(1967). Rational proportioning of preformed foam cellular concrete. ACI Material Journal,(64),104–9.

McGovern, G.,(2000).Manufacture and supply of ready-mix foamed concrete. One day awareness seminar on Foamed concrete: Properties, applications and potential held at University of Dundee, 12-25.

Mehta, P. K. and Monteiro, P. J. M., (2006). Concrete: Microstructure, Properties and Materials. 3rd Edition, McGraw-Hill.

Meier, R., Anderson, J., Verryn, S., (2012). Industrial X-ray Diffraction Analysis of Building Materials. Reviews in Mineralogy & Geochemistry,(74), 147-165.

Mindess,S., Young, J. F. and Darwin, D.,(2002). Concrete, 2nd Edition, Prentice Hall, Englewood Cliffs.

Milovanovic, B., Banjad, P. I. and Gabrijel, I., (2011). Measuring thermal properties of hydrating cement pastes. 31st Cement and Concrete Science Conference Novel Developments and Innovation in Cementitious Materials, 12-13.

Murashov, V. V. and Mary, A. W., (2002).Thermal properties of zeolites: effective thermal conductivity of dehydrated powdered zeolite 4A. Materials Chemistry and Physics,(75), 178–180.

Mydin,M.A.O., (2010). Lightweight foamed concrete (LFC) thermal and mechanical properties at elevated temperatures and its application to composite walling system. Ph.d Thesis, School of Mechanical, Aerospace and Civil Engineering.

Mydin,M.A.O., Awang,H. and Roslan,A.F.,(2012). Determination of lightweight foamed concrete thermal properties integrating various additives. Elixir Cement and Concrete Composite,(48), 9286-9291.

Mydin,M.A.O., (2011). Effective thermal conductivity of foamcrete of different densities. Cement Research Letters,(2),(1),March.

Nambiar, E. K. K., and Ramamurthy, K., (2006). Models relating mixture composition to the density and strength of foam concrete using response surface methodology. Cement Concrete Composite, (28), 752–760.

Nambiar, E. K. K. and Ramamurthy, K., (2007). Air-void characterisation of foam concrete. Cement and concrete research,(37).

Nambiar, K. E. K., and Ramamurthy, K., (2008). Fresh State Characteristics of Foam Concrete. Journal of Materials in Civil Engineering, ASCE, 111-117.

Narayanan, N. and Ramamurthy, K., (2000). Structure and properties of aerated concrete: a review. Cement and concrete composite, (22).

Neville,A.M.,(2011).Properties of Concrete.5th Edition, Pearson Education Limited.

Ochsner, A. and Murch, G., and Lemos, M., (2008). Cellular and Porous Materials. Wiley-Vch.

Odler, and Abdul-Maula, S., (1984). Possibilities of Quantitative Determination of the aft-(ettringite) and afm-(monosulphate) phases in hydrated cement pastes. Cement and Concrete Research, (14), 133-141.

Ou, Z., Mab, B. and Jian, S., (2011). Comparison of FT-IR, Thermal Analysis and XRD for Determination of Products of Cement Hydration. Advanced Materials Research, (168-170), 518-522.

Pande, R. N., Kumar, V. and Chandhary, D. R.,(1984).Thermal conduction in a homogeneous two-phase system. Pramana Journal of Physics, (22).

Petrov, I, and Schlegel, E.,(1994). Application of Automatic Image Analysis for the Investigation of Autoclaved Aerated Concrete Structure, Cement and Concrete Research, (24),(5),830-840.

Puttappa, C.G., Rudresh, Ibrahim, A., Muthu, K.U., Raghavendra, H.S., (2008). Mechanical Properties of Foamed Concrete. ICCBT,(43),491-500.

Raheem, A.A. and Adesanya, D.A., (2011). A Study of Thermal Conductivity of Corn Cob Ash Blended Cement Mortar. The Pacific Journal of Science and Technology, (12),(2),106-111.

Rahmanian, I. and Wang, Y., (2009).Thermal Conductivity of Gypsum at High Temperatures: A Combined Experimental and Numerical Approach. Acta Polytechnica,(49),(1).

Ramachandran, V. S., Paroli, R. M., Beaudoin, J. J. and Delgado, A. H., (2002). Handbook of thermal analysis of construction material. Noyes Publications.

Ramamurthy, K., Nambiar, E. K. K. and Ranjan, G. I. S., (2009). A classification of studies on properties of foam concrete. Cement and Concrete Composites,(31).

Rattanasak, U. and Kendall, K., (2005). Pore structure of cement/pozzolan composites by X-ray microtomography. Cement and Concrete Research, (35), 637–640.

Rietveld, H. M., (1969). A profile refinement method for nuclear and magnetic structures. Journal of Applied Crystallography,(2), 65–71.

Rietveld, H.M., (1967). Line profiles of neutron powder-diffraction peaks for structure refinement. Acta Crystallography,(22),151-152.

Rietveld, H.M., (2010). The Rietveld method. Conference at the 10th Spanish Summer School on the Rietveld Method, Castellon (Spain).

Roussel, N. and Roy, L., R., (2005).The Marsh cone: a test or a rheological apparatus. Cement and Concrete Research, (35), 823-830.

Roszczynialski, W., (2002). Determination of Pozzolanic Activity of Materials by Thermal Analysis. Journal of Thermal Analysis and Calorimetry,(70),387–392.

Russell, H. W., (1935).Principles of Heat Flow in Porous Insulators. Journal of the American Ceramic Society,(18),(1).

Russ, J.C., (2002). The image processing. Handbook, CRC Press,boca,4th edition.

Scott, J.D. and Seta, A.C., (1986). Thermal property measurements on oil sands. The Journal of Canadian Petroleum Technology, 70-75.

Scrivener , K. L. and Nonat, A., (2011). Hydration of cementitious materials, present and future. Cement and Concrete Research Volume (41),(7), 651–665.

Scrivener, K.L., Fu¨llmanna, T., Galluccia, E., Walentabb, G. and Bermejob, E.,(2004). Quantitative study of Portland cement hydration by X-ray diffraction/Rietveld analysis and independent methods. Cement and Concrete Research, (34) 1541–1547.

Shekarchi, M., Bonakdar, A., Bakhshi, M., Mirdamadi, A. and Mobasher, B.,(2010). Transport properties in metakaolin blended concrete. Construction and Building Materials, (24), (1), 2217–2223.

Sharma, R. L. and Pandey, S. P., (1999). Influence of mineral additives on the hydration characteristics of ordinary Portland cement. Cement and Concrete Research, (29), 1525–1529.

Shen, H., Nutt, S. and Hull, D., (2004).Direct observation and measurement of fiber architecture in short fiber-polymer composite foam through micro-CT imaging. Composites Science and Technology, (64), 2113–2120.

Siddique, R. and Kahn, M. I., (2011). Supplementary Cementing Materials. 1st edition, Springer.

Soin, A. V., Catalan, L. J.J. and Kinrade, S. D. A., (2013). Combined QXRD/TG method to quantify the phase composition of hydrated Portland cements.Cement and Concrete Research, (48), 17–24.

Snellings, R., Mertens, G. and Elsen, J., (2012). Supplementary Cementitious Materials. Reviews in Mineralogy & Geochemistry,(74), 211-278.

Snyder, K. A., (1998). A Numerical Test of Air Void Spacing Equations. Advanced Cement Based Material, (8), 28-44.

Straube, B. and Walther, H., (2011). AAC with low thermal conductivity. Xella Technical Report.

www.xella.com/de/docs/SKMBT_C253_12091713140.pdf.

Tikalsky, P.J., Pospisil, J. and MacDonald, W., (2004). A method for assessment of the freezethaw resistance of preformed foam cellular concrete. Cement and concrete Research, (34),(5),889–93.

Thomas, M., (2013).Supplementary Cementing Materials in Concrete. CRC Press Taylor & Francis Group.

Torre, De. La. A. G.,Bruque, S. and Aranda, M.A.G., (2001). Rietveld quantitative amorphous content. Journal of Applied Crystallography,(34), 196–202.

Torre, De. La. A. G.,Bruque, S. and Aranda, M.A.G.,(2003). Accuracy in Rietveld quantitative phase analysis of Portland cements. Journal of Applied Crystallography, (36),1169–1176.

Toby, B.H.,(2006). R Factors in Rietveld analysis: How good is good enough? Powder Diffraction,(21),(1).

Valore, R.C., (1954). Cellular concrete Part 1 Composition and methods of production. Journal of American Concrete Institute, (50), 773-796.

Vedalakshmi, R., Raj, A. S., Srinivasan, S., Babu, K. G.,(2003).Quantification of hydrated cement products of blended cements in low and medium strength concrete using TG and DTA technique. Thermochimica Acta,(407),49–60.

Veluchamy, P., Barathan, S., Sivakumar, G. and Anandhan, N.,(2009). X-Ray Diffraction Analysis on the Effect of Silica Fume and Water in Blended Cement Paste. International Journal of Applied Engineering Research, (4),(11) 2369–2376.

Verma, L. S., Shrotriya, A. K. and Chaudhary, D. R., (1991).Thermal conduction in two-phase materials with spherical and non-spherical inclusions. Journal of Physics D: Applied Physics,1729-1737.

Visagie, M., (2000).The effect of microstructure on the properties of foamed concrete. Dissertation for M (Eng), University of Pretoria.

Wang, J., Carson, J., North, M. and Cleland D., (2008). A new approach to modelling the effective thermal conductivity of heterogeneous materials. International Journal of Heat and Mass Transfer, (49), 3075–3083.

Wee, T. B. D., Tamilselvan, T. and Lim, H.,(2006).Air-Void System of Foamed Concrete and Its Effect on Mechanical Properties. ACI Materials Journal, (103),(1), 45-52.

Weiner, O., (1904).Phys Ztschr.332.

Wild, S. and Khatib, J.M., (1997). Portlandite consumption in metakaolin cement pastes and mortars. Cement and Concrete Research, (27), (1), 137–146.

www.engineering.com/Library/
www.brucite.cn/products_8.php

Wyrwał, J., Marynowicz, A. and Świrska, J., (2008). Effective thermal conductivity of porous building materials – analysis and verification. Ernst & Sohn Verlag für Architektur und technische Wissenschaften GmbH & Co. KG, Berlin. Bauphysik (30),(6).

Zhang, M. and Gjcrv, O. E.,(1991). Effect of Silica Fume on Cement Hydration in Low Porosity Cement Pastes. Cement and Concrete Research, (21), 800-808.

Zhang, W. M., Sun, W. and Chen, H. S., (2010). 3D visualisation of pore structures in cement based materials by LSCM. Advances in Cement Research, (22), (1), January, 53–57.

Appendix A

Fresh State Properties

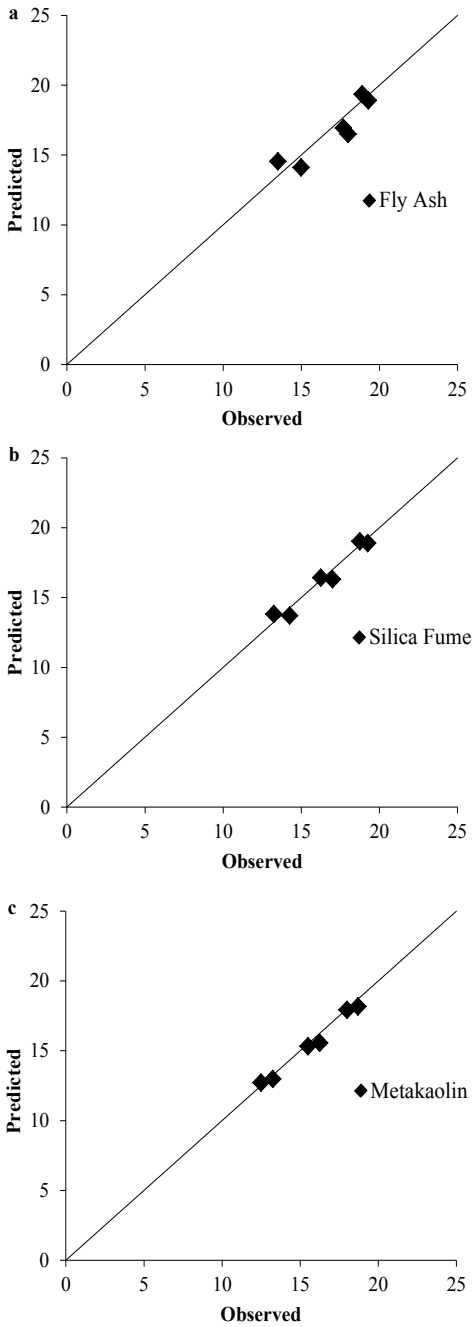

Figure A.1: Comparison between the predicted values using equation 4.1 and tested values; a) Fly Ash Mix; b) Silica Fume Mix; c) Metakaolin Mix.

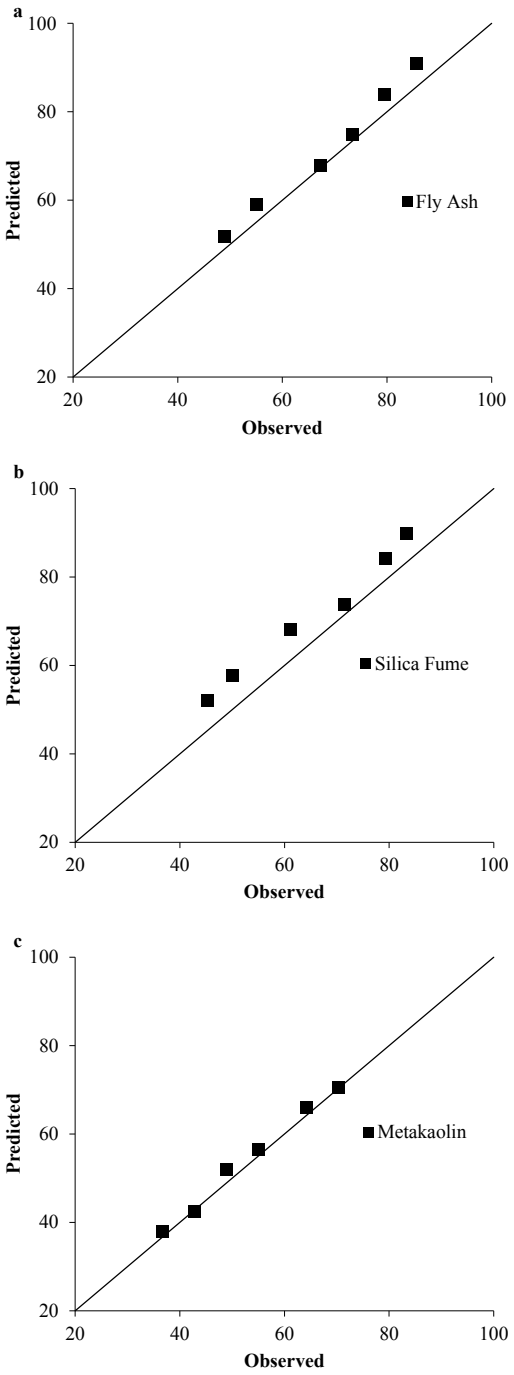

Figure A.2: Comparison between the predicted values using equation 4.2 and tested values; a) Fly Ash Mix; b) Silica Fume Mix; c) Metakaolin Mix.

Quantitative Analysis

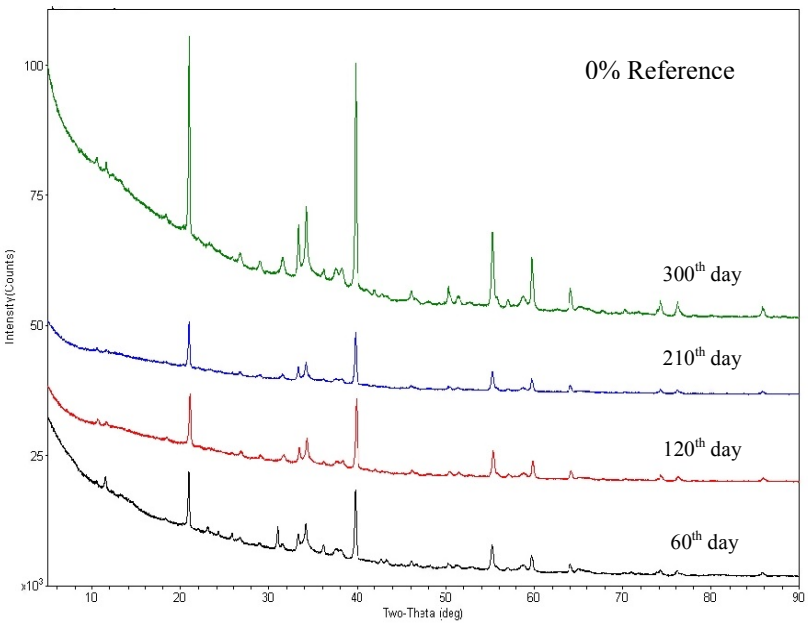

Figure A.3: X-ray diffraction patterns for 0% Reference mix.

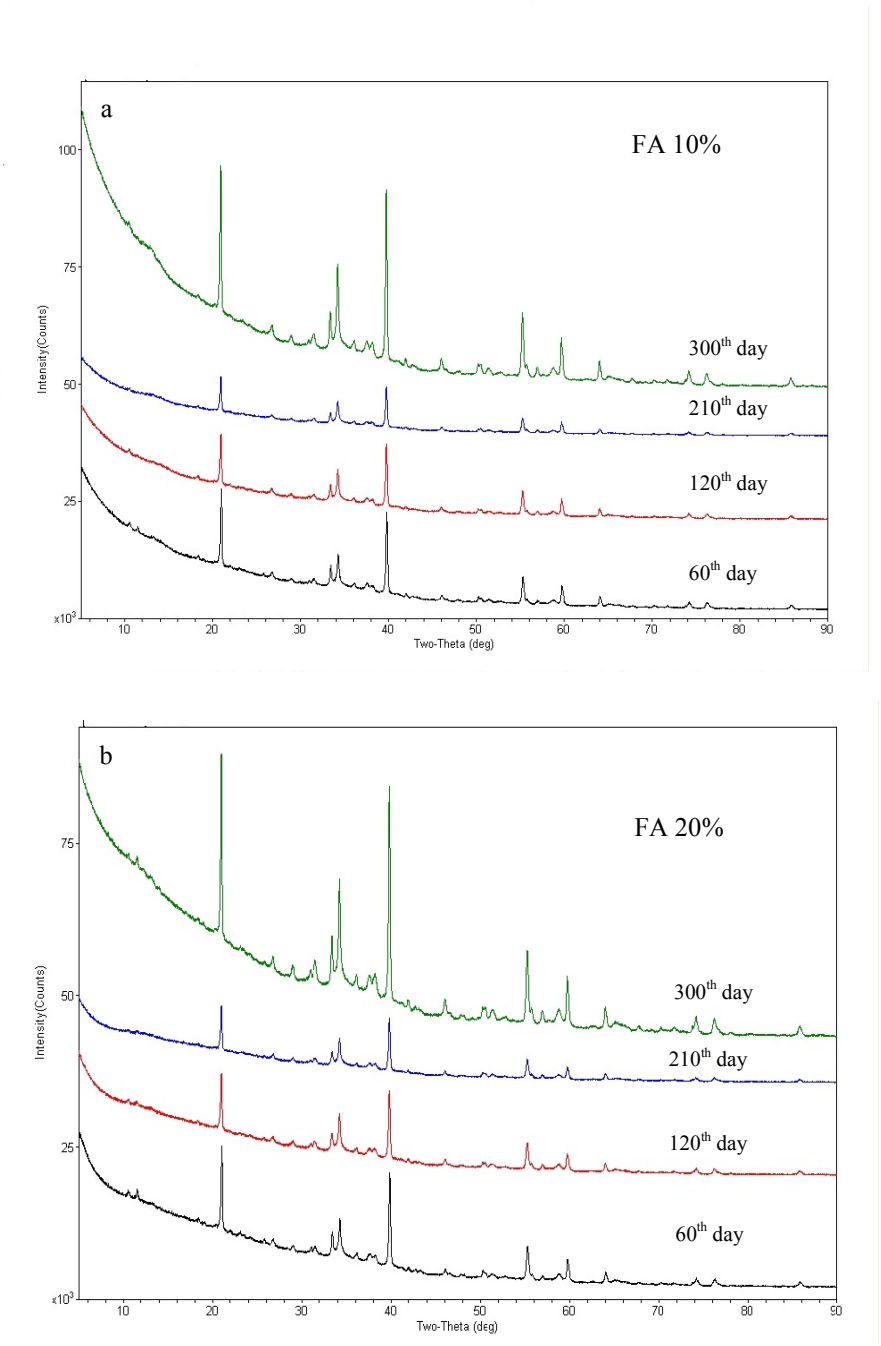

Figure A.4: X-ray diffraction patterns for Fly ash mix; a) 10% FA; b) 20% FA.

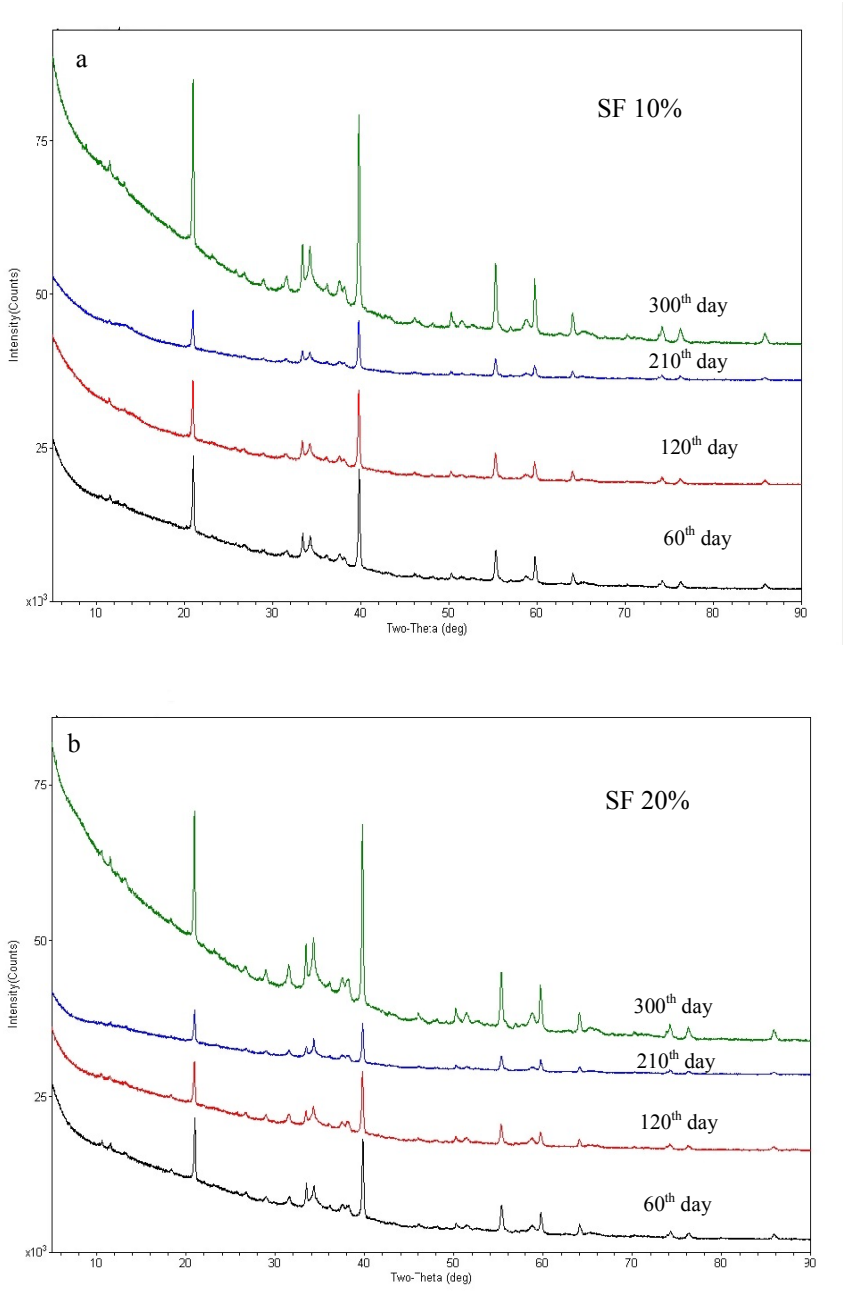

Figure A.5: X-ray diffraction patterns for Silica Fume mix; a) 10% SF; b) 20% SF

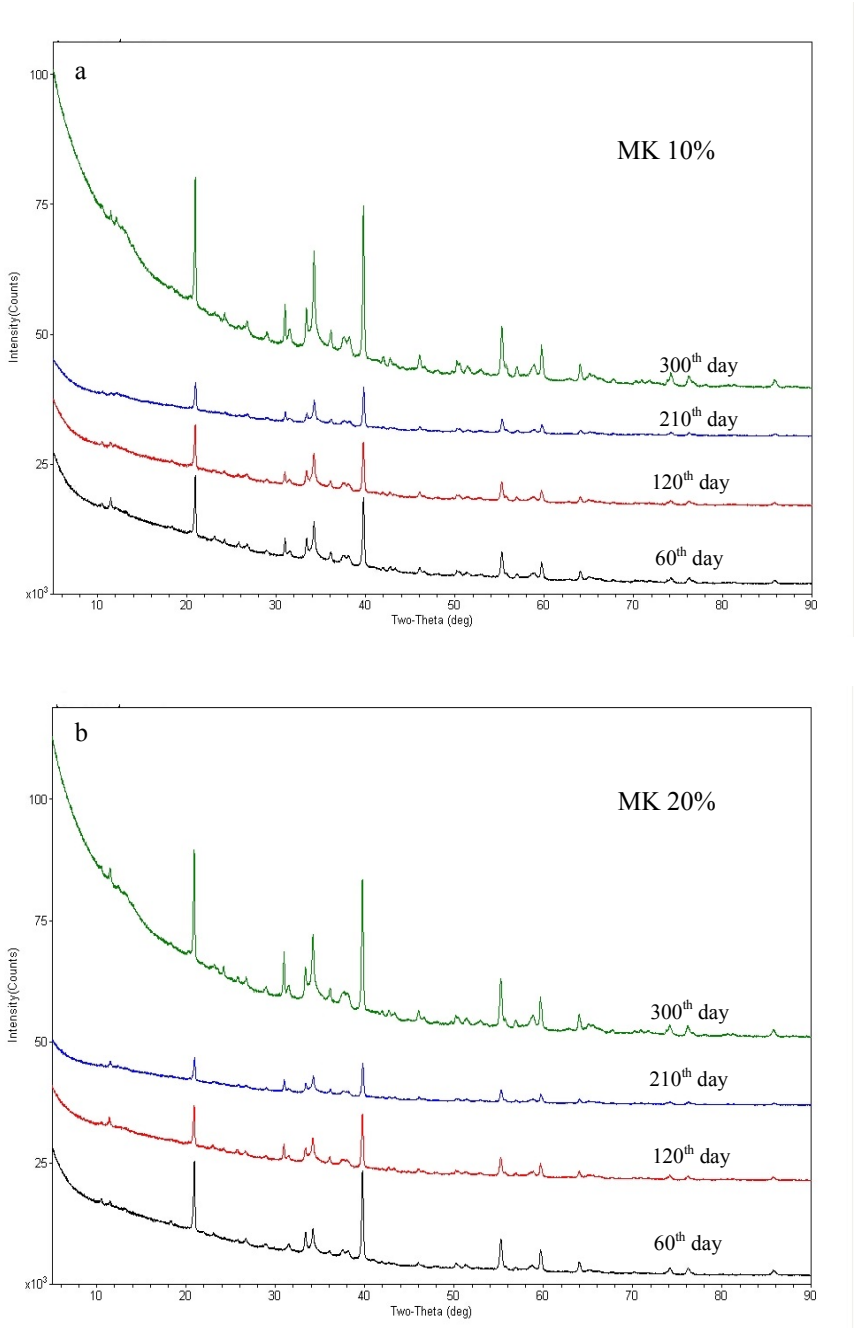

Figure A.6: X-ray diffraction patterns for Metakaolin mix; a) 10% MK; b) 20% MK

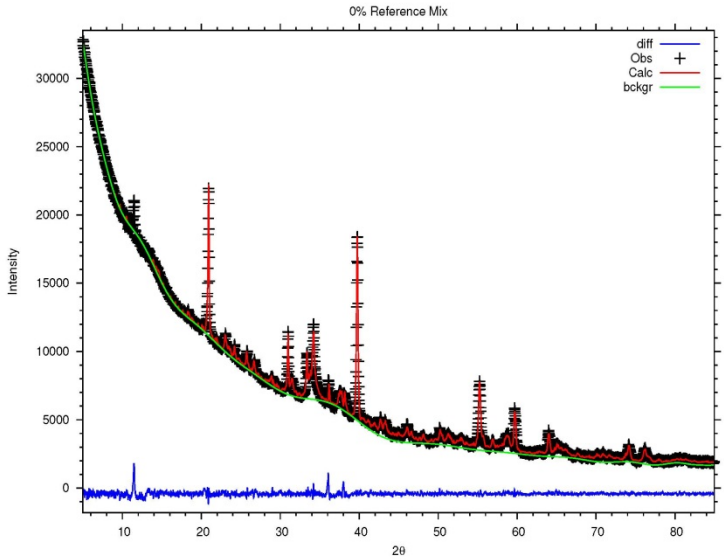

Figure A.7: Rietveld refinement plot for the 0% Reference mix.

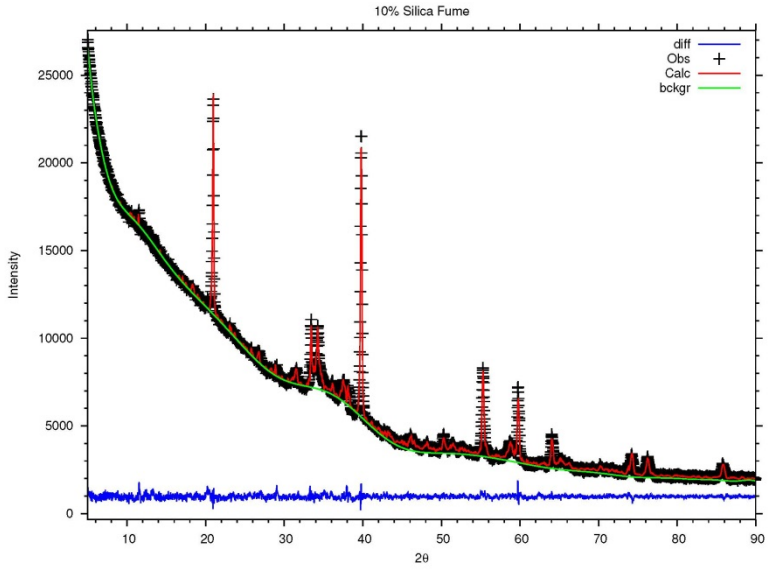

Figure A.8: Rietveld refinement plot for the 10% Silica fume mix.

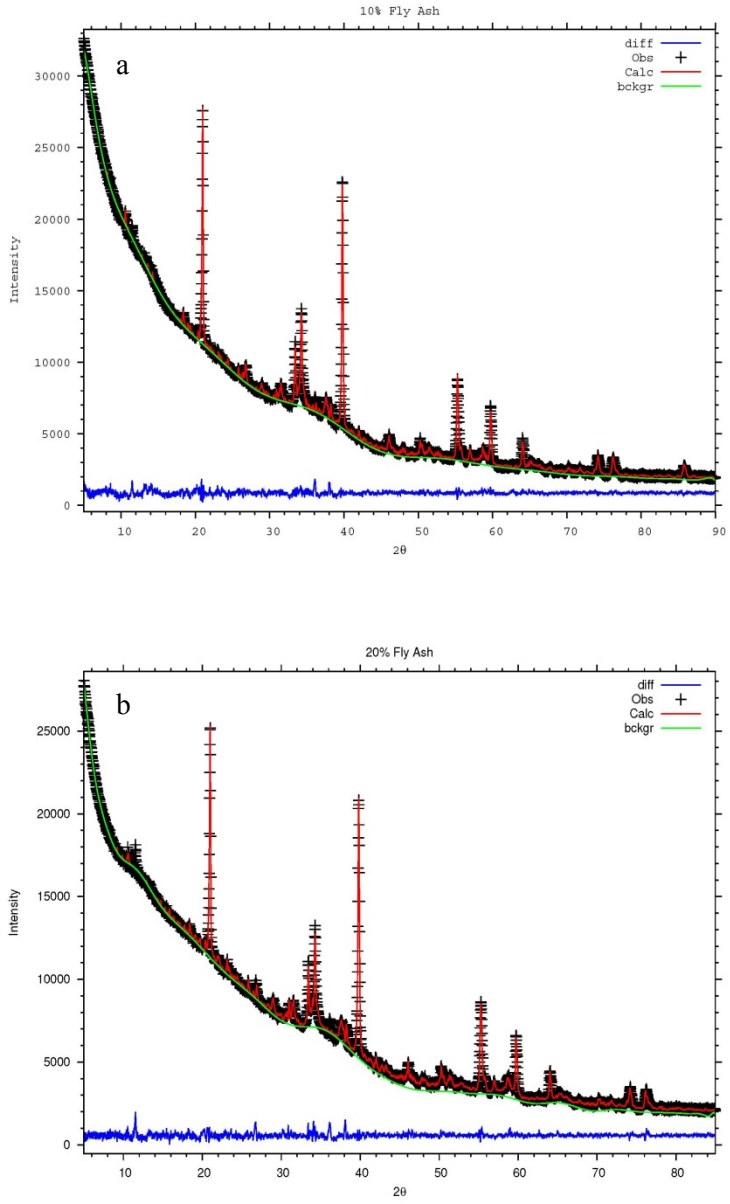

Figure A.9: Rietveld refinement plot for the fly ash mix; a) 10% FA; b) 20% FA

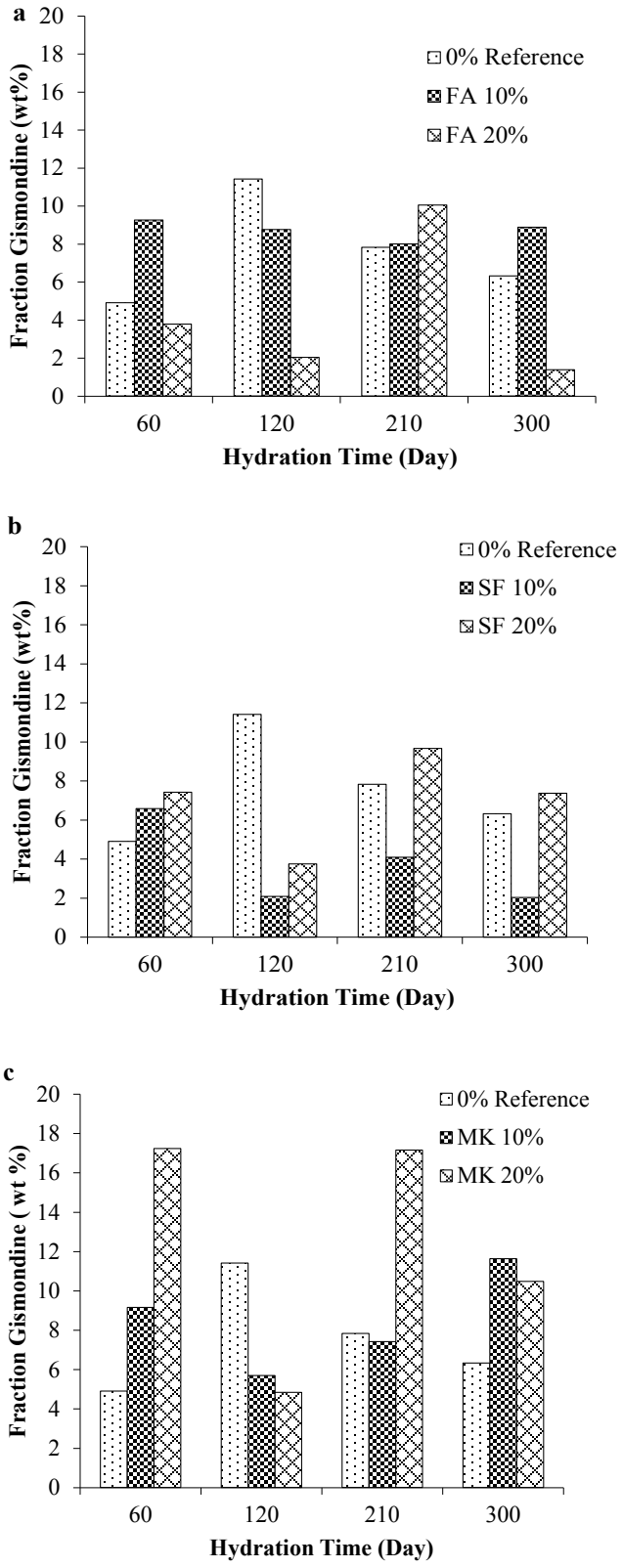

Figure A-10: Time-dependent formation of Gismondine; a) Fly Ash mix; b) Silica fume mix; c) Metakaolin mix.

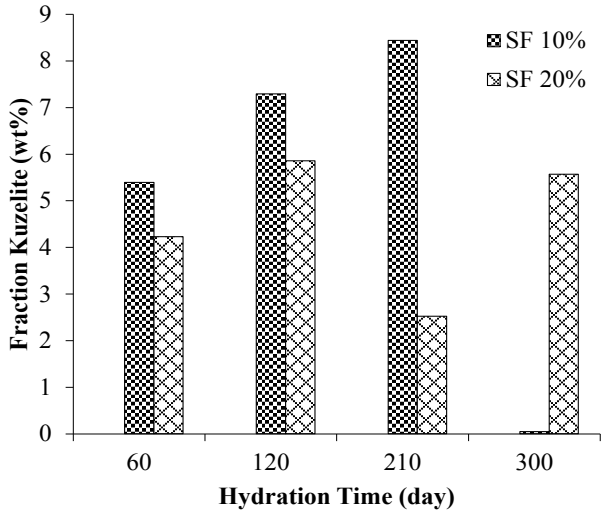

Figure A-11: Time-dependent formation of Kuzelite for Silica fume mix.

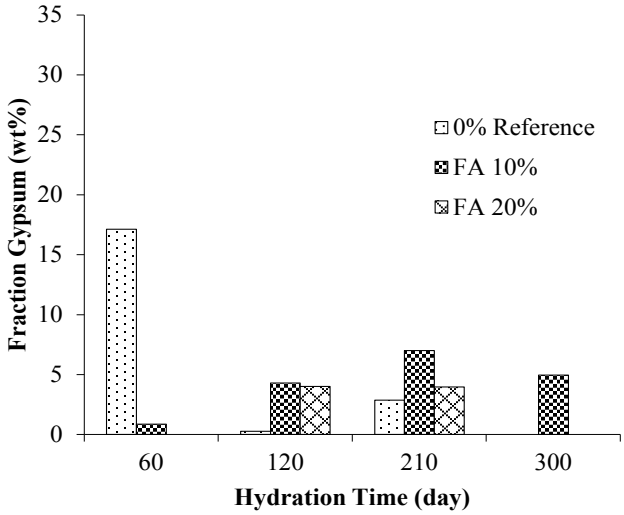

Figure A-12: Time-dependent formation of gypsum for Fly Ash mix.

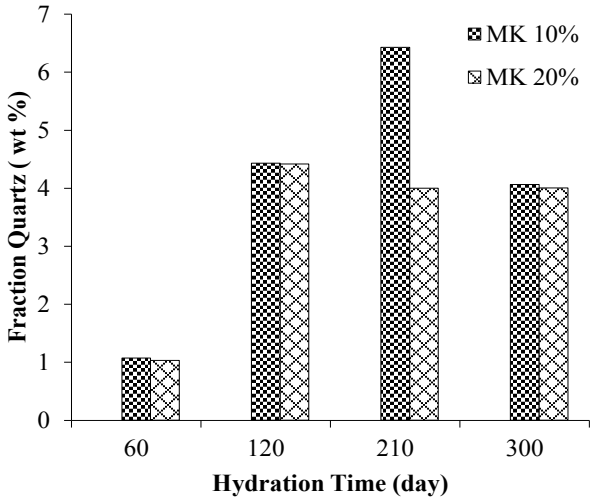

Figure A-13: Time-dependent formation of quartz for metakaolin mix.

Air-Void Characterization

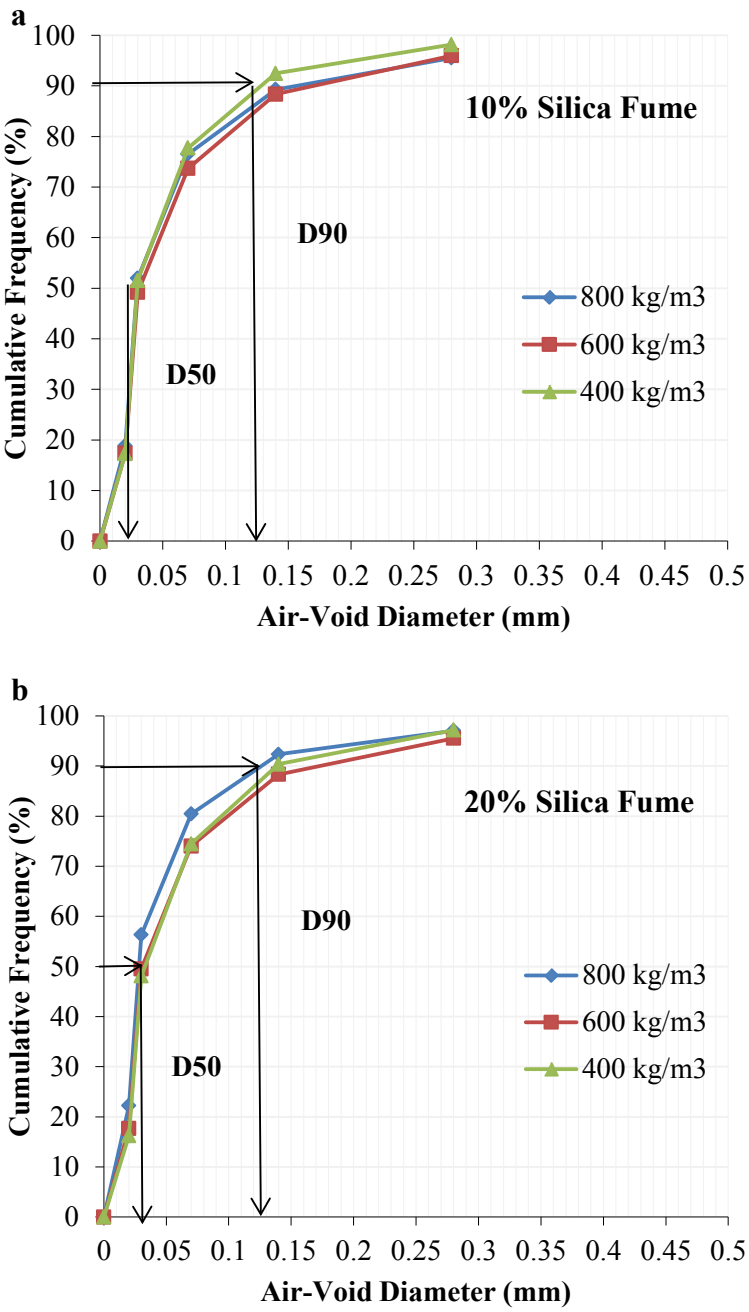

Figure A.14: Cumulative frequency distribution of air-void size for three cast density; a) Mix with 10% Silica fume; b) Mix with 20% Silica Fume.

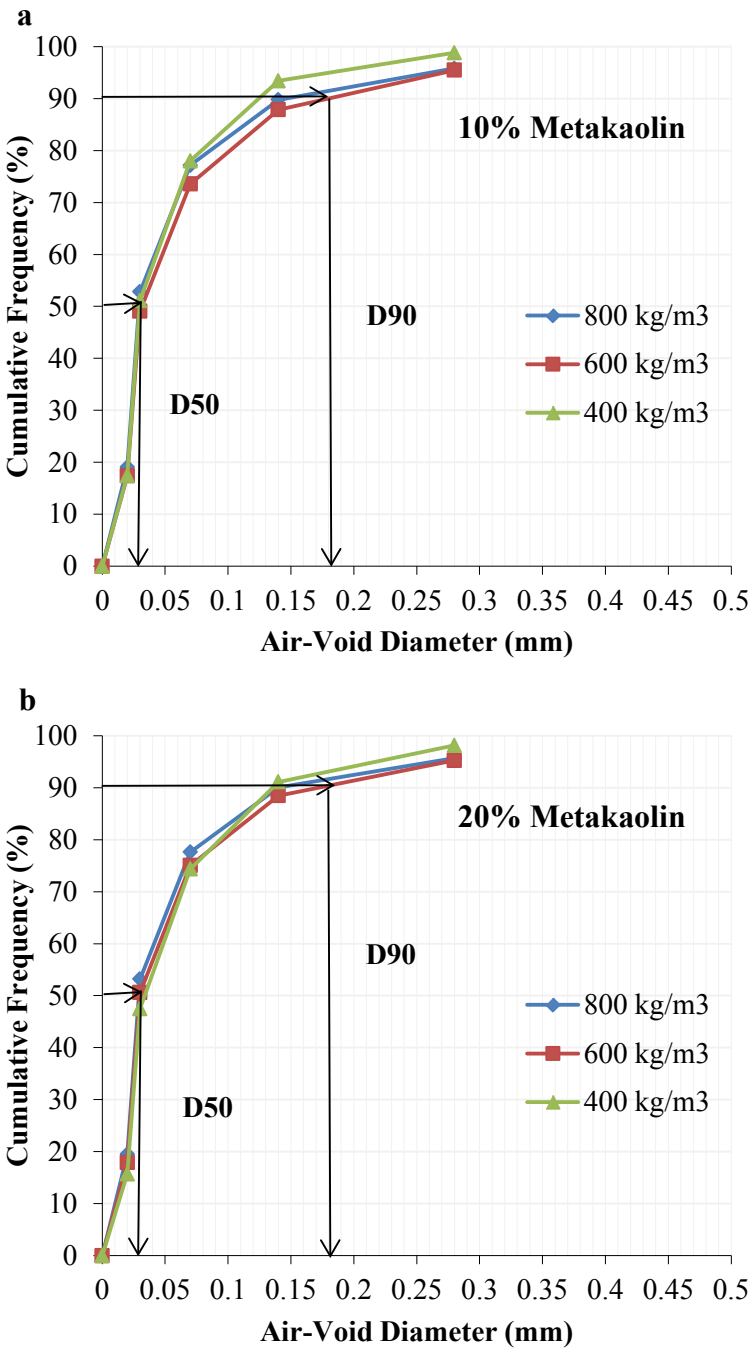

Figure A.15: Cumulative frequency distribution of air-void size for three cast density; a) Mix with 10% Metakaolin; b) Mix with 20% Metakaolin.

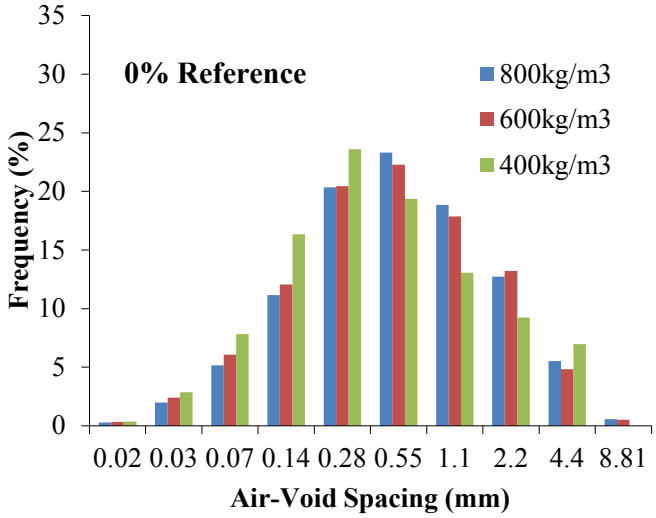

Figure A.16: Air- void size distribution for 0% reference for three cast densities.

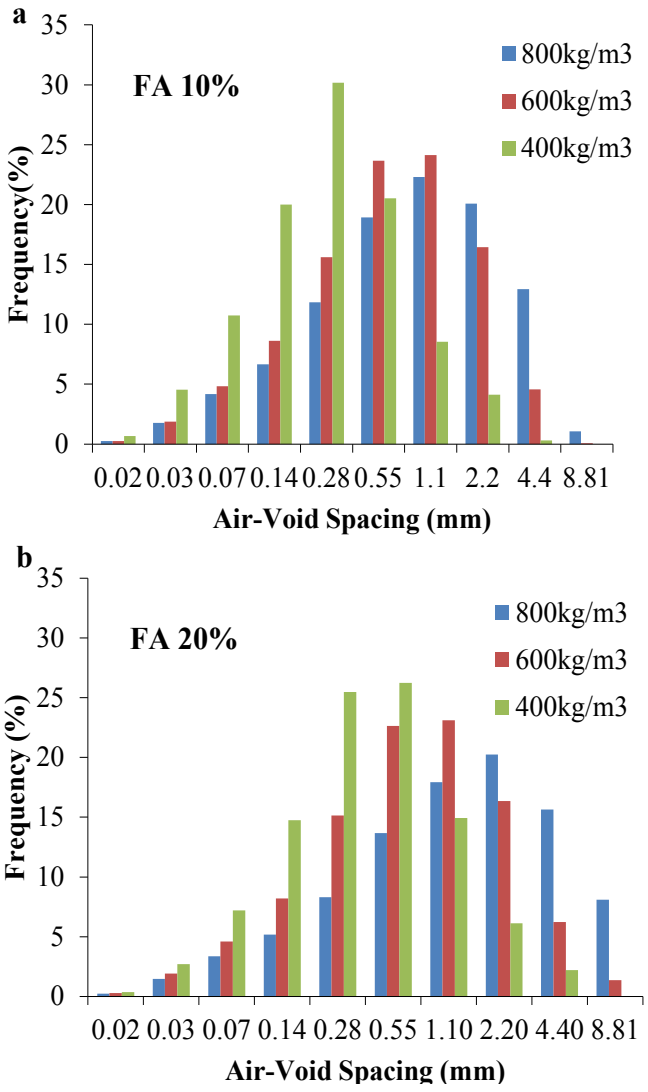

Figure A.17: Air- void Spacing for Fly Ash mix for three case densities; a) Mix with 10% Fly Ash; b) Mix with 20% Fly Ash.

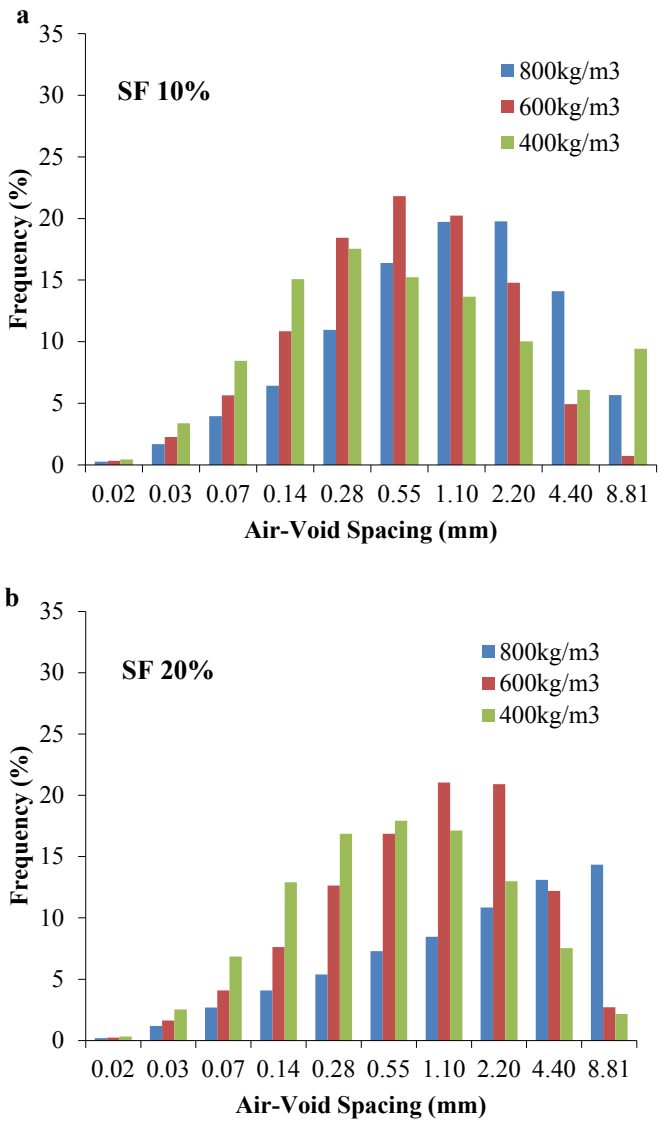

Figure A.18: Air-void Spacing for Silica Fume mix for three case densities; a) Mix with 10% Silica Fume; b) Mix with 20% Silica Fume.

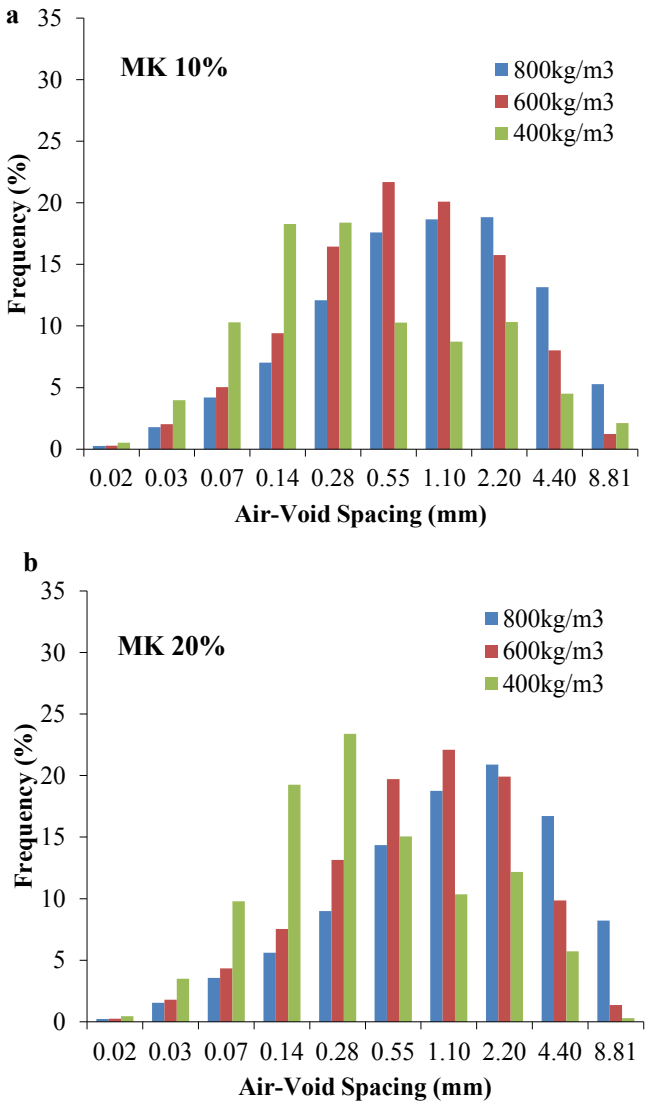

Figure A.19: Air-void Spacing for Metakaolin mix for three case densities; a) Mix with 10% Metakaolin; b) Mix with 20% Metakaolin.

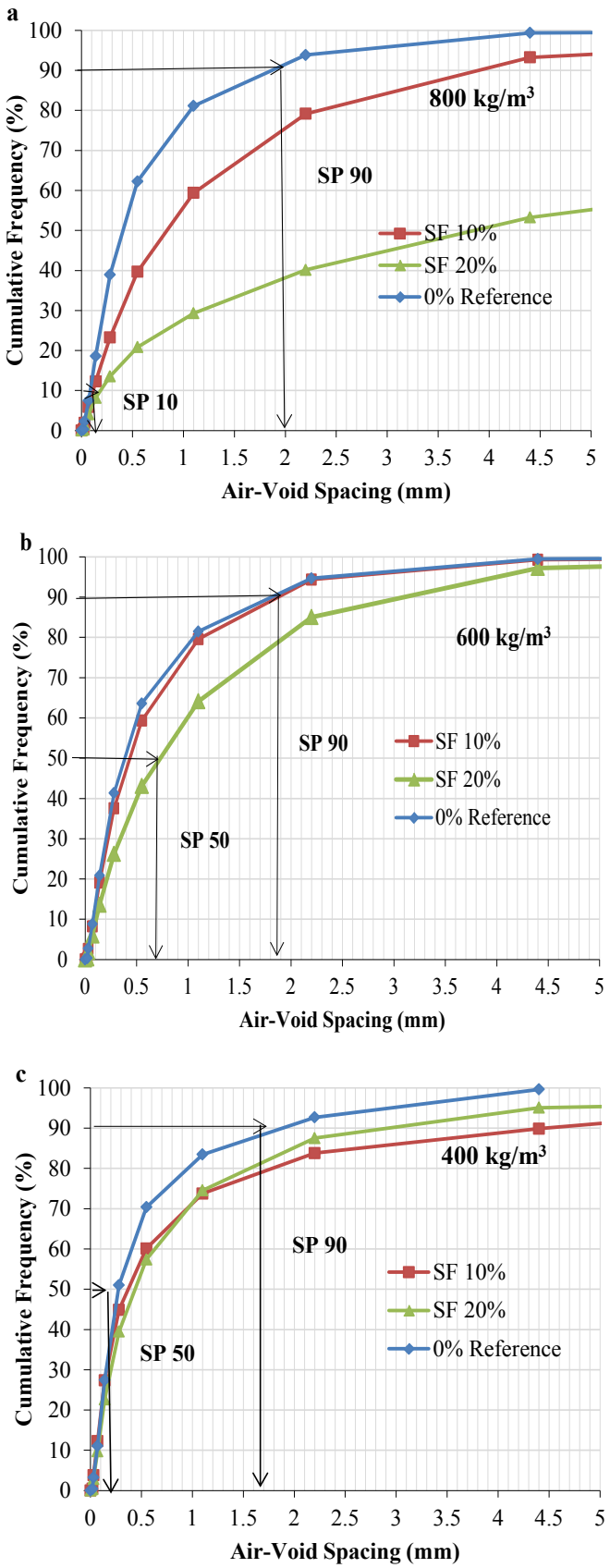

Figure A.20: Cumulative frequency distributions of air-void spacing for Silica fume mix; a) 800kg/m^3; b) 600kg/m^3; c) 400kg/m^3 .

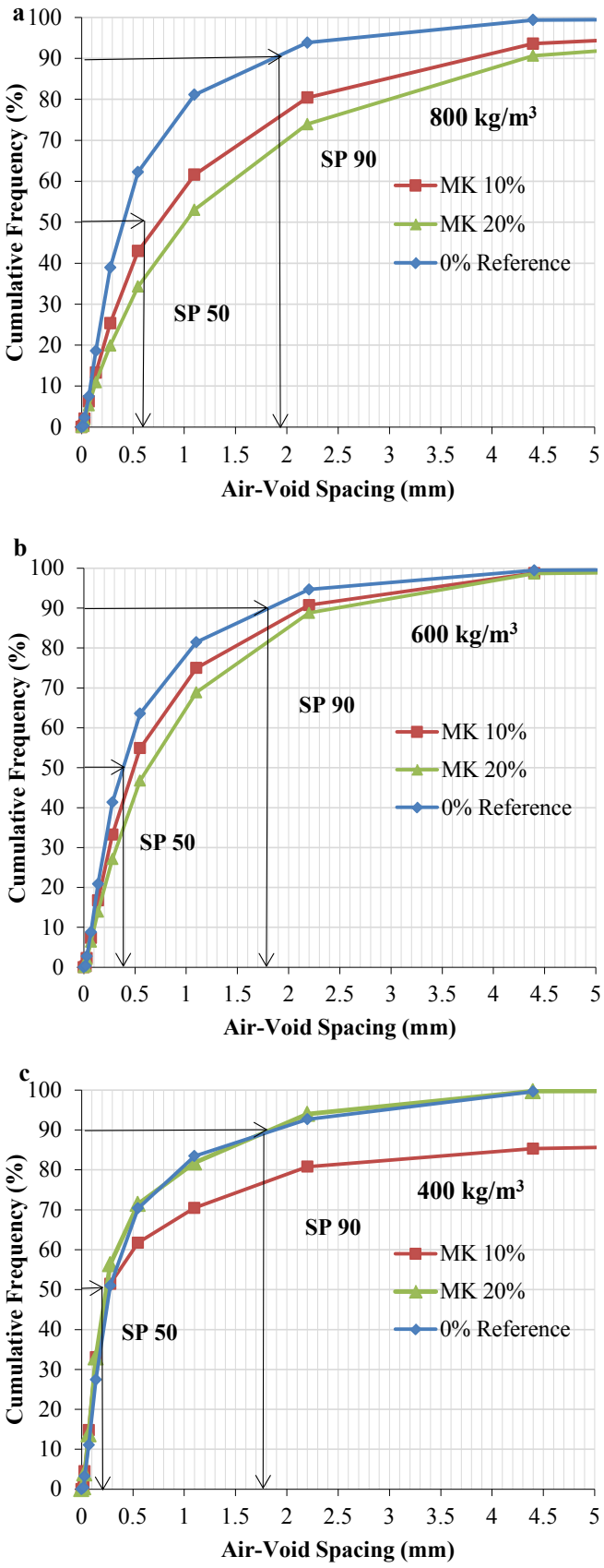

Figure A.21: Cumulative frequency distributions of air-void spacing for Metakaolin mix; a) 800kg/m^3; b) 600kg/m^3; c) 400kg/m^3 .

Table A.1: Measured frequency of occurrence of Air-void size distribution for 0% reference mix.

Sample Id	Sizes (mm)	Frequency of Occurrence of Air-Void Size Distribution					
		800 kg/m^3	COV	600 kg/m^3	COV	400 kg/m^3	COV
		(%)	(%)	(%)	(%)	(%)	(%)
0% Reference	**0.02**	16.770	5.595	17.364	4.833	15.725	6.574
	0.03	29.889	2.253	31.136	2.077	31.320	2.295
	0.07	23.660	1.705	24.437	1.762	25.581	1.918
	0.14	15.798	3.523	15.167	3.145	16.535	4.131
	0.28	9.184	4.367	8.064	4.160	8.085	5.568
	0.55	3.628	4.920	2.977	5.807	2.291	7.046
	1.10	0.893	6.151	0.704	9.063	0.392	8.045
	2.20	0.159	7.876	0.135	13.337	0.061	20.744
	4.40	0.019	25.696	0.015	26.413	0.010	44.092
	8.81	0.000	147.105	0.001	116.929	0.000	299.742

Table A.2: Measured frequency of occurrence of Air-void size distribution for Fly Ash mix.

Sample Id	Sizes	Frequency of Occurrence of Air-Void Size Distribution					
		800 kg/m^3	COV	600 kg/m^3	COV	400 kg/m^3	COV
	(mm)	(%)	(%)	(%)	(%)	(%)	(%)
10% Fly Ash	**0.02**	19.628	4.863	18.061	4.842	16.013	5.191
	0.03	33.588	1.523	32.256	1.760	30.942	2.170
	0.07	24.518	1.962	24.107	1.693	24.999	1.561
	0.14	12.254	2.893	13.424	3.066	15.717	3.134
	0.28	5.556	4.624	7.198	4.113	8.566	4.936
	0.55	2.822	4.833	3.520	4.521	3.115	7.881
	1.10	1.152	5.677	1.162	7.747	0.581	12.705
	2.20	0.380	10.508	0.242	9.125	0.061	16.198
	4.40	0.086	10.310	0.027	18.091	0.006	45.469
	8.81	0.014	25.923	0.002	51.020	0.000	0.000
20% Fly Ash	**0.02**	17.611	6.011	16.468	5.817	18.489	4.835
	0.03	33.766	1.704	31.975	2.132	33.101	1.778
	0.07	24.908	3.464	24.924	2.111	24.764	1.973
	0.14	12.572	3.930	13.921	3.397	14.575	3.013
	0.28	6.303	8.740	7.434	4.442	7.113	4.287
	0.55	3.237	7.531	3.752	6.823	1.742	6.357
	1.10	1.211	11.571	1.236	9.900	0.197	7.892
	2.20	0.326	23.784	0.263	9.271	0.019	20.359
	4.40	0.064	32.039	0.026	33.813	0.000	175.271
	8.81	0.002	93.387	0.000	412.311	0.000	178.929

Table A.3: Measured frequency of occurrence of Air-void size distribution for Silica Fume mix.

Sample Id	Sizes	Frequency of Occurrence of Air-Void Size Distribution					
		800 kg/m^3	COV	600 kg/m^3	COV	400 kg/m^3	COV
	(mm)	(%)	(%)	(%)	(%)	(%)	(%)
10% SilicaFume	**0.02**	18.812	4.955	17.366	4.735	17.315	4.746
	0.03	33.130	1.777	31.820	1.597	34.220	1.678
	0.07	24.578	2.001	24.505	1.565	26.182	1.881
	0.14	12.772	3.368	14.670	2.657	14.746	3.201
	0.28	6.262	4.910	7.631	3.774	5.700	5.440
	0.55	2.983	5.774	3.004	5.036	1.447	7.909
	1.10	1.080	6.937	0.819	6.759	0.325	13.670
	2.20	0.310	9.808	0.167	11.367	0.056	13.965
	4.40	0.063	13.381	0.017	23.707	0.008	41.268
	8.81	0.008	30.589	0.001	110.230	0.002	59.392
20% SilicaFume	**0.02**	22.202	4.690	17.651	4.814	16.239	4.852
	0.03	34.104	1.696	31.867	1.639	31.846	2.208
	0.07	24.125	2.051	24.507	1.451	26.398	1.657
	0.14	11.922	1.328	14.315	3.206	15.905	3.359
	0.28	4.708	2.294	7.188	4.671	6.799	5.039
	0.55	1.922	3.095	3.014	4.159	2.134	6.126
	1.10	0.661	4.878	1.085	5.658	0.553	8.824
	2.20	0.241	5.892	0.312	7.676	0.107	12.130
	4.40	0.082	13.259	0.057	13.938	0.017	34.019
	8.81	0.025	22.181	0.004	47.479	0.001	89.994

Table A.4: Measured frequency of occurrence of Air-void size distribution for Metakaolin mix.

Sample Id	Sizes	Frequency of Occurrence of Air-Void Size Distribution					
		800 kg/m^3	COV	600 kg/m^3	COV	400 kg/m^3	COV
	(mm)	(%)	(%)	(%)	(%)	(%)	(%)
10% Metakaolin	**0.02**	19.061	4.765	17.386	4.537	17.424	5.159
	0.03	33.755	9.441	31.705	1.741	33.689	2.711
	0.07	24.318	2.289	24.455	1.554	26.878	1.940
	0.14	12.618	9.471	14.316	2.647	15.419	4.626
	0.28	6.044	14.765	7.596	4.133	5.404	11.800
	0.55	2.863	17.764	3.334	6.565	0.972	17.698
	1.10	0.986	19.114	0.960	9.259	0.163	18.101
	2.20	0.278	20.648	0.212	10.577	0.043	20.012
	4.40	0.066	25.563	0.035	21.844	0.007	38.712
	8.81	0.011	42.452	0.002	70.808	0.001	118.265
20% Metakaolin	**0.02**	19.490	3.956	17.895	4.797	15.715	4.769
	0.03	33.698	1.558	32.695	1.647	31.785	1.690
	0.07	24.421	1.500	24.440	1.846	26.848	1.470
	0.14	12.405	2.526	13.419	3.067	16.754	2.859
	0.28	5.660	4.282	6.785	4.120	7.024	4.542
	0.55	2.774	5.172	3.282	4.872	1.556	6.921
	1.10	1.105	6.298	1.146	7.515	0.244	9.862
	2.20	0.352	8.312	0.291	11.590	0.062	13.409
	4.40	0.083	16.825	0.044	19.201	0.011	29.669
	8.81	0.012	35.557	0.002	85.616	0.001	120.000

Table A.5: Measured frequency of occurrence of Air-void spacing distribution for reference mix

Sample Id	Sizes (mm)	Frequency of Occurrence of Air-Void Spacing Distribution					
		800 kg/m^3	COV	600 kg/m^3	COV	400 kg/m^3	COV
		(%)	(%)	(%)	(%)	(%)	(%)
0% Reference	**0.02**	0.291	10.408	0.349	10.020	0.376	11.840
	0.03	1.998	6.397	2.392	6.807	2.877	7.031
	0.07	5.161	2.709	6.061	3.876	7.823	3.772
	0.14	11.152	1.980	12.054	2.554	16.352	3.018
	0.28	20.335	1.719	20.453	1.889	23.589	4.231
	0.55	23.306	1.939	22.274	2.300	19.362	5.309
	1.10	18.851	3.654	17.859	4.789	13.053	4.836
	2.20	12.741	6.534	13.213	8.874	9.234	24.512
	4.40	5.522	21.806	4.817	25.300	6.963	49.656
	8.81	0.576	161.444	0.528	125.606	0.000	0.000

Table A.6: Measured frequency of occurrence of Air-void spacing distribution for Fly Ash mix

Sample Id	Sizes (mm)	Frequency of Occurrence of Air-Void Spacing Distribution					
		800 kg/m^3	COV	600 kg/m^3	COV	400 kg/m^3	COV
		(%)	(%)	(%)	(%)	(%)	(%)
10% Fly Ash	**0.02**	0.228	12.061	0.282	9.754	0.363	9.602
	0.03	1.470	7.591	1.916	5.581	2.698	6.349
	0.07	3.372	4.676	4.604	2.887	7.208	4.472
	0.14	5.187	4.820	8.207	3.332	14.755	4.170
	0.28	8.317	4.865	15.134	2.803	25.471	2.419
	0.55	13.674	4.717	22.630	2.369	26.232	3.636
	1.10	17.926	3.334	23.112	5.452	14.936	8.614
	2.20	20.239	5.654	16.344	5.916	6.120	12.996
	4.40	15.653	9.369	6.232	23.380	2.195	53.814
	8.81	8.104	20.869	1.349	64.308	0.000	0.000
20% Fly Ash	**0.02**	0.238	17.369	0.248	11.750	0.666	8.936
	0.03	1.762	12.134	1.877	7.718	4.528	5.008
	0.07	4.167	7.820	4.817	4.357	10.746	2.303
	0.14	6.666	12.825	8.616	4.438	20.004	1.900
	0.28	11.849	17.877	15.608	4.499	30.174	1.210
	0.55	18.928	12.233	23.652	4.535	20.513	3.461
	1.10	22.300	8.558	24.136	5.849	8.546	6.768
	2.20	20.089	14.744	16.432	8.113	4.117	16.484
	4.40	12.927	28.566	4.555	27.472	0.304	173.010
	8.81	1.073	97.765	0.059	412.311	0.402	188.723

Table A.7: Measured frequency of occurrence of Air-void spacing distribution for Silica Fume Mix

Sample Id	Sizes (mm)	Frequency of Occurrence of Air-Void Spacing Distribution					
		800 kg/m^3	COV	600 kg/m^3	COV	400 kg/m^3	COV
		(%)	(%)	(%)	(%)	(%)	(%)
10% Silica Fume	**0.02**	0.249	10.408	0.324	9.491	0.447	10.080
	0.03	1.679	6.746	2.270	5.979	3.367	6.871
	0.07	3.951	3.509	5.650	3.403	8.440	4.616
	0.14	6.422	2.406	10.839	2.795	15.083	4.875
	0.28	10.965	1.519	18.423	3.310	17.537	6.020
	0.55	16.390	1.736	21.810	2.971	15.231	7.729
	1.10	19.721	4.633	20.235	4.031	13.655	12.773
	2.20	19.760	7.867	14.787	7.077	10.032	13.040
	4.40	14.094	12.272	4.930	26.008	6.076	44.049
	8.81	5.662	36.073	0.731	127.863	9.431	64.270
20% Silica Fume	**0.02**	0.200	7.503	0.238	9.104	0.334	11.787
	0.03	1.189	4.965	1.638	5.804	2.526	9.625
	0.07	2.698	2.999	4.083	3.758	6.854	6.782
	0.14	4.079	2.713	7.621	2.941	12.905	6.028
	0.28	5.383	3.368	12.635	3.011	16.860	7.294
	0.55	7.281	3.715	16.862	2.722	17.917	7.420
	1.10	8.468	5.556	21.038	4.326	17.135	8.656
	2.20	10.857	7.384	20.902	6.738	12.999	10.531
	4.40	13.106	13.199	12.193	10.122	7.527	29.486
	8.81	14.339	33.739	2.713	50.383	2.163	114.916

Table A.8: Measured frequency of occurrence of Air-void spacing distribution for Metakaolin Mix

Sample Id	Sizes (mm)	Frequency of Occurrence of Air-Void Spacing Distribution					
		800 kg/m^3	COV	600 kg/m^3	COV	400 kg/m^3	COV
		(%)	(%)	(%)	(%)	(%)	(%)
10% Metakaolin	**0.02**	0.264	10.270	0.289	9.714	0.534	9.928
	0.03	1.778	7.468	2.020	6.755	3.963	7.448
	0.07	4.200	6.610	5.042	4.958	10.301	7.272
	0.14	7.022	6.927	9.414	4.673	18.275	10.499
	0.28	12.084	7.443	16.453	4.143	18.386	17.842
	0.55	17.599	5.504	21.686	4.846	10.284	22.778
	1.10	18.644	4.574	20.087	5.964	8.738	21.811
	2.20	18.835	5.808	15.766	7.256	10.309	24.170
	4.40	13.160	14.350	8.018	23.331	4.508	43.803
	8.81	5.281	33.775	1.226	86.029	2.116	101.003
20% Metakaolin	**0.02**	0.238	8.913	0.258	10.851	0.448	9.131
	0.03	1.552	6.265	1.794	7.755	3.502	5.461
	0.07	3.560	5.318	4.332	5.649	9.791	2.952
	0.14	5.600	4.967	7.552	4.082	19.267	2.249
	0.28	8.987	7.086	13.149	3.715	23.385	3.321
	0.55	14.354	6.540	19.703	3.461	15.059	5.643
	1.10	18.756	5.267	22.100	4.896	10.363	8.025
	2.20	20.890	5.266	19.907	7.383	12.170	14.130
	4.40	16.714	13.202	9.850	15.569	5.735	33.599
	8.81	8.213	32.526	1.356	88.487	0.289	205.300

Appendix B

Quantitative Analysis

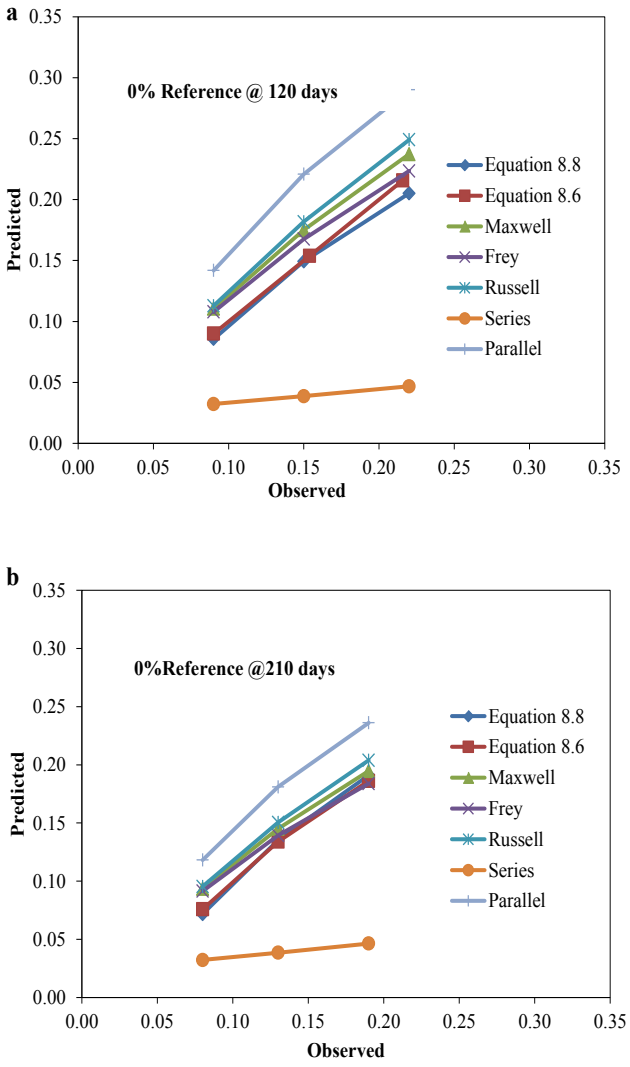

Figure B.1: Comparison between the predicted and the tested values of conductivity measured by the current authors' and other researchers; 0% Reference mix.

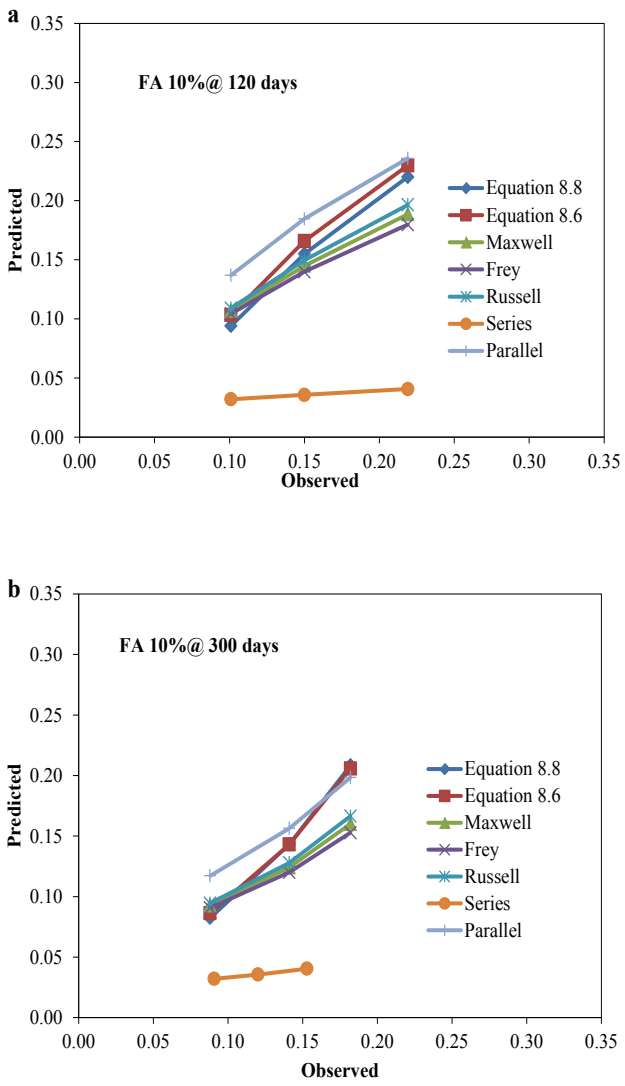

Figure B.2: Comparison between the predicted and the tested values of conductivity measured by the current authors' and other researchers; 10% fly ash mix.

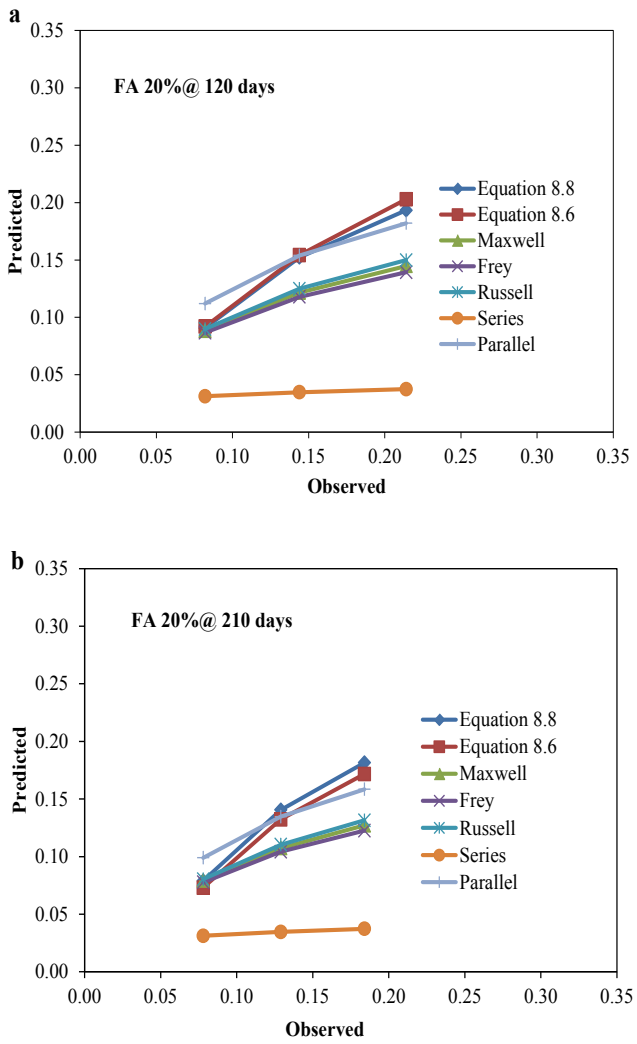

Figure B.3: Comparison between the predicted and the tested values of conductivity measured by the current authors' and other researchers; 20% fly ash mix.

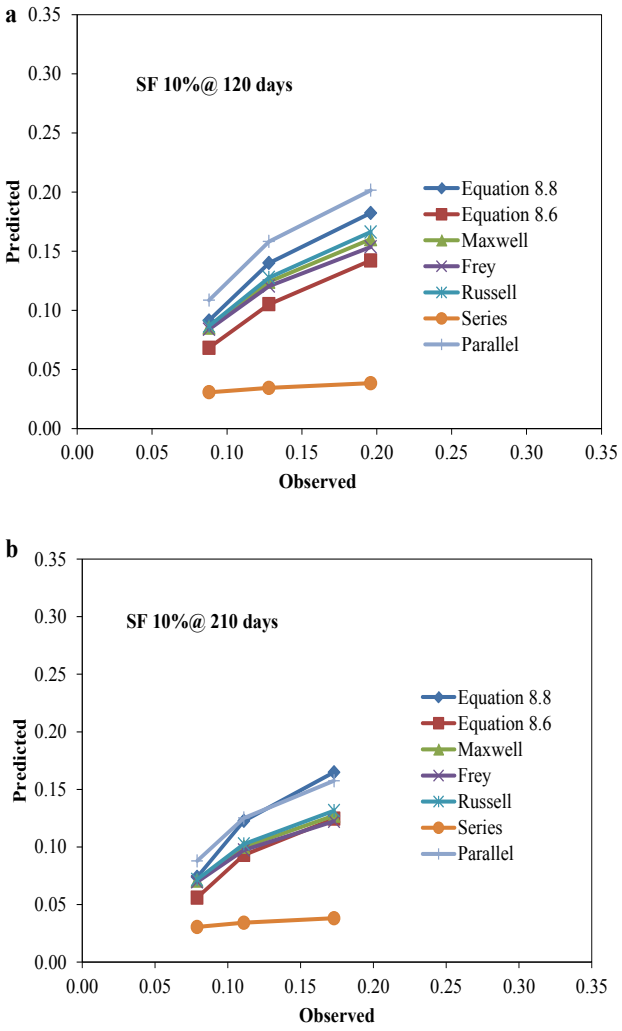

Figure B.4: Comparison between the predicted and the tested values of conductivity measured by the current authors' and other researchers; 10% Silica Fume mix.

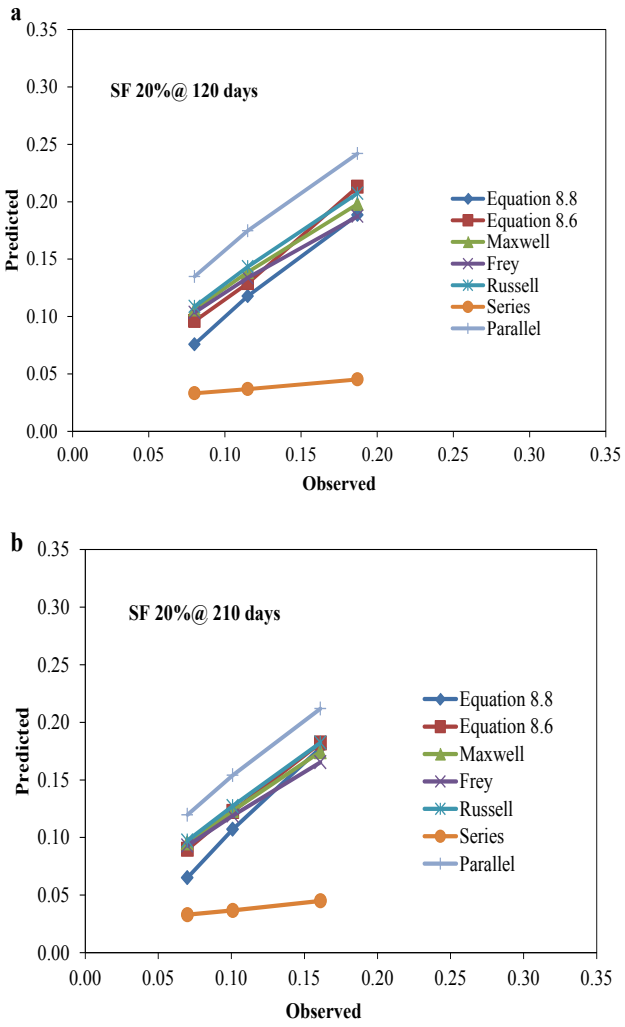

Figure B.5: Comparison between the predicted and the tested values of conductivity measured by the current authors' and other researchers; 20% Silica Fume mix.

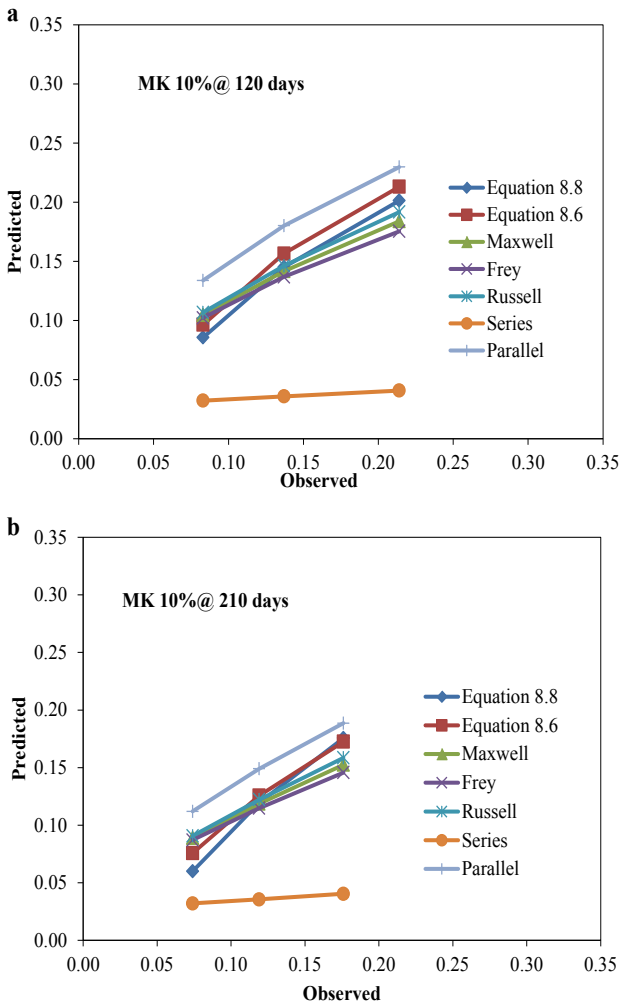

Figure B.6: Comparison between the predicted and the tested values of conductivity measured by the current authors' and other researchers; 10% Metakaolin mix.

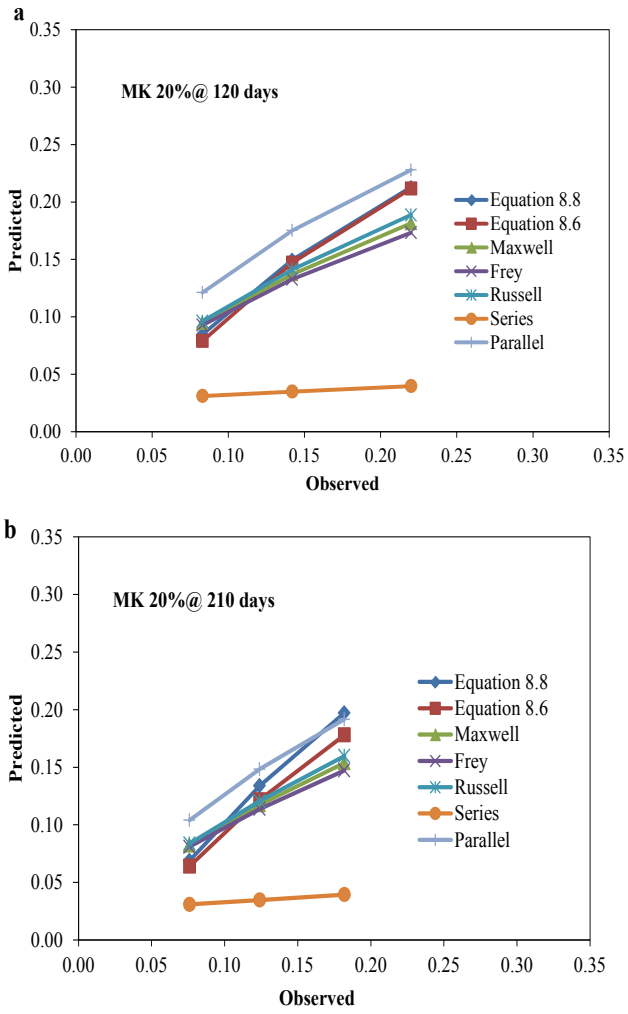

Figure B.7: Comparison between the predicted and the tested values of conductivity measured by the current authors' and other researchers; 20% Metakaolin mix.

Model Summary[b]

Model	R	R Square	Adjusted R Square	Std. Error of the Estimate	Change Statistics					Durbin-Watson
					R Square Change	F Change	df1	df2	Sig. F Change	
1	.974[a]	.948	.947	.0116794	.948	847.622	3	140	.000	.565

a. Predictors: (Constant), porosity, Lndays, Ratio

b. Dependent Variable: TC

ANOVA[a]

Model		Sum of Squares	df	Mean Square	F	Sig.
1	Regression	.347	3	.116	847.622	.000[b]
	Residual	.019	140	.000		
	Total	.366	143			

a. Dependent Variable: TC

b. Predictors: (Constant), porosity, Lndays, Ratio

Coefficients[a]

Model		Unstandardized Coefficients		Standardized Coefficients	t	Sig.	95.0% Confidence Interval for B		Correlations			Collinearity Statistics	
		B	Std. Error	Beta			Lower Bound	Upper Bound	Zero-order	Partial	Part	Tolerance	VIF
1	(Constant)	.038	.010		3.857	.000	.018	.057					
	Ratio	.121	.020	.120	6.035	.000	.081	.161	-.109	.454	.117	.943	1.060
	Lndays	-.021	.002	-.259	-13.413	.000	-.025	-.018	-.259	-.750	-.259	1.000	1.000
	porosity	.769	.016	.960	48.281	.000	.738	.801	.931	.971	.932	.943	1.060

a. Dependent Variable: TC

Correlations

		TC	Ratio	Lndays	porosity
Pearson Correlation	TC	1.000	-.109	-.259	.931
	Ratio	-.109	1.000	.000	-.239
	Lndays	-.259	.000	1.000	.000
	porosity	.931	-.239	.000	1.000
Sig. (1-tailed)	TC	.	.097	.001	.000
	Ratio	.097	.	.500	.002
	Lndays	.001	.500	.	.500
	porosity	.000	.002	.500	.
N	TC	144	144	144	144
	Ratio	144	144	144	144
	Lndays	144	144	144	144
	porosity	144	144	144	144

Figure B.8: Output for equation 8.8;Fly Ash mix.

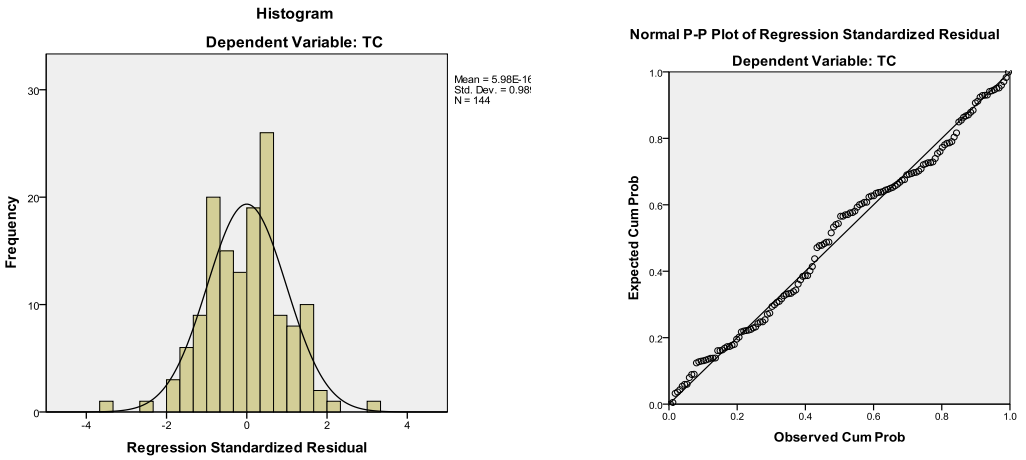

Figure B.9: Histograms and normal P-P plots of normally distributed residuals and non-normally distributed residuals for equation 8.8;Fly Ash mix.

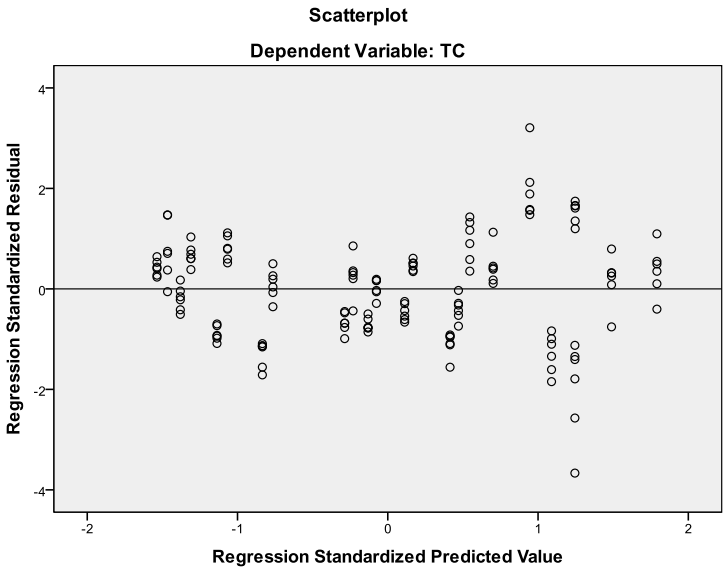

Figure B.10: Plot of standardized predicted values against standardized residuals; Fly Ash mix.

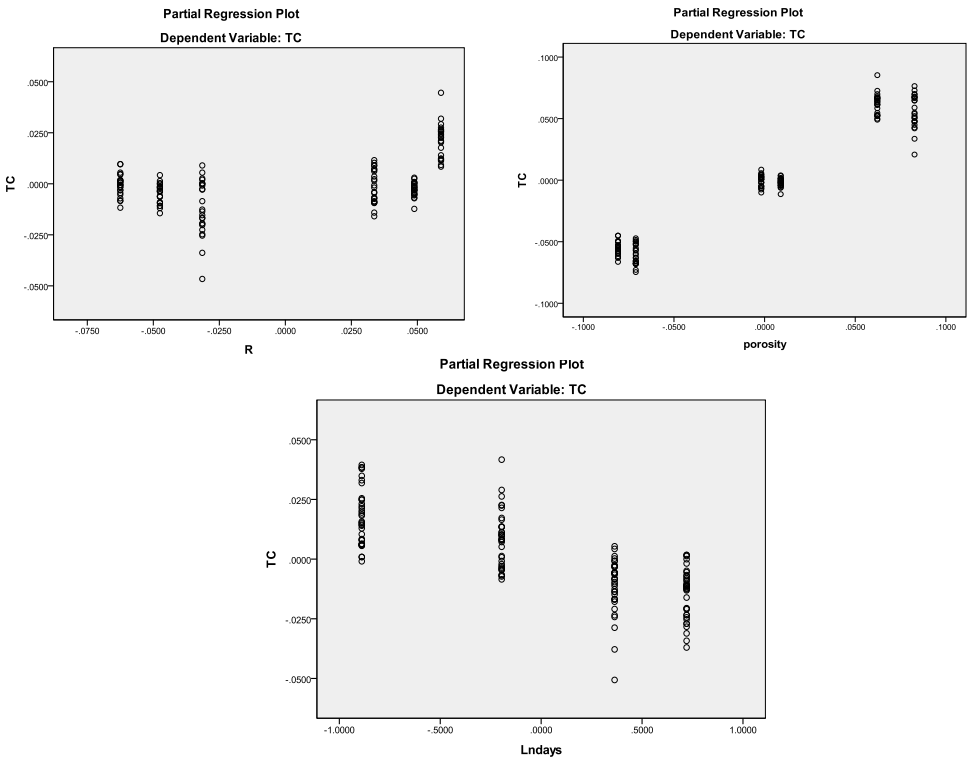

Figure B.11: Plot of thermal conductivity values against independent variables; Fly Ash mix.

Tests of Normality

	Kolmogorov-Smirnov[a]			Shapiro-Wilk		
	Statistic	df	Sig.	Statistic	df	Sig.
Standardized Residual	.066	144	.200*	.986	144	.138

*. This is a lower bound of the true significance.

a. Lilliefors Significance Correction

Figure B.12: Output of Tests of Normality for Plot; Fly Ash mix.

Model Summary[b]

Model	R	R Square	Adjusted R Square	Std. Error of the Estimate	Change Statistics					Durbin-Watson
					R Square Change	F Change	df1	df2	Sig. F Change	
1	.979[a]	.958	.957	.0108523	.958	796.820	2	69	.000	1.189

a. Predictors: (Constant), Indays, Porosity

b. Dependent Variable: TC

ANOVA[a]

Model		Sum of Squares	df	Mean Square	F	Sig.
1	Regression	.188	2	.094	796.820	.000[b]
	Residual	.008	69	.000		
	Total	.196	71			

a. Dependent Variable: TC

b. Predictors: (Constant), Indays, Porosity

Coefficients[a]

Model		Unstandardized Coefficients		Standardized Coefficients	t	Sig.	95.0% Confidence Interval for B		Correlations			Collinearity Statistics	
		B	Std. Error	Beta			Lower Bound	Upper Bound	Zero-order	Partial	Part	Tolerance	VIF
1	(Constant)	.110	.011		9.715	.000	.087	.133					
	Porosity	.498	.013	.936	38.164	.000	.472	.524	.936	.977	.936	1.000	1.000
	Indays	-.025	.002	-.287	-11.712	.000	-.029	-.020	-.287	-.816	-.287	1.000	1.000

a. Dependent Variable: TC

Correlations

		TC	Porosity	Indays
Pearson Correlation	TC	1.000	.936	-.287
	Porosity	.936	1.000	.000
	Indays	-.287	.000	1.000
Sig. (1-tailed)	TC	.	.000	.007
	Porosity	.000	.	.500
	Indays	.007	.500	.
N	TC	72	72	72
	Porosity	72	72	72
	Indays	72	72	72

Figure B.13: Output for equation 8.8; Reference Mix.

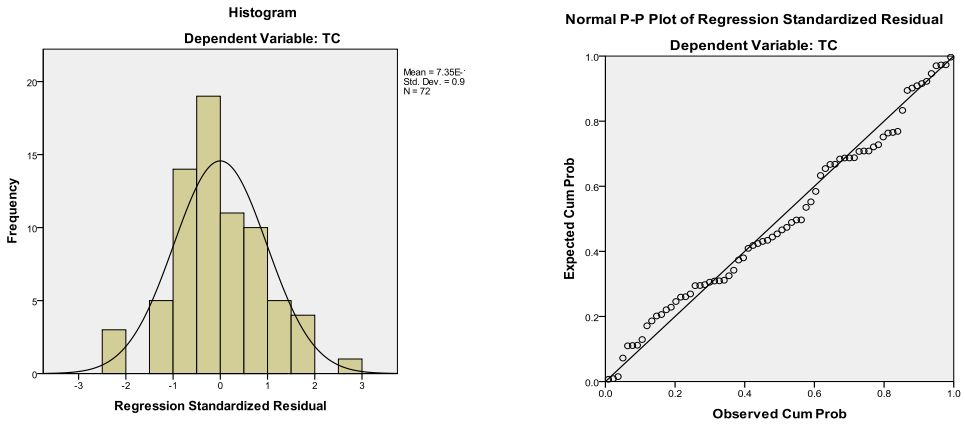

Figure B.14: Histograms and normal P-P plots of normally distributed residuals and non-normally distributed residuals for equation 8.8; Reference Mix.

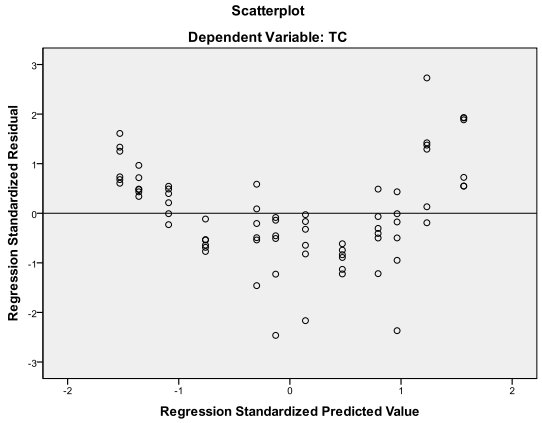

Figure B.15: Plot of standardized predicted values against standardized residuals; Reference Mix.

Tests of Normality

	Kolmogorov-Smirnov[a]			Shapiro-Wilk		
	Statistic	df	Sig.	Statistic	df	Sig.
Standardized Residual	.075	72	.200*	.981	72	.365

*. This is a lower bound of the true significance.

a. Lilliefors Significance Correction

Figure B.16: Output of Tests of Normality for Plot; Reference Mix.

Model Summary[b]

Model	R	R Square	Adjusted R Square	Std. Error of the Estimate	Change Statistics					Durbin-Watson
					R Square Change	F Change	df1	df2	Sig. F Change	
1	.974[a]	.948	.947	.0104653	.948	847.548	3	140	.000	.568

a. Predictors: (Constant), porosity, Lndays, Ratio

b. Dependent Variable: TC

ANOVA[a]

Model		Sum of Squares	df	Mean Square	F	Sig.
1	Regression	.278	3	.093	847.548	.000[b]
	Residual	.015	140	.000		
	Total	.294	143			

a. Dependent Variable: TC

b. Predictors: (Constant), porosity, Lndays, Ratio

Coefficients[a]

Model		Unstandardized Coefficients		Standardized Coefficients	t	Sig.	95.0% Confidence Interval for B		Correlations			Collinearity Statistics	
		B	Std. Error	Beta			Lower Bound	Upper Bound	Zero-order	Partial	Part	Tolerance	VIF
1	(Constant)	.149	.008		18.940	.000	.134	.165					
	Ratio	-.495	.019	-.548	-25.731	.000	-.533	-.457	-.116	-.909	-.497	.823	1.215
	Lndays	-.019	.001	-.260	-13.459	.000	-.022	-.016	-.260	-.751	-.260	1.000	1.000
	porosity	.552	.011	1.026	48.221	.000	.529	.574	.796	.971	.931	.823	1.215

a. Dependent Variable: TC

Correlations

		TC	Ratio	Lndays	porosity
Pearson Correlation	TC	1.000	-.116	-.260	.796
	Ratio	-.116	1.000	.000	.420
	Lndays	-.260	.000	1.000	.000
	porosity	.796	.420	.000	1.000
Sig. (1-tailed)	TC	.	.083	.001	.000
	Ratio	.083	.	.500	.000
	Lndays	.001	.500	.	.500
	porosity	.000	.000	.500	.
N	TC	144	144	144	144
	Ratio	144	144	144	144
	Lndays	144	144	144	144
	porosity	144	144	144	144

Figure B.17: Output for equation 8.8; Silica fume Mix

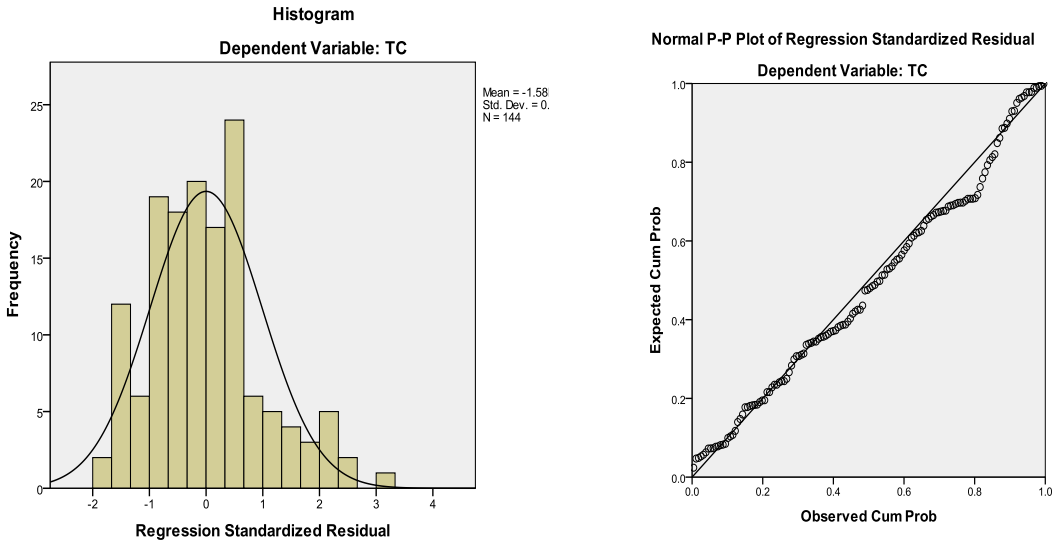

Figure B.18: Histograms and normal P-P plots of normally distributed residuals and non-normally distributed residuals for equation 8.8; Silica fume Mix

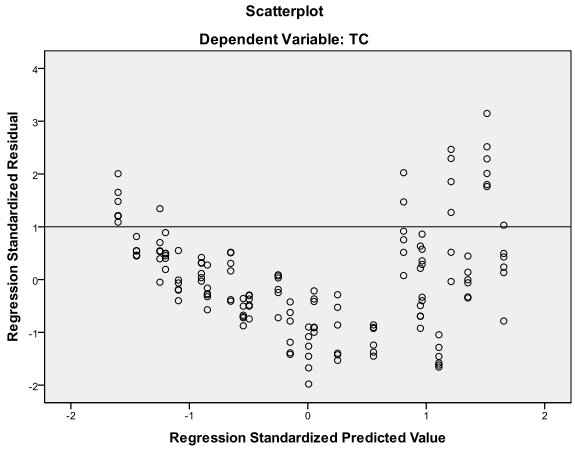

Figure B.19: Plot of standardized predicted values against standardized residuals; Silica fume Mix.

Tests of Normality

	Kolmogorov-Smirnov[a]			Shapiro-Wilk		
	Statistic	df	Sig.	Statistic	df	Sig.
Standardized Residual	.095	144	.003	.971	144	.004

a. Lilliefors Significance Correction

Figure B.20: Output of Tests of Normality for Plot; Silica fume Mix.

Model Summary[b]

Model	R	R Square	Adjusted R Square	Std. Error of the Estimate	Change Statistics					Durbin-Watson
					R Square Change	F Change	df1	df2	Sig. F Change	
1	.979[a]	.958	.957	.0111923	.958	1066.634	3	140	.000	.773

a. Predictors: (Constant), Porosity, Lndays, Ratio

b. Dependent Variable: TC

ANOVA[a]

Model		Sum of Squares	df	Mean Square	F	Sig.
1	Regression	.401	3	.134	1066.634	.000[b]
	Residual	.018	140	.000		
	Total	.418	143			

a. Dependent Variable: TC

b. Predictors: (Constant), Porosity, Lndays, Ratio

Coefficients[a]

Model		Unstandardized Coefficients		Standardized Coefficients	t	Sig.	95.0% Confidence Interval for B		Correlations			Collinearity Statistics	
		B	Std. Error	Beta			Lower Bound	Upper Bound	Zero-order	Partial	Part	Tolerance	VIF
1	(Constant)	.062	.009		6.864	.000	.044	.080					
	Ratio	.198	.019	.184	10.509	.000	.161	.235	.047	.664	.182	.979	1.022
	Lndays	-.028	.002	-.317	-18.338	.000	-.031	-.025	-.317	-.840	-.317	1.000	1.000
	Porosity	.734	.014	.935	53.443	.000	.706	.761	.908	.976	.925	.979	1.022

a. Dependent Variable: TC

Correlations

		TC	Ratio	Lndays	Porosity
Pearson Correlation	TC	1.000	.047	-.317	.908
	Ratio	.047	1.000	.000	-.146
	Lndays	-.317	.000	1.000	.000
	Porosity	.908	-.146	.000	1.000
Sig. (1-tailed)	TC	.	.287	.000	.000
	Ratio	.287	.	.500	.040
	Lndays	.000	.500	.	.500
	Porosity	.000	.040	.500	.
N	TC	144	144	144	144
	Ratio	144	144	144	144
	Lndays	144	144	144	144
	Porosity	144	144	144	144

Figure B.21: Output for equation 8.8; Metakoalin Mix

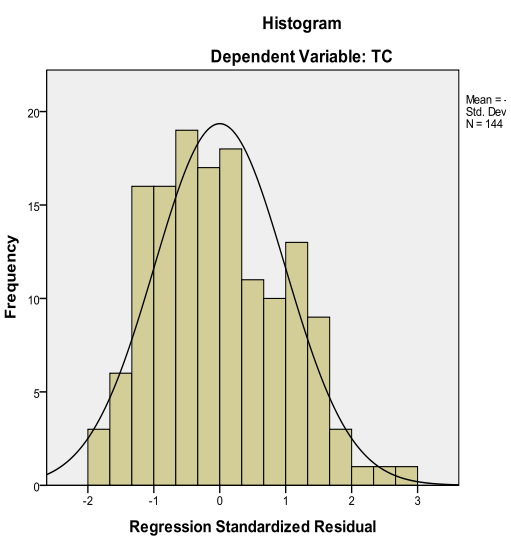

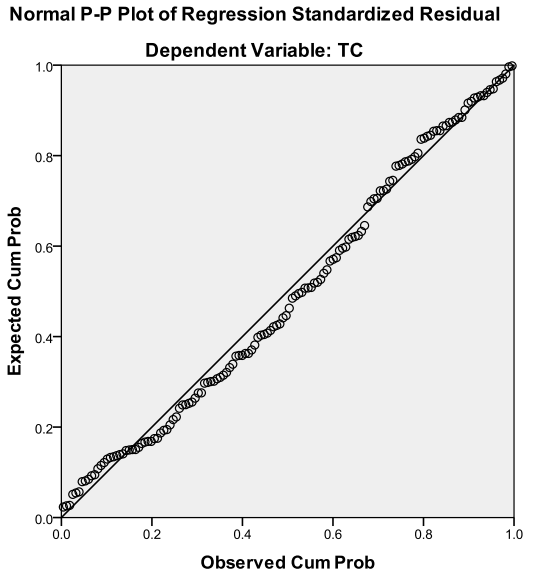

Figure B.22: Histograms and n[illegible] non-normally distributed residuals for equation 8.8; Metakaolin Mix

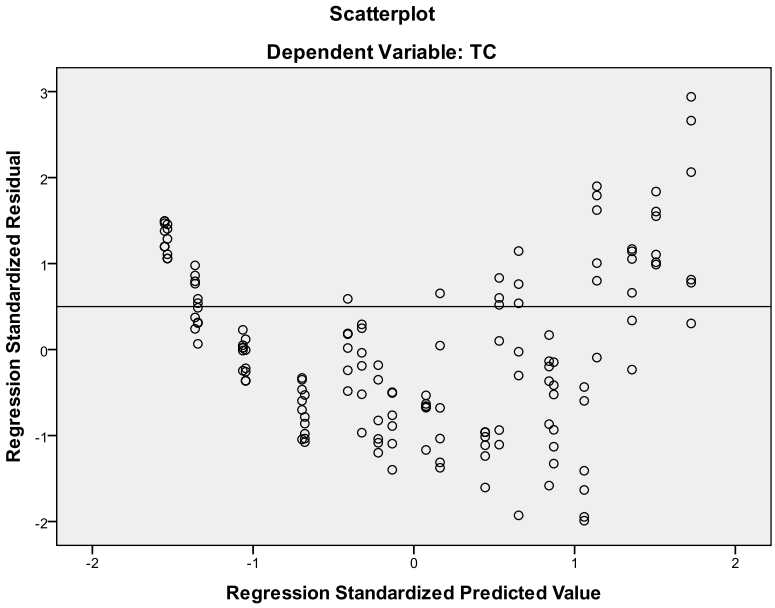

Figure B.23: Plot of standardized predicted values against standardized residuals; Metakaolin Mix.

Tests of Normality

	Kolmogorov-Smirnov[a]			Shapiro-Wilk		
	Statistic	df	Sig.	Statistic	df	Sig.
Standardized Residual	.059	144	.200*	.982	144	.062

*. This is a lower bound of the true significance.

a. Lilliefors Significance Correction

Figure B.24: Output of Tests of Normality for Plot; Metakaolin

Table B.1: Detail of Fly Ash model input

Mix	Cast Density	Tc (W/m/k)	Ratio	Days	ln(days)	Porosity (%)	Tcp(1- p)	Tcv (p- Mc)	Tcw (Mc)	Tc Eq(8.6) (W/m/k)	Ψ (Eq 8.7)	Tc Eq(8.8) (W/m/k)
Fly Ash	800	0.245	0.1	60	4.094	62.2	0.251	0.014	0.006	0.223	0.351	0.234
		0.234	0.1	60	4.094	62.2	0.251	0.014	0.006	0.223	0.351	0.234
		0.238	0.1	60	4.094	62.2	0.251	0.014	0.006	0.223	0.351	0.234
		0.236	0.1	60	4.094	62.2	0.251	0.014	0.006	0.223	0.351	0.234
		0.239	0.1	60	4.094	62.2	0.251	0.014	0.006	0.223	0.351	0.234
		0.228	0.1	60	4.094	62.2	0.251	0.014	0.006	0.223	0.351	0.234
	600	0.159	0.1	60	4.094	71.4	0.190	0.016	0.005	0.160	0.267	0.169
		0.164	0.1	60	4.094	71.4	0.190	0.016	0.005	0.160	0.267	0.169
		0.164	0.1	60	4.094	71.4	0.190	0.016	0.005	0.160	0.267	0.169
		0.167	0.1	60	4.094	71.4	0.190	0.016	0.005	0.160	0.267	0.169
		0.161	0.1	60	4.094	71.4	0.190	0.016	0.005	0.160	0.267	0.169
		0.162	0.1	60	4.094	71.4	0.190	0.016	0.005	0.160	0.267	0.169
	400	0.106	0.1	60	4.094	80.0	0.133	0.019	0.004	0.102	0.188	0.109
		0.109	0.1	60	4.094	80.0	0.133	0.019	0.004	0.102	0.188	0.109
		0.110	0.1	60	4.094	80.0	0.133	0.019	0.004	0.102	0.188	0.109
		0.107	0.1	60	4.094	80.0	0.133	0.019	0.004	0.102	0.188	0.109
		0.112	0.1	60	4.094	80.0	0.133	0.019	0.004	0.102	0.188	0.109
		0.102	0.1	60	4.094	80.0	0.133	0.019	0.004	0.102	0.188	0.109
	800	0.227	0.1	120	4.787	62.2	0.221	0.014	0.006	0.230	0.351	0.220
		0.221	0.1	120	4.787	62.2	0.221	0.014	0.006	0.230	0.351	0.220
		0.221	0.1	120	4.787	62.2	0.221	0.014	0.006	0.230	0.351	0.220
		0.209	0.1	120	4.787	62.2	0.221	0.014	0.006	0.230	0.351	0.220
		0.218	0.1	120	4.787	62.2	0.221	0.014	0.006	0.230	0.351	0.220
		0.220	0.1	120	4.787	62.2	0.221	0.014	0.006	0.230	0.351	0.220
	600	0.156	0.1	120	4.787	71.4	0.167	0.016	0.005	0.166	0.267	0.155
		0.158	0.1	120	4.787	71.4	0.167	0.016	0.005	0.166	0.267	0.155
		0.160	0.1	120	4.787	71.4	0.167	0.016	0.005	0.166	0.267	0.155
		0.158	0.1	120	4.787	71.4	0.167	0.016	0.005	0.166	0.267	0.155
		0.157	0.1	120	4.787	71.4	0.167	0.016	0.005	0.166	0.267	0.155
		0.158	0.1	120	4.787	71.4	0.167	0.016	0.005	0.166	0.267	0.155
	400	0.105	0.1	120	4.787	80.0	0.117	0.019	0.004	0.103	0.188	0.094
		0.101	0.1	120	4.787	80.0	0.117	0.019	0.004	0.103	0.188	0.094
		0.101	0.1	120	4.787	80.0	0.117	0.019	0.004	0.103	0.188	0.094
		0.099	0.1	120	4.787	80.0	0.117	0.019	0.004	0.103	0.188	0.094
		0.104	0.1	120	4.787	80.0	0.117	0.019	0.004	0.103	0.188	0.094
		0.098	0.1	120	4.787	80.0	0.117	0.019	0.004	0.103	0.188	0.094
		0.189	0.1	210	5.347	62.2	0.184	0.015	0.002	0.206	0.351	0.208
	800	0.190	0.1	210	5.347	62.2	0.184	0.015	0.002	0.206	0.351	0.208
		0.175	0.1	210	5.347	62.2	0.184	0.015	0.002	0.206	0.351	0.208
		0.163	0.1	210	5.347	62.2	0.184	0.015	0.002	0.206	0.351	0.208
		0.192	0.1	210	5.347	62.2	0.184	0.015	0.002	0.206	0.351	0.208
		0.185	0.1	210	5.347	62.2	0.184	0.015	0.002	0.206	0.351	0.208
		0.137	0.1	210	5.347	71.4	0.140	0.018	0.002	0.143	0.267	0.143
	600	0.142	0.1	210	5.347	71.4	0.140	0.018	0.002	0.143	0.267	0.143
		0.142	0.1	210	5.347	71.4	0.140	0.018	0.002	0.143	0.267	0.143
		0.143	0.1	210	5.347	71.4	0.140	0.018	0.002	0.143	0.267	0.143
		0.140	0.1	210	5.347	71.4	0.140	0.018	0.002	0.143	0.267	0.143
		0.140	0.1	210	5.347	71.4	0.140	0.018	0.002	0.143	0.267	0.143
		0.088	0.1	210	5.347	80.0	0.098	0.020	0.002	0.086	0.188	0.082
	400	0.089	0.1	210	5.347	80.0	0.098	0.020	0.002	0.086	0.188	0.082
		0.092	0.1	210	5.347	80.0	0.098	0.020	0.002	0.086	0.188	0.082
		0.084	0.1	210	5.347	80.0	0.098	0.020	0.002	0.086	0.188	0.082
		0.087	0.1	210	5.347	80.0	0.098	0.020	0.002	0.086	0.188	0.082
		0.087	0.1	210	5.347	80.0	0.098	0.020	0.002	0.086	0.188	0.082
	800	0.186	0.1	300	5.704	62.2	0.173	0.016	0.001	0.198	0.351	0.201
		0.188	0.1	300	5.704	62.2	0.173	0.016	0.001	0.198	0.351	0.201
		0.185	0.1	300	5.704	62.2	0.173	0.016	0.001	0.198	0.351	0.201
		0.176	0.1	300	5.704	62.2	0.173	0.016	0.001	0.198	0.351	0.201
		0.179	0.1	300	5.704	62.2	0.173	0.016	0.001	0.198	0.351	0.201
		0.182	0.1	300	5.704	62.2	0.173	0.016	0.001	0.198	0.351	0.201
	600	0.137	0.1	300	5.704	71.4	0.131	0.018	0.001	0.137	0.267	0.136
		0.143	0.1	300	5.704	71.4	0.131	0.018	0.001	0.137	0.267	0.136
		0.137	0.1	300	5.704	71.4	0.131	0.018	0.001	0.137	0.267	0.136
		0.128	0.1	300	5.704	71.4	0.131	0.018	0.001	0.137	0.267	0.136
		0.135	0.1	300	5.704	71.4	0.131	0.018	0.001	0.137	0.267	0.136
		0.136	0.1	300	5.704	71.4	0.131	0.018	0.001	0.137	0.267	0.136
	400	0.081	0.1	300	5.704	80.0	0.092	0.021	0.000	0.075	0.188	0.075
		0.080	0.1	300	5.704	80.0	0.092	0.021	0.000	0.075	0.188	0.075
		0.071	0.1	300	5.704	80.0	0.092	0.021	0.000	0.075	0.188	0.075
		0.076	0.1	300	5.704	80.0	0.092	0.021	0.000	0.075	0.188	0.075
		0.089	0.1	300	5.704	80.0	0.092	0.021	0.000	0.075	0.188	0.075
		0.089	0.1	300	5.704	80.0	0.092	0.021	0.000	0.075	0.188	0.075
	800	0.226	0.2	60	4.094	67.7	0.167	0.015	0.006	0.205	0.301	0.208
		0.221	0.2	60	4.094	67.7	0.167	0.015	0.006	0.205	0.301	0.208
		0.224	0.2	60	4.094	67.7	0.167	0.015	0.006	0.205	0.301	0.208
		0.225	0.2	60	4.094	67.7	0.167	0.015	0.006	0.205	0.301	0.208
		0.225	0.2	60	4.094	67.7	0.167	0.015	0.006	0.205	0.301	0.208
		0.220	0.2	60	4.094	67.7	0.167	0.015	0.006	0.205	0.301	0.208
	600	0.152	0.2	60	4.094	73.5	0.137	0.017	0.005	0.158	0.248	0.167
		0.146	0.2	60	4.094	73.5	0.137	0.017	0.005	0.158	0.248	0.167
		0.154	0.2	60	4.094	73.5	0.137	0.017	0.005	0.158	0.248	0.167
		0.154	0.2	60	4.094	73.5	0.137	0.017	0.005	0.158	0.248	0.167
		0.153	0.2	60	4.094	73.5	0.137	0.017	0.005	0.158	0.248	0.167
		0.152	0.2	60	4.094	73.5	0.137	0.017	0.005	0.158	0.248	0.167
	400	0.090	0.2	60	4.094	82.2	0.092	0.020	0.004	0.092	0.168	0.105
		0.090	0.2	60	4.094	82.2	0.092	0.020	0.004	0.092	0.168	0.105
		0.085	0.2	60	4.094	82.2	0.092	0.020	0.004	0.092	0.168	0.105
		0.090	0.2	60	4.094	82.2	0.092	0.020	0.004	0.092	0.168	0.105
		0.083	0.2	60	4.094	82.2	0.092	0.020	0.004	0.092	0.168	0.105
		0.090	0.2	60	4.094	82.2	0.092	0.020	0.004	0.092	0.168	0.105
	800	0.215	0.2	120	4.787	67.7	0.157	0.015	0.005	0.203	0.301	0.193
		0.213	0.2	120	4.787	67.7	0.157	0.015	0.005	0.203	0.301	0.193
		0.208	0.2	120	4.787	67.7	0.157	0.015	0.005	0.203	0.301	0.193
		0.228	0.2	120	4.787	67.7	0.157	0.015	0.005	0.203	0.301	0.193
		0.209	0.2	120	4.787	67.7	0.157	0.015	0.005	0.203	0.301	0.193
		0.209	0.2	120	4.787	67.7	0.157	0.015	0.005	0.203	0.301	0.193
	600	0.143	0.2	120	4.787	73.5	0.129	0.017	0.004	0.154	0.248	0.152
		0.142	0.2	120	4.787	73.5	0.129	0.017	0.004	0.154	0.248	0.152
		0.146	0.2	120	4.787	73.5	0.129	0.017	0.004	0.154	0.248	0.152
		0.147	0.2	120	4.787	73.5	0.129	0.017	0.004	0.154	0.248	0.152
		0.143	0.2	120	4.787	73.5	0.129	0.017	0.004	0.154	0.248	0.152
		0.145	0.2	120	4.787	73.5	0.129	0.017	0.004	0.154	0.248	0.152
	400	0.075	0.2	120	4.787	82.2	0.087	0.020	0.003	0.092	0.168	0.091
		0.080	0.2	120	4.787	82.2	0.087	0.020	0.003	0.092	0.168	0.091
		0.077	0.2	120	4.787	82.2	0.087	0.020	0.003	0.092	0.168	0.091
		0.080	0.2	120	4.787	82.2	0.087	0.020	0.003	0.092	0.168	0.091
		0.077	0.2	120	4.787	82.2	0.087	0.020	0.003	0.092	0.168	0.091
		0.077	0.2	120	4.787	82.2	0.087	0.020	0.003	0.092	0.168	0.091
	800	0.184	0.2	210	5.347	67.7	0.146	0.017	0.002	0.172	0.301	0.181
		0.180	0.2	210	5.347	67.7	0.146	0.017	0.002	0.172	0.301	0.181
		0.192	0.2	210	5.347	67.7	0.146	0.017	0.002	0.172	0.301	0.181
		0.184	0.2	210	5.347	67.7	0.146	0.017	0.002	0.172	0.301	0.181
		0.183	0.2	210	5.347	67.7	0.146	0.017	0.002	0.172	0.301	0.181
		0.181	0.2	210	5.347	67.7	0.146	0.017	0.002	0.172	0.301	0.181
	600	0.129	0.2	210	5.347	73.5	0.120	0.018	0.002	0.132	0.248	0.140
		0.131	0.2	210	5.347	73.5	0.120	0.018	0.002	0.132	0.248	0.140
		0.128	0.2	210	5.347	73.5	0.120	0.018	0.002	0.132	0.248	0.140
		0.132	0.2	210	5.347	73.5	0.120	0.018	0.002	0.132	0.248	0.140
		0.129	0.2	210	5.347	73.5	0.120	0.018	0.002	0.132	0.248	0.140
		0.129	0.2	210	5.347	73.5	0.120	0.018	0.002	0.132	0.248	0.140
	400	0.076	0.2	210	5.347	82.2	0.080	0.021	0.002	0.073	0.168	0.079
		0.071	0.2	210	5.347	82.2	0.080	0.021	0.002	0.073	0.168	0.079
		0.074	0.2	210	5.347	82.2	0.080	0.021	0.002	0.073	0.168	0.079
		0.078	0.2	210	5.347	82.2	0.080	0.021	0.002	0.073	0.168	0.079
		0.070	0.2	210	5.347	82.2	0.080	0.021	0.002	0.073	0.168	0.079
		0.074	0.2	210	5.347	82.2	0.080	0.021	0.002	0.073	0.168	0.079
	800	0.186	0.2	300	5.704	67.7	0.131	0.017	0.001	0.166	0.301	0.174
		0.185	0.2	300	5.704	67.7	0.131	0.017	0.001	0.166	0.301	0.174
		0.178	0.2	300	5.704	67.7	0.131	0.017	0.001	0.166	0.301	0.174
		0.175	0.2	300	5.704	67.7	0.131	0.017	0.001	0.166	0.301	0.174
		0.188	0.2	300	5.704	67.7	0.131	0.017	0.001	0.166	0.301	0.174
		0.182	0.2	300	5.704	67.7	0.131	0.017	0.001	0.166	0.301	0.174
	600	0.122	0.2	300	5.704	73.5	0.108	0.019	0.001	0.126	0.248	0.133
		0.124	0.2	300	5.704	73.5	0.108	0.019	0.001	0.126	0.248	0.133
		0.121	0.2	300	5.704	73.5	0.108	0.019	0.001	0.126	0.248	0.133
		0.122	0.2	300	5.704	73.5	0.108	0.019	0.001	0.126	0.248	0.133
		0.118	0.2	300	5.704	73.5	0.108	0.019	0.001	0.126	0.248	0.133
		0.125	0.2	300	5.704	73.5	0.108	0.019	0.001	0.126	0.248	0.133
	400	0.073	0.2	300	5.704	82.2	0.072	0.021	0.001	0.064	0.168	0.071
		0.075	0.2	300	5.704	82.2	0.072	0.021	0.001	0.064	0.168	0.071
		0.074	0.2	300	5.704	82.2	0.072	0.021	0.001	0.064	0.168	0.071
		0.076	0.2	300	5.704	82.2	0.072	0.021	0.001	0.064	0.168	0.071
		0.071	0.2	300	5.704	82.2	0.072	0.021	0.001	0.064	0.168	0.071
		0.072	0.2	300	5.704	82.2	0.072	0.021	0.001	0.064	0.168	0.071

Table B.2: Detail of Silica Fume model input

Mix	Cast Density	Tc (W/m/k)	Ratio	Days	ln(days)	Porosity (%)	Tcp(1- p)	Tcv (p- Mc)	Tcw (Mc)	Tc Eq(8.6) (W/m/k)	Ψ (Eq 8.7)	Tc Eq(8.8) (W/m/k)
Silica fume	800	0.213	0.1	60	4.094	66.2	0.211	0.014	0.065	0.187	0.315	0.195
		0.216	0.1	60	4.094	66.2	0.211	0.014	0.065	0.187	0.315	0.195
		0.221	0.1	60	4.094	66.2	0.211	0.014	0.065	0.187	0.315	0.195
		0.218	0.1	60	4.094	66.2	0.211	0.015	0.065	0.180	0.315	0.195
		0.227	0.1	60	4.094	66.2	0.211	0.015	0.065	0.180	0.315	0.195
		0.213	0.1	60	4.094	66.2	0.211	0.015	0.065	0.180	0.315	0.195
	600	0.143	0.1	60	4.094	74.5	0.159	0.017	0.055	0.145	0.238	0.153
		0.143	0.1	60	4.094	74.5	0.159	0.017	0.055	0.145	0.238	0.153
		0.143	0.1	60	4.094	74.5	0.159	0.017	0.055	0.145	0.238	0.153
		0.137	0.1	60	4.094	74.5	0.159	0.017	0.055	0.140	0.238	0.153
		0.139	0.1	60	4.094	74.5	0.159	0.017	0.055	0.140	0.238	0.153
		0.138	0.1	60	4.094	74.5	0.159	0.017	0.055	0.140	0.238	0.153
	400	0.098	0.1	60	4.094	84.1	0.099	0.020	0.048	0.103	0.150	0.105
		0.097	0.1	60	4.094	84.1	0.099	0.020	0.048	0.103	0.150	0.105
		0.100	0.1	60	4.094	84.1	0.099	0.020	0.048	0.103	0.150	0.105
		0.094	0.1	60	4.094	84.1	0.099	0.019	0.048	0.114	0.150	0.105
		0.096	0.1	60	4.094	84.1	0.099	0.019	0.048	0.114	0.150	0.105
		0.096	0.1	60	4.094	84.1	0.099	0.019	0.048	0.114	0.150	0.105
	800	0.181	0.1	120	4.787	66.2	0.184	0.014	0.063	0.186	0.315	0.182
		0.201	0.1	120	4.787	66.2	0.184	0.014	0.063	0.186	0.315	0.182
		0.207	0.1	120	4.787	66.2	0.184	0.014	0.063	0.186	0.315	0.182
		0.194	0.1	120	4.787	66.2	0.184	0.015	0.063	0.177	0.315	0.182
		0.205	0.1	120	4.787	66.2	0.184	0.015	0.063	0.177	0.315	0.182
		0.187	0.1	120	4.787	66.2	0.184	0.015	0.063	0.177	0.315	0.182
	600	0.136	0.1	120	4.787	74.5	0.139	0.017	0.050	0.140	0.238	0.140
		0.124	0.1	120	4.787	74.5	0.139	0.017	0.050	0.140	0.238	0.140
		0.133	0.1	120	4.787	74.5	0.139	0.017	0.050	0.140	0.238	0.140
		0.123	0.1	120	4.787	74.5	0.139	0.018	0.050	0.135	0.238	0.140
		0.130	0.1	120	4.787	74.5	0.139	0.018	0.050	0.135	0.238	0.140
		0.124	0.1	120	4.787	74.5	0.139	0.018	0.050	0.135	0.238	0.140
	400	0.088	0.1	120	4.787	84.1	0.087	0.020	0.042	0.097	0.150	0.091
		0.087	0.1	120	4.787	84.1	0.087	0.020	0.042	0.097	0.150	0.091
		0.093	0.1	120	4.787	84.1	0.087	0.020	0.042	0.097	0.150	0.091
		0.089	0.1	120	4.787	84.1	0.087	0.021	0.042	0.085	0.150	0.091
		0.087	0.1	120	4.787	84.1	0.087	0.021	0.042	0.085	0.150	0.091
		0.084	0.1	120	4.787	84.1	0.087	0.021	0.042	0.085	0.150	0.091
		0.166	0.1	210	5.347	66.2	0.152	0.016	0.024	0.142	0.315	0.172
	800	0.176	0.1	210	5.347	66.2	0.152	0.016	0.024	0.142	0.315	0.172
		0.174	0.1	210	5.347	66.2	0.152	0.016	0.024	0.142	0.315	0.172
		0.173	0.1	210	5.347	66.2	0.152	0.016	0.024	0.138	0.315	0.172
		0.179	0.1	210	5.347	66.2	0.152	0.016	0.024	0.138	0.315	0.172
		0.167	0.1	210	5.347	66.2	0.152	0.016	0.024	0.138	0.315	0.172
		0.117	0.1	210	5.347	74.5	0.115	0.019	0.019	0.105	0.238	0.129
	600	0.111	0.1	210	5.347	74.5	0.115	0.019	0.019	0.105	0.238	0.129
		0.119	0.1	210	5.347	74.5	0.115	0.019	0.019	0.105	0.238	0.129
		0.115	0.1	210	5.347	74.5	0.115	0.019	0.019	0.104	0.238	0.129
		0.113	0.1	210	5.347	74.5	0.115	0.019	0.019	0.104	0.238	0.129
		0.107	0.1	210	5.347	74.5	0.115	0.019	0.019	0.104	0.238	0.129
		0.077	0.1	210	5.347	84.1	0.072	0.021	0.017	0.068	0.150	0.081
	400	0.079	0.1	210	5.347	84.1	0.072	0.021	0.017	0.068	0.150	0.081
		0.085	0.1	210	5.347	84.1	0.072	0.021	0.017	0.068	0.150	0.081
		0.079	0.1	210	5.347	84.1	0.072	0.021	0.017	0.063	0.150	0.081
		0.078	0.1	210	5.347	84.1	0.072	0.021	0.017	0.063	0.150	0.081
		0.075	0.1	210	5.347	84.1	0.072	0.021	0.017	0.063	0.150	0.081
	800	0.169	0.1	300	5.704	66.2	0.140	0.017	0.009	0.125	0.315	0.165
		0.185	0.1	300	5.704	66.2	0.140	0.017	0.009	0.125	0.315	0.165
		0.173	0.1	300	5.704	66.2	0.140	0.017	0.009	0.125	0.315	0.165
		0.171	0.1	300	5.704	66.2	0.140	0.017	0.009	0.124	0.315	0.165
		0.179	0.1	300	5.704	66.2	0.140	0.017	0.009	0.124	0.315	0.165
		0.164	0.1	300	5.704	66.2	0.140	0.017	0.009	0.124	0.315	0.165
	600	0.117	0.1	300	5.704	74.5	0.106	0.019	0.008	0.093	0.238	0.123
		0.109	0.1	300	5.704	74.5	0.106	0.019	0.008	0.093	0.238	0.123
		0.113	0.1	300	5.704	74.5	0.106	0.019	0.008	0.093	0.238	0.123
		0.115	0.1	300	5.704	74.5	0.106	0.019	0.008	0.092	0.238	0.123
		0.107	0.1	300	5.704	74.5	0.106	0.019	0.008	0.092	0.238	0.123
		0.106	0.1	300	5.704	74.5	0.106	0.019	0.008	0.092	0.238	0.123
	400	0.078	0.1	300	5.704	84.1	0.066	0.022	0.006	0.056	0.150	0.074
		0.078	0.1	300	5.704	84.1	0.066	0.022	0.006	0.056	0.150	0.074
		0.087	0.1	300	5.704	84.1	0.066	0.022	0.006	0.056	0.150	0.074
		0.080	0.1	300	5.704	84.1	0.066	0.019	0.006	0.090	0.150	0.074
		0.077	0.1	300	5.704	84.1	0.066	0.019	0.006	0.090	0.150	0.074
		0.072	0.1	300	5.704	84.1	0.066	0.019	0.006	0.090	0.150	0.074
	800	0.193	0.2	60	4.094	55.2	0.266	0.012	0.057	0.216	0.416	0.202
		0.212	0.2	60	4.094	55.2	0.266	0.012	0.057	0.216	0.416	0.202
		0.202	0.2	60	4.094	55.2	0.266	0.012	0.057	0.216	0.416	0.202
		0.206	0.2	60	4.094	55.2	0.266	0.013	0.057	0.199	0.416	0.202
		0.205	0.2	60	4.094	55.2	0.266	0.013	0.057	0.199	0.416	0.202
		0.203	0.2	60	4.094	55.2	0.266	0.013	0.057	0.199	0.416	0.202
	600	0.121	0.2	60	4.094	69.1	0.183	0.017	0.032	0.137	0.288	0.131
		0.126	0.2	60	4.094	69.1	0.183	0.017	0.032	0.137	0.288	0.131
		0.128	0.2	60	4.094	69.1	0.183	0.017	0.032	0.137	0.288	0.131
		0.121	0.2	60	4.094	69.1	0.183	0.017	0.032	0.131	0.288	0.131
		0.126	0.2	60	4.094	69.1	0.183	0.017	0.032	0.131	0.288	0.131
		0.120	0.2	60	4.094	69.1	0.183	0.017	0.032	0.131	0.288	0.131
	400	0.092	0.2	60	4.094	77.4	0.134	0.019	0.023	0.097	0.212	0.089
		0.091	0.2	60	4.094	77.4	0.134	0.019	0.023	0.097	0.212	0.089
		0.088	0.2	60	4.094	77.4	0.134	0.019	0.023	0.097	0.212	0.089
		0.088	0.2	60	4.094	77.4	0.134	0.018	0.023	0.117	0.212	0.089
		0.089	0.2	60	4.094	77.4	0.134	0.018	0.023	0.117	0.212	0.089
		0.091	0.2	60	4.094	77.4	0.134	0.018	0.023	0.117	0.212	0.089
	800	0.184	0.2	120	4.787	55.2	0.228	0.012	0.052	0.213	0.416	0.189
		0.184	0.2	120	4.787	55.2	0.228	0.012	0.052	0.213	0.416	0.189
		0.187	0.2	120	4.787	55.2	0.228	0.012	0.052	0.213	0.416	0.189
		0.192	0.2	120	4.787	55.2	0.228	0.013	0.052	0.194	0.416	0.189
		0.187	0.2	120	4.787	55.2	0.228	0.013	0.052	0.194	0.416	0.189
		0.189	0.2	120	4.787	55.2	0.228	0.013	0.052	0.194	0.416	0.189
	600	0.115	0.2	120	4.787	69.1	0.157	0.017	0.023	0.129	0.288	0.118
		0.118	0.2	120	4.787	69.1	0.157	0.017	0.023	0.129	0.288	0.118
		0.114	0.2	120	4.787	69.1	0.157	0.017	0.023	0.129	0.288	0.118
		0.117	0.2	120	4.787	69.1	0.157	0.017	0.023	0.127	0.288	0.118
		0.117	0.2	120	4.787	69.1	0.157	0.017	0.023	0.127	0.288	0.118
		0.109	0.2	120	4.787	69.1	0.157	0.017	0.023	0.127	0.288	0.118
	400	0.079	0.2	120	4.787	77.4	0.115	0.019	0.021	0.096	0.212	0.076
		0.084	0.2	120	4.787	77.4	0.115	0.019	0.021	0.096	0.212	0.076
		0.080	0.2	120	4.787	77.4	0.115	0.019	0.021	0.096	0.212	0.076
		0.080	0.2	120	4.787	77.4	0.115	0.019	0.021	0.098	0.212	0.076
		0.077	0.2	120	4.787	77.4	0.115	0.019	0.021	0.098	0.212	0.076
		0.079	0.2	120	4.787	77.4	0.115	0.019	0.021	0.098	0.212	0.076
	800	0.160	0.2	210	5.347	55.2	0.198	0.013	0.024	0.182	0.416	0.178
		0.160	0.2	210	5.347	55.2	0.198	0.013	0.024	0.182	0.416	0.178
		0.163	0.2	210	5.347	55.2	0.198	0.013	0.024	0.182	0.416	0.178
		0.166	0.2	210	5.347	55.2	0.198	0.014	0.024	0.177	0.416	0.178
		0.159	0.2	210	5.347	55.2	0.198	0.014	0.024	0.177	0.416	0.178
		0.161	0.2	210	5.347	55.2	0.198	0.014	0.024	0.177	0.416	0.178
	600	0.101	0.2	210	5.347	69.1	0.136	0.017	0.017	0.123	0.288	0.107
		0.102	0.2	210	5.347	69.1	0.136	0.017	0.017	0.123	0.288	0.107
		0.103	0.2	210	5.347	69.1	0.136	0.017	0.017	0.123	0.288	0.107
		0.103	0.2	210	5.347	69.1	0.136	0.017	0.017	0.121	0.288	0.107
		0.101	0.2	210	5.347	69.1	0.136	0.017	0.017	0.121	0.288	0.107
		0.098	0.2	210	5.347	69.1	0.136	0.017	0.017	0.121	0.288	0.107
	400	0.070	0.2	210	5.347	77.4	0.100	0.019	0.015	0.090	0.212	0.065
		0.069	0.2	210	5.347	77.4	0.100	0.019	0.015	0.090	0.212	0.065
		0.069	0.2	210	5.347	77.4	0.100	0.019	0.015	0.090	0.212	0.065
		0.072	0.2	210	5.347	77.4	0.100	0.020	0.015	0.085	0.212	0.065
		0.069	0.2	210	5.347	77.4	0.100	0.020	0.015	0.085	0.212	0.065
		0.070	0.2	210	5.347	77.4	0.100	0.020	0.015	0.085	0.212	0.065
	800	0.162	0.2	300	5.704	55.2	0.198	0.014	0.008	0.163	0.416	0.171
		0.162	0.2	300	5.704	55.2	0.186	0.014	0.008	0.164	0.416	0.171
		0.160	0.2	300	5.704	55.2	0.186	0.014	0.008	0.164	0.416	0.171
		0.176	0.2	300	5.704	55.2	0.186	0.014	0.008	0.163	0.416	0.171
		0.172	0.2	300	5.704	55.2	0.186	0.014	0.008	0.163	0.416	0.171
		0.165	0.2	300	5.704	55.2	0.186	0.014	0.008	0.163	0.416	0.171
	600	0.101	0.2	300	5.704	69.1	0.128	0.018	0.007	0.111	0.288	0.100
		0.104	0.2	300	5.704	69.1	0.128	0.018	0.007	0.111	0.288	0.100
		0.104	0.2	300	5.704	69.1	0.128	0.018	0.007	0.111	0.288	0.100
		0.102	0.2	300	5.704	69.1	0.128	0.018	0.007	0.110	0.288	0.100
		0.095	0.2	300	5.704	69.1	0.128	0.018	0.007	0.110	0.288	0.100
		0.095	0.2	300	5.704	69.1	0.128	0.018	0.007	0.110	0.288	0.100
	400	0.068	0.2	300	5.704	77.4	0.094	0.020	0.005	0.079	0.212	0.058
		0.070	0.2	300	5.704	77.4	0.094	0.020	0.005	0.079	0.212	0.058
		0.070	0.2	300	5.704	77.4	0.094	0.020	0.005	0.079	0.212	0.058
		0.073	0.2	300	5.704	77.4	0.094	0.020	0.005	0.075	0.212	0.058
		0.074	0.2	300	5.704	77.4	0.094	0.020	0.005	0.075	0.212	0.058
		0.078	0.2	300	5.704	77.4	0.094	0.020	0.005	0.075	0.212	0.058

Table B.3: Detail of Metakaolin model input

Mix	Cast Density	Tc (W/m/k)	Ratio	Days	ln(days)	Porosity (%)	Tcp(1- p)	Tcv (p- Mc)	Tcw (Mc)	Tc Eq(8.6) (W/m/k)	Ψ (Eq 8.7)	Tc Eq(8.8) (W/m/k)
Metakaolin	800	0.239	0.1	60	4.094	62.8	0.222	0.014	0.057	0.226	0.346	0.221
		0.241	0.1	60	4.094	62.8	0.222	0.014	0.057	0.226	0.346	0.221
		0.232	0.1	60	4.094	62.8	0.222	0.014	0.057	0.226	0.346	0.221
		0.233	0.1	60	4.094	62.8	0.222	0.014	0.057	0.225	0.346	0.221
		0.232	0.1	60	4.094	62.8	0.222	0.014	0.057	0.225	0.346	0.221
		0.238	0.1	60	4.094	62.8	0.222	0.014	0.057	0.225	0.346	0.221
	600	0.154	0.1	60	4.094	71.2	0.172	0.016	0.051	0.166	0.269	0.164
		0.146	0.1	60	4.094	71.2	0.172	0.016	0.051	0.166	0.269	0.164
		0.153	0.1	60	4.094	71.2	0.172	0.016	0.051	0.166	0.269	0.164
		0.150	0.1	60	4.094	71.2	0.172	0.016	0.051	0.166	0.269	0.164
		0.152	0.1	60	4.094	71.2	0.172	0.016	0.051	0.166	0.269	0.164
		0.154	0.1	60	4.094	71.2	0.172	0.016	0.051	0.166	0.269	0.164
	400	0.094	0.1	60	4.094	80.0	0.119	0.019	0.046	0.103	0.188	0.105
		0.099	0.1	60	4.094	80.0	0.119	0.019	0.046	0.103	0.188	0.105
		0.095	0.1	60	4.094	80.0	0.119	0.019	0.046	0.103	0.188	0.105
		0.093	0.1	60	4.094	80.0	0.119	0.018	0.046	0.104	0.188	0.105
		0.096	0.1	60	4.094	80.0	0.119	0.018	0.046	0.104	0.188	0.105
		0.093	0.1	60	4.094	80.0	0.119	0.018	0.046	0.104	0.188	0.105
	800	0.221	0.1	120	4.787	62.8	0.215	0.014	0.053	0.218	0.346	0.201
		0.222	0.1	120	4.787	62.8	0.215	0.014	0.053	0.218	0.346	0.201
		0.210	0.1	120	4.787	62.8	0.215	0.014	0.053	0.218	0.346	0.201
		0.200	0.1	120	4.787	62.8	0.215	0.014	0.053	0.218	0.346	0.201
		0.212	0.1	120	4.787	62.8	0.215	0.014	0.053	0.218	0.346	0.201
		0.219	0.1	120	4.787	62.8	0.215	0.014	0.053	0.218	0.346	0.201
	600	0.139	0.1	120	4.787	71.2	0.166	0.016	0.047	0.161	0.269	0.145
		0.132	0.1	120	4.787	71.2	0.166	0.016	0.047	0.161	0.269	0.145
		0.137	0.1	120	4.787	71.2	0.166	0.016	0.047	0.161	0.269	0.145
		0.137	0.1	120	4.787	71.2	0.166	0.017	0.047	0.160	0.269	0.145
		0.137	0.1	120	4.787	71.2	0.166	0.017	0.047	0.160	0.269	0.145
		0.138	0.1	120	4.787	71.2	0.166	0.017	0.047	0.160	0.269	0.145
	400	0.081	0.1	120	4.787	80.0	0.115	0.019	0.043	0.099	0.188	0.086
		0.085	0.1	120	4.787	80.0	0.115	0.019	0.043	0.099	0.188	0.086
		0.082	0.1	120	4.787	80.0	0.115	0.019	0.043	0.099	0.188	0.086
		0.081	0.1	120	4.787	80.0	0.115	0.020	0.043	0.097	0.188	0.086
		0.087	0.1	120	4.787	80.0	0.115	0.020	0.043	0.097	0.188	0.086
		0.083	0.1	120	4.787	80.0	0.115	0.020	0.043	0.097	0.188	0.086
		0.184	0.1	210	5.347	62.8	0.185	0.015	0.023	0.190	0.346	0.186
	800	0.183	0.1	210	5.347	62.8	0.185	0.015	0.023	0.190	0.346	0.186
		0.168	0.1	210	5.347	62.8	0.185	0.015	0.023	0.190	0.346	0.186
		0.176	0.1	210	5.347	62.8	0.185	0.015	0.023	0.189	0.346	0.186
		0.181	0.1	210	5.347	62.8	0.185	0.015	0.023	0.189	0.346	0.186
		0.187	0.1	210	5.347	62.8	0.185	0.015	0.023	0.189	0.346	0.186
		0.116	0.1	210	5.347	71.2	0.143	0.018	0.021	0.139	0.269	0.129
	600	0.117	0.1	210	5.347	71.2	0.143	0.018	0.021	0.139	0.269	0.129
		0.117	0.1	210	5.347	71.2	0.143	0.018	0.021	0.139	0.269	0.129
		0.127	0.1	210	5.347	71.2	0.143	0.018	0.021	0.139	0.269	0.129
		0.120	0.1	210	5.347	71.2	0.143	0.018	0.021	0.139	0.269	0.129
		0.125	0.1	210	5.347	71.2	0.143	0.018	0.021	0.139	0.269	0.129
		0.076	0.1	210	5.347	80.0	0.099	0.020	0.020	0.085	0.188	0.070
	400	0.070	0.1	210	5.347	80.0	0.099	0.020	0.020	0.085	0.188	0.070
		0.076	0.1	210	5.347	80.0	0.099	0.020	0.020	0.085	0.188	0.070
		0.073	0.1	210	5.347	80.0	0.099	0.020	0.020	0.085	0.188	0.070
		0.075	0.1	210	5.347	80.0	0.099	0.020	0.020	0.085	0.188	0.070
		0.073	0.1	210	5.347	80.0	0.099	0.020	0.020	0.085	0.188	0.070
	800	0.175	0.1	300	5.704	62.8	0.169	0.015	0.023	0.173	0.346	0.176
		0.181	0.1	300	5.704	62.8	0.169	0.015	0.023	0.173	0.346	0.176
		0.154	0.1	300	5.704	62.8	0.169	0.015	0.023	0.173	0.346	0.176
		0.172	0.1	300	5.704	62.8	0.169	0.015	0.023	0.172	0.346	0.176
		0.184	0.1	300	5.704	62.8	0.169	0.015	0.023	0.172	0.346	0.176
		0.188	0.1	300	5.704	62.8	0.169	0.015	0.023	0.172	0.346	0.176
	600	0.121	0.1	300	5.704	71.2	0.131	0.018	0.020	0.126	0.269	0.119
		0.114	0.1	300	5.704	71.2	0.131	0.018	0.020	0.126	0.269	0.119
		0.119	0.1	300	5.704	71.2	0.131	0.018	0.020	0.126	0.269	0.119
		0.116	0.1	300	5.704	71.2	0.131	0.018	0.020	0.126	0.269	0.119
		0.121	0.1	300	5.704	71.2	0.131	0.018	0.020	0.126	0.269	0.119
		0.126	0.1	300	5.704	71.2	0.131	0.018	0.020	0.126	0.269	0.119
	400	0.076	0.1	300	5.704	80.0	0.091	0.020	0.020	0.076	0.188	0.060
		0.074	0.1	300	5.704	80.0	0.091	0.020	0.020	0.076	0.188	0.060
		0.072	0.1	300	5.704	80.0	0.091	0.020	0.020	0.076	0.188	0.060
		0.075	0.1	300	5.704	80.0	0.091	0.018	0.020	0.081	0.188	0.060
		0.071	0.1	300	5.704	80.0	0.091	0.018	0.020	0.081	0.188	0.060
		0.071	0.1	300	5.704	80.0	0.091	0.018	0.020	0.081	0.188	0.060
	800	0.262	0.2	60	4.094	64.1	0.214	0.014	0.069	0.215	0.334	0.232
		0.241	0.2	60	4.094	64.1	0.214	0.014	0.069	0.215	0.334	0.232
		0.241	0.2	60	4.094	64.1	0.214	0.014	0.069	0.215	0.334	0.232
		0.265	0.2	60	4.094	64.1	0.214	0.014	0.069	0.214	0.334	0.232
		0.255	0.2	60	4.094	64.1	0.214	0.014	0.069	0.214	0.334	0.232
		0.236	0.2	60	4.094	64.1	0.214	0.014	0.069	0.214	0.334	0.232
	600	0.157	0.2	60	4.094	73.4	0.158	0.017	0.055	0.149	0.248	0.169
		0.158	0.2	60	4.094	73.4	0.158	0.017	0.055	0.149	0.248	0.169
		0.178	0.2	60	4.094	73.4	0.158	0.017	0.055	0.149	0.248	0.169
		0.176	0.2	60	4.094	73.4	0.158	0.017	0.055	0.148	0.248	0.169
		0.175	0.2	60	4.094	73.4	0.158	0.017	0.055	0.148	0.248	0.169
		0.170	0.2	60	4.094	73.4	0.158	0.017	0.055	0.148	0.248	0.169
	400	0.096	0.2	60	4.094	83.1	0.101	0.019	0.048	0.081	0.160	0.104
		0.100	0.2	60	4.094	83.1	0.101	0.019	0.048	0.081	0.160	0.104
		0.092	0.2	60	4.094	83.1	0.101	0.019	0.048	0.081	0.160	0.104
		0.097	0.2	60	4.094	83.1	0.101	0.019	0.048	0.082	0.160	0.104
		0.099	0.2	60	4.094	83.1	0.101	0.019	0.048	0.082	0.160	0.104
		0.100	0.2	60	4.094	83.1	0.101	0.019	0.048	0.082	0.160	0.104
	800	0.226	0.2	120	4.787	64.1	0.202	0.014	0.066	0.202	0.334	0.213
		0.216	0.2	120	4.787	64.1	0.202	0.014	0.066	0.202	0.334	0.213
		0.220	0.2	120	4.787	64.1	0.202	0.014	0.066	0.202	0.334	0.213
		0.224	0.2	120	4.787	64.1	0.202	0.014	0.066	0.201	0.334	0.213
		0.225	0.2	120	4.787	64.1	0.202	0.014	0.066	0.201	0.334	0.213
		0.210	0.2	120	4.787	64.1	0.202	0.014	0.066	0.201	0.334	0.213
	600	0.134	0.2	120	4.787	73.4	0.150	0.017	0.051	0.140	0.248	0.150
		0.135	0.2	120	4.787	73.4	0.150	0.017	0.051	0.140	0.248	0.150
		0.157	0.2	120	4.787	73.4	0.150	0.017	0.051	0.140	0.248	0.150
		0.138	0.2	120	4.787	73.4	0.150	0.017	0.051	0.140	0.248	0.150
		0.150	0.2	120	4.787	73.4	0.150	0.017	0.051	0.140	0.248	0.150
		0.142	0.2	120	4.787	73.4	0.150	0.017	0.051	0.140	0.248	0.150
	400	0.082	0.2	120	4.787	83.1	0.095	0.020	0.047	0.074	0.160	0.085
		0.085	0.2	120	4.787	83.1	0.095	0.020	0.047	0.074	0.160	0.085
		0.085	0.2	120	4.787	83.1	0.095	0.020	0.047	0.074	0.160	0.085
		0.084	0.2	120	4.787	83.1	0.095	0.021	0.047	0.072	0.160	0.085
		0.087	0.2	120	4.787	83.1	0.095	0.021	0.047	0.072	0.160	0.085
		0.085	0.2	120	4.787	83.1	0.095	0.021	0.047	0.072	0.160	0.085
	800	0.179	0.2	210	5.347	64.1	0.174	0.016	0.024	0.177	0.334	0.197
		0.192	0.2	210	5.347	64.1	0.174	0.016	0.024	0.177	0.334	0.197
		0.181	0.2	210	5.347	64.1	0.174	0.016	0.024	0.177	0.334	0.197
		0.175	0.2	210	5.347	64.1	0.174	0.016	0.024	0.177	0.334	0.197
		0.190	0.2	210	5.347	64.1	0.174	0.016	0.024	0.177	0.334	0.197
		0.175	0.2	210	5.347	64.1	0.174	0.016	0.024	0.177	0.334	0.197
	600	0.118	0.2	210	5.347	73.4	0.128	0.018	0.022	0.121	0.248	0.134
		0.121	0.2	210	5.347	73.4	0.128	0.018	0.022	0.121	0.248	0.134
		0.128	0.2	210	5.347	73.4	0.128	0.018	0.022	0.121	0.248	0.134
		0.124	0.2	210	5.347	73.4	0.128	0.018	0.022	0.121	0.248	0.134
		0.128	0.2	210	5.347	73.4	0.128	0.018	0.022	0.121	0.248	0.134
		0.125	0.2	210	5.347	73.4	0.128	0.018	0.022	0.121	0.248	0.134
	400	0.078	0.2	210	5.347	83.1	0.082	0.021	0.021	0.064	0.160	0.069
		0.073	0.2	210	5.347	83.1	0.082	0.021	0.021	0.064	0.160	0.069
		0.071	0.2	210	5.347	83.1	0.082	0.021	0.021	0.064	0.160	0.069
		0.078	0.2	210	5.347	83.1	0.082	0.021	0.021	0.064	0.160	0.069
		0.077	0.2	210	5.347	83.1	0.082	0.021	0.021	0.064	0.160	0.069
		0.080	0.2	210	5.347	83.1	0.082	0.021	0.021	0.064	0.160	0.069
	800	0.174	0.2	300	5.704	64.1	0.166	0.016	0.023	0.168	0.334	0.187
		0.182	0.2	300	5.704	64.1	0.166	0.016	0.023	0.168	0.334	0.187
		0.172	0.2	300	5.704	64.1	0.166	0.016	0.023	0.168	0.334	0.187
		0.181	0.2	300	5.704	64.1	0.166	0.016	0.023	0.167	0.334	0.187
		0.185	0.2	300	5.704	64.1	0.166	0.016	0.023	0.167	0.334	0.187
		0.176	0.2	300	5.704	64.1	0.166	0.016	0.023	0.167	0.334	0.187
	600	0.118	0.2	300	5.704	73.4	0.122	0.018	0.021	0.114	0.248	0.124
		0.123	0.2	300	5.704	73.4	0.122	0.018	0.021	0.114	0.248	0.124
		0.113	0.2	300	5.704	73.4	0.122	0.018	0.021	0.114	0.248	0.124
		0.122	0.2	300	5.704	73.4	0.122	0.018	0.021	0.114	0.248	0.124
		0.127	0.2	300	5.704	73.4	0.122	0.018	0.021	0.114	0.248	0.124
		0.126	0.2	300	5.704	73.4	0.122	0.018	0.021	0.114	0.248	0.124
	400	0.072	0.2	300	5.704	83.1	0.078	0.021	0.021	0.059	0.160	0.059
		0.075	0.2	300	5.704	83.1	0.078	0.021	0.021	0.059	0.160	0.059
		0.072	0.2	300	5.704	83.1	0.078	0.021	0.021	0.059	0.160	0.059
		0.075	0.2	300	5.704	83.1	0.078	0.022	0.021	0.057	0.160	0.059
		0.074	0.2	300	5.704	83.1	0.078	0.022	0.021	0.057	0.160	0.059
		0.075	0.2	300	5.704	83.1	0.078	0.022	0.021	0.057	0.160	0.059